EVALUATION OF REMOTE SENSING METHODS FOR CONTINUOUS COVER FORESTRY

GLORIA OLAYA – GONZALEZ

Ph.D.
The University of Edinburgh
2006

DECLARATION

I declare that this thesis has been composed by myself and the work presented and described is my own, unless otherwise stated.

ACKNOWLEDGEMENTS

Many people and organizations have helped to make this work possible. Firstly, I would like to express my profound gratitude to my supervisors Dr. Tim Malthus and Prof. Peter Furley for all their patience and support. This work owes much to their assistance, advice and involvement in every aspect of it.

I gratefully acknowledged the help and cooperation received from the staff at the Institute of Geography, University of Edinburgh, especially from Chris Place who kindly guided me through the image processing work.

I am very grateful to Juan Suarez who provided the LiDAR data and aerial photography for this research. I also extend my sincere gratitude to the friends that dedicated their valuable time to assist me in the data collection in the Aberfoyle area.

I acknowledged the collaboration of the following institutions: Natural Environment Research Council (UK), Forestry Commission Scotland, and Universidad del Zulia which provided data, logistics, and financial support for this research.

Finally, I am greatly indebted to all my friends in the UK and family and friends in Venezuela. Their help, encouragement, appreciation, friendly contributions and advices made this stage of my life very enjoyable. To Nedzad, many thanks for waiting so long.

ABSTRACT

The overall aim of the project was to investigate the potential and challenges in the application of high spatial and spectral resolution remote sensing to forest stands in the UK for Continuous Cover Forestry (CCF) purposes. Within the context of CCF, a relatively new forest management strategy that has been implemented in several European countries, the usefulness of digital remote sensing techniques lie in their potential ability to retrieve parameters at sub-stand level and, in particular, in the assessment of natural regeneration and light regimes. The idea behind CCF is the support of a sustainable forest management system reducing disturbance of the forest ecosystem and encouraging the use of more natural methods, e.g. natural regeneration, for which the light environment beneath the forest canopy plays a fundamental role.

The study was carried out at a test area in central Scotland, situated within the Queen Elizabeth II Forest Park (lat. 56°10' N, long. 4° 23' W). Six plots containing three different species (Norway spruce, European larch and Sessile oak), characterized by their different light regimes, were established within the area for the measurement of forest variables using a forest inventory approach and hemispherical photography. The remote sensing data available for the study consisted of Landsat ETM+ imagery, a small footprint multi-return lidar dataset over the study area, Airborne Thematic Mapper (ATM) data, and aerial photography with same acquisition date as the lidar data.

Landsat ETM+ imagery was used for the spectral characterisation of the species under study and the evaluation of phenological change as a factor to consider for future acquisitions of remotely sensed imagery. Three approaches were used for the discrimination between species: raw data, NDVI, and Principal Component Analysis (PCA). It can be concluded that no single date is ideal for discriminating the species studied (early summer was best) and that a combination of two or three datasets covering their phenological cycles is optimal for the differentiation. Although the approaches used helped to characterize the forest species, especially to the discrimination between spruces, larch and the deciduous oak species, further work is needed in order to define an optimum approach to discriminate between spruce species (e.g. Sitka spruce and Norway spruce) for which spectral responses are very similar. In general, the useful ranges of the indices were small, so a careful and accurate preprocessing of the imagery is highly recommended.

Lidar, ATM, and aerial photographic datasets were analysed for the characterisation of vertical and horizontal forest structure. A slope-based algorithm was developed for the extraction of ground elevation and tree heights from multiple return lidar data, the production of a Digital Terrain Model (DTM) and Digital Surface Model (DSM) of the area under study, and for the comparison of the predicted lidar tree heights with the true tree heights, followed by the building of a Digital Canopy Model (DCM) for the determination of percentage canopy cover and tree crown delineation. Mean height and individual tree heights were estimated for all sample plots. The results

showed that lidar underestimated tree heights by an average of 1.49 m. The standard deviation of the lidar estimates was 3.58 m and the mean standard error was 0.38 m.

This study assessed the utility of an object-oriented approach for deciduous and coniferous crown delineation, based on small-footprint, multiple return lidar data, high resolution ATM imagery, and aerial photography. Special emphasis in the analysis was made in the fusion of aerial photography and lidar data for tree crown detection and classification, as it was expected that the high vertical accuracy of lidar, combined with the high spatial resolution aerial photography would render the best results and would provide the forestry sector with an affordable and accurate means for forest management and planning. Most of the field surveyed trees could be automatically and correctly detected, especially for the spruce and larch plots, but the complexity of the deciduous plots hindered the tree recognition approach, leading to poor crown extent and gap estimations. Indicators of light availability were calculated from the lidar data by calculation of laser hit penetration rates and percentage canopy cover. These results were compared to estimates of canopy openness obtained from hemispherical pictures for the same locations.

Finally, the synergistic benefits of all datasets were evaluated and the forest structural variables determined from remote sensing and hemispherical photography were examined as indicators of light availability for regenerating seedlings.

TABLE OF CONTENTS

LIST OF FIGURES

LIST OF TABLES

LIST OF ACRONYMS

ATM	Airborne Thematic Mapper
CASI	Compact Airborne Spectrographic Imager
CCF	Continuous Cover Forestry
CSIRO	Commonwealth Scientific and Industrial Research Organization
COST-method	Cosine-T method
Dbh	Diameter at breast height
DN	Digital Number
DOS	Dark Object Subtraction
GESAVI	Generalised Soil Adjusted vegetation Index
GPS	Global Positioning System
HYMAP	HyMAP Hyperspectral Scanner
IUFRO	International Union
LAI	Leaf Area Index
Landsat ETM+	Landsat Enhanced Thematic Mapper Plus
MSAVI	Modified Soil Adjusted Vegetation Index
MSARVI	Modified Soil and Atmospherically Resistant Vegetation Index
NERC	Natural Environmental Research Council
NDMI	Normalized Difference Moisture Index
NDVI	Normalized Difference Vegetation Index
NPCI	Normalized Pigments Chlorophyll Ratio Index
OSGB	Ordnance Survey Great Britain
PCA	Principal Components Analysis
PIF method	Pseudo Invariant Features method
PRI	Photochemical Reflectance Index

RSA	Regeneration Study Area
RTC	Radiative Transfer Code
SPOT	Satellite Pour l'Observation de la Terre
UK	United Kingdom
UKWAS	United Kingdom Woodland Assurance Standard
UNCED	United Nations Commission on Economic Development

Evaluation of Remote Sensing Methods in Continuous Cover Forestry (CCF)

Chapter 1

Introduction and objectives of the research

1.1 Introduction

Remote sensing techniques have experienced significant development in the last decades, which has brought new opportunities and challenges to the interpretation of environmental processes. In the last years it has become widely and routinely used for environmental and natural resources applications including commercial forestry, which has benefited from new techniques that are improving the availability and accessibility to the forest information (Chen and Cihlar 1996; Jensen *et al.* 1999; Lefsky *et al.* 1999; Verstraete *et al.* 1996; Dymond *et al.* 2002; Hagiwara *et al.* 2004; Hajek 2005). Remote sensing can be expected to be used increasingly to collect needed data, especially related to the monitoring of changes in forest cover, assessing land use and forest land degradation, evaluating the productivity of the land and providing information not only for forest inventory but also for direct inputs into forest management and strategic planning (Howard 1991). With the increasing availability of satellite data remote sensing products are being utilised more widely.

Traditional remote sensing techniques have been successfully used for forestry applications, especially for monitoring of resources and to support land management. Although the status of photography is challenged by continuing innovations in digital imaging technology, aerial photography remains the most practical and widely used means of remote sensing (Campbell 1996). Continued reliance on aerial photography is largely a sign of its superior spatial resolution in comparison to conventional satellite images (e.g. Landsat, Satellite pour l'Observation de la Terre SPOT). However, more sophisticated remote sensing techniques have been shown to provide additional

information overcoming limitations in spectral resolution of aerial photography and limitations in spatial resolution of conventional remote sensors, which represent a barrier to applicational levels and scales. That is the case for hyperspectral data such as that acquired by HYMAP and CASI sensors and Radar and LiDAR data, which have proved to be very useful for the retrieval of forest parameters (Bunting and Lucas 2006; Hyde *et al.* 2006; Schlerf *et al.* 2005; Pulliainen *et al.* 2003; St-Onge and Vepakomma 2004; Yu *et al.* 2004; Hu *et al.* 2000).

Within the context of Continuous Cover Forestry (CCF), a relatively new forest management strategy that has been implemented in several European countries, the usefulness of digital remote sensing techniques lies in their ability to retrieve parameters at sub-stand level and in the assessment of natural regeneration and light regimes. The aim of CCF management is to maintain continuous woodland conditions through time, rather than periodically removing whole crops of trees as clearfelling culture systems do, transforming even-aged plantations to a mixed, uneven-aged woodland. The main advantage of this conversion is the increase in ecological stability (Mason *et al.* 1999; Hale *et al.* 2004). Other positive effects of CCF include (Pommerening and Murphy, 2004): increased horizontal and vertical structure of trees within the stand; reduction of biotic, abiotic and economic risks; and less visual impact compared to clearfelling. But with the diversity in species and age of the trees within the stand, there is also significant increase in canopy complexity for management purposes, for which more detailed and precise data will be needed at individual tree level. This would include information such as breast-height diameters, tree positions, tree heights, in order to quantify spatial forest structure through the calculation of the diversity of tree positions, tree species diversity, and the diversity of tree dimensions (Pommerening 2006). The acquisition of this data is currently carried out through forest inventories which are both very time and cost consuming. Remote sensing technologies offer significant potential and an alternative means to retrieve desired forest canopy variables that could decrease field work effort and be potentially as reliable as conventional methods for forest inventory.

The idea behind CCF is the support of a sustainable forest management system reducing the disturbance of the forest ecosystem to a minimum and encouraging the use of natural methods (Sterba and Ledermann 2006). Natural regeneration, natural pruning and self-thinning are stimulated. There has been increasing interest in the use of natural regeneration in Britain's forest in preference to planting in order to favour more natural approaches to forest management (Mason *et al.* 1999; Hale 2001, Hale *et al.* 2004). While successful natural regeneration can reduce costs and provide environmental benefits, uncertainties such as the variability between and within sites can make it difficult for forest managers to decide when and where to rely on natural regeneration in preference to, or alongside traditional planting methods (Nixon and Worrell, 1999). Moreover, the success of natural regeneration depends greatly upon the light environment as the primary factor in determining the survival and growth of seedlings beneath a forest canopy (Lieffers *et al.* 1999), but there is a significant lack of information on the required understory light regimes for planted species as the methods traditionally used for stand management (clearfelling and restocking) did not need such information.

Thus CCF represents a new challenge not only for the U.K. forestry community but also for remote sensing techniques. New approaches have to be developed in order to consider these two important aspects (regeneration and light environment) for the implementation of the CCF system. Such approach involve the analysis of available techniques and their appropriateness to these issues, for example, if their spectral and spatial resolutions are capable of retrieving the information needed.

In this way, the scope of this research is to evaluate the usefulness of different remote sensing platforms (Landsat TM, LiDAR, ATM) for CCF implementation. Considerable research has already been carried out on the applications of data from each of these platforms to forest management and more generally, to the monitoring of the character of the vegetation at the surface (Hill and Thomson 2005; Ager and Owens 2004; Blaschke et al. 2004; Collins et al. 2004; Basham et al. 1997; Danson and Curram 1993; Brockhaus and Khorram 1992). This includes studies at different scales such as the mapping and

monitoring changes in major ecological regions (Maselli *et al.* 2005; Holmgren and Jonsson 2004; Jiang *et al.* 2004) or more local studies like the analysis of timber volume and tree heights (Watt *et al.* 2004; Means *et al.* 2000). However, there is at the moment a lack of information about the advantages and disadvantages of the use of these techniques towards the CCF management system. The synergy among the techniques has also to be evaluated to gain an understanding about how different sets of data can complement each other, thereby taking full advantage of their characteristics and providing a potentially wider and deeper view of canopy structure.

1.2 Aims and objectives

The overall aim of the project is to investigate the potential, and challenges, in the application of high spatial and spectral resolution remote sensing to forest stands in transition to, and managed under the Continuous Cover Forestry system in the UK. The evaluation of the Landsat ETM+ imagery, ATM imagery, aerial photography, and LiDAR data available for the research, along with the field measurements, will allow the identification of reliable techniques and methods that can be applied at tree and stand level to meet cost-effectively the specific data requirements of CCF. These techniques and methods will be explored on mature even-aged stands, in order to assess their ability for the retrieval of key CCF parameters such as tree height, gaps and crown recognition, and estimates of light environment. The goal is to identify the techniques that directly serve the objectives of CCF and provide information for the mapping and monitoring of the transition of existing forest stands to CCF in a cost-effective manner.

Specific objectives will be:

- To analyse the influence of seasonal changes on the surface reflectance by using Landsat imagery.
- To examine LiDAR data for the determination of forest variables such as tree height.
- To evaluate the application of crown identification methods, using both high-resolution ATM imagery, LiDAR data and aerial photography.

- To evaluate the synergistic benefits of Lidar and high resolution ATM data for forest structure retrieval.
- To examine forest structural variables determined from remote sensing and hemispherical photography as indicators of light environment underneath a canopy.

1.3 Relevance of the research and expected outcomes

Remote sensing offers several advantages with respect to CCF. Evaluation of the transition from traditional forestry methods to a CCF approach demands close monitoring of several ecological parameters. These include tree height, canopy structure, incidence of gaps and light requirements. Since the measurement of these variables by ground survey is time-consuming and expensive, it is likely that remote sensing may offer a less labour intensive and lower cost approach.

The project has great significance since national and international initiatives are encouraging more ecologically sound management practices for commercial forestry. Due to limited British experience in the application of the CCF system and considering that, under the recent UKWAS certification standard (2000; FSC approved), managers are required to "increasingly favour" lower impact silvicultural systems, it is necessary to strengthen the research in this area.

It is therefore argued that remote sensing may prove a cost-effective way to obtain the information that is needed to help with the planning, establishment and monitoring of the CCF system in UK. Landsat products have been increasingly used in forestry for the production of forest thematic maps due to their low cost, high geographic coverage and good resolution. The monitoring of change detection in more sustainable forest practices, such as CCF, is a good example of the type of application that can be achieved using Landsat data. However, the difficulties in calibrating long time series or adjacent images accurately enough to comparable radiometric levels have hampered its application on a day-to-day basis for this purpose. Other uncertainties such as the effect of the

phenological cycles on the signal recorded by the sensor have not been fully explored either. The analysis of the Landsat ETM+ imagery available for this research will allow the investigation of these issues with respect to the most common forest species in Britain and the determination of the most suitable acquisition dates where the phenological effects (if they exist) can be clearly distinguished.

On the other hand, because CCF implies greater diversity of both tree species and age, the identification of reliable methods for the extraction and monitoring of tree height is vital. The use of natural regeneration as a preferred restocking method also demands the identification of techniques and methods that can provide information about light requirements and crown and gap detection. The analysis of LiDAR, multispectral and high resolution optical data in this study will allow the evaluation of the individual/combined datasets that provide those parameters for CCF management information. The estimation of the operational cost and feasibility of the implementation of each technique will also allow the evaluation of their practical use.

Key outcomes will be:

- Improved understanding of the applications of high spatial resolution remote sensing for providing forest structure information.
- Improved understanding of the influence of management practices on regeneration dynamics.
- Development of field-validated procedures for the retrieval of forest structure parameters in forest regions in transition to a Continuous Cover Forestry system.
- Evaluation of the synergistic value of ATM and Lidar data for forest structural parameter retrieval.

1.4 Thesis Outline

Chapter two comprises an introduction to Continuous Cover Forestry, describing its history, advantages, disadvantages, and topics within the CCF debate. This chapter also includes the description of the test site and the species studied and reports the results of fieldwork undertaken in six contrasting plots in the study area.

Chapter three will present the bibliographic review, methodology and the results obtained from the correction and analysis of Landsat imagery in connection with seasonal changes and how they affect the reflectance surface for the retrieval of spectral signatures of the species under study. Through this analysis it is expected to determine the best time of the year and best spectral resolution for the retrieval of forest structure information.

Chapter four consists of a bibliographic review, methodology and results obtained from the analysis of the LiDAR datasets. The outcomes of the research will demonstrate that this technique is suitable for the modelling of the forest canopy and that in combination with aerial photography, will allow more objectives of the Continuous Cover Forestry to be addressed.

Chapter five will focus on the analysis of aerial photography, LiDAR and the Airborne Thematic Mapper dataset for tree crown delineation.

Chapter six describes the results achieved from the analysis of the hemispherical photography in relation to canopy openness and percent direct transmitted light, essential factors for the understanding of the natural regeneration objective.

Chapter seven will analyse the synergy among Landsat, Lidar, ATM, hemispherical photography, and ground information and its usefulness for the Continuous Cover Forestry system approach.

Chapter 2

Introduction to the Continuous Cover Forestry (CCF) system and description of the study site

2.1 Introduction

The aim of this chapter is to provide a more detailed insight into the Continuous Cover Forestry system, carrying out a bibliographical review at first, followed by the definition of the term and the description of the concepts related to the CCF system. This section also introduces the study area for the project and outlines the key characteristics of the species and plots chosen for the analysis and studied during the project.

Continuous Cover Forestry (CCF) is an approach to forest management that envisions shifts in emphasis from sustainable yield to sustainable forests in the broadest sense. The system requires the substitution of the mechanistic and systematic silvicultural methods used until now, which have produced reasonable economic profits but also have created concerns in relation to ecology, biodiversity and aesthetics (Pommerening 2006a), for others characterized by the introduction of several species of different ages within the stand and the use of natural regeneration as the main restocking method. There has been an increasing interest in the idea of diverse forest structure for the potential it has to meet wider sustainability requirements.

In concept and practice, CCF is not entirely new, having long-established precedents. The formal history of CCF or uneven-aged silviculture began in Europe in the middle of the 19th century. In 1886 the German professor Karl Gayer emphasized the advantages of uneven-aged forests and in 1913 his colleague Alfred Möller, influenced by several writers, and by impressions gained in German managed forests and in natural forests in

the Amazon and North America, conceptualized the idea of "dauerwald" (continuous forestry) (Schabel and Pecore 1997). Möller published a book in 1922 that unleashed a storm in the forest establishment, and which precipitated a flood of other publications and heated discussions. However, there was a decline in interest in CCF following Möller's death (Pommerening and Murphy 2004).

The debate on CCF was revived in the 1980s in relation to the discussions on impacts of acid rain, forest decline, restoration and certification (Brundtland Report 1987). It was in 1992 that interest in CCF acquired greater relevance due to the discussion in the United Nations Commission on Economic Development (UNCED) summit at Rio de Janeiro, when the terms and scope of sustainable forest management were redefined and it was suggested that they become an integral part of modern forest practices worldwide. This new silvicultural approach has been welcomed in Britain and shows its strongest commitment in the Welsh Woodland Strategy which aims for the 50 per cent of public forests to be transformed to CCF by 2020, where feasible (Mason *et al.* 2004).

According to Malcolm *et al.* (2001), there are about 1.5 Mha of conifer high forest in Great Britain composed almost entirely of even-aged plantations of non-native species established since 1900, and of which around 500-750 kha are established on sites sufficiently windfirm to be managed under CCF. The task of transforming these even-aged stands into ones that comprise several species and different ages implies the adoption of alternative silvicultural methods referred to as "lower impact" (UKWAS 2000). CCF does not describe a set management system, rather a range of management options that can reflect the characteristics and management requirements of a particular stand (Lincoln 2005). These options include "group selection, shelterwood or underplanting, small coupe felling systems, minimum intervention and single tree selection systems" (Mason 2001). The description of these management systems and their local variants is the subject of numerous forestry books (Young and Giese 1990; Hibberd 1991; Hart 1995; Barnes 1998). Table 2.1 outlines the main characteristics of the traditional silvicultural systems used in the UK.

System	Description	Microclimatic criteria	Typical area of canopy openings (in ha)
• Clearcut	Removes part or all of a stand, or several stands in one cut	Open conditions dominate over canopy effects	> 0.5 or > 1.0 (depending on canopy tree height) to > 100
• Seedtree	Retains a small number of well spaced seed-producing trees (15-50/ha) on a cleared area for a short time	Open conditions dominate over canopy effects	> 0.5 to > 0.1 after seed tree removal
• Shelterwood	System of successive regeneration fellings that retains a forest cover over all or part of the stand until regeneration phase is completed	Protective cover during regeneration phase	See below
- Uniform	Opening a canopy even; young trees more or less even aged	Protective cover during a brief regeneration period, then full open conditions	< 0.01 to 0.1
- Group	Opening a canopy by scattered gaps; young trees more or less even aged	Gaps expanded successively to full open conditions over 20-40 yr	< 0.01 to 0.1 initially; enlarged over time
- Irregular	Opening of canopy irregular and gradual; young trees more or less uneven-aged	Canopy openings expanded successively over more than 50 yr; some mature trees may be retained at all times	< 0.01 to 0.1 initially; enlarged over time
- Strip or wedge	Opening of canopy in well-defined strips or wedges; regeneration even-aged in advancing strips or spanding wedges	Some canopy shading during regeneration, then full open conditions	Depends on length of strip or wedge and canopy tree height; typically <2 times stand height
• Selection	Forest canopy is more or less retained over all of stand area	Canopy effects dominate over open conditions	
- Single tree	Trees remove individually across entire stand	Continuous forest cover	< 0.01
- Group	Trees periodically removed in small groups	Continuous forest cover	0.01 to 0.1
• Coppice	Trees originating by vegetative means	Open conditions dominate over canopy effects	

Table 2.1: Traditional silvicultural systems in the UK (Coates 1997)

These European silvicultural methods, mainly selection and shelterwood systems, were introduced to the colonies at the beginning of the 20th century with the opposite aim of CCF, that is, to simplify the complex composition of the forests by reducing the number of species and to convert it into as regular a stand as possible for easier treatment and management. The problems of the implementation of these methods in Cameroon and the assessment of the usefulness of alternative methods was analysed by Ngeh (1989). The problems were mainly related to the lack of natural regeneration and strong competition with unwanted species. This led to the introduction of alternative systems in which adequate light conditions are provided by the progressive removal of the existing forest cover, either manually or by machinery, to encourage the survival and growth of the useful species. Ngeh study is an example of modification of silvicultural methods to adapt to particular characteristics and requirements of the management. However, the conversion to CCF is a large and long term project which is hampered by a lack of experience of irregular systems in Britain. Furthermore, Price and Price (2006) state that to date there is a dearth of information on the economic efficiency of irregular stands and on the transformation process from regular stands in a British context.

However, the exploration of the possibilities for the transformation to CCF has begun with the establishment of trials and research. For instance, Malcolm *et al.* (2001) analysed diverse factors influencing the success of the transformation process, pointing out that the main problem in Britain is related to the species that, with exception of Scots pine which is native of northern Scotland, have been introduced and planted in afforestation schemes over the last century. Thus, these stands are in their first or second rotation, established on sites that may not have carried forest in the recent past, that is, artificial ecosystems for which there are few natural models.

The role which remote sensing techniques could play in the implementation of CCF in Britain is manifold. The more complex stand structure that characterises this approach creates a need for more within-stand information and a more continuous level of monitoring.

It has been demonstrated that remote sensing can provide more rapid and frequent data acquisition, faster and automated processing to deliver information, maps and information delivered at a much greater sampling intensity, and maps of forest attributes at below the sub-compartment level (Malthus 2002).

The implementation of CCF will require information on the following general aspects: site conditions, stock quality, species diversity, light climate and regeneration, continuous monitoring, and aesthetic factors.

The specific CCF information needs that can be explored using remote sensing data available for this research (Landsat ETM+, ATM, and Lidar) are:

- Characterisation of seasonal variations in spectral signatures of forest species.
- Characterisation of within-stand vertical structure: measurement of tree heights, within-stand height variability and its spatial distribution, and derivative parameters (diameter at breast height, crown size, crown depth, etc.).
- Characterisation of within-stand horizontal structure: quantification and spatial distribution of gaps.
- Monitoring of stands' variability (landscape scale).

2.2 The CCF system

There exist many different terms to define and describe Continuous Cover Forestry. According to the International Union of Forest Research Organisations (IUFRO) Multilingual Forest Terminology Database, the term describes a highly structured forest ecosystem managed to maintain continuous tree cover over the total forest area (IUFRO 2002).

Mason *et al.* (1999) state "continuous cover is defined as the use of silvicultural systems whereby the forest canopy is maintained at one or more levels without clear felling".

There exist also some terms associated with the system such as "continuity of forest cover", "permanent forest", "low impact silviculture", "ecological silviculture", "holistic forestry", etc., but all of them stress the idea of the continuity of woodland conditions over time which do not imply a lack of management but emphasize the need to avoid clearfelling over large areas. Within this broad concept a range of silvicultural systems are possible (Pommerening and Murphy 2004).

CCF has a long history in Europe and it is known that the system or forms of it have been practised long ago in parts of Switzerland, France, Germany, Austria and Slovenia (Pommerening and Murphy 2004). The success of the German forestry is recognised worldwide. The development of a sustainable forest production on a scientific basis began in Germany nearly 300 years ago. Its success lies in the adaptability of the silvicultural methods to the sites and native species and in the utilization of the forest in other ways, for instance for the increasing of wood quality in stands with low volume production, or to make use of other forest products as well as the wood (Wild and Weidenbach 1998).

Until now, yield timber management principles have guided forest management practices in the UK. Thus, experience in the management of forest under CCF is far more limited in Great Britain. In 1952 Professor M. L. Anderson (Edinburgh University) began a conversion trial of 30 year old conifer stand with the aim to create a mixed forest of irregular structure (Anderson plots) (Hart 1995). It has taken 30 to 40 years for the diversity of the structure in these plots to become apparent and for it to be possible to start to judge the success of this trial (Mason *et al.* 1999). During the 1990s some factors such as the Rio-Helsinki process, the requirements of certification and the international movement in favour of a more natural forest management, influenced a rethinking about the appropriate silvicultural systems for plantation forests in Britain (Mason *et al.* 2005). Given that transformation to irregular forest structures can take 50-100 years, it should be noted that the implementation of CCF, among others, requires both long time and great patience in order to achieve its objectives.

Figure 2.1 describes the characteristic structure of a stand managed under CCF.

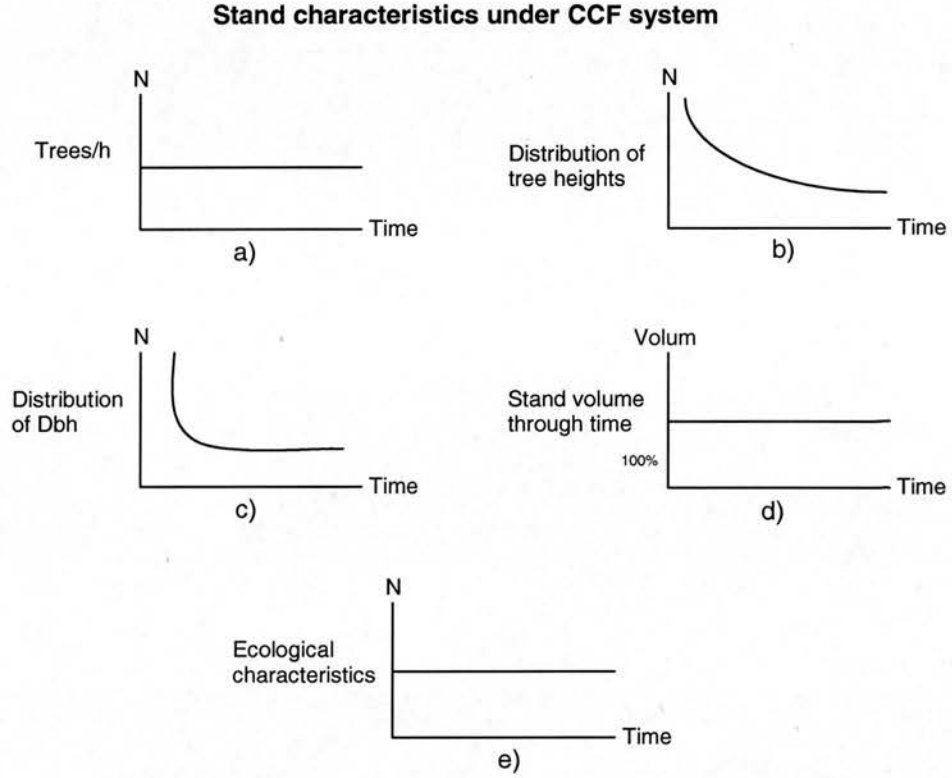

Figure 2.1: Structure and evolving characteristics of stands under CCF system (adapted from Oesten and Roeder 2001).

The figures show the ideal behaviour of some relationships through time: a) the number of trees per area unit is kept constant through time; b) there will be a majority of small trees (seedlings and saplings) after a complete transition from other systems is achieved; c) the distribution of diameter at breast height (Dbh) will also represent the majority of small trees; d) stand volume will be approximately the same through time; e) under successful management there will be no ecological disturbances apart from natural events or illnesses.

There are many possible advantages in the application of CCF (Continuous Cover Forestry Group 1994) which include:

- Less visual impact than clearfelling.
- Increased within-stand structural and species diversity.
- Less disturbance of forest ecosystem and greater shelter for regenerating seedlings.
- Harvesting operations dispersed across the forest and through time, higher average tree size, and greater output of saw logs.

However, CCF also implies some disadvantages:

- More complex stand management requiring skilled personnel.
- Yield prediction and regulation is more difficult.
- Greater monitoring is required.
- Greater harvesting costs because of small dispersed felling sites.

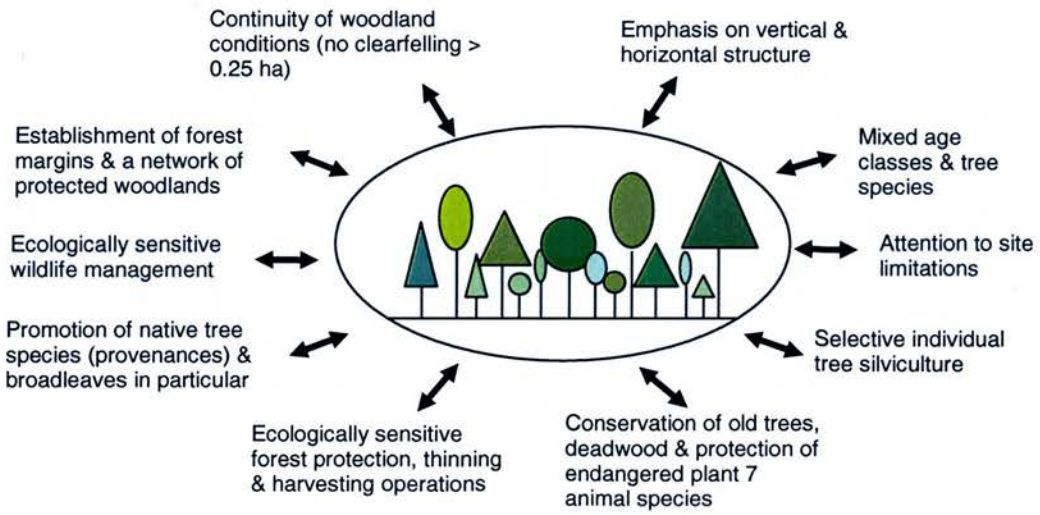

Figure 2.2: Main components of the contemporary international continuous cover forestry debate (Pommenering and Murphy 2004).

CCF is not just a silvicultural method but an approach to forest management for multipurpose objectives that encompasses diverse aspects as shown in figure 2.2.

Pommerening and Murphy (2004) highlighted the main components of the continuous cover forestry debate:

- Continuity of woodland conditions: this is the most important part of the CCF concept. Continuity of woodland conditions is a requirement for the survival of some species and is also an important feature of protection forests, securing and stabilizing watersheds, mountain slopes and coastlands, and for recreational purposes. A millenary experience about the use of techniques to guarantee the continuity and diversity and make use of the forests' multipurpose benefits is seen in the Maya culture. Increasingly evidence is being uncovered which illustrates how the Mayas agro-silvicultural techniques made use of succesional stages of natural forest growth and regrowth. Forest management consisted of various activities to select, cultivate, protect and introduce trees in shifting cultivation plots or follow land coppicing of numerous species (by cutting down to c. 50 cm above the ground and encouraging multi-bole regrowth), "plantations" of favoured species within the natural forest and deliberate plantings around houses and urban centres, as living fences, and along trails (Furley 1998).

Continuity of the woodland implies also some considerations about light regime beneath the forest. As clearfelling is necessary to open up the canopy and allow the target species to grow, there is still a lack of agreement about the size of clearfell allowed and whether it should take tree species and site types into consideration. Regarding the clearfell, some studies in Britain (Hale 2001, Hale 2003) seem to indicate that the actual gap fraction levels beneath Sitka spruce (between 5 and 10%) do not provide the appropriate light regime environment for natural regeneration to occur. Because of the relative shade intolerance of the major tree species and the lower irradiance and greater cloudiness in Britain, appropriate gap sizes for regeneration may be quite large (Malcolm *et al.* 2001). Group felling is often seen as an appropriate way of transforming stand structure in northern temperate forest as the removal of individual trees do not provide sufficient opening of canopy for less shade tolerant species (Price and Price 2006). This result is supported by findings by Mason et al. (2005) about the survival of different seedlings species after planting in a Sitka spruce spacing trial

with different light environments, suggesting that heavy thinning should be employed to promote growth of advance regeneration.

- Emphasis on vertical and horizontal structure: achieving a varied structure of vertical and horizontal elements provides some advantages: establishment and tending costs decrease, greater biodiversity and more attractive view.
- Mixed age classes and tree species: mixed forest provide a wider range of size classes and timber products, improves soil composition, and provide more habitats.

The issue of mixed species stands, whether of introduced and native species or of introduced species alone, is new territory for British silviculture, therefore any transformation must be considered to be on a trial basis and eventual species compositions of these forests is still to be determined (Malcolm *et al.* 2001).

- Attention to site limitations: tree species grown should be dependent on the site. Since the interaction between thinning, stand structure and wind risk will largely determine the extent of use of CCF in upland Britain, research is conducted to investigate wind forces upon trees in irregular stands (Mason et al. 2005). Successful transformations are likely to occur on windfirm sites with freely-draining soils and where there are strong aesthetic, conservation or heritage reasons for adopting a silvicultural syatem based on gap regeneration (Malcolm *et al.* 2001).
- Selective individual tree silviculture: trees are individually marked, thinned and harvested in a compromise between silvicultural, economical and conservation needs.
- Conservation of old trees, deadwood and protection of rare and endangered plant and animal species: all these elements contribute to the biodiversity aspects and must be acknowledge in the management.
- Promotion of native tree species/provenances and broadleaves: this aims for the restoration of the forest to native species, which are better adapted to local conditions, and the removal of invasive non-native tree species.

- Ecologically sensitive forest protection, thinning and harvesting operations: the disturbance of forest has to be reduced to a minimum by carrying out only limited forest protection and promoting biological methods.
- The establishment of forest margins and a network of protected forests: the forest margins will act as transition zones between the open landscape and woodlands.

CCF aims to create and maintain an ecologically healthy, productive, profitable and aesthetically pleasing forest. This means that the forest is perceived in a more holistic way, trying to balance the economic benefits with the interests of the community regarding ecology, landscape and recreation. Ideally, this type of forest can be harvested lightly and frequently, removing only those trees no longer producing timber value at an acceptable rate of return, and leaving a mature looking forest, or at least a forest that doesn't look heavily logged (Schabel and Pecore 1997). To date, the profitability of other forest products is hardly mentioned. These products consist of forest plant materials that may include fungi, mosses, lichens, herbs, vines, shrubs, trees, or plant parts that are harvested, including the roots, tubers, leaves, bark, twigs, branches, fruit, sap, and resin, in addition to the wood. For many temperate forests, little more is known about non timber forest products (NTFP) than basic taxonomy and the geographic distribution. There is a general lack of knowledge about the reproductive biology, inventories, and sustainable yields of these resources. Furthermore, in industrialized countries, NTFP use is often viewed as a marginal activity, though in reality the trade of these products provide significant economic benefits to many rural households and communities (Chamberlain *et al.* 2000).

Experiences in tropical forests have shown that the financial gain from NTFP could be as good as the one generated by the wood trade. Peters *et al.* (1989) carried out a valuation of an Amazonian forest. The results of their study clearly demonstrate the importance of non-wood forest products. Compared to timber, the benefits have not been recognised because non-wood resources are collected and sold in local markets.

Some of the criticism for the embrace of a NTFP culture is related to the risk involved in the developing of a "new" product and its possibly limited market. This contrasts with the results of the Forestry Commission's 2005 GB Survey of Public Opinion of Forestry that were published in June 2005. Of respondents who said that they had visited woodlands in the last few years, 27% said that they had gathered some kind of woodland product: 13% had gathered material for food or drink, 13% had gathered decorative, floral or craft materials, 9% had gathered "items for seasonal, cultural or religious use" (e.g. holly, ivy, hazel), and just 2% gathered medicinal or dietary supplements. There is a clear window of opportunities and many local communities and organisations are already working with the overall goal to increase knowledge and stimulate wider use and appreciation of NTFPs (http://www.reforestingscotland.org/projects/rural_alternatives.php)

During the transition from even-aged to CCF some economic issues have to be addressed (Hanewinkel 2001, Price and Price 2006). The harvest of quality timber may need to be deferred, administrative and management procedures modified and harvesting technology adjusted to the new realities. One advantage is the production of large diameter, high quality sawlogs. One of the disadvantages is the greater harvesting costs because of small dispersed felling sites (Mason *et al.* 1999) and that the stand will require a regular network of racks linked to extraction roads so that harvesting machinery does not damage regenerating seedlings (Mason and Kerr 2001). Another problem is the demise of skilled harvesting thinning teams equipped with purpose-built machines for both motor manual and fully mechanised work (Yorke 2001).

The object of the transformation is to achieve the heterogeneous composition of the forest by lengthening the regeneration period, breaking up the existing structure, and using systems other than extensive clearcutting. The process must begin early and at not later than 40 years in conifer stands and 60 to 80 years in broadleaved stands (Hart 1995, Malcolm *et al.* 2001).

To recreate a semblance of the diversity of fauna and flora, which may have been greatly altered in the traditional age-class forest, reintroductions of non-commercial, "serving" species may be necessary. To achieve and eventually maintain a mixed forest, frequent silvicultural interventions through-out the forest are called for (ranging from a gap created by felling one tree up to a maximum of 0.25 ha), always in ways which eliminate the "lesser" tree to eventually provide permanence in stand, site and timber quality (Bode 1992). Figure 2.3 depicts the phases in the transition from even-aged forests to CCF, according to Oesten and Roeder (2001).

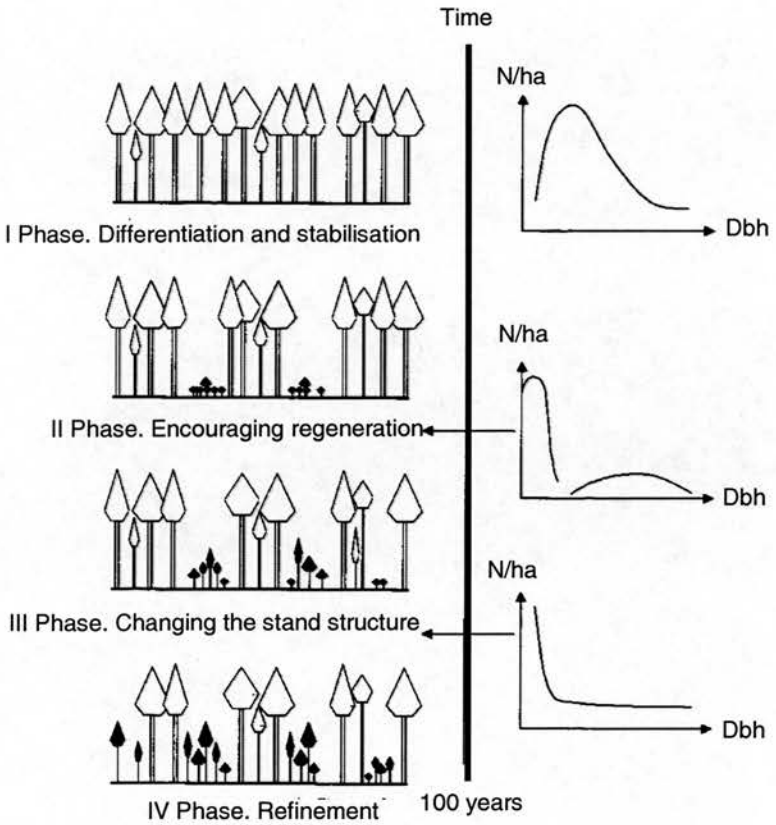

Figure 2.3: Idealised scheme of the transition of the even-aged stands to Continuous Cover Forestry. The graph shows how stand structure and Dbh change through time (Oesten and Roeder 2001).

This analysis, considering a time scale of 100 years, is supported by more recent studies by Sterba and Ledermann (2006) who conducted a study on two forest management

districts in Austria, natural regeneration and single tree selection, with the aim to model forests in transition from even-aged to uneven-aged management. They found that after a simulated 100 years, species diversity, structural diversity and between-stand variation was enhanced in the natural regeneration system, but the equilibrium of harvests and growth was reached in the single tree selection system after 80 years.

2.3 Emphasis on natural regeneration

CCF relies greatly on natural regeneration as the preferred method of restocking stands. The term "natural regeneration" refers to the natural process by which plants replace or re-establish themselves by reproduction from self-sown seeds or by vegetative recovery (sprouting from stumps, lignotubers, rhizomes or roots) (Young and Giese 1990). In some instances seed may not be available at the site immediately but may be carried in from nearby sources by water, wind or wildlife.

The problems affecting the controlling factors for natural regeneration are (Petrie 1999):

- Seed supply: no seed, or seed of poor viability. This may be due to the absence of fertile plants with viable seed; seed harvesting by ants and predation by other insects, birds and mammals; lack of pollinators or seasonal variations.
- Soil conditions: seed germination and establishment may be impaired by "unhealthy" soil conditions. Such conditions might include: a lack of suitable sites for germination as a result of soil compaction, loss of top soil, poor drainage or excess of soil moisture, an unstable site, or unfavourable soil chemistry.
- Competition: competition from the same or other plant species may prevent successful seedling recruitment. This may be due to weeds, parent plant allelopathy (chemical inhibition) or fungal attack.
- Predation of young plants: seedlings may be destroyed by predators such as insects and other invertebrates, stock or wildlife. Seedlings and young stems may lack natural deterrents (toxic or unpalatable chemicals, hard leaves or leaf

structures such as torns and hairs) and so are relatively defenceless compared to mature plants.

- Natural hazards and controls: there may be natural climatic, biological and physical constraints upon natural regeneration. These include fire, flood, wind, drought, temperature extremes (e.g. frosts), and time of year and light conditions.

The most common factors of failure of regeneration in the plots under study are browsing and competition. However, anecdotal evidence indicates that the level of browsing of coniferous natural regeneration is rarely significant except where the red deer population is totally out of control, or where there is negligible alternative browse vegetation (Yorke 2001). The absence or failure of regeneration due to vegetation competition is commonly due to excessive opening up of the woodland canopy in "expectation" of regeneration. The result is often an influx of competing vegetation particularly on the more fertile site types. If the layer of invasive species is dense, as it often is, invaders may largely or entirely preclude the establishment of the regeneration of desired species (Young and Giese 1990).

The successful use of natural regeneration depends upon the manipulation of the stand microclimate to ensure satisfactory germination and growth of seedlings. One of the factors determining the survival and growth of seedlings beneath a forest canopy is the light environment (Lieffers *et al.* 1999). Thus, to better understand mechanisms involved in understorey tree regeneration it is important to know how forest canopy and light interact and which are the light requirements of the target species.

2.4 Regeneration and light

The light environment beneath a forest canopy is heterogeneous, varying both spatially and temporally (Gay *et al.* 1971 in Hale 2001). Even in a relatively uniform stand with a relatively dense overstorey, there is significant spatial variation in light transmitted to the understorey (Lieffers *et al.* 1999). The effect of the forest itself in intercepting radiation is

obvious. Only a small percentage of the incident sunlight reaches the floor of a dense forest (Barnes *et al.* 1998).

A hierarchy of factors determines the microclimate experienced by any organism within a forest. The prevailing climate is modified first by local weather conditions and then by the vegetation, mainly the upper canopy. Crucially, the structure of the canopy controls the quantity, quality, spatial and temporal distribution of light (Jennings *et al.* 1999). Because light is often the most limiting resource for growth of understorey seedlings and saplings (Ricard *et al.* 2003), light availability in the understorey is frequently associated with regeneration process and the long-term survival of forest tree species (Mcllure *et al.* 2000, Woods 2000). The growth and survival of understorey trees is closely dependent on their ability both to acclimate to sudden increases in irradiance caused by a break in the canopy and to tolerate low irradiances for lengthy periods until a canopy gap occurs (Delagrange *et al.* 2004).

Most of the studies have concentrated solely on the ability of trees to grow in shade, and in particular on the concept of shade tolerance (Messier *et al.* 1999). The response of a particular species to light may be referred to as its shade tolerance. Shade-tolerant species are characterised by more efficient net assimilation at low light levels, partly as result of morphological and physiological acclimation responses including reduced respiration rates (Malcolm *et al.* 2001). Shade-intolerant species are unable to maintain a positive photosynthesis/respiration balance at low-light levels and cannot survive. On the other hand, shade-intolerant species tend to respond better to high-light conditions.

Findings indicate that shade-tolerant species exhibit greater changes in crown morphology along a light gradient than do the more shade intolerant species (Barnes *et al.* 1998). These morphological changes are of ecological importance in understanding the capacity of a given species to become adjusted to shaded conditions and the reaction of such a plant when suddenly released to the light, following windstorm or by cutting of the overstorey. When logging occurs, there is an immediate and dramatic impact on saplings

and seedlings: they undergo a change in their light environment and microclimate. These changes alter the competitive relations in the stand, as each species has its own capacity to respond to a change in resource availability. Thus some species are favoured, others discriminated against, and the future structure and species composition of the stand may not be the same as the preceding one (Canell and Grace 1993).

Numerous studies have stated that canopy gaps are necessary for many tree species to attain canopy status (e.g. Canham 1989, Poulson and Platt 1989, Runkle *et al.* 1995 in Yoshida *et al.* 1998). The modelling of the transmission of solar radiation through a forest canopy has proven challenging owing to the highly variable nature of the gaps within and between tree crowns, particularly in discontinuous canopies (Hardy *et al.* 2004). Canopy gaps create a range of light conditions within and around the gap opening depending of the sun angle, tree height, and sky condition (Lieffers *et al.* 1999). Like canopy gaps created by natural tree death or windthrow, gaps are also generated by silvicultural systems which remove dominant trees (Coates and Burton 1997). Large gaps in the canopy permit long periods of uninterrupted transmission of direct-beam light to the understorey. As canopy gaps are regarded as important factors in forest dynamics, considerable research has been dedicated to the methods to define and estimate gap sizes (Ferreira de Lima 2005).

The prediction of light levels under a canopy gap is thus important for evaluating forest management practices which attempt to create an artificial canopy gap in order to facilitate regeneration (Yoshida *et al.* 1997). While managers have no control of above-canopy light, they can control the light levels in the understorey by controlling the amount, position, and type of vegetation that absorbs the incoming light. It will be desirable to match the light transmission to the understory with the light requirements for growth of target species. Messier *et al.* (1999) have developed a concept that relates the maximum sustainable height of surviving understorey trees to gap sizes for a number of boreal species.

The literature review carried out in this chapter has proved the important role of gaps for the ecology of natural regeneration, which as mentioned before, is considered the main method for restocking under CCF management. An understanding of the role of small-scale disturbance in forest ecosystem can help foresters to develop cutting prescriptions that maintain functional mature or old-growth conditions and lead to the achievement of timber production objectives without compromising ecosystem management principles. The potential of remote sensing techniques for gap detection and quantification was explored in this work and will be presented in Chapter 5.

2.5 Site description

The study site used for this project is situated within the Queen Elizabeth II Forest Park, a series of extensive tracts of forest cover in the greater Trossachs in central Scotland (figure 2.4). The entire forest park covers 50,000 acres consisting of a mixture of commercial forest, semi-natural and ancient woodlands and open space, managed by Forest Enterprise. It forms a significant part of the Loch Lomond and Trossachs National Park, the first national park in Scotland, established in July 2002. As well as supporting commercial forestry, the region supports a rich variety of animal and non-commercial forest plant species and is an important region for recreation.

The QEII Forest Park lies in the Central Lowlands, a low-lying belt of fertile valleys with an average elevation of 150 m (500 ft). Rich soils and most of Scotland's coal deposits are found in the Lowlands. This region, which comprises just one-tenth of Scotland's surface area, is home to Scotland's leading industries and cities and the majority of the country's population.

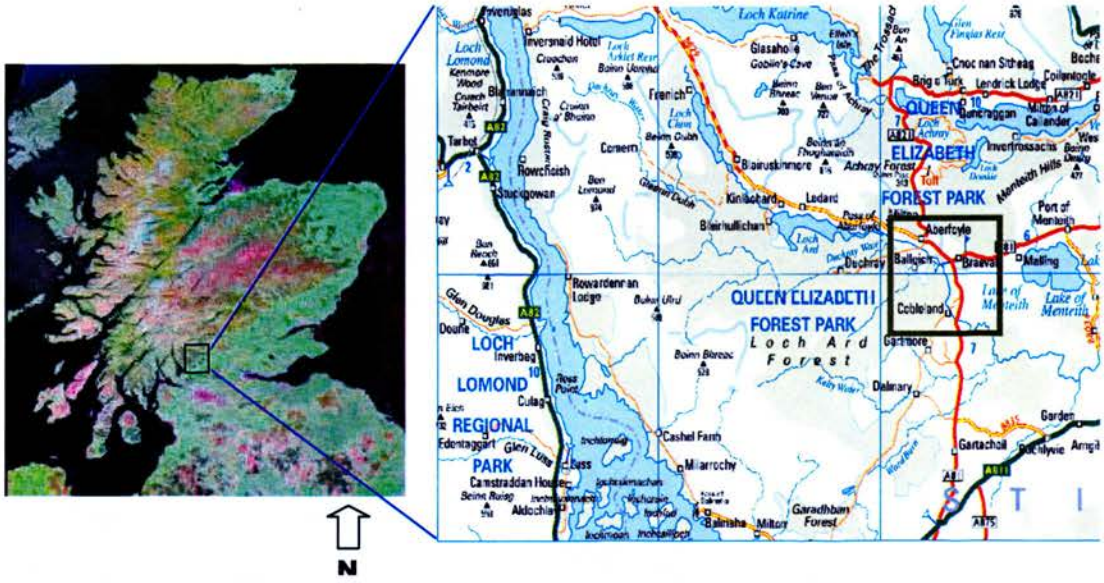

Figure 2.4: Satellite imagery and map showing the study area (Digital map data Bartholomew © 1:100000)

Specific blocks of interest within the park are located within the Achray and Loch Ard Forest Districts surrounding Aberfoyle village (approximate coordinates 56°10'27"N and 4°22'39"W). A Regeneration Study Area (RSA), comprising over 200 ha, was established in 1998 in the Achray Forest District with the purpose of management under the Continuous Cover Forestry system. The objectives of the RSA are to provide information on the effect of different canopy manipulations upon stand microclimates, in particular light regimes, and to determine the interaction between canopy manipulations and stand development with an emphasis on natural regeneration. Thus the plots serve as a means of gaining and transferring experience about alternative silvicultural practices.

2.5.1 Field Sites

For the purposes of this remote sensing study, six plots were established within the area (figure 2.5), to measure forest variables using a forest inventory approach as well as for hemispherical photography.

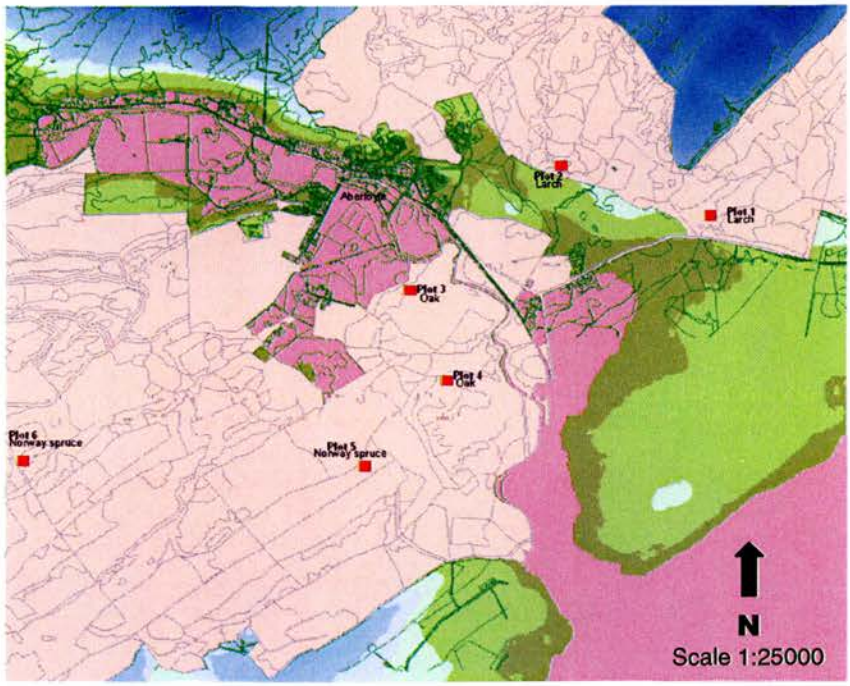

Figure 2.5: Location of plots within stand compartments (adapted from Forestry Commission Achray Database)

The candidate sites were personally visited during a pilot field reconnaissance including an assessment of disturbance, and also to verify that every plot appeared clearly on the aerial photography. Two plots per specie were selected to have replicas of the information for validating purposes. The plots chosen were as homogeneous as possible, to ensure minimum spectral variance of pixels within sites, but also with the maximum contrast possible between sites, in order to achieve the ideal case for the analysis of species reflectance for the Landsat data. The selection of even-aged, single species plots responds to the need for establishing ground truth plots that provide information that can be compared to the remote sensing results from satellite as well as airborne data. This is regarded as a first step offering base line data, necessary before the methods can be extrapolated to mixed age and multi-species treats. In any case, the selection of more diverse plots both in species and age was not practical owing to the lack of such stands on the three species analysed in an area small enough that could have been surveyed in the limited time available for this study. The complexity of stand characteristics that have to

be considered for image processing and model development would have made the study of diverse species excessively complicated at this stage in the research.

The size of the plots (50 x 50m) was chosen to be large enough to allow their location on the medium resolution Landsat ETM+ imagery (30m), and small enough to avoid unaffordable, intensive fieldwork. Six plots corresponding to three of the species (European larch, Sessile oak, and Norway spruce) were marked within the stands and positioned using GPS. Two plots corresponding to the Sitka spruce species were generated from the Achray Forest Database (Forestry Commission). See also Chapter Three, Section 3.5.2, page 75 for further explanation. The sites are also representative of three species with different light regimes. These species were especially chosen because of their differences of shade tolerance, so in this way is possible to establish comparisons regarding light conditions and distribution of gaps as one of the most important factors influencing stand microclimate. The plots also differ in density and age and were selected in locations with minimum disturbance but close enough to the access roads. Differences in density and small variations in topography allowed the assessment of the effect of these factors especially on the LiDAR data.

2.6 Field sampling strategy

Once the sites were visited and the experimental plots chosen, they were marked on the ground using meter tapes, sticks and compass to orientate them to the North. These were afterwards precisely located using Global Positioning System (GPS) Trimble Pro XL dual frequency receiver. Measurements were post-processed for ephemeredes to correct for satellite positions obtained at sub-meter accuracies. Within each 50x50 m plots, an inventory of the most important forest structural attributes was carried out: tree-counting, tree height and Dbh (diameter at breast height). Tree height was one of the most important variables measured, as it is critical for the accuracy assessment of the LiDAR-derived Digital Canopy Model. In plots of low density (e.g. European larch) the height of all trees within the plot was measured (40 trees). For all other plots sample size was

extracted from the tables developed by Snedecor that relate two measures of variation, range and standard deviation, giving the expected value of their ratio for a given sample size (http://forestry.oxfordjournals.org/cgi/reprint/25/1/66.pdf). According to this method, a sample size of 20 trees gives an approximate standard deviation of ±3.08 m that is within the range expected for the even-aged trees in the sample plots. However, sample size was increased to 25 in order to have as much data as possible for comparisons with LiDAR estimates. Other structural measurements were taken in order to have a complete inventory of the plots under study as a baseline for future research. These measurements included: identification of dead/alive trees, identification and marking of forked trees, dominance, and crown diameter measurements of the 25 biggest trees. Top height was considered as the height of the tree with largest dbh. This parameter was used for the comparison of ground to LiDAR heights (see Chapter 4, Section, page).

Plots 1 and 2 are located in the RSA area. Plot 1 is located within a pure stand of European larch (*Larix decidua* P. Mill.) and Plot 2 within a mixed stand of European larch (*Larix decidua* P. Mill.) and Douglas fir (*Pseudotsuga menziesi*). Plots 3 and 4 are located in small hills known as Doon Hill and Fairy Knowe, respectively, within Sessile oak (*Quercus petraea*) stands of about 130 years old. Analysis of grow rates indicates a steady reduction in growth since 1907. A thinning operation was completed in winter 2001 which opened gaps in the canopy and thinned the matrix. Plots 5 and 6 are located within Norway spruce (*Picea abies* (L.) Karst) stands.

The measurement of individual parameters was undertaken for the six plots. A total of 807 trees were labelled and their Dbh measured with a metric tape. The height was measured using a hypsometer model Vertex II; the crown diameter was measured with metric tape along the two perpendicular axes. Field work for forest inventory was carried out throughout March 2003. Acquisition of hemispherical pictures was performed during the first week of May 2003. The Natural Environmental Research Council (NERC) also overflew these field sites in August 2003, where ATM data was collected. Lidar and aerial photography were acquired by NERC in September 2002.

The methodology used for the analysis of each data set will be explained in following chapters. The key characteristics and features of each plot are outlined..

2.7 Description of the plots

- **Plot1**

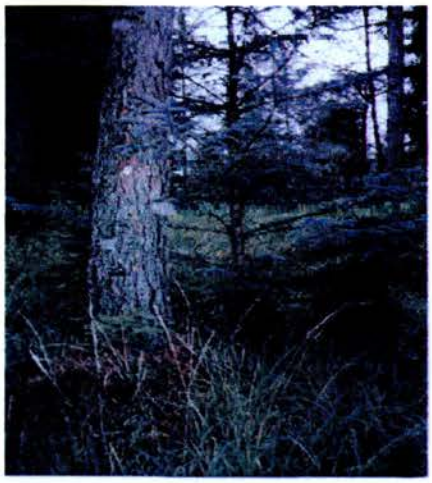

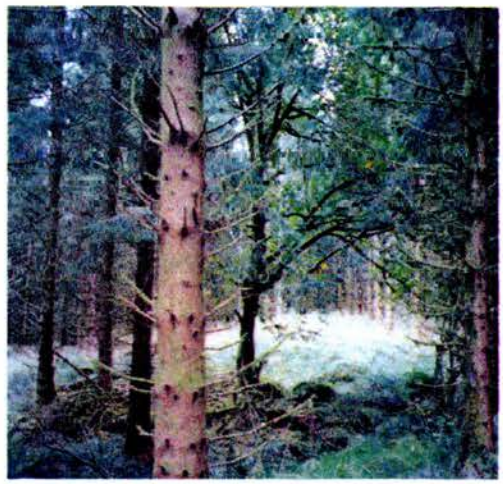

Figure 2.6: Views of Plot 1: **a)** regeneration, and.. **b)** ..trees around gap

Characteristics

Area: 50x50m

Species: Norway spruce (*Picea abies* (L.) karst.)

*Age: 35 years

Number of trees: 222

*Soil: Upland brown earth

*Yield class: 12

Terrain: relatively flat

*Mean elevation: 40 m

*(Forestry Commission Database)

Observations

Other species present:

Sitka spruce (*Picea sitchensis* (Bong.) Carr.) 20%

Scots pine (*Pinus sylvestris*) 5%

Hinberry (*Vaccinium myrtillus*) 5%

Grass 70%

High presence of regeneration. Many Sitka spruce (*Picea sitchensis* (Bong.) Carr.) saplings but no mature trees of that species within the plot. The regenerating Norway spruce seedlings and saplings are located around the borders of the gaps.

- **Plot2**

a)

b)

Figure 2.7: Views of Plot 2: a) general and b) within stand.

Characteristics

Area: 50x50m

Species: Norway spruce (*Picea abies* (L) Karst.)

*Age: 36 years

Number of trees: 115

*Soil: Upland brown earth

*Yield class: 20

Terrain: Relatively flat

*Mean elevation: 40 m

*(Forestry Commission Database)

Observations

Other species present:

Grass 90%

Bracken (*Pteridum aquilinum)* 5%

Moss 5%

High density of trees. This plot presents some gaps but no regeneration.

- **Plot3**

a)

b)

Figure 2.8. Views of Plot 3: a) general and b) within stand

Characteristics	**Observations**
Area: 50x50m	Other species present:
Species: Sessile oak (*Quercus petraea)*	Hinberry (*Vaccinium myrtillus*) 40%
*Age: 135 years	Raspberry (*Rubus idaeus*) 10%
Number of trees: 168	Blackberry-bramble (*Rubus fruticosa*) 10%
*Soil: Upland brown earth	Moss 40%
*Yield class: 12	The plot is located at the top of Drummond
Terrain: 10% slope	Hill and exhibits a light slope. The trees are
*Mean elevation: 70 m	more or less aligned and present extended crowns and considerable heights.
*(Forestry Commission Database)	High density of trees. Presence of dead trees. Bad quality of the trunks making the wood of low commercial value. Locally very wet soil.

- **Plot4**

a)

b)

Figure 2.9: Views of Plot 4: a) general and b) within stand

Characteristics

Area: 50x50m

Species: Sessile oak (*Quercus petraea)*

*Age: 135 years

Number of trees: 174

*Soil: Upland brown earth

*Yield class: 12

Terrain: 10% slope

*Mean elevation: 70 m

*(Forestry Commission Database)

Observations

Other species present:

Hazel (*Corylus avellana*) 10%

Holly (*Ilex acquifolium*) 20%

Beech (*Fagus sylvatica*) 10%

Moss 300%

Grass 30%

This plot is located at the top of a hill known as Fairy Knowe. The site presents few seedlings but no saplings. Most of the plot is dominated by grass. High density of trees.

- **Plot5**

a)

b)

Figure 2.10: Views of Plot 5: a) general and b) within stand

Characteristics

Area: 50X50 m

Species: European Larch (*Larix decidua* P. Mill.)

*Age: 68 years

Number of trees: 45

*Soil: Upland brown earth

*Yield class: 12

Terrain: 20% slope

*Mean elevation: 70m

*(Forestry Commission Database)

Observations

Other species present:

Bracken (*Pteridum aquilinum*) 70%, Hinberry (*Vaccinium myrtillus*) 20%, Grass 10%.

Nearly all of the trees situated in the southern part of the plot lack almost half of the branches that form the crown. The loss of these branches, which should be orientated to the north, could be due to competition from thinned trees, operation carried out in 1998. Light levels are adequate for regeneration but the problem is the control of vegetation competition.

- **Plot6**

Figure 2.11: View of Plot 6: **a)** general and **b)** ..within stand

Characteristics

Area: 50x50m

Species: European Larch (*Larix decidua*) and Douglas Fir (*Pseudotsuga menziesi*)

*Age: 67 years

Number of trees: 83

*Soil: Gley

*Yield class: 12

Terrain: 60% slope

*Mean elevation: 100m

*(Forestry Commission Database)

Observations

Other species present:

Bracken (*Pteridum aquilinum)* 5%,
Hinberry (*Vaccinium myrtillus*) 10%,
Holly (*Ilex acquifolium*) 10%
Wild service tree (*Sorbus torminalis*) 5%
Grass 70%.

The dominant species is European larch, covering approximately 60% of the plot. The trees are distributed in parallel lines and the terrain presents a slope of 40° approximately. This stand is included within the Regeneration Study Area.

The regeneration consists of a few seedlings of Norway spruce and Douglas fir which exhibit deer grazing damage. The side of the crowns that are south orientated are more developed maybe due to effects of the wind.

2.8 Description of the species under study

The retrieval of forest parameters and requirements for light regime were analysed on 3 different species: European larch (*Larix decidua* P. Mill.), Sessile oak (*Quercus petraea)*, and Norway spruce (*Picea abies* (L.) Karst.). A view of these species is shown in figure 2.12.

The species' botanical and ecological characteristics are described as follows and are useful to relate their morphological and seasonal changes to the reflectances values obtained from the remotely sensed imagery, as well as to have an understanding of their light regimes. This information was mainly extracted from the internet site (http://www.fs.fed.us/database/feis/plants/tree/picabi/botanical_and_ecological_characteristics.html) unless another source it is stated.

Figure 2.12: Norway spruce, European larch and Oak. ©Copyright 2005-2006 Virginia Tech Forestry Department.

- **European Larch (*Larix decidua* (P.) Mill.) in Great Britain**

  European larch been widely planted throughout Europe and Great Britain, and has also been planted in southern Canada and the north-eastern United States. European

larch wood is durable and strong, of moderately high density, with excellent toughness and stiffness. It is used for pulp, framing timber, roof tiles, flooring, and log houses. It is suitable for veneer and other decorative purposes.

General botanical characteristics

In the UK European larch is an introduced deciduous conifer. Mature height usually ranges from 9-40 m in the United States and Canada; larger individuals have occasionally been reported, particularly from Europe (up to 54 m). The crown of young trees is symmetrical, open, and narrowly conic. European larch is characterized as deep-rooted.

Figure 2.13: European larch's (*Larix decidua*) bark, leaf, form, fruit and twig.
©Copyright 2005-2006 Virginia tech Forestry Department

Trunk: straight, 1 – 1.5 m in girth.

Bark: On young trees smooth, on old trees grey or brown and fissured, shredding in small plates.

Branches: on young trees, dense, short and compact; on old trees spreading, upturned or drooping.

Branchlets: drooping, thin, grey or yellowish, glabrous, furrowed. Short spurs dark brown, nearly black, marked with as many rings as they are old, rings downy.

Winter buds: on main shoots ovoid, short-pointed; scales pointed, slightly resinous; golden to chestnut brown.

Leaves: on growth shoots single, varying in size up to 6 – 7 cm long; on the spurs – in clusters of 30 – 40, 1.5 – 3.5 cm long. All leaves turn to yellow in autumn.

Flowers: male strobili stalkless, rounded, yellow, 5 – 10 mm long, ripening in April and May.

Mature cones: ovoid, to 4 cm long, 2 cm broad, light brown ripening to grey the first year.

Seeds: about 4.5 mm long, greyish. Wing: mostly 12.5 mm long, 8-9 mm wide, reaching to the top of the scales.

Regeneration processes

European larch is monoecious which means that in this species male and female organs are found on the same plant but in different flowers. Minimum age of first reproduction is around 10 years. Large seed crops are produced at 3 to 10 year intervals. The seeds are wind dispersed. Most larch seeds germinate without pre-treatment. Viable seeds may remain in the cone for 1 to 2 years.

Site characteristics

European larch grows best on uniformly moist, deep, fertile soils. It does not do well on pure sand. Preferred soil textures include loamy sands, loams, and salty loams. European larch does not occur on poorly drained or very wet sites.

Light regime

European larch is intolerant of shade at any age (Hibberd 1991). Its open crown transmits a considerable amount of light so that it does not tend to suppress more tolerant understory species (McComb, 1955).

Seasonal development

In Great Britain, European larch cones do not open until spring. European larch needles die and are abscised in early November in Britain; some are retained through December.

Silvicultural systems

Group selection silvicultural system is successful with European larch. This is a system that promotes uneven-aged stands with clumps of even-aged trees well distributed throughout the cutting unit. These even-aged groups are large enough to accommodate some shade-intolerant seral species in addition to more tolerant climax species. Small gaps or openings are created on short intervals to develop into a mosaic of at least three or more age classes throughout the stand.

Group selection provides that advanced regeneration has not been suppressed for very long; suppressed seedlings do not respond well to release. Planting in mixtures with more tolerant species works well if the stands are thinned to allow European larch to maintain a dominant crown position; it does not usually suppress its more tolerant neighbours. European larch planted on slopes are susceptible to stem bending and breakage from snow.

- **Norway Spruce (*Picea abies* (L.) Karst.)**

  Norway spruce is native to the European Alps, the Balkan Mountains, and the Carpathians, its range extending north to Scandinavia. It was introduced to Britain as early as 1500 AD.

General botanical characteristics

Norway spruce is an introduced evergreen tree. In central Europe, heights of up to 61 m have been reported; the range is usually between 30-61 m and 100-150 cm dbh. The crown of young trees is narrowly conic, that of older trees becoming broadly columnar. Norway spruce cones are large (10-18 cm long). The root system is typically shallow, with several lateral roots and no taproot.

Figure 2.14: Norway spruce (*Picea abies*) bark, leaf, fruit, twig and form. ©Copyright 2005-2006 Virginia Tech Forestry Department.

Trunk: usually straight and symmetrical, with no tendency to fork.

Bark: orange-brown, finely flaking, becoming gray-brown, scaly on old trees.

Branches: short and stout, the upper level ascending, the lower drooping; twigs orange-brown.

Buds: reddish brown, 5-7 mm, apex acute.

Leaves: needles that persist for 3 to 4 years, stiff and pointed 1-2.5 cm long. Needles tend to point downwards and towards the stem tip, light to dark green.

Seed cones: cones found at the ends of branches long and narrow: 12-16 cm long; light green color turning to a medium brown at maturity; scales diamond-shaped.

Regeneration process

Norway spruce usually first reproduces at 30 to 40 years of age. Good seed crops are produced every 3 to 4 years in Britain. Most of the seeds are produced in the crowns of dominant stems; seed yield is lower in smaller stems in stands of the same age. Norway spruce seeds are wind dispersed, but do not usually travel much farther than the height of the parent tree. Movement after dispersal, however, can be considerable when seeds are dispersed onto crusted snow and are pushed along on the surface by wind. Seeds germinate promptly and do not require pretreatment or exacting light regimes. Optimum germination temperature for Norway spruce seeds is around 73 degrees Fahrenheit (23 deg C) but germination will occur up to about 91 degrees Fahrenheit (33 deg C).

Seedling growth is best at constant low temperature (9 deg C), rather than with fluctuating temperatures or steady high temperatures. The seedlings are sensitive to drought and/or overheating, particularly when the soil surface is exposed to direct insolation. Other studies support the hypothesis that shading improves early seedling survival.

Site characteristics

Norway spruce grows best in cool, humid climates on rich soils. Preferred soils include well-drained sandy loams. It also grows well on almost all other types of soils.

Light regime

Norway spruce is tolerant of shade. Seeds of Norway spruce are probably not long lived in the soil, although under good storage conditions remain viable for up to 7 years. Disturbance events such as windfalls, snow damage, disease and insect attack

create small-scale gaps in the mature canopy. Norway spruce depends largely on advance regeneration (seedling banks) to capture such canopy gaps. Norway spruce is the most common gapmaker and it is also the most common seedling in gaps. Seedlings survive in an extremely stunted condition for many years. This reservoir of seedlings functions in a way analogous to soil seedbanks. Suppressed Norway spruce saplings can persist for several decades, retaining the ability to respond to canopy gaps with increased growth.

Seasonal development

Norway spruce cones open from May to June. Seeds ripen in late autumn the same year. They are released on warm days in late autumn and winter, but are sometimes retained until spring.

- **Sessile Oak (*Quercus petraea* (Matt.) Lieblein)**

The Sessile oak (*Quercus petraea*), is native to most of Europe. It is a large deciduous tree of about 40 m tall, similar to English oak, with which it overlaps in range. Significant botanical differences with English oak include stalked leaves, and stalkless (sessile) acorns. It is found more often than English oak in upland areas with higher rainfall, but also with lighter soils with better drainage. The Sessile Oak has an age of up to 1000 years or more.

General botanical characteristics

It is a large deciduous tree, which grows slowly as a seedling, but of much faster growth later, with a maximum height of about 30-40m. The Sessile Oak is propagated by its seeds that are not dormant.

Trunk: Pale brown hard wood, grows faster than Common oak with straighter branches.

Bark: is deeply fissured with age.

Leaf: Elliptical leaves, 5-12 cm long, have 5-6 various sized lobes on either side, and no ears at the base which narrows gradually into a leaf stalk 10-25 mm long, on stalks with clusters of sessile acorns, flowers appear in May.

Figure 2.15: Sessile oak (*Quercus petraea)* bark, acorn, leaf, and terminal buds. ©Copyright 2005-2006 Virginia Tech Forestry Department.

Site characteristics

The habitat of the Sessile Oak is mainly in acid upland soils, often in its own pure stands. It generally prefers lighter well drained soils and not tolerant of flooding.

Light regime

European oaks require high solar irradiances, especially at the seedling stage.

Seasonal development

Acorns in autumn: the Sessile oak fruits less frequently than the Common Oak, and its acorns are smaller.

The tree in winter: growth ceases during the winter because there are no leaves to carry out photosynthesis.

The tree in spring: spring is the time when the previous year's acorns germinate to produce the young oak seedlings. Paradoxically, oak seedlings appear almost anywhere except beneath oak trees.

Female flowers in spring: female flowers are almost stalkless, and are borne in small groups on twigs, in the axils of leaves.

Male flowers in spring: the male catkins shed their pollen during late spring, and each catkin produces several million pollen grains. Oak trees are probably self-sterile (the pollen cannot fertilize female flowers from the same tree).

The tree in autumn: Oaks start to lose their leaves in the middle of autumn, but yellow leaves can still be seen on the trees in a mild winter. The autumn leaf fall produces a blanket of leaves, called litter, which forms a protective bed for germinating acorns.

Table 2.2 outlines the main aspects of the seed production of the species under study and the suggested times for seed collection.

Common Name	Age of first good seed crop (years)	Age of maximum production (years)	Average interval between good seed crops (years)	Recommended time of seed collection		
				Earliest	Normal	Latest
European larch	15 - 20	40 - 60	3 - 5	November	Feb/March	April
Norway spruce	30 - 35	50 - 60	-	October	October	November
Sessile oak	40 - 50	80 - 120	3 - 5	September	October	November
Sitka spruce	30 - 35	40 - 50	3 - 5	September	Sep./Oct.	December

Table 2.2: Seed production of trees in Great Britain (adapted from Hibberd 1991).

2.9 Summary

This chapter has introduced the theoretical aspects about Continuous Cover Forestry system, its definitions and main characteristics.

The definition of CCF used in this work corresponds to the one presented by Mason et al. (1999) that defines continuous cover as "the use of silvicultural systems whereby the forestry canopy is maintained at one or more levels without clearfelling", although in general, all terms that define the system emphasize its most important aspects which are the continuity of woodland conditions over time and the need to avoid clearfelling over large areas.

The use of natural regeneration as a restocking method is highly encouraged by CCF. The successful use of natural regeneration depends upon the manipulation of the stand microclimate to ensure satisfactory germination and growth of seedlings. One of the factors determining the survival and growth of the seedlings beneath a forest canopy is the light environment (Lieffers et al. 1999). Thus, to better understand mechanisms involved in understorey tree regeneration it is important to know how forest canopy and light interact and which are the light requirements of the target species.

In this chapter the area and species chosen for the study were also introduced. The study area consists in six sample plots located within the Elizabeth Forest Park in Aberfoyle, Scotland, and the species analysed were European larch (*Larix decidua* P. Mill.), Sessile oak (*Quercus petraea*) and Norway spruce (*Picea abies* (L.) Karst).

These species were especially chosen because of their differences of shade tolerance, so in this way is possible to establish comparisons regarding light conditions as well as size and distribution of gaps as one of the most important factors influencing stand microclimate.

Chapter 3

Analysis of the spectral reflectances of European larch, Norway spruce, Sessile Oak, and Sitka Spruce using Landsat ETM+ imagery

3.1 Introduction

The existence of up-to-date and accurate forestry related information is relevant for all forest management tasks and especially for continuous cover forestry (CCF) purposes. This information comprises variables or stand parameters such as tree height, diameter at breast height (dbh), basal area or volumes, which are often used in forestry to aid planning of forest resources. Although detailed measurements could and should be acquired *in situ*, remote sensing from space platforms appears to be the only economically feasible way to gather information repetitively over large areas with a high spatial, spectral, and temporal resolution (Verstraete *et al.* 1996). Optical remote sensing offers opportunities to determine forest parameters using forest reflectance to monitor forest stands, and to predict their current and possibly future characteristics as well as their mapping. Thus, the accurate determination of forest reflectance plays a key role in the improvement of forest classification, mapping, forest inventory and management goals in a cost effective manner.

The applicability of Landsat Thematic Mapper (TM) for estimating structural forest variables based on the vegetation spectral characteristics has been researched over the past three decades. Stand structure attributes such as tree size, density, and basal area were reliably quantified using Landsat TM data by Cohen and Spies (1992). Ripple *et al.* (1991) utilised TM and SPOT (Satellite Pour l'Observation de la Terre) data over coniferous forest and established that significant inverse relationships existed between forest volume and the near infrared bands of both sensors. Similar results were shown by Gemmell (1995) who also reported that forest volume was strongly related to the reflectance characteristics of the stand and could thus be estimated from the remote

sensing data. Trotter *et al.* (1997) performed a Landsat TM spectral analysis on bands 3,4,5, and 7 and found that acceptable accuracies of wood volume calculations were obtained for forest-stand areas of about 40 ha therefore limiting its use for inventory at more detailed scales. Brockhaus and Khorram (1992) found several TM spectral bands to be significantly and positively correlated to basal area and age classes of trees, but they concluded that the correlation coefficients were so low as to limit any use in model development. Significant positive correlations between forests stand parameters and Landsat TM spectral bands were found by Mallinis *et al.* (2004) with bands 4 and 7 showing the strongest correlations. Strong positive relationships have been observed between the Leaf Area Index (LAI) of temperate coniferous forests and the ratio of near infrared and red radiance measured by Landsat TM (Spanner1990).

Considerable work has focussed on spectral vegetation indices and correlations between remotely sensed data and biophysical properties. These indices derived from satellite data are one of the primary sources of information for operational characterisation and monitoring of the vegetation cover. The most frequently used spectral vegetation index is the Normalized Difference Vegetation Index (NDVI) described by Rouse *et al.* in 1974 (Jensen 2000, Perry and Lautenschlager 1984), although improved vegetation indices have been developed such as the Modified Soil Adjusted Vegetation Index (MSAVI) (Qi *et al.* 1994), the Modified Soil and Atmospherically Resistant Vegetation Index (MSARVI) (Huete and Liu 1994), the Normalised Pigments Chlorophyll Ratio Index (NPCI) (Peñuelas *et al.* 1994), the Photochemical Reflectance Index (PRI) (Peñuelas *et al.* 1995), and the Generalised Soil Adjusted Vegetation Index (GESAVI) (Gilabert *et al.* 2002).

Price *et al.* (2002) evaluated the use of Landsat TM to determine optimal vegetation indices and band combinations for discriminating among six forest management practices. They found that increasing the number of TM bands by using multiple datasets of imagery improved discrimination accuracy up to a point, but that the use of too many bands (greater than 10) could actually decrease discrimination accuracy. The usefulness

of spectral methods applied to Landsat TM data for differentiating old growth from younger Spruce-Fir stands was evaluated by Nel *et al.* (1994), showing that the NDVI and the Simple Ratio were the best discriminators between the two types.

The correlation between NDVI and Leaf Area Index (LAI) has been a topic of considerable research (Vieira *et al.* 2003, Chen and Cihlar 1996, Gilabert *et al.* 1996, Chen *et al.* 1996), as LAI is one of the most important biophysical factors controlling many processes such as photosynthesis, respiration, transpiration, carbon and nutrient cycle, and rainfall interception (Qi *et al.* 1996, Chen *et al.* 1996).

Time series of Landsat TM imagery have been used successfully in the production of detailed land cover maps (Ager and Owens 2004, Oetter *et al.* 2000, Basham *et al.* 1997, Wolter *et al.* 1995). The applications of such data for forestry mapping are also well documented: Wilson and Sader (2002) used multiple dates of Landsat TM imagery for the detection of forest types, concluding that the Normalised Difference Moisture Index (NDMI) applied to imagery collected every 2 – 3 years proved to be useful in the detection of harvesting and other disturbances that do not remove the entire overstorey canopy. Almeida-Filho and Shimabukuro (2002) applied a Principal Components Analysis to a 12-year Landsat series of data in order to map and monitor land cover changes in Brazil.

Despite previous research efforts, the question remains as to how spectral Landsat TM bands respond to the variation of forest parameters or species over time. The analysis of spectral responses is more complex because most types of land cover exhibit different spectral behaviour within species in a single season, mainly related to plant growth (Jakubauskas 1996, Nilson and Peterson 1994) and development, as well as to changing background properties (Danson and Curran 1993, Elvidge and Chen 1995). Furthermore, the relationships between spectral and biophysical attributes do not extrapolate to other sites and years as they depend on viewing and radiation geometries, canopy morphology and background, and the spectral characteristics of individual plant parts (Gilabert *et al.*

1996). Danson and Curran (1993), analysing the remotely sensed response of coniferous forest plantations, concluded that one of the main factors affecting such responses is related primarily to stand structure. A study carried out by Vogelmann and DeFelice (2003) for the characterisation of reflectance properties in South Dakota using Landsat TM and ETM+ data, concluded that the degree to which the land cover classes could be separated spectrally and radiometrically depended on the time of year during which the datasets were acquired, and that no single dataset appeared to be adequate for separating all types of land cover.

While a number of investigations have examined the long-term variation of forest reflectance, the use of information relating to the seasonal variation of forest reflectance appears to be relatively untested (Gemmell *et al.* 2001) and certainly little has been done or at least reported in the UK. Some studies are published on this topic: Kodani *et al.* (2002) analyzed the seasonal variations in the reflectance factor with respect to the seasonal variations in the biophysical or biochemical attributes of deciduous canopy in Japan using four bands of the moderate resolution imaging spectrometer MODIS; Huete *et al.* (2002) produced multitemporal profiles of the MODIS VIs over numerous biome types in North and South America representing their seasonal phenologies; Ustin *et al.* (1994) reported the observed seasonal changes in AVIRIS images of vegetation communities in California.

The investigation of multi-seasonal data-sets for forests is important to facilitate a better understanding and classification of land cover and further work needs to be undertaken to identify optimal image acquisition dates and to understand better the biophysical aspects of the temporal changes in forest reflectance in specific conditions.

The approach in this study for the spectral characterisation of four different species is the detection of phenological change on a Landsat 7 Enhanced Thematic Mapper Plus (ETM+) time series. The results indicate patterns of seasonal reflectance properties and

the time of the year in which data acquisition should be made to obtain the best discrimination of species.

3.2 Objectives

The analysis of Landsat ETM+ data already available for the area was considered appropriate for this project due to that is one of the most widely used remote sensing datasets for forestry applications. The main advantages of Landsat ETM+ are its availability soon after acquisition and more affordable price in comparison with other remote sensing data sources. At Landsat resolution it is possible to explore phenological patterns within and between stands. Given the continued demand for Landsat imagery from the forestry sector and the growing supply of imagery from Landsat 7, it was felt that the scenes available for the study area owed to be analysed and that this sensor provides the most accessible data for the research objectives. The spectral signatures from stands of four species: European larch (*Larix decidua* P. Mill.), Norway spruce (*Picea abies*), Sessile Oak (*Quercus petraea*), and Sitka Spruce (*Picea Sitchensis* (Bong.) Carr.) were investigated to determine the extent to which their reflectances varied seasonally and whether the species could be discriminated better by remote sensing using this seasonal reflectance data. The spectral reflectance of those species was collected from Landsat ETM+ images over the Aberfoyle area at different times of the year through two years, 2000 and 2001. The analysis of the spectral signatures for mapping purposes therefore stimulates the following questions:

- To what extent do the spectral signatures of different tree species vary seasonally?
- Are seasonal reflectance spectra sufficiently different between species?
- What potential impact does seasonal variation have on monitoring intra-annual change in forests?
- What utility does intra-annual variation have for improved species classification?

In order to answer these questions, the study aims at evaluating a range of features derived from ETM+ data for discriminating the marked species in the test site, which included single bands, NDVI, Principal Components Analysis, and the assessment of the image acquisition time that provided a better discrimination of the species under analysis.

The understanding of the influence of seasonal changes on the reflectance from different forest species is important as:

- seasonal influence may be useful for classification, taking advantage of different species' phenologies. It is therefore useful to determine whether the observed reflectance differences between species are significant and consistent, over different seasons and areas, before they can be generally applied with success in remote sensing mapping or in the retrieval of other forest parameters.
- Seasonal variation will lead to errors in detection of change over longer time scales if a) seasonal influence is marked; b) a part of the difference recorded is a seasonal one, unrelated to longer term changes; c) images are acquired at different times of the year.

Therefore, the developing of accurate measurements for forested areas using satellite data requires finding out what actual ground-level changes trigger remotely sensed signal variations. If the changes are caused by overstorey phenological events, then appropriate model parameterisations may need to be employed to assess the process accurately.

Limitations of the study arise mainly from the short series to be evaluated which do not follow closely key phenological events, and the lack of field measurements to tie up the results derived from remotely sensed products as explored by Fisher et al. (2006) in which work, through the analysis of 57 Landsat scenes and corresponding field work, achieved an effective scaling from plot to satellite phenological observations.

3.3 Remote sensing of the marked vegetation

The basic premises for optical remote sensing of vegetation are that the solar radiation received by a remotely located sensor upon interaction with the plant stand (e.g. a forest) carries in it the signature of the vegetation and that this spectral signature can be deciphered to obtain the important characteristics of the stand (Rautiainen *et al.* 2004).

Within the electromagnetic spectrum, different wavebands will produce different levels of reflectance when radiation interacts with the canopy cover. Vegetation shows a marked increase in reflectance at spectral bands immediately past the range of human vision. Through the visible light region, vegetation is low in reflectance, with the exception of a small rise in the green (figure 3.1). For example, in the visible bands (0.4 – 0.7 μm), lower reflectance will occur as more light is absorbed by leaf pigments than is reflected. The blue (0.40 – 0.50 μm) and red (0.60 – 0.70 μm) wavelengths include two main absorption bands where light is absorbed by leaf pigments. This broad chlorophyll absorption continues into the infrared with the long-wavelength side of chlorophyll absorption extending beyond 0.7 μm (Howard 1991).

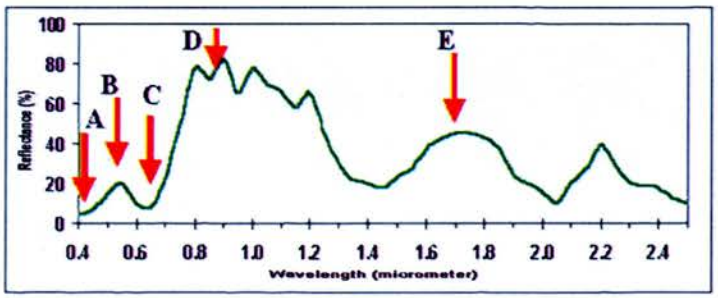

Figure 3.1: Typical spectral reflectance characteristics of healthy vegetation. The labelled arrows indicate the common wavelength bands used in optical remote sensing of vegetation: A: blue band, B: green band; C: red band; D: near IR band; E: short-wave IR band (adapted from Jensen 2000).

The change in reflectance from red into the near infrared is usually large, ranging from a low of about 5% at 0.68 μm to a maximum of about 50% at 0.73 μm. This rapid change in reflectance has been called the "red edge" and it was reported for first time by Collins in 1978 (Campbell 2002). The properties of reflectance spectra indicate that the

chlorophyll absorption band is "saturated" such that the minimum will not change much with changes in absorption.

Since all vegetation is composed of the same chlorophyll and associated photosynthetic material, the reflectance spectra from widely differing plants will look similar. However, either seasonal variation or vegetation stress will cause a difference in the amount of the chlorophyll absorption, which results in a small shift of the side of the absorption peak as the absorption decreases and therefore in an observed reflectance change in the near infrared, or "red edge shift". Since different plants may have differing levels of stress and thus different depths of chlorophyll absorption, the amount of red edge shift can be used to differentiate between plant types (Jensen 2000).

Canopy structure also affects the remotely sensed response of vegetation. Nilson and Peterson (1994) have found that the reflectance factors of forest stands are greatly influenced by the values of leaf reflection coefficients. Thus, in a coniferous forest, the stand reflectance may be sensitive to changes in the proportion of needles of the current year and previous years. Gerard and North (1997) found that the spectral reflectances of the red and near infrared bands are influenced by structural characteristics such as canopy cover, tree pattern distribution, and canopy gaps. Asner (1998) indicated that the variability in canopy structure is the dominant factor on canopy reflectance with the exception of soil reflectance and vegetation cover in sparse canopies. More recent studies (Rautiainen *et al.* 2004) indicate that crown size and shape are important factors influencing stand reflectance. Further research (Rautiainen 2005) shows that the main explanation for the low reflectance of coniferous in comparison to broadleaved stands, especially in near infrared wavelengths, is the high level of within-shoot scattering within coniferous species. All these studies seem to indicate the fact that the smaller the crown volume, the lower the canopy reflectance.

The effects of canopy structure on forest reflectance have been modelled, among others, by Li and Strahler (1985). This geometric-optical model, formulated for use in

discontinuous canopies, allows for the retrieval of forest parameters from the remotely sensed images and has been tested several times on a limited number of stands. The inversion of this model by Woodcock et al. (1997) showed that the means for tree geometry parameters vary between forest types; the estimates of forest cover are reliable, and that the estimates of tree size are unreliable due to the breakdown in the relationship between image intra-stand variance and tree size. This study suggests that improvements in estimates of tree size require the use of a series of Landsat TM data rather than a single image.

Another source of spectral difference between plant species is differences in the amount of water in the leaf or canopy structure. This spectral difference can be seen in leaves from the same species after a period of drying, and can be an indicator of stress, as leaves from stressed plants had higher reflectance in the visible and lower in the near infrared (Peñuelas *et al.* 1994). Spectral differences can also be seen in leaves from trees of different species. Throughout the wavelength range beyond 1.3 μm, leaf reflectance is approximately inversely related to the total water present in a leaf. This total is a function of both the moisture content and the thickness of a leaf (Lillesand 1990).

Normally, there is an inverse relationship between vegetation amount and reflectance in the visible and mid-infrared region of the electromagnetic spectrum because of the absorption from plant pigments and water content, respectively. In contrast, the relationship between vegetation amount and reflectance in the near-infrared is positive (Mallinis 2004). However, it has been found that this positive relationship does not always exist; it can be flat (Franklin 1986) or even inverse depending on understorey or background reflectance (Danson and Curran 1993).

3.3.1 Factors affecting vegetation spectral reflectance

The classification of species of forest types by remote sensing assumes that the features to be classified in an image reflect or emit light energy in different and often unique ways

(Lillesand and Kieffer 1994), and that therefore, those unique patterns of response can be analysed and discriminated by species. However, there are other physical and physiological parameters that affect the reflectance from vegetation which can vary according to the species or over an individual plant over space and time (Fyfe 2003). As a result of these effects it is important to know if the observed reflectance differences between species are significant and consistent over different seasons and areas so they can be applied in remote sensing mapping.

There are several factors that influence the reflectance quality of vegetation on satellite and remote sensing images. These include brightness, greenness and moisture (Cohen and Spies 1992). Brightness is calculated as a weighted sum of all the bands and is defined in the direction of principal variation in reflectance. Greenness is orthogonal to brightness and is a contrast between the near-infrared and visible bands. It is related to the amount of green vegetation in the scene. Moisture in vegetation will reflect more energy than dry vegetation. Leaf properties that influence leaf optical properties include the internal or external structure, age, water status, mineral stresses, and the health of the leaf. It is important to note that the reflectance of the optical properties of leaves is the same, regardless of the species. What may differ for each leaf are the typical spectral features recorded for the three main optical spectral domains: leaf pigments, cell structure and water content.

Electromagnetic radiation of all wavelengths will interact differently with different parts of plants and trees. These parts include leaves, stems, stalks and limbs of the plants. The density of the tree or plant canopy will also affect the scattering of the wavelengths (http://ucalgary.ca/geog/Virtual/Remote%20Sensing/rsveg.html). Identifying vegetation in remote sensing images depends on several plant characteristics. For instance, in general, broad deciduous leaves tend to be more reflective than evergreen needles. It has also been demonstrated that crown shape affects reflectance. Stands with conical crowns had much smaller reflectance than ellipsoidal crowns, where larger crown volume results in higher single scattering from crowns (Rautiainen *et al.* 2004).

Soil background is one source of variation that has received much attention in recent years (Danson and Curran 1993, Elvidge and Chen 1995, Gilabert 2002). The sensitivity of NDVI to soil background lead to the development of new indices such as the Soil Adjusted Vegetation Index (SAVI), Transformed Soil Adjusted Vegetation Index (TSAVI), and Modified Soil Adjusted Vegetation Index (MSAVI), which are less sensitive to this external influence (Rondeaux *et al.* 1996). Gemmell (1999) inverted a forest reflectance model to estimate the biophysical characteristics of coniferous forest stands. Emphasis was placed in incorporating the effects of variation in background signatures into the inversion process. Results indicated that the inversion model performed better than spectral indices when the background signatures were included.

Plant age or maturity is also a factor to consider (Nilson and Peterson 1994). It is recognized that changes in leaf chlorophyll and internal structure during the phenological cycle of a plant significantly affects its spectral response pattern (Jensen *et al.* 1999). Mature plant canopy leaves tend to increase the contrast between infrared (NIR) and red reflectance (Nel *et al.* 1994). The possibility that the amount of shade will increase with stand age has also been documented (Nilson and Peterson 1994, Leblon *et al.* 1996).

Reflectance from vegetative cover may vary significantly over the course of a growing season. Thus, acquisition of multiple dates of coverage, e.g., early and late in the growing season, often allows a further refinement of spectral signatures, and thus a higher degree of resolution among vegetation types. For example, plant species that have spectrally similar signatures early in the growing season may diverge in this regard later in the season, thus allowing their unique identities to be resolved. Where multiple layers of vegetation exist, such as forest canopy and understorey, the measured reflectance is that of the top-most layer. Consequently, a closed forest canopy would not allow understorey vegetation to be identified, and an open canopy forest would yield a mix of both tree canopy and understorey reflectance (Nilson and Peterson 1994). Other factors that influence the vegetation spectral response are time of day, sun angle, atmospheric haze, clouds, processing errors.

Landsat imagery from more than one date may provide additional information over single-date imagery in three ways (Gemmell *et al.* 2001): First, the spectral characteristics of both foliage and background vary with time, affecting the contrast between crowns and background, thus influencing the separability of different stands using multispectral reflectances. Second, if two separate Landsat TM scenes had a sufficient solar zenith angle, this would give two samples of stand bidirectional reflectance, thus providing more information on the structural characteristics of the stand. Third, differences in atmospheric conditions affect the ratio of direct to diffuse sky irradiance, which also affects the contrast between sunlit and shadow component reflectances.

3.4 Data collection

A set of eight 1G level Landsat 7 Enhanced Thematic Mapper Plus (ETM+) images was available for the study (figure 3.2 and 3.3). The 1G level product is radiometrically and geometrically corrected. These images were the best and most cloud free obtained by this sensor during this period. As the images of a point are taken only every 16 days by the Landsat system, this makes more difficult the acquisition of cloud-free images, especially in Britain. Two images are representative of the beginning and peak of summer 2000 (17 July 2000 and 25 August 2000, respectively), one winter 2000 image (24 December), one mid-spring 2001 image (01 May), two representative images of the beginning and middle of winter 2001 (31 October and 11 December, respectively), while the last one was taken at the beginning of spring 2002 (01 March).

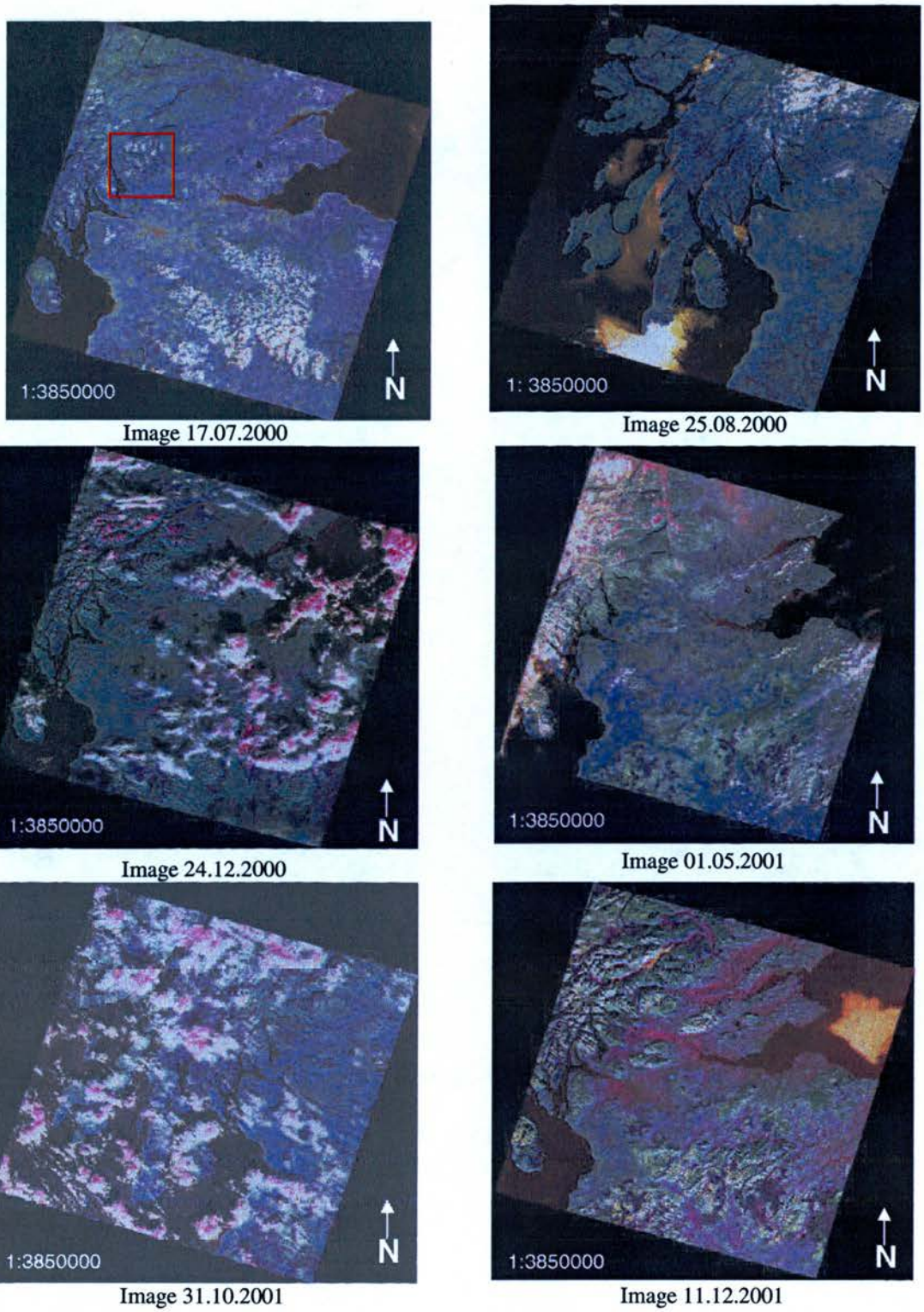

Figure 3.2: Colour composites of Landsat 7 Enhanced Thematic Mapper Plus (ETM+) imagery acquired for the study. The study site is enclosed in the red box on image 17.07.2000.

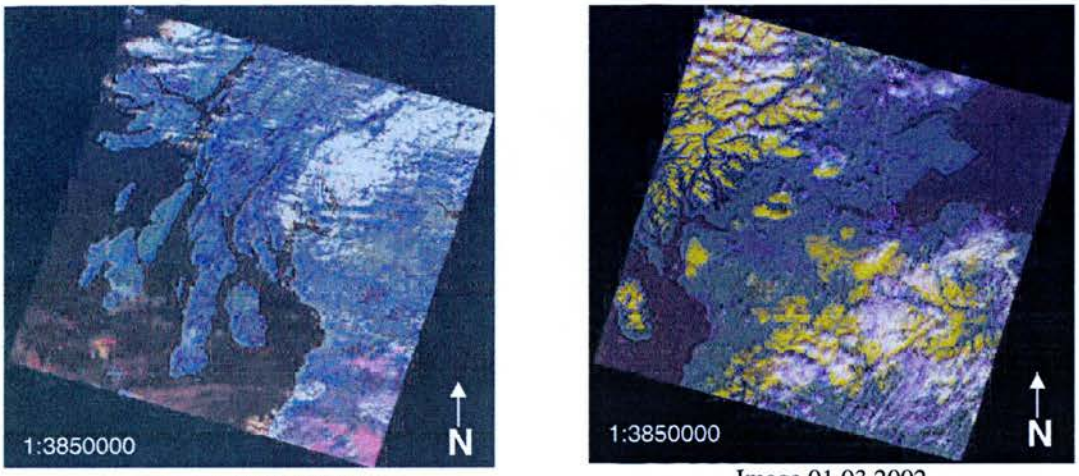

Image 23.08.1999 Image 01.03.2002

Figure 3.3: Colour composites of Landsat 7 Enhanced Thematic Mapper Plus (ETM+) imagery with clouds over the study site, non suitable for analysis.

From the group of images available, the ones acquired on the 23.08.1999 and 01.03.2002 (figure 3.3) were cloud dominated making the extraction of information over the area of interest difficult. The images taken in late October and December (24.12.2000, 31.10.2001, and 11.12.2001) present very low sun angles which produces a strong shadowing and highlights terrain features. Normal time of acquisition of the satellite data for the study area was about 11:07 GMT.

ETM+ data are organized by rectangular areas referred to as scenes, each 185 km on a side. A scene is comprised of millions of pixels, each representing a 30 m square, or an on-the-ground area of 900 square m.

There are also other useful parameters obtained from Landsat imagery, such as illumination differences (Table 3.1).

Path	Date acquired	Sun azimuth	Sun elevation	Comments
206	23.08.1999	156.40	43.79	Cloudy
205	17.07.2000	150.87	52.73	Cloud-free
206	25.08.2000	156.23	42.78	Cloud-free
205	24.12.2000	164.18	9.53	Very dark
205	01.05.2001	156.04	47.49	Cloud-free
206	31.10.2001	166.13	19.14	Dark
205	11.12.2001	165.19	10.09	Very dark
205	01.03.2002	157.48	24.44	Cloudy

Table 3.1: Acquisition characteristics of the Landsat ETM+ imagery used in the study.

The ETM+ sensor measures the sun's energy as reflected from elements of the land surface. The full spectrum of reflected energy is measured at discrete intervals, referred to as bands, with each band capturing a narrow range of wavelengths, including visible (blue, green, red) and non-visible (near infrared, and two mid-infrared) wavelengths. An ETM+ data set includes reflectance values for each pixel for each of the six bands. A unique combination of reflectance values comprises a spectral "signature", and potentially allows each element of the landscape to be identified as a particular type of land cover.

The multi-temporal set of images allowed the study of the range of spectral variability through time between species. The six ETM+ optical bands were used to analyze the spectral response of four forest species in the Elizabeth II Forest Park. The thermal band was not included in the analysis. ERDAS Imagine Software v 8.7 (ERDAS 2003) was used for the analysis of the satellite imagery data.

3.4.1 Atmospheric correction and normalisation

The use of multitemporal imagery requires the removal of the atmospheric effects on radiation (Du *et al.* 2002, Hall *et al.* 1991), especially in this study in where the aim is to

identify spectral signatures of tree species through time. If the data are not corrected, the subtle differences in reflectance among the species may be lost.

Optical radiation from the Earth's surface, which highly characterizes surface inherent properties, is largely contaminated by the atmosphere (Myneni and Asrar 1994). The atmospheric window through which many of the high resolution sensors scan the Earth lie within the visible and near infrared regions of the electromagnetic spectrum. Within this region in particular, atmospheric scattering has an additive effect on the radiation reaching the satellite sensor, thereby increasing the Earth's reflected response (CSIRO 1995). Absorption and scattering of radiation in the atmosphere is assumed to be primarily due to gases and aerosols (Myneni and Asrar 1994). The atmospheric particles (aerosols and molecules) scatter and absorb the solar photons reflected by the surface in such a way that only part of the surface radiation can be detected by the sensor. On the other hand, atmospheric particles scatter sunlight into the sensor's field of view directly, resulting in a radiation that does not contain any surface information at all. The combined atmospheric effects of scattering and absorption are wavelength dependent, vary in time and space, and also depend on the surface reflectance and its spatial variation (Kaufman 1989).

As a result, any image processing technique that analyses the relative spectral responses of different spectral bands, or requires quantitative analysis, will be affected by the composition of the atmosphere at the time of data capture. Thus, the development of empirical relationships between satellite measured radiance responses and ground cover variables will also be affected by changing atmospheric conditions. Changing atmospheric composition thereby alters the responses detected in each of the spectral bands and this can, in turn, affect the predicted responses during the analysis. To ensure that the results are independent of the atmospheric conditions, it is necessary to remove or minimise the atmospheric effect on the dataset.

Although qualitative evaluation of raw remotely sensed data has been useful, the quantitative analysis to link at-sensor reflectances and surface characteristics greatly depends on the removal of the atmospheric effects. The objective of atmospheric correction is thus to retrieve surface reflectance from the at sensor signal. In order to calculate surface reflectance from remotely measured radiance, radiative transfer codes play an important role for removal of atmospheric scattering and gaseous effects under varying illumination and viewing conditions (Staenz *et al.* 2002).

Thus, the quality of the results achieved through the temporal analysis depends highly on the corrections and calibrations performed on the imagery. For example, contributions from the atmosphere to NDVI are significant and can amount to 50 percent or more over thin or broken vegetation cover (Jensen 2005). For multitemporal studies, where variation in atmospheric parameters such as aerosol optical depth and water vapor content is to be expected, the use of NDVI is not recommended unless atmospheric correction can be accurately performed because of the sensitivity of this index to atmospheric perturbations (McDonald *et al.* 1998).

In order to correct for atmospheric effects, the relationship between the upward radiance L^m measured by the satellite and surface reflectance ρ has to be established. Radiative transfer theory is used for this purpose. Assuming that the atmosphere is bounded by a Lambertian surface (reflects solar energy isotropically), the upward radiance at the top of a cloud-free, horizontally homogeneous atmosphere can be expressed by [1]:

$$L^m = L_0 + \frac{\rho F_d T}{\pi(1 - s\rho)} \quad \text{.....[1]}$$

where L_0 is the upward radiance of the atmosphere with zero surface reflectance, often called path radiance, F_d is the downward flux (total integrated radiance) at the ground, T is the transmittance from the surface to the sensor (the probability that a photon travels through a path without being scattered or absorbed), and s is the atmospheric albedo (the probability that a photon reflected from the surface is reflected back to the surface). The

factor $\frac{\rho}{1-\rho s}$ is the sum of the infinite series of interactions between the surface and the atmosphere (Fallah-Adl *et al.* 1995).

Theory shows that the path radiance effect (Rayleigh and aerosol scattering) is dominant in the visible region of the electromagnetic spectrum and approaches zero in the infrared region. The opposite occurs for atmospheric attenuation, which presents its minimum in the visible region and increases in the infrared region.

An image standardization process was applied to the imagery analyzed in this study to normalize pixel values for differences in sun illumination geometry, atmospheric effects and instrument calibration. Several attempts were made in order to perform an absolute correction using a Radiative Transfer Code (RTC) program such as 6S (Second Simulation of the Satellite Signal in the Solar Spectrum) developed by Vermote *et al.* (1997) and for which atmospheric information on the dates of image acquisition was collected from the Meteorological Office, Edinburgh, consisting of monthly returns of daily observations. However, use of 6S model was restricted due to the lack of information about water vapor content (H_2O) and ozone concentrations (O_3) in the atmosphere at the time of the image acquisition, parameters required for the input file in 6S to ensure accuracy in the correction process. Other input parameters for this model were: Sun-sensor geometry, ground reflectance, type of atmospheric model, type of aerosol model, aerosol optical depth, and spectral band.

The selected procedure for the correction, known as COST, is image-based so that *in situ* atmospheric measurements are not required. Of image correction methods, the COST method is one of the most sophisticated as it attempts to correct for both additive scattering and multiplicative absorption effects of the atmosphere, and it has been shown by Chavez (1996) to be as accurate as those that have used *in situ* atmospheric field measurements and radiative transfer code (RTC) software. This correction converts the image's raw DN values to at-sensor reflectance values and corrects for procedure

distortions caused by the following: gains and offsets from the sensor, path radiance, atmospheric transmittance along the path from the sun to the earth's surface (which is approximated by the cosine of the solar zenith angle in this equation), and atmospheric transmittance along the path from the earth's surface to the sensor. The actual method is an improvement to the DOS (Dark Object Subtraction) model (Chavez 1988), which only corrects for the additive scattering effect.

The COST model calculates the following equation:

$$\rho_{BandN} = \frac{\pi((L_{BandN} * Gain_{BandN} + Bias_{BandN}) - (H_{BandN} * Gain_{BandN} + Bias_{BandN})) * D^2}{E_{BandN} * (COS((90 - \theta) * \pi / 180))} \quad \ldots.[2]$$

Where,

ρ_{BandN} = Reflectance for Band N

L_{BandN} = Digital Number for Band N

H_{BandN} =Digital Number representing Dark Object for Band N

D = Normalized Earth-Sun Distance

E_{BandN} = Solar Irradiance for Band N

$Bias_{BandN}$= the data product bias contained in the Level 1 product header in watts

The correction was performed using software available from the GIS Laboratory at Utah State University (www.gis.usu.edu/docs/projects/swgap/ImageStandardization.htm), which generated a spatial model per image to be run in ERDAS Imagine. The required input parameters were the header file of each image and the minimum DN values per band. The result was a spatial model that could then be used to perform the correction on the image.

The normalisation process is not error free. Although there is a hope that site-specific predictive reflectance trajectories ("reflectance tables") can be determined, the problems of reliable normalisation of multidate data still remain to be solved (Nilson and Peterson 1994). Naturally, it has to be considered that the reflectance factors or radiances depend

not only on the characteristic wavelength but also on the bandwidth. As a consequence, reflectance trajectories determined by a particular sensor cannot be directly extended to sensors viewing in another spectral region.

After atmospheric correction the reflectance values of five of the images were normalised to a baseline data set (the remaining scene) using the PIF method developed by Schott *et al.* (1988) that performs a radiometric scene normalisation using Pseudo-Invariant Features. The method corrects for atmospheric degradations, illumination effects, and sensor response differences in multispectral imagery (Schott *et al.* 1988). The technique is based on the statistical invariance of the reflectance of man-made in-scene elements such as concrete, asphalt, and rooftops. This approach does not give an absolute radiometric scale, but has the advantage of compensating for all sources of radiometric distortion simultaneously and has been shown to be preferable to other simplified approaches to image calibration (Joyce 2005).

The PIF normalisation process assumes that the relationship between the at-sensor radiances recorded at two different times from regions of constant reflectance is spatially homogeneous and can be approximated by linear functions, and its most difficult and time-consuming aspect is the determination of suitable time-invariant features upon which to base the normalization (Canty *et al.* 2004). In practice, targets with constant reflectance do not exist; therefore, the concept of PIFs is adopted, with the assumption that their reflectances are constant over time (Du *et al.* 2002). That makes the selection of PIFs the key to the image regression. In the present study, these features were extracted directly from the imagery. The baseline scene selected was the Landsat ETM+ 25 August 2000 data set as this image was particularly clear and haze free.

The normalisation process was carried out through the selection of 10 pseudoinvariant targets covering a range of brightnesses. The selection of a higher number of PIFs was limited by the availability of invariant features identifiable in all the images. These targets were located within the study area and its surroundings. They included large

lakes, Glasgow airport, and the tops of large buildings. The largest targets were the water bodies and the smallest target was a building comprising 4 pixels in size.

Attempts were made to avoid mixed pixels and targets that were characterized by high levels of heterogeneity. For each band, mean values extracted from each target in each scene were plotted against their counterpart mean values from the baseline scene (25 August 2000).

Regression equations derived from these plots generally had r^2 values of 0.98 or higher, implying an excellent relationship between the individual pairs of bands from the different acquisitions of data being compared (Appendix 1).

The appropriate regression equations were then used to normalise each band of each non-baseline data set to the same band of the baseline data set to ensure that the resulting reflectances were comparable among data sets. For this purpose normalisation models were built using the parameters from the regression equations for each band in the Model Maker module in ERDAS Imagine. To check the appropriateness of the correction and normalisation process, reflectance values corresponding to four deep-water bodies for every image and their respective reflectance values obtained after atmospheric correction and normalisation were compared (Figures 3.4 and 3.5).

The results indicate that for each image, the PIF normalisation led to significant improvements in reflectances, which for each lake can be expected to be very low. The main reflectance variability for lakes after normalisation was observed for the images acquired in December 2000 and December 2001. The rest of the scenes showed more consistency between bands.

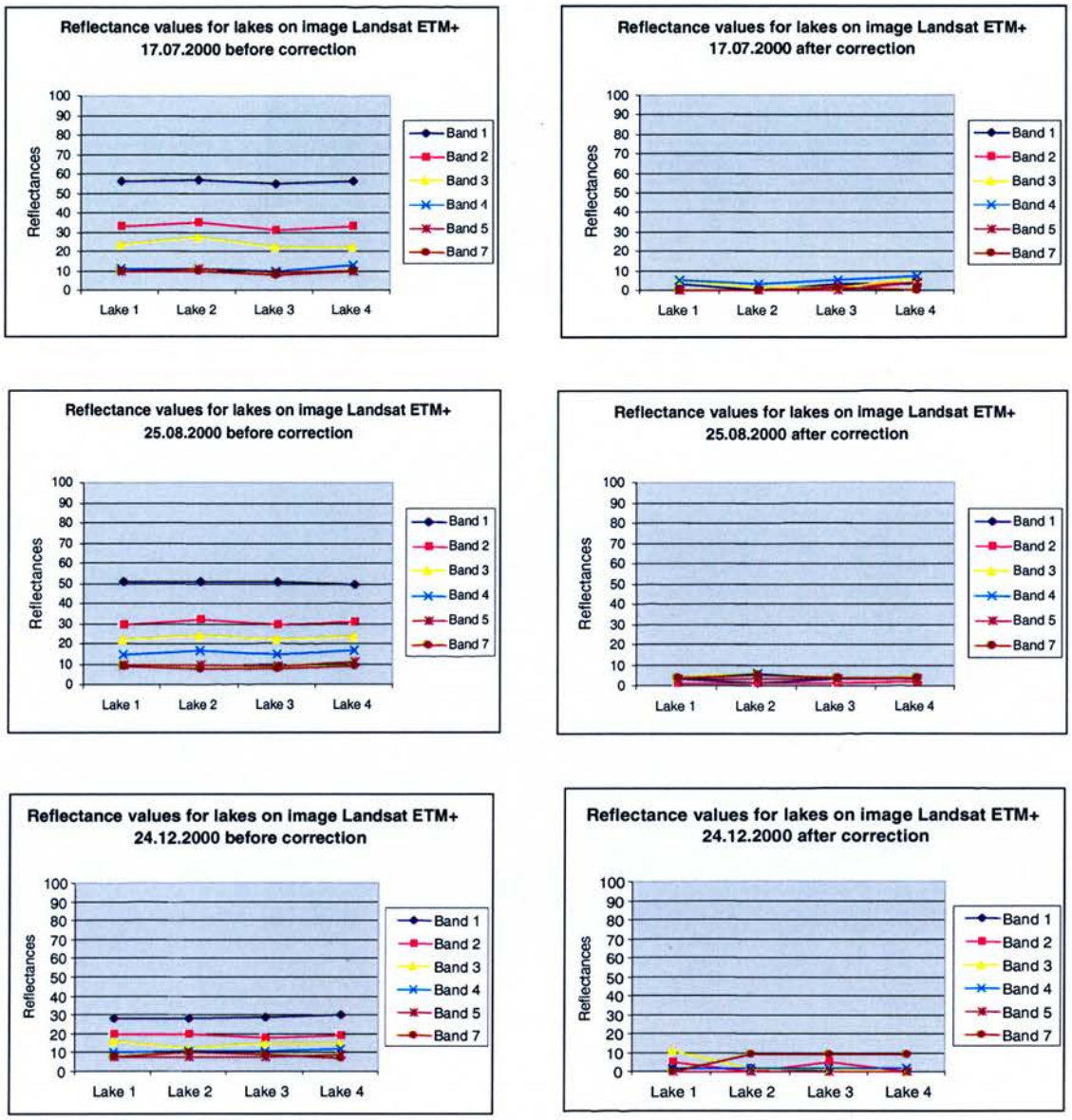

Figure 3.4: Reflectance values of water bodies before and after atmospheric correction and normalisation correspondent to images taken on 17.07.2000, 25.08.2000 and 24.12.2000. Greater variations after correction can be seen in the 24.12.2000 scene, indicating that the normalisation of this image could not be achieved accurately.

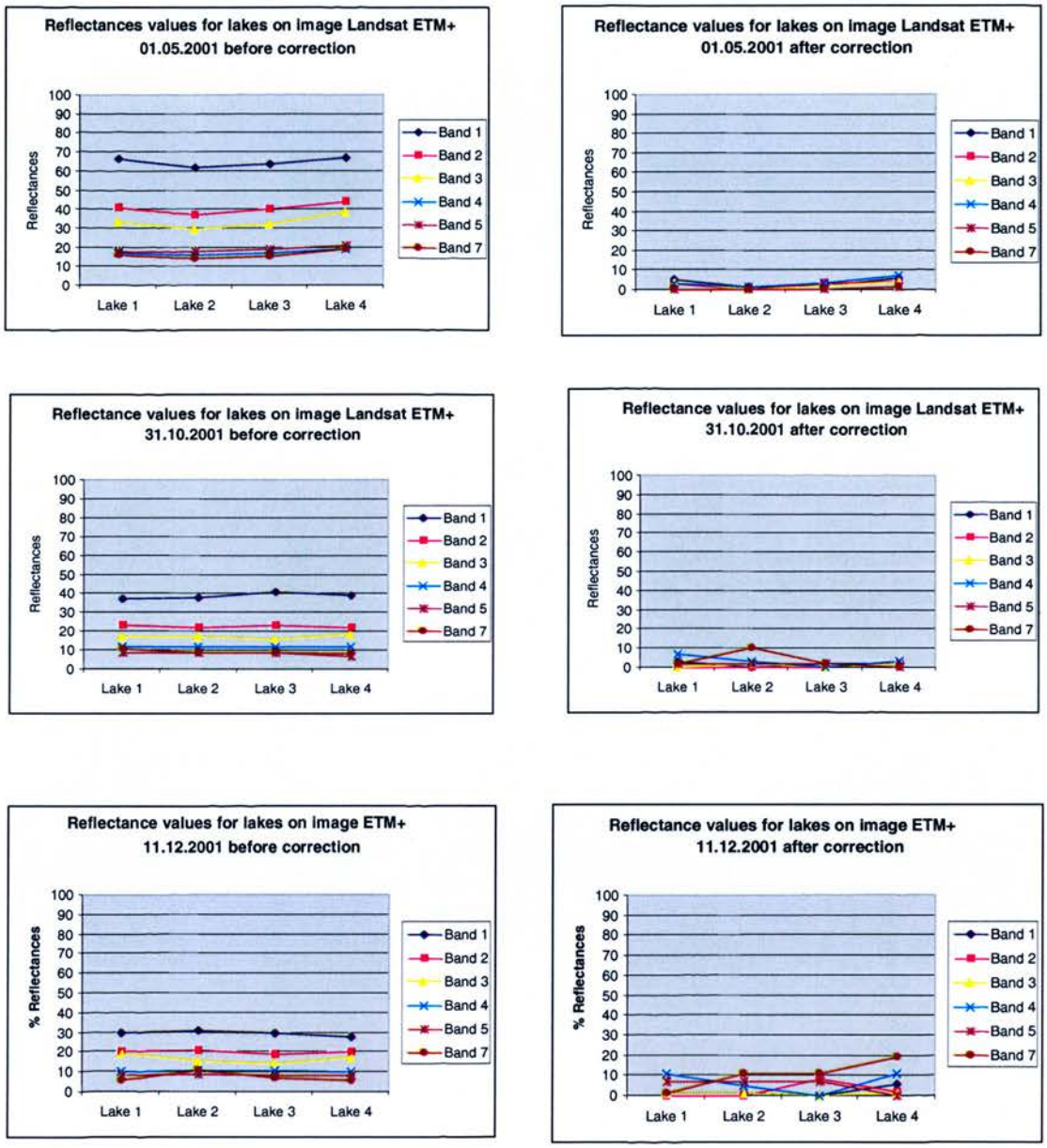

Figure 3.5: Reflectance values of water bodies before and after atmospheric correction and normalisation correspondent to images taken on 01.05.2001, 31.10.2001 and 11.12.2001. Greatest variations after correction can be seen in the 11.12.2001 scene, indicating that the normalisation of this image could not be achieved accurately.

However, recent research (Paolini *et al.* 2006) has showed that high positive correlations between PIFs as the ones found in this study (Appendix 2), do not necessarily mean that radiometric effects haven been eliminated.

In the light of this latter publication and although further processing and analysis of the reflectance and the phenological effects was already carried out, it was decided that the accuracy of the radiometric normalisation should be tested further to evaluate the extent of the radiometric normalisation errors during the process.

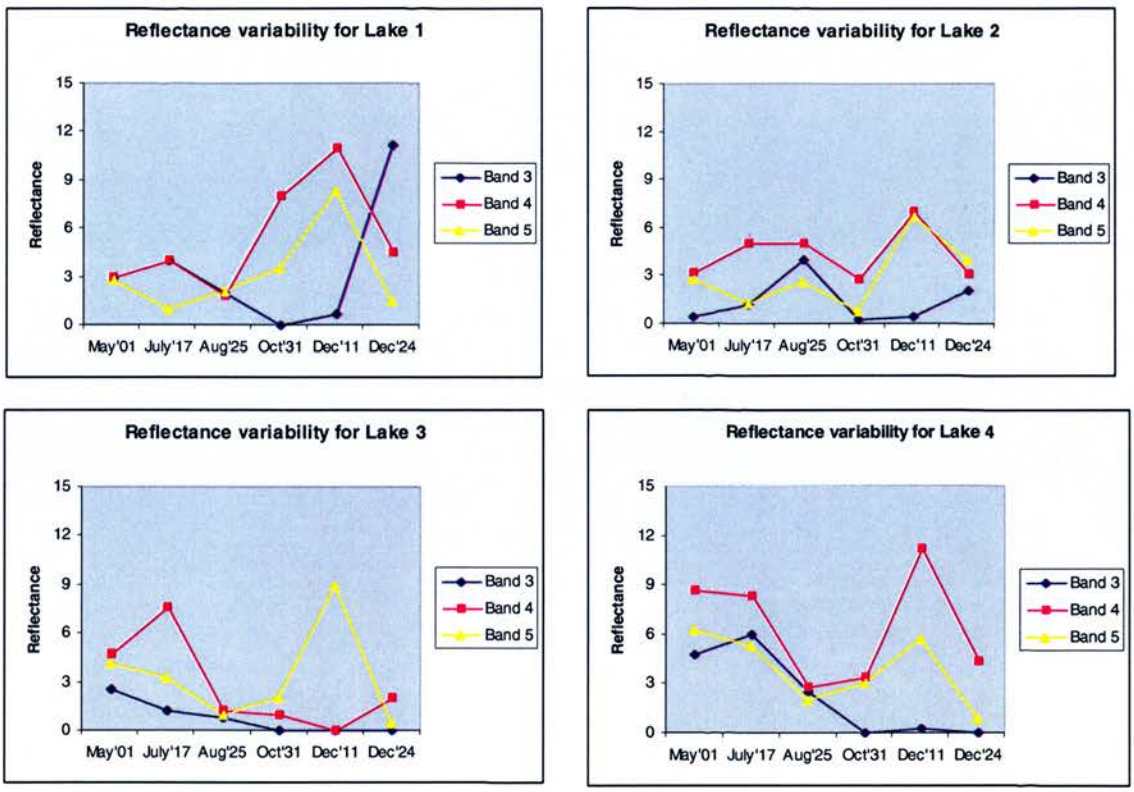

Figure 3.6: Assessment of the PIFs targets. The figure shows the reflectance variability trough time of four targets used in the normalisation process.

This analysis showed that despite the good positive correlations found for all the PIFs used for radiometric normalisation (Appendix 2), the variability of the reflectance for these targets trough time was considerable and may have introduced a margin of error to

be taken in account when evaluating the reflectance responses of the species considered. Figure 3.6 shows the reflectance variability for 4 of the most invariant targets located on lakes surrounding the study area.

The figure shows the variability of the reflectance values trough time. Important departures from the base-image reflectance (25 August) are observed especially for the winter imagery (up to 10 reflectance units). The inclusion of these targets in the normalisation process will therefore introduce bias in subsequent estimations.

The lack of better pseudo-invariant features to be selected lead to the culmination of the analysis process in the knowledge that possible phenological effects could be diminished or exacerbated by the errors introduced for this reflectance variability. The use of a methodology to establish the accuracy of the PIFs and the radiometric correction, as the one proposed by Paolini *et al.* (2006), should be used in future research to overcome this problem.

Once the images were normalized, the radiance images of the 2000 and 2001 dates are assumed to appear as if they had been imaged through the same sensor response function and similar atmospheric conditions as the reference reflectance image.

The analysis of the spectral responses of the species under study was carried out on reflectance data so calculated for each TM scene and for each band. The Landsat ETM+ bands that were used in the analysis include the following: TM1(blue-green), TM2(green), TM3(red), TM4(NIR), TM5(mid-infrared(MIR)) and TM7(MIR). The Normalised Difference Vegetation Index (NDVI) and the first three components from Principal Components Analysis (PCA1,2,3) were also calculated for each of the six images used in the study.

3.4.2 Geometric correction

After radiometric and normalisation corrections, the 25.08.2000 base line scene was rectified to the Ordnance Survey Great Britain (OSGB) coordinate system using an empirical correction method based in the positional relationship between points in the image and their correspondent locations in a map. The correction was performed using 25 common control points extracted from topographic maps at the scale 1:100.000. These points were characterised for being clearly identifiable both in the map and in the image and for being features that have no tendency to change over time. They were chosen at the intersection of main roads, corners of buildings, and other man made features. Exceptionally, geographical features were chosen where no roads or buildings were clearly identified. Particular attention was placed on the selection of points in the surroundings of the study area as these empirical models only correct locally at ground control points. A first order polynomial rectification algorithm was used, which achieved a registration accuracy of 0.7 pixels (21 m). The nearest neighbour resampling method was used.

The 25.08.00 scene was used as a reference to co-register the rest of the images. This was carried out with the use of the first order polynomial algorithm selecting a mean of 25 points per scene that were identified in both images at a time. The ground control points were preferably chosen in areas of high contrast, land clearing, geometric features, and bare ground patches amongst dense vegetation, trying to avoid water bodies, areas covered by clouds and features subject to shadowing. Control points with a residual greater than 1 pixel were discarded. The overall root mean square error of the transformation was of about 1 pixel (30m) for all scenes (Table 3.2).

In order to preserve radiometric integrity, a nearest neighbour procedure was used for resampling. The images were then spatially subset to the extent of the study site in order to have a more manageable format size and working area.

Acquisition date	Total RMS error (pixel)
17.07.2000	0.9461
25.08.2000	0.7162
24.12.2000	0.8882
01.05.2001	0.8946
31.10.2001	0.9416
11.12.2001	0.80634

Table 3.2: Geometric correction accuracies of Landsat ETM+ scenes.

3.5 Patterns of seasonal reflectance

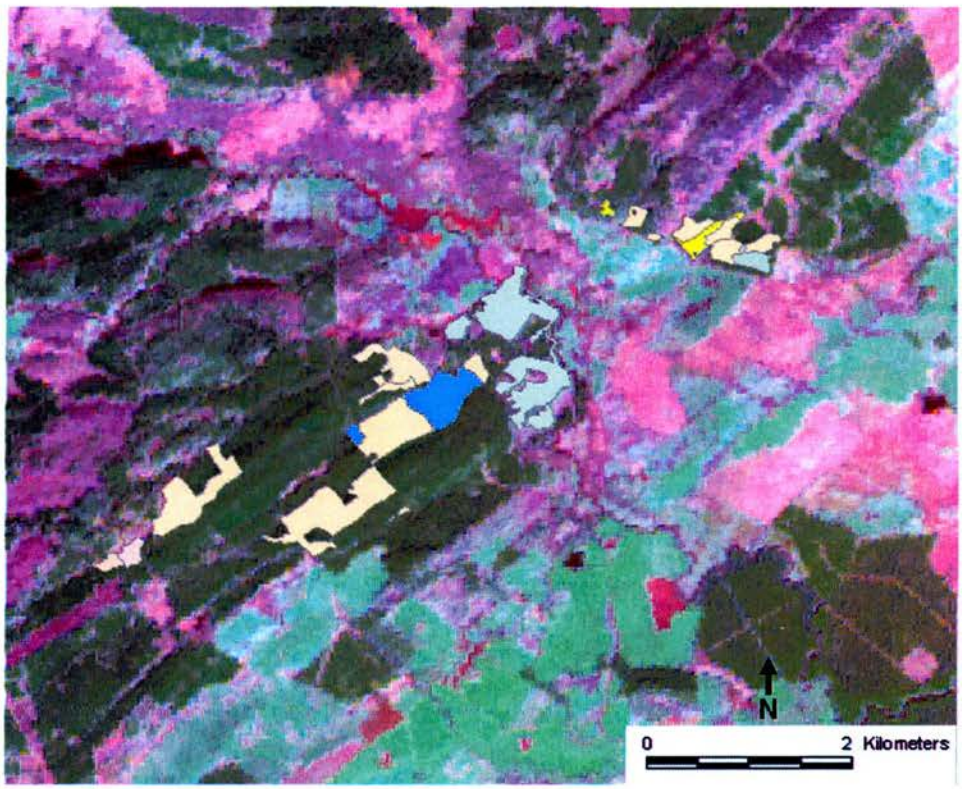

Figure 3.7: Subset of the Landsat ETM+ image obtained on 25.08.2000 showing the location of the study plots within the Aberfoyle area. The bright yellow plots correspond to the European Larch plots, the pale green to Oak plots, the blue to the Norway spruce plots, and the pale yellow to the Sitka Spruce plots.

While structural vegetation variables such as height, dbh, and basal area, are required for CCF conversion and monitoring purposes, the question remains about how spectral Landsat TM bands respond to their variation within and between species and over time. In order to collect information about the species spectral responses, two training sites were identified for each of the tree species under evaluation. The training sites encompassed the plots in which height and dbh measurements were taken. A false colour composite of the August 2000 scene with indication of the sample plots is shown in figure 3.7.

3.5.1 Selection of optimal band combination

The correlation matrix of the spectral bands contains useful information about data redundancy and selection of optimal band combinations for interpretation purposes. If the bands show strong correlation (value near to 1.00) this indicates that the bands usually contain similar information to each other. When those bands are visualized minimum separability among different features would be noticed. The following table (3.3) represents the correlation matrix of the baseline image obtained on 25th August 2000.

Correlation matrix						
Base-line image (25.08.2000)						
Bands	1	2	3	4	5	7
1	1.0					
2	0.979	1.0				
3	0.977	0.993	1.0			
4	0.361	0.515	0.497	1.0		
5	0.637	0.754	0.761	0.884	1.0	
7	0.838	0.898	0.915	0.686	0.922	1.0

Table 3.3: Correlation matrix for the Landsat ETM+ data obtained on 25 August 2000

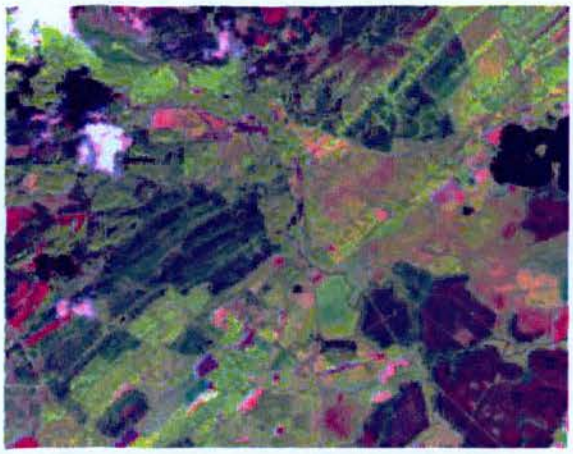

a) Image 17.07.2000

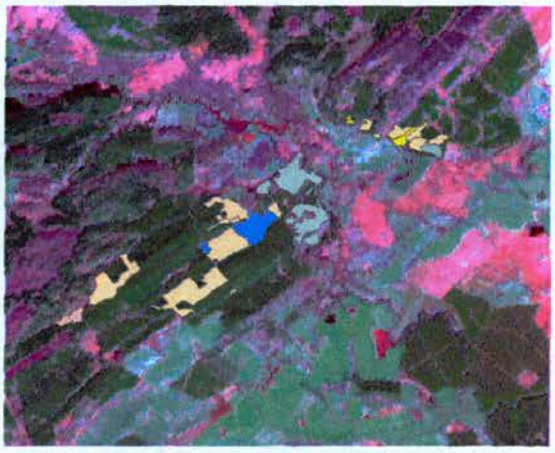

b) Image 25.08.2000

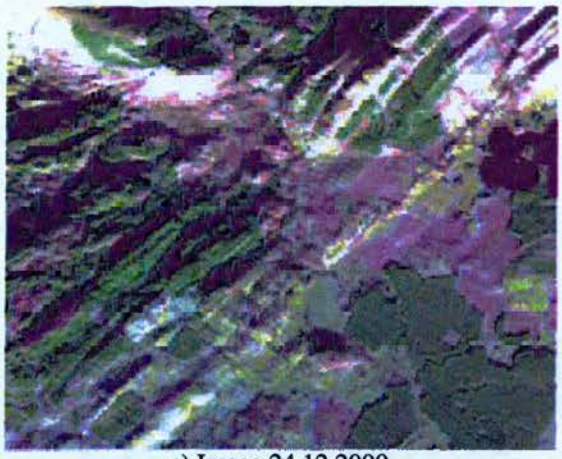

c) Image 24.12.2000

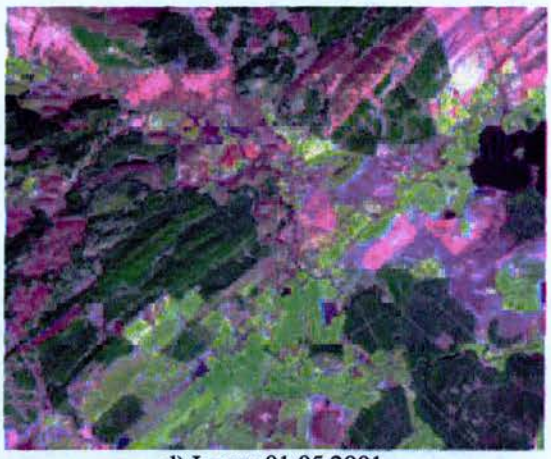

d) Image 01.05.2001

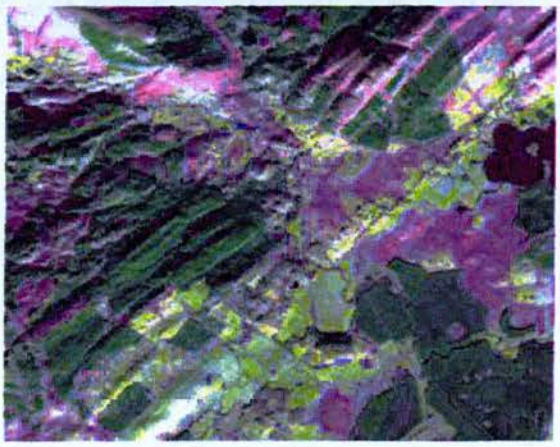

d) Image 31.10.2001

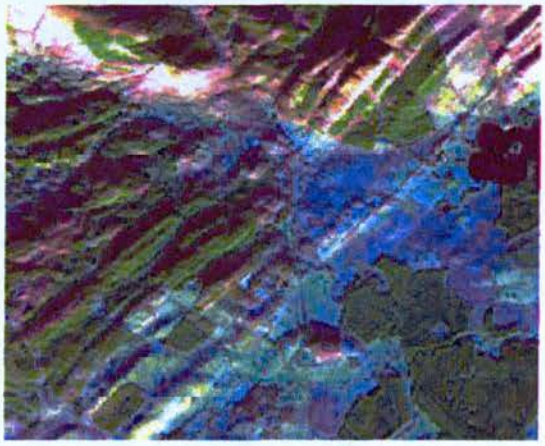

e) Image 11.12.2001

Figure 3.8: Subsets of the images selected for the analysis of the spectral reflectances of the marked species (scale 1:145000). Figure b) also denotes the location of the sample plots (yellow for European larch, green for oaks, blue for Norway spruce and pink for Sitka spruce).

The correlation matrices of all Landsat ETM+ imagery available for this study were calculated and the correlations between bands for all the images showed approximately the same behavior as for the baseline dataset. From Table 3.2 it is observed that high correlation exists among visible (band 1-3) and mid-infrared bands (band 5-7), which means there is a high redundancy of information within these bands. According to Gemmell (2001), Horler and Ahern (1986) showed that bands 3, 4 and 5 are relatively independent of one another for coniferous forest.

A combination of bands that includes one from the visible region, the near-infrared and one from mid-infrared are commonly selected to achieve the best separability in the vegetated areas using Landsat ETM+ data. However, the analysis of the reflectance pattern for the selected forest species was carried out on all raw ETM+ bands.

A Principal Components Analysis was also performed to determine the combination of bands that portrayed the greatest significance for the study. When displayed as images, the band combination 4, 5 and 3 in the order of red, green and blue was effective in portraying the changing patterns of reflectance for the different species studied. Subsets of these colour composite images of the study area are shown in figure 3.8.

3.5.2 Interpretation of observed spectral reflectances in ETM+ bands

Spectral signatures of all forest sampling plots were extracted from the optical bands (bands 1, 2, 3, 4, 5 and 7) of the six ETM+ acquisitions. Although sample plots of the species Sitka spruce were not established on the field, it was decided to include plots of this species to complement the study and for comparisons with the other species, being Sitka spruce a non-native coniferous commonly found in forest plantations in the UK. Location of Sitka spruce stands as well as the other stands in which sampling plots were established in the Aberfoyle area, were obtained from the Achray Forest Database (Forestry Commission). Sampling plots were located in a GIS layer containing the Achray Forest sub-compartments and two new plots 50 x 50 m were created in two

different sub-compartments of the Sitka spruce species. This GIS layer was afterwards overlaid on the imagery. All spectral signatures were averaged over the ground plots for the same species to have mean spectral values for each species. Some spectral variability was found within and between plots of the same species. This was especially significant for the European larch plots. Variations between the spectral values of European larch samples from these two plots might be due to the different characteristics they exhibit related to: topography (Plot 1 was relatively flat and Plot 2 had a high slope); understorey vegetation cover (Plot 1 had mainly bracken and grass and Plot 2 had mainly grasses); stand density (Plot 1 had low density and Plot 2 had high density). All other plots from where reflectances were extracted showed more homogeneous values per image.

As the acquisition of cloud-free images that correspond to phenological events is difficult, the spectral values are displayed by day and month of acquisition, regardless of the year. This allowed the interpretation and visualization of seasonal events as if they were registered in a single year. The resulting pattern of spectral values over time gives an indication of the typical phenological development in the field.

Leaf-flush or senescence is phenological change that can be captured by satellite images (Jensen 2000). Species can be distinguished when they are in different phenological stages in the same image, or when they change differently from one image to the next (Dymond *et al.* 2002). However, as stated before, the appearance of the profile is determined by a variety of interrelated factors, including phenology, plant morphology, canopy structure, and environmental conditions (Odenweller and Johnson 1984).

Kuusk *et al.* (2004) investigated another factor that plays a significant role in the spectral response of forest such as the understorey vegetation. They acknowledge the fact that too few systematic data are available on the spectral signatures of forest understorey species and that due to the complexity of their ecosystem it is not possible to describe them quantitatively. This lack of information has caused problems in the modelling of

reflectance of sub-boreal forests as well as in the interpretation of the measured reflectance spectra.

Figure 3.9 illustrates the spectral curves of the four species that were sampled, for all six images. Band 1, 2 and 3 of Landsat ETM+ represent the visible light of blue-green, green and red reflectance, respectively. Vegetation containing large amounts of green leaves and biomass usually shows more absorption in the visible green and red spectral region. Vegetation that has fewer amounts of those components exhibits relatively higher reflectance in that spectral region. In this case, all the species appear with relatively high absorption in these bands, with the deciduous species oak and larch showing the highest reflectance in all dates. Visible band reflectances (1, 2, and 3) are slightly higher in these species during the leaf-off periods (24 December 2000, 11 December 2001) than during leaf-on periods (May through August). The overall appearance of the profile is highly dependant upon acquisition history. If key observations are missing, discriminating features may not be detected (Odenweller and Johnson 1984).

Band 4 corresponds to reflectance of the near infrared region which is typically high for vegetation and is thus widely used to separate vegetation from other types of land use. Sessile oak and European larch appear to have more reflectance in this band than the spruce species as seen in figure 3.9 a,b,c (July'00, May'01, and August'00). However, this pattern changes for Oak in figure 3.9 d,e,f corresponding to the winter images (October'01, December'01, and December'01) where it appears to have a lower reflectance than European larch and Sitka Spruce, consistent with the expected decrease in reflectivity as a result of the leaf-off conditions.

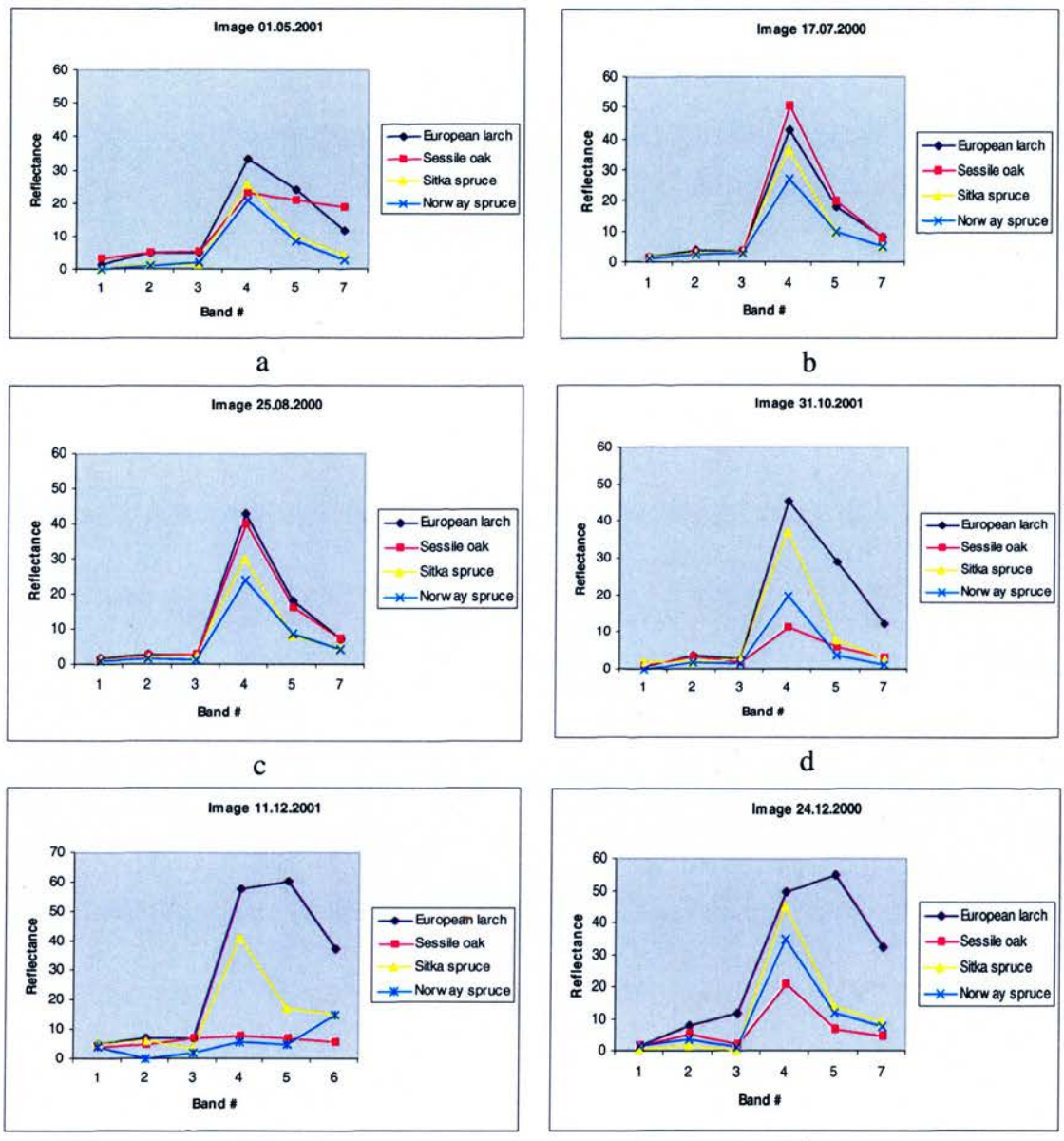

Figure 3.9: Spectral profile for Sitka Spruce, European Larch, Sessile Oak and Norway Spruce for the Landsat ETM+ imagery displayed in phenological order and obtained on a) 01.05.2001, b) 17.07.2000, c) 25.08.2000, d) 31.10.2001, e) 11.12.2001, and f) 24.12.2000.

Residual NIR reflectances at these times may be due to the influence of the understorey vegetation, which mainly consisted of blackberry, bramble, hazel and holy, but may also be due to the ground contribution to reflectance by wet soils and the thick moss layer which characterised the Oak plots. As mentioned before, shadows can be another factor

influencing the NIR reflectance decrease. In winter the reflectance of deciduous forests is also much influenced by the projected area of the woody part of the trees and by the area of the shade cast by the tree trunks on the ground (Nilson and Peterson 1994).

The contrasting high reflectance values of European larch in band 4 on winter imagery could be explained by two main factors: as the contribution of understorey vegetation (as the sites are dominated by bracken and grasses which are highly reflective) and due to the viewing and illumination angle. The usual physical interpretation that the subcanopy components such as grass are more reflective than the forest canopy was demonstrated by Trotter *et al.* (1997). In relation to the second factor, the spectral signal typically referred to as a bidirectional signal, is a function of the prevailing sensor view and solar geometric characteristics. Depending on these conditions, the target stand can look darker or brighter (Kuusk *et al.* 2002).

On the other hand, the European larch plots were also considerably less dense than their Oak counterparts so that the effect of shadows due to woody parts on reflectance response was reduced. Stands with a lower overstorey density, as in the case of the European larch in this work, allow a greater proportion of the incident light to reach the forest floor, where the amount of understorey cover influences stand spectral response (Jakubauskas 1996). An understorey dominated by green vegetation will increase absorption in the visible bands and augment the vegetation component of the overstorey spectral reflectance. If the understorey of the low-density stands is sparse or dominated by soil, reflectance is increased in the visible bands. Shadow remains a minor factor, as the trees are of similar height (low size diversity) and there is little depth to the foliated canopy. It has been demonstrated that open stands with broadleaved understorey vegetation or other highly reflective background have elevated near infrared radiances. Old growth stands with considerable shadows and dark backgrounds have near infrared radiances lower than expected (Spanner *et al.* 1990).

In figure 3.9 it can be seen that the best differentiation between species appears to be in band 4 for the images taken in July 2000, May 2001 and October 2001. Figures 3.9f and 3.8e corresponding to December 2000 and 2001, show a sudden increase in band 5 reflectance for European Larch. These values do not fit the trend for spectral responses that is observed in the other figures with peaks in band 4. Again it should be noted that the winter images are very dark and the spectral response of the selected features could be biased by radiometric errors no eliminated, and shadowing of woody parts due to the low solar angle.

Band 5 corresponds to the shortwave-infrared region, which is sensitive to the amount of water present in plant leaves. The most important contributors to band 5 reflectances are thus shadows and canopy moisture content (Trotter *et al.* 1997). Studies have noted the utility of the shortwave infrared wavelength (bands 5 and 7) region in forest discrimination (Gemmell 1995). It is expected that the species that contain the greatest quantity of water in their leaves show the lower reflectance. In this study Norway and Sitka spruce exhibited the lowest reflectances in this band and European larch was the species that showed consistently the higher reflectance. This is evident especially during the leaf-off period for the latter species (late October to April). However, in the same images (December 2000, October 2001, and December 2001), although the deciduous Sessile oak was also in leaf-off stage, its band 5 reflectance values contrast highly with those for European larch, being as low as those corresponding to Norway spruce (figure 3.8 d,e,f). This phenomenon could be explained by background effects, considering that the oak sites were characterised by wet bare soil and moss. However, what is evident is that band five has a high variability for different vegetation classes, indicating that the band could be useful for the separation of different types of vegetation.

Band 7 contains information on shortwave-infrared reflectance, which is also an indicator of the presence of water in leaves. However, other studies indicate that it might contain only redundant information, as band 5 suffices, as the Principal Component Analysis in the next section will show. Figures 3.8f and 3.8e correspond to the spectral responses in

the images 24.12.2000 and 11.12.2001 and also show a great degree of differentiation between species in band 7. However, information from images with such a low solar angle is thought to be unreliable, besides the difficulties for species identification due to excessive shadowing.

Figure 3.10 corresponds to the observed mean intra-seasonal reflectances obtained from the image datasets.

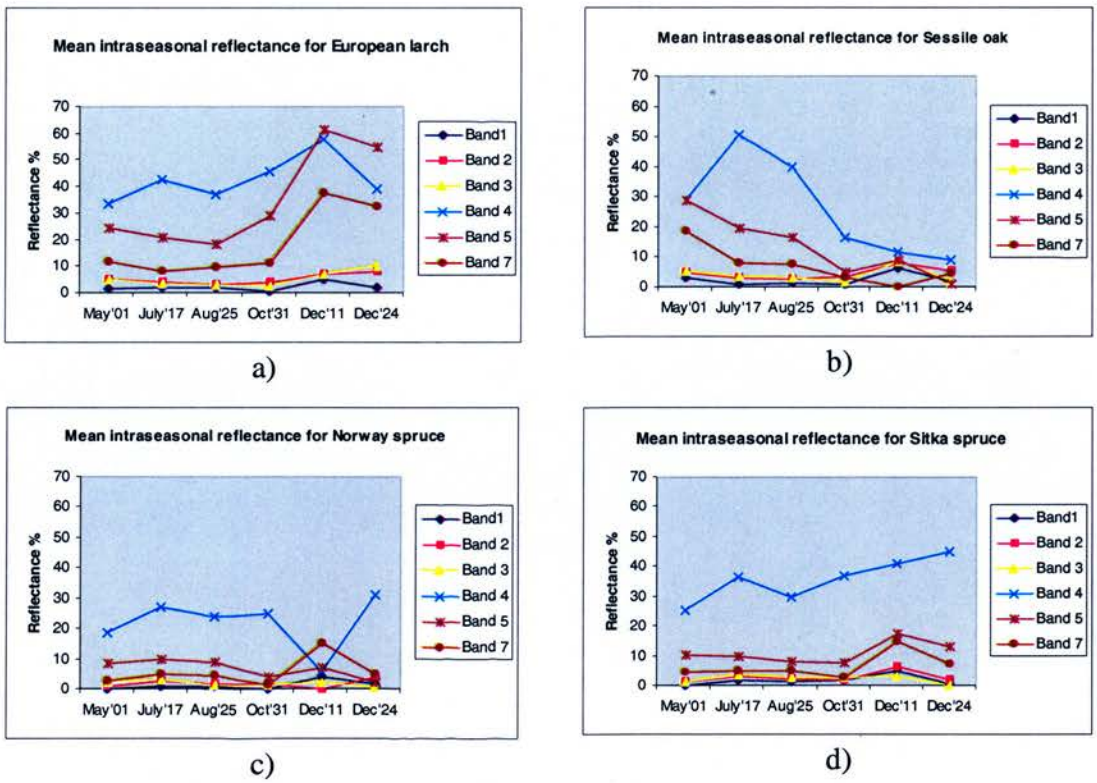

Figure 3.10: Mean intra-seasonal reflectance values for European larch (a), Sessile oak (b), Norway spruce (c), and Sitka spruce (d) .

The effect of normalisation errors is shown in figure 3.11.

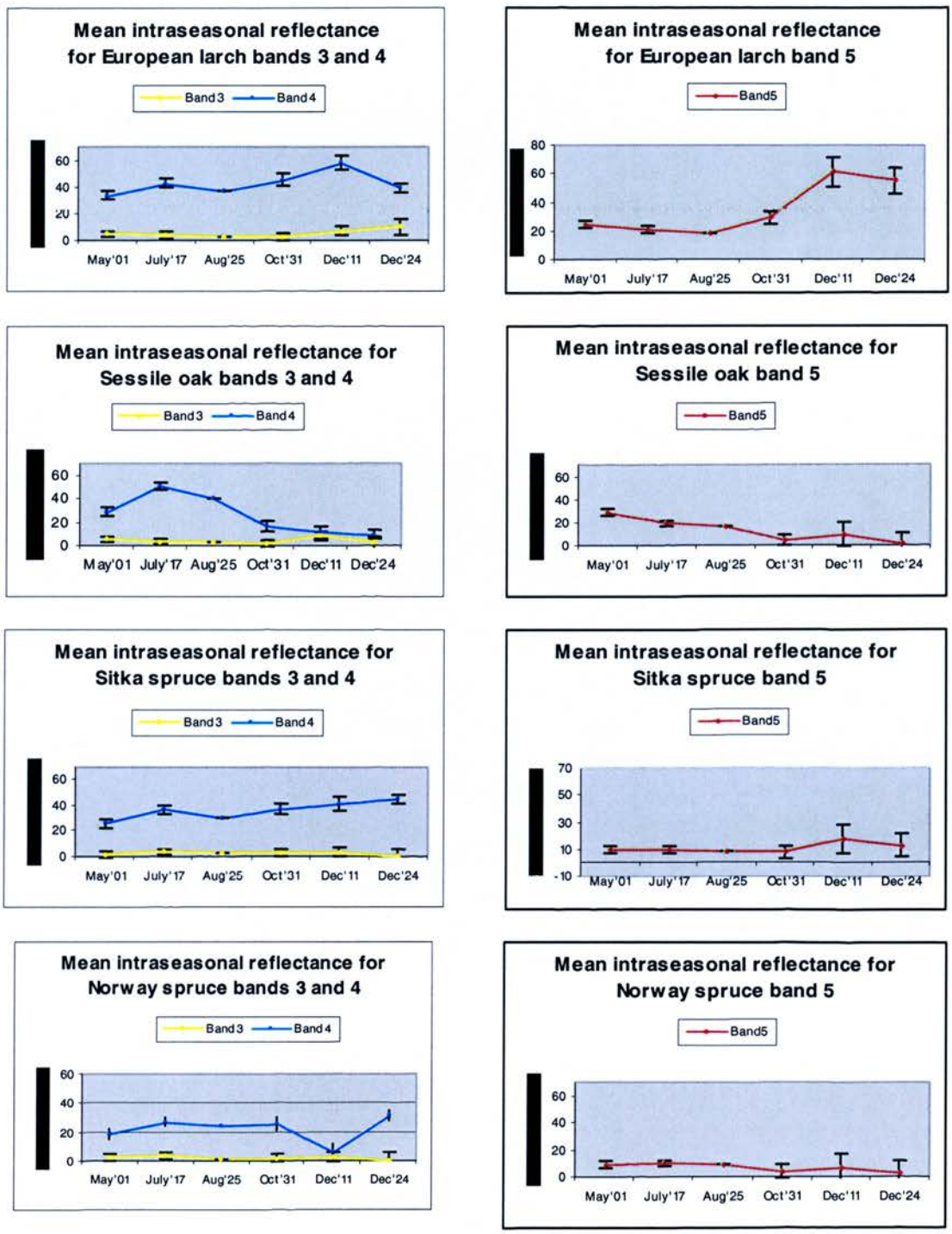

Figure 3.11: Mean intraseasonal spectral reflectances bands 3,4,5 for the species analysed with expected errors due to radiometric correction.

In figure 3.11, the largest error bars correspond to the winter imagery, indicating that the reflectance values extracted from these scenes might not be comparable with the ones extracted from the base-line dataset. Very low or high reflectance values specifically in band 4 for all species do not certainly conform to present research in the area. Although conifers have been shown to exhibit phenologies (Duchemin 1999), the satellite-observable manifestation of new needle and shoot growth is not as clear and marked as deciduous leaf development. Goetz and Prince (1996) have found that the phenological variation in spruce stands is negligible in closed-canopy stands, whereas discontinuous stands exhibit a slight seasonality due to variations in the amount of understorey vegetation background illuminated as solar zenith angles varies through the year. This emphasizes the necessity of acquiring ground data about the reflectivity of the understorey and overstorey, and the following of a rigorous processing method to minimize radiometric and atmospheric effects over the recorded species reflectance.

The observed reflectance for European larch in individual Landsat ETM+ bands is shown in figure 3.10a. The pattern is similar throughout the growing season and with rising reflectances in all bands taken in the midwinter imagery which might be a result of low leaf cover, low sun angles and bias introduce by the normalisation process. Visible bands (bands 1, 2, and 3) reflectances are slightly higher during leaf-off conditions (Dec'11 and Dec'24) than during leaf-on periods (May, July and August).

Sessile oak has a peak in reflectance in band 4 in the growing season and then has a declining reflectance through August. The sample size is small but both sites analysed showed this pattern (figure 3.10 b). Band 5 has a peak in May and continues decreasing to October, then reaches its lowest value throughout the winter period. This might be again the result of the combined effects from shadows, understorey vegetation cover and processing errors. Visible bands have expected lower reflectances from May to October. Bands 5 and 7 closely track visible band reflectance values for the imagery from October to December.

Figure 3.10 c corresponds to the observed mean intra-seasonal reflectance of Norway spruce species. Again, bands 1, 2, and 3 almost overlap showing that just one of them needs to be used in the band combination. Bands 5 and 7 follow almost the same pattern with peak in the December 2000 image. Band 4 reflectances exhibit a certain degree of stability except for the low value in the December 11 image. The reflectance value for the December'24 image, unusually high, might be product of radiometric errors.

Figure 3.10 d shows the mean intra-seasonal reflectances for Sitka spruce. The spectral response of this species is characterised by very low values for the visible bands, along with bands 5 and 7 and which show a very similar pattern to Norway spruce with peaks for all bands in the December'11 image. Band 4 for this species presents reflectance values higher than those of Norway spruce and unusually high reflectances during the winter period due to the errors on the normalisation process explained before.

One trend observed in all the species study plots is the consistent increase in Near Infrared Reflectance (NIR - band 4) between May and July indicating that this is a feature of the growing season. Other increases in NIR observed between August and December for European larch and Sitka spruce species were potentially linked to understorey reflectance and low sun angles. NIR reflectance was expected to be higher during leaf-on conditions and significantly lower during leaf off conditions for European larch but the reflectance values for the imagery taken in October and December are high, mainly as a consequence of radiometric normalisation errors. However, band 4 could be a good discriminator of this species as its values in all seasons are distinct from those for the other species.

In general, these results suggest that a multitemporal approach may be effective in characterizing the seasonal phenology of the species studied and in differentiating among them. The reduction of errors due to radiometric corrections may increase the correspondence of the patterns derived here with other work. Norway spruce and Sitka spruce have quite similar reflectance (visible, 5, and 7 bands), being higher in winter.

Band 4 reflectances are higher for Sitka spruce compared to Norway spruce in all seasons. European larch and Sessile oak had both the highest band 4 and 5 reflectances and the largest variability among seasons. European larch also had somewhat elevated band 5 and 7 reflectances compared to other species, while Norway spruce had lower reflectances in the same bands during May through August and Sessile oak the lowest band 4,5,7 reflectances in winter. The unusually low reflectance in band 4 for Norway spruce in the December 11 image and the high reflectance value in the same band and date observed for Sitka spruce might be explained by a combination of errors introduced in the processing, especially related to problems with the radiometric correction, and low sun angle and background effects (shadows and canopy cover). Reflectances extracted from the December imagery showed the most variable and unexpected values for all species and also the largest error bars derived for the radiometric correction and normalization process.

The potential for spectral discrimination of European larch and Sessile oak species was apparent even before correction of the reflectance data. Differences were apparent in the relative magnitude of reflectance of NIR wavelengths by these species. It was more difficult to establish reflectance differences between the spruce species. However, their spectral signatures show small but discrete differences in the magnitude of the NIR reflectance which could potentially aid in their mapping. In conclusion, the band in which a better separation of species can be carried out is band 4 and the date of imagery that best show a maximum contrast among spectral reflectances was the July 2000 image when differences in band 4 were maximal. However, no single date appeared to be ideal to discriminate the four species suggesting that a combination of two or three datasets covering their phenological cycles will be optimal for their differentiation. In this study the images that best portrayed the spectral characteristics of the marked species, apart from the July image, were 01.05.2001 and 31.10.2001. The main phenological characteristics observed in the imagery are that earlier in the seasonal cycle (May 01), the foliage is definitely not fully developed while in the latter imagery (August 25) the

deciduous species (Sessile oak) and European larch have maximum foliage and chlorophyll content.

Chen and Cihlar (1996) found that late spring TM images (such as the May 2001 in this study) were superior to summer images for determining overstorey leaf area index in boreal forest because the effect of the understorey was minimized in the spring, before the full growth of the understorey. However, they also reported that spectral differentiation for the species under study was too small to allow species identification using this imagery. Maselli *et al.* (2005), in the retrieval of forest attributes from multitemporal Landsat ETM+ images, reported that image dates that rendered best results were at the beginning or end of the growing season.

The imagery captured in December showed potential problems that mainly resulted from a combination of poor radiometric correction and low sun angles that cause excessive shadowing of the features. The general spectral responses for different species and seasons might be explained by shadowing effects related not only to the topography but to the heterogeneous nature of the forest as it is known that the multispectral signatures derived from sensors such as Landsat ETM+ are the measure of a composite of stand structure, tree density, and cover condition impacted to varying degrees by atmospheric and terrain influence (Jiang *et al.* 2004). Other factors include solar zenith angle, background reflectance and stand structure. Further studies should be carried out to develop a rigorous spectral characterisation of the species in question utilising a longer sequence of images. The calibration of such scenes with in situ measurements is highly desirable.

This study has analyzed a number of Landsat ETM+ images to characterize the vegetative phenology of four tree canopies in order to understand the advantages in considering multitemporal datasets. Much of the spectral change is related to plant growth and development, but some also relates to changing background properties and processing errors. All the species analyzed had particular seasonal patterns of reflectance.

In the earlier images (17.07.2000, 25.08.2000, and 01.05.2001), European larch and Sessile oak showed a similar pattern as did also Norway and Sitka spruce. The most significant spectral differences occur in the late October image when European larch and Sessile oak are in a leaf-off stage. However, lack of available ground information by the time of data acquisition, such as status of vegetation and type of vegetation during a particular time interval, often makes it difficult to determine the biological reasons behind the reflectance changes (Vogelmann and DeFelice 2003). Nilson and Peterson (1994) have found that the stability of crown closure and LAI accounts for the relative stability of forest reflectance over a long time of period, in spite of the fact that essential forest inventory parameters (tree height, dbh, volume) keep increasing until maturity.

3.6 Normalized Difference vegetation Index (NDVI)

Since information contained in a single spectral band is usually insufficient to characterize vegetation status, vegetation indices are usually developed by combining spectral bands (Qi *et al.* 1994). The combination may be in the form of a ratio, a slope, or some other information (Rondeaux *et al.* 1996) and aims is to enhance the spectral characteristics of the vegetation in order to derive its biophysical properties. Vegetation Indices (VI's) are dimensionless, radiometric measures that indicate relative abundance and activity of green vegetation, including Leaf Area Index (LAI), percentage green cover, chlorophyll content, green biomass, and absorbed photosynthetically active radiation (PAR) (Jensen 2005).

A vegetation index is formed from combinations of reflectances in several spectral wave bands that are added, divided, or multiplied in a manner designed to yield a single value that indicates the amount or vigour of vegetation within a pixel (Campbell 2002).

The NDVI is an intrinsic index that does not involve any external factor other than the measured spectral reflectances and is calculated by the following expression (Gemmell 1999):

$$NDVI = \frac{\rho_{NIR} - \rho_R}{\rho_{NIR} + \rho_R} \quad \text{.....[3]}$$

where ρ_{NIR} is the near infrared reflectance and ρ_R is the red reflectance. The index operates by contrasting intense chlorophyll pigment absorptions in the red against the high reflectivity of plant materials in the NIR (Elvidge and Chen 1995). Thus high NDVI values indicate high leaf biomass, canopy closure, or leaf area.

There are a significant number of studies that show that NDVI values can be affected by atmospheric effects (Myneni and Asrar 1994), spectral bandwidth (Teillet *et al.* 1997) and background reflectance (McDonald *et al.* 1998, Trotter *et al.* 1997, Nel *et al.* 1994). The latter issue was further explored by Gemmell (1999) in a study to determine the background effects on coniferous forest spectral signatures, concluding that NDVI, although it does not specifically account for soil line effects, performed better than the Soil Adjusted Vegetation Index (SAVI), and was insensitive to near-infrared background variations and slope-aspect effects.

The literature reports that several biotic and abiotic factors may influence the seasonal trends of the NDVI of a particular forest site. These factors include the phenological changes in forest Leaf Area Index (LAI) caused by climate, the proportion of the surface cover types contributing to the overall reflectance, and the effects resulting from variations in the solar zenith angle (Spanner *et al.* 1990). Shadowing effects are also important in the case of sparse vegetation canopies, low sun elevations, for example, in winter or at high latitudes, or in the case of large satellite view angles. Leblon *et al.* (1996) showed that NDVI is highly sensitive to the amount of shadowing in a forest canopy.

Solar zenith angle effects are also pronounced when comparing NDVI values at different times during the year. Lower sun angles and increased shadow in the winter months also serve to reduce NDVI values. Shadowing probably plays an important part in the response of all bands and is thought to be at least as important as canopy water content in determining the mid-infrared response (Trotter *et al.* 1997)

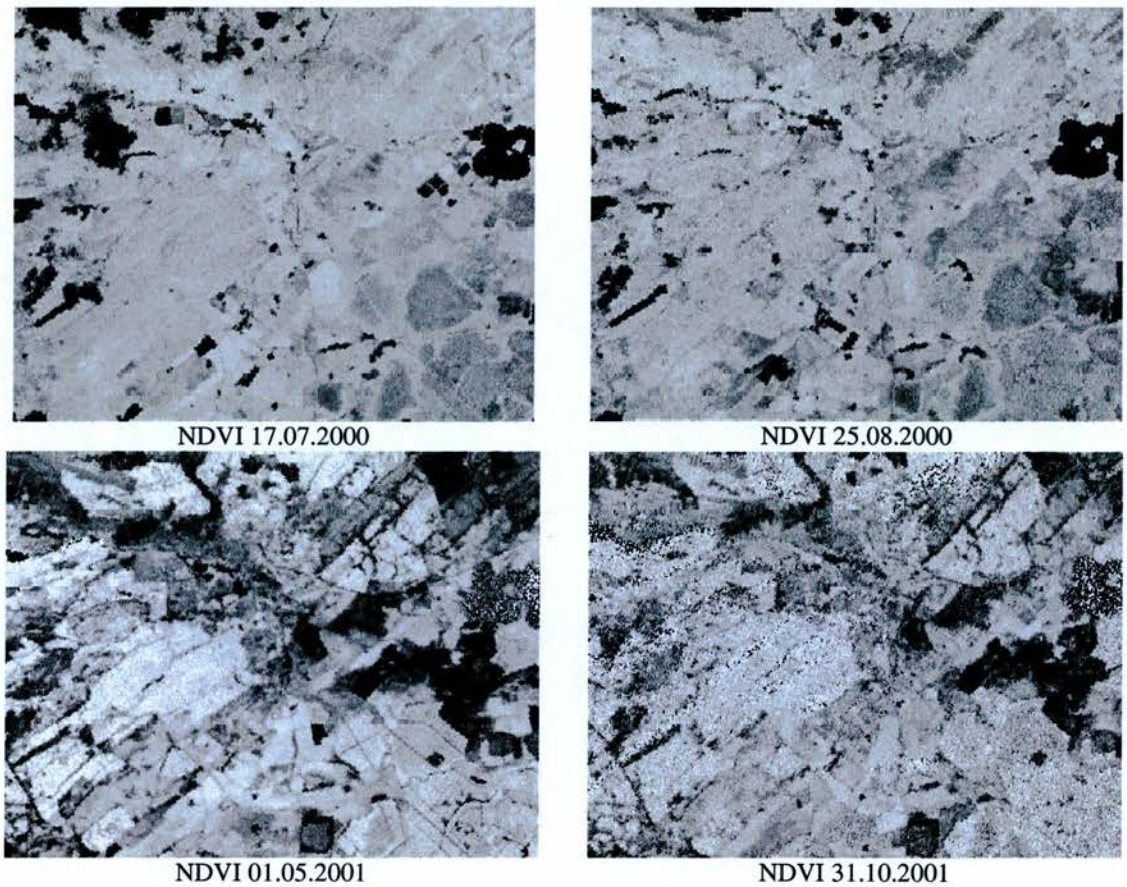

Figure 3.12: NDVI imagery scale 1:140000 over Aberfoyle area derived from four Landsat ETM+ scenes.

Despite its influence from extraneous factors, the ease of calculating NDVI from various types of satellite data, the success of the NDVI in detecting vegetation and its ease in interpretation has made it a popular vegetation index (Wilson and Sader 2002). NDVI was computed for each date of imagery 1G level (radiometrically and geometrically corrected) and the images derived from four of the dates are shown in figure 3.11.

Differences in brightness intensities for the imagery are evident in these NDVI images, with the October imagery showing saturated values in darker areas. Figure 3.13 shows the extracted seasonal NDVI values for the species and stands studied.

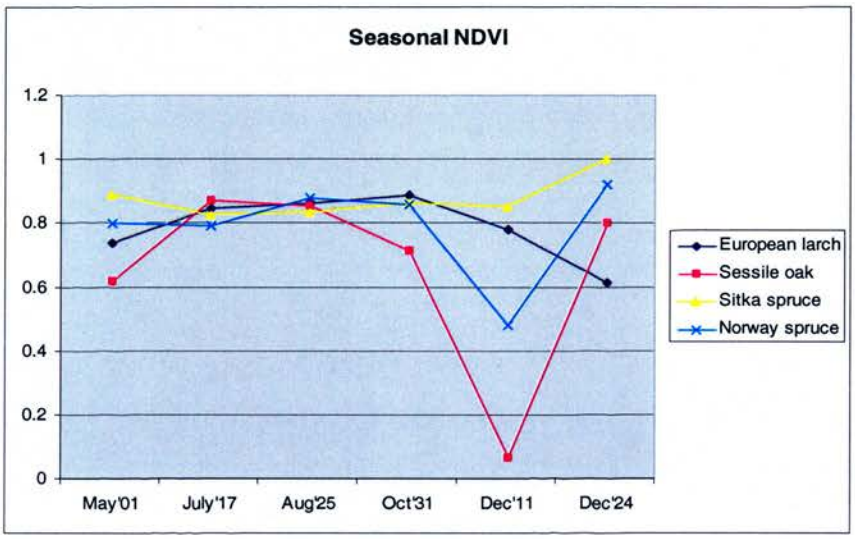

Figure 3.13: Seasonal NDVI values for the species under study.

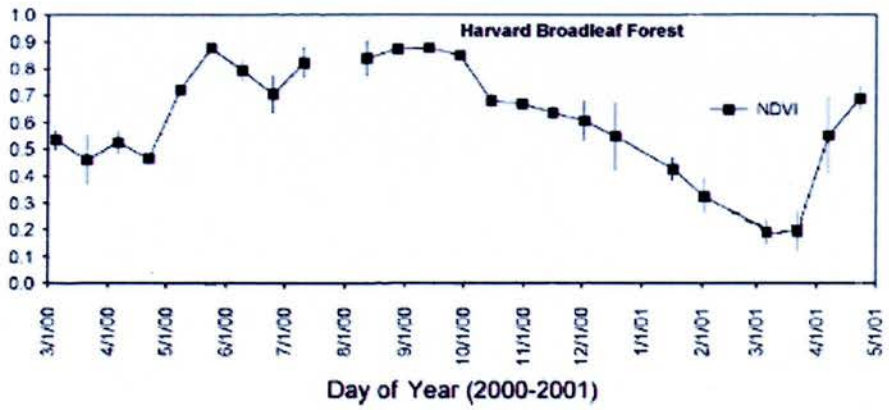

Figure 3.14: Seasonal NDVI values from a broadleaf forest in USA (adapted from Huete *et al.* 2002).

On a seasonal basis, there are similar trends in the NDVI response between species. NDVI values were almost constant for Sitka spruce and Norway spruce, ranging between 0.8 and 0.9, except for the values observed in the December imagery. Although the Sitka

spruce NDVI kept within that range for most of the observed time, the Dec'24 image registered an increase for this species. This increase might not represent a phenological change but an effect from sun angle, background reflectance, or/and radiometric errors as discussed before. In contrast, NDVI decreased dramatically in the Dec'11 scene for the Norway spruce species. For that scene, oak and Norway spruce stands appear very dark leading to low NDVI values (figure 3.15). The lack of ground information about the particular conditions of sites on those dates makes it difficult to explain the exact reasons behind the changes in reflectance for those sites at this time but the low sun angle along with shadow combined with the background effects and radiometric errors may be responsible for this spectral response.

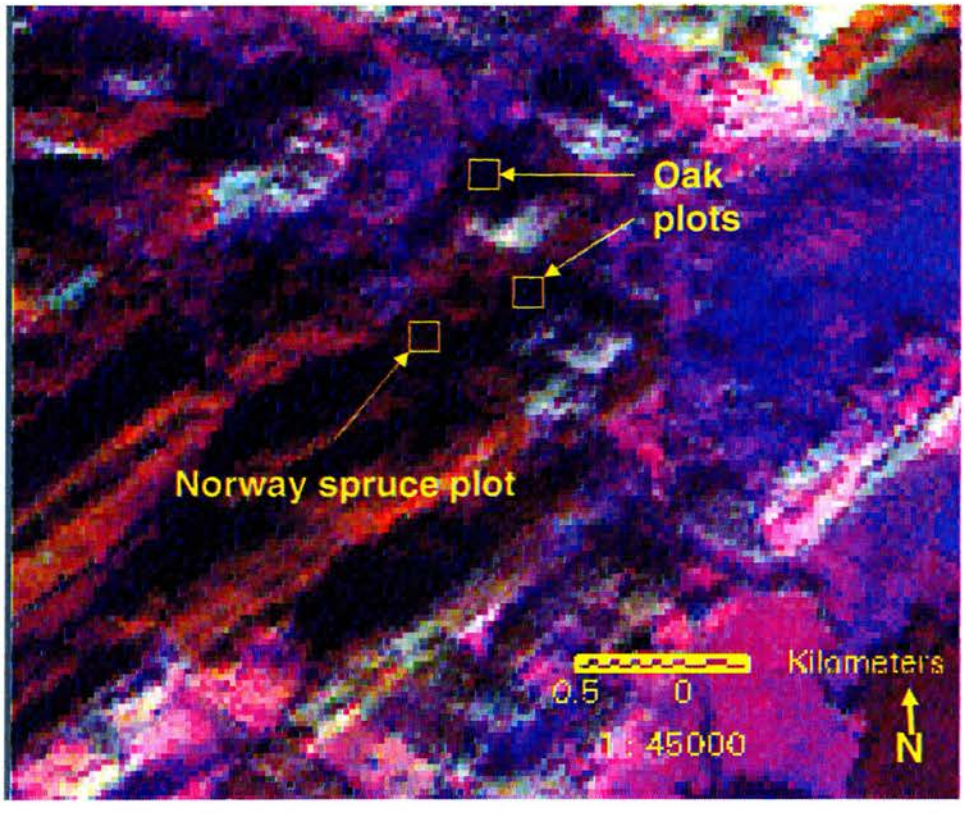

Figure 3.15: ETM+ image acquired on 11.12.2001. The yellow boxes show the location of Oak and Norway spruce plots which appear very dark in this scene.

Sessile oak presents an increasing NDVI value from May to July, remaining relatively stable until late August when it decreased through October until December. Other studies investigating phenology have reported a similar pattern (figure 3.12) for other deciduous

species (Vogelmann and DeFelice 2003, Kodani *et al.* 2002, Huete *et al.* 2002). In a phenological study on a broadleaved deciduous stand of Japanese beech (*Fagus crenata*), Kodani *et al.* (2002) measured continuous reflectance during the growing season for this species. The results showed that canopy attributes increased rapidly in spring, were stable in summer, and decreased in autumn so that patterns of the reflectance clearly changed during the growing season. They also reported that to detect the processes and the turning points of the canopy phenology in the deciduous forest, it was necessary to measure reflectance at least once a week, especially in the flushing season.

Both Sessile oak and European larch species showed a trapezoidal response, being more defined in the oak species. In other words, NDVIs rose during the spring and decrease during autumn, closely tracking the development of the forest vegetation on these sites. However, in the October image an increase in the European larch NDVI occurred while the Sessile oak NDVI decreased. At this leaf-off stage, the influence of background reflectance on radiometric response is more accentuated. Given that these sites are different in density and in vegetation cover, this dissimilar response might be influenced by these two factors.

The amplitudinal differences in the species NDVI values observed in May suggests that discrimination between species may be more successful at this time of the year as opposed to periods later in the growing season. However, these differences are in a limited range of 0.6 to 0.9 which might not be good enough for species discrimination. Winter imagery also shows similar differences between coniferous and broadleaved species but as has been discussed other factors may make the retrieval of reflectance values a difficult task with no reliable results at this time of the year. In conclusion, NDVI has showed less ability to portray spectral differences between species than raw band reflectances.

Another problem related to NDVI is that it tends to saturate at high levels of leaf area index. In addition, problems related to the use of NDVI in the boreal zone have been reported (Eklundh *et al.* 2001, Nilson *et al.* 1999, Häme *et al.* 1997, Chen & Cihlar,

1996). These studies indicate that NDVI may not be a dynamic enough index to be suitable for leaf area index estimation in coniferous regions as the range of NDVI of boreal coniferous forests is typically narrow, and where the index reaches nearly saturated values at moderate values of LAI.

3.7 Principal Components Analysis (PCA)

PCA is an approach that can be used to characterize land cover types from multitemporal datasets. It has been successfully employed in remote sensing for image data transformation, information compression, and change detection analysis (Hirosawa *et al.* 1996, Cihlar *et al.* 1996). In essence, PCA identifies the optimum linear combinations of the original bands from satellite data that can account for the variation in pixel values in an image (Campbell 2002). Linear combinations are of the form

$$A = C_1X_1 + C_2X_2 + C_3X_3 + C_4X_4 \quad [4]$$

where X_1, X_2, X_3, and X_4 are pixel values in four spectral bands, and C_1, C_2, C_3, and C_4 are coefficients applied individually to the values in the respective bands. Principal components are derived from the original data such that the first principal component accounts for the maximum proportion of the variance of the original dataset (usually variations in intensity), and subsequent orthogonal components account for the decreasing proportions of the remaining variance (Jensen 2005). Thus, this method reduces the number of bands to be examined while simultaneously retaining as much information as possible and reducing contributions from noise and other data errors.

PCA was applied to all ETM+ images acquired for the study but only the data corresponding to the base line image (25.08.2000) is shown in the following tables. Table 3.4 shows the statistics used in the Principal Components Analysis of this image.

Univariate statistics						
Band Number (μm)	**1 0.45 – 0.52**	**2 0.52 – 0.60**	**3 0.63 – 0.69**	**4 0.76 – 0.90**	**5 1.55 – 1.75**	**7 2.08 – 2.35**
Mean	14.57	17.53	19.062	76.262	47.512	26.935
Standard deviation	24.799	27.273	28.716	61.469	41.425	26.906
Minimum	1	1	1	1	1	1
Maximum	154	185	180	255	255	194
Correlation Matrix						
1	1					
2	0.979	1				
3	0.977	0.993	1			
4	0.361	0.515	0.497	1		
5	0.637	0.754	0.761	0.884	1	
7	0.838	0.898	0.915	0.686	0.922	1

Table 3.4: Statistics for the base-line imagery (25.08.2000) used in the Principal Components Analysis (PCA).

The linear transformation required is derived from the correlation matrix of the original dataset. The transformation is computed from the original spectral statistics as in Jensen (2005). Eigenvalues $E = [\lambda_{11}, \lambda_{22}, \lambda_{33}, ..., \lambda_{nn}]$ and eigenvectors $EV = \lfloor a_{kp} ...\text{for } k = 1 \text{ to } n \text{ bands, and } p = 1 \text{ to } n \text{ components} \rfloor$ of the correlation matrix were calculated for the imagery (table 3.5).

	Component *p*					
Band	1	2	3	4	5	6
1	0.028	-0.093	-0.402	-0.076	0.289	-0.860
2	0.084	-0.134	-0.475	-0.399	0.602	0.477
3	0.060	-0.207	-0.570	-0.276	-0.740	0.067
4	0.866	0.491	-0.075	0.056	-0.030	-0.005
5	0.456	-0.702	0.443	-0.306	-0.002	-0.090
7	0.176	-0.443	-0.292	0.813	0.073	0.143
Eigenvalues	1981.82	198.12	15.45	3.47	1.97	1.42

Table 3.5: Eigenvector matrix for Principal Components Analysis for the 25.08.2000 image.

Analysis of the PCA statistics for all the multidate images showed that correlation matrices and derived eigenvalues and eigenvectors were similar to those for the 25.08.2000 image presented above, as shown in table 3.6.

Image 17.07.2000						Image 24.12.2000					
0.11	-0.35	-0.43	0.21	0.60	0.50	0.02	-0.01	-0.06	-0.17	0.19	-0.96
0.16	-0.35	-0.40	0.09	0.11	-0.81	0.09	-0.01	-0.12	-0.42	0.85	0.26
0.13	-0.40	-0.32	0.13	-0.78	0.27	0.14	-0.13	-0.28	-0.79	-0.48	0.07
0.83	0.49	-0.20	-0.06	-0.02	0.03	0.66	0.73	-0.09	0.05	-0.04	0.00
0.43	-0.38	0.68	0.42	0.05	-0.02	0.64	-0.50	0.57	0.00	0.00	0.00
0.21	-0.42	0.15	-0.85	0.06	0.06	0.33	-0.42	-0.75	0.38	0.03	0.00
Image 01.05.2000						**Image 31.10.2001**					
0.08	-0.08	-0.34	-0.05	-0.48	-0.79	0.03	-0.04	-0.22	-0.08	-0.52	-0.81
0.15	-0.07	-0.46	-0.02	-0.61	0.60	0.10	-0.04	-0.34	-0.08	-0.72	0.57
0.21	-0.26	-0.68	0.30	0.56	-0.02	0.11	-0.22	-0.82	0.36	0.35	-0.02
0.55	0.81	-0.10	-0.08	0.09	-0.03	0.77	0.62	-0.04	-0.03	0.07	-0.02
0.68	-0.34	0.42	0.45	-0.15	-0.02	0.55	-0.63	0.37	0.38	-0.11	-0.01
0.38	-0.35	0.03	-0.83	0.16	0.02	0.25	-0.40	-0.12	-0.84	0.22	0.01

Table 3.6: Eigenvector matrix of four images for Principal Components Analysis.

The eigenvalues contain important information. For example, it is possible to determine the percent of total variance ($\%_p$) explained by each of the principal components, using the equation:

$$\%_p = \frac{eigenvalue\lambda_p \times 100}{\sum_{p=1}^{6} eigenvalue\lambda_p} \quad \text{.....[5]}$$

Where λ_p is the pth eigenvalue out of the possible n eigenvalues. For example, the first principal component (eigenvalue λ_1) of the ETM+ base-line image accounts for 89.99% of the variance in the entire dataset (table 3.7). Component 2 accounts for 8.99% of the remaining variance. Cumulatively, these first two principal components account for 98.98% of the variance. The third component just accounts for another 0.7%, bringing the total to 99.68% of the variance explained by the first three components. Thus, the seven band ETM+ image might be compressed into just two or three new principal components images (or bands) that explain 98.98% to 99.68% of the variance.

Component	**1**	**2**	**3**	**4**	**5**	**6**
Variance(%)	89.99	8.99	0.70	0.17	0.09	0.06
Cumulative	89.99	98.98	99.68	99.85	99.94	100.00
			Component *p*			
Band	**1**	**2**	**3**	**4**	**5**	**6**
1	0.209	-0.459	-0.309	0.015	0.721	-0.365
2	0.262	-0.419	-0.313	-0.204	-0.075	0.781
3	0.273	-0.454	-0.161	-0.065	-0.677	-0.481
4	0.697	0.587	-0.385	0.141	-0.008	-0.037
5	0.494	-0.017	0.667	-0.541	0.130	-0.037
7	0.297	-0.250	0.432	0.801	0.002	0.148

Table 3.7: Eigenvectors computed for the covariance matrix found in table 3.3 for the ETM+ 25.08.2000 image.

Once the eigenvectors for the covariance matrix has been calculated, it is possible to calculate a new matrix filled with factor loadings which indicate the correlations between ETM+ bands and principal components.

This new matrix is calculated as:

$$R_{kp} = \frac{a_{kp} \times \sqrt{\lambda_p}}{\sqrt{Var_k}} \quad \text{.....[6]}$$

Where

a_{kp} = eigenvector for band k and component p

λ_p = pth eigenvalue

Var_k = variance of band k in the covariance matrix

The calculated factor loadings are displayed in table 3.8.

	Component *p*					
Band	**1**	**2**	**3**	**4**	**5**	**6**
1	0.37	-0.270	-0.048	0.001	0.040	-0.017
2	0.421	-0.213	-0.044	-0.014	-0.003	0.033
3	0.417	-0.219	-0.022	-0.004	-0.033	-0.019
4	0.496	0.132	-0.024	0.004	-0.002	-0.007
5	0.534	0.006	0.063	-0.024	0.004	-0.001
7	0.485	0.129	0.062	0.055	0.001	0.006

Table 3.8: Correlations (factor loadings) between principal components and ETM+ bands for image 25.08.2000.

The structure of the principal components extracted from the ETM+ data were similar to those observed in other studies (Basham *et al* 1997, Almeida-Filho and Shimabukuro 2002, Price *et al.* 2002). For the base line image, the first principal component (Component 1) accounted for >89 per cent of the total variance (table 3.7) and was positively correlated with all bands (table 3.8). Thus, this component could be interpreted as an overall brightness component. The second component had negative correlations with bands 1, 2, 3 (table 3.8) and positive correlation with the near-infrared band and could be interpreted as a vegetation component.

The third component consists of both near and middle infrared information (bands 4, 5 and 7). This component explained a negligible amount (i.e., <1 per cent) of the total variance along with the subsequent components. Thus, the six-band ETM+ data can be reduced in dimension to just two principal components (1 and 2) which account for 98.98 % of the variance.

The highest correlations (i.e., factor loadings) for principal component 1 were for bands 4, 5, and 7 (0.496, 0.534, and 0.485, respectively; table 3.8). These values correspond to the near and middle infrared reflectance bands and could explain the brightness exhibited

by golf courses and other types of vegetation including some forested regions (figure 3.16a).

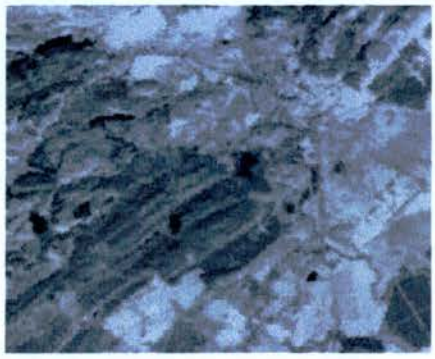

a) Principal Component 1

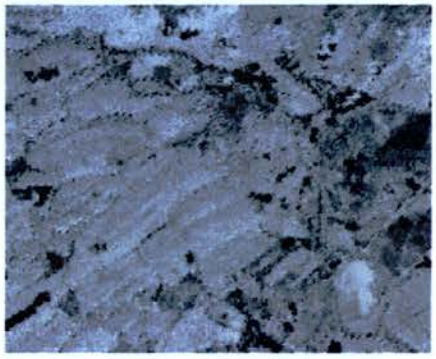

b) Principal Component 2

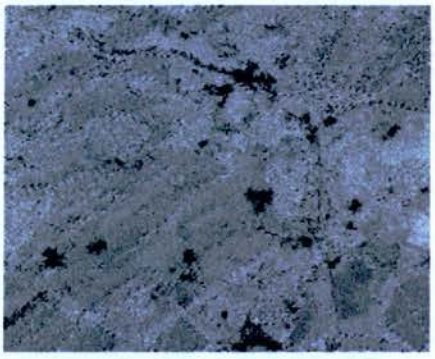

c) Principal Component 3

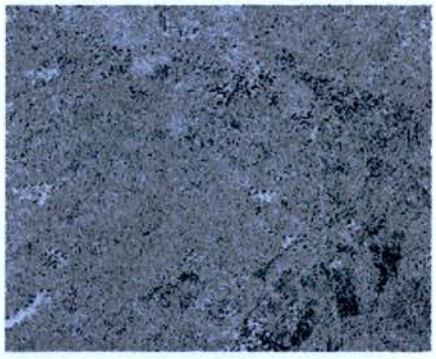

d) Principal Component 4

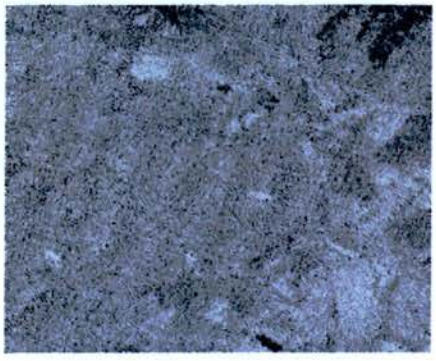

e) Principal Component 5

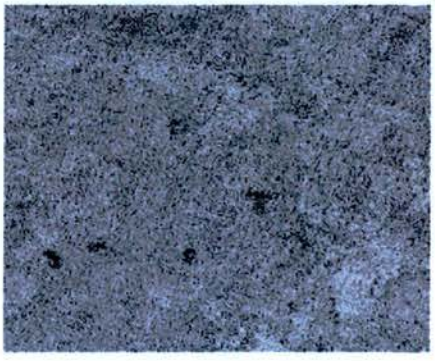

f) Principal Component 6

Figure 3.16: Principal Component images of Elizabeth Forest Park II derived from Landsat ETM+ imagery obtained on 25 August 2000.

Results showed that the first three PCA images concentrated more than 99% of the total variability of the data, for all the dates considered. A false colour composite of those first three components is showed in figure 3.16 for four of the images analysed.

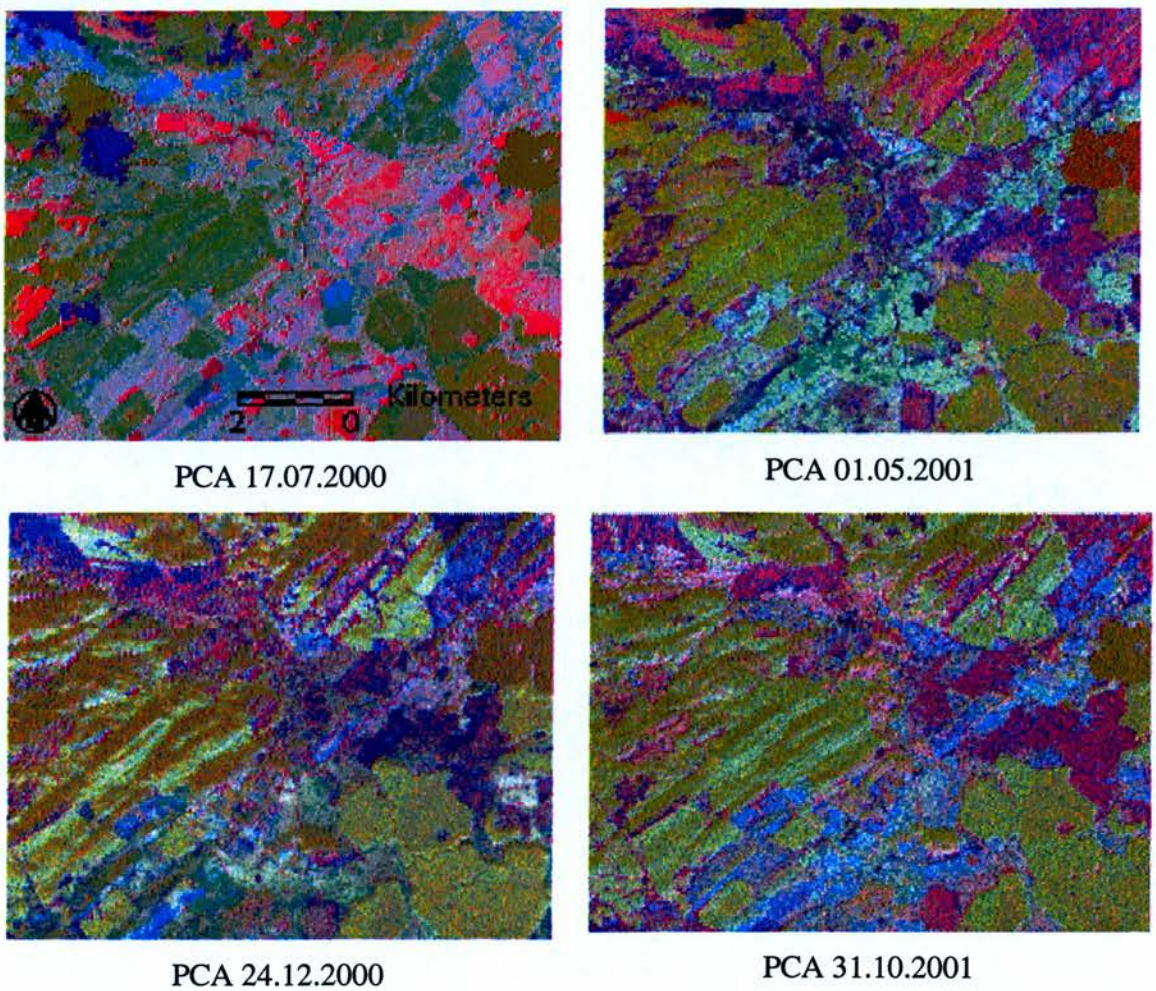

Figure 3.17: False colour composite of the three first principal components for four acquisition dates.

As has been demonstrated in previous multitemporal research (Hirosawa *et al.* 1996), the first two PCs may represent accumulated greenness during the temporal analysis period of analysis (the first PC) and the seasonal variation of vegetation (the second PC). These authors found that the elements of the first PC eigenvector were positive, higher in value, and very consistent over the period of analysis, while the elements of the second PC

exhibited a cyclical pattern or seasonal variation. They concluded that the first PC serves as a means of quantifying the density and photosynthetic activity of vegetation while the second PC can quantify the seasonal pattern of vegetation change.

Figure 3.18 displays the eigenvector coefficients plotted against date for the highest, lowest, and mean PCA second component scores. The profile of the second PC appears to explain a pattern of vegetation change for the study area throughout the year. The higher score of the second PC indicates a seasonal vegetation change pattern for the subset data from May to December, with greater photosynthetic activity in spring (May) and decreased activity during summer (August) after which it begins to increase again. The lower score of the second PC pixels exhibit the opposite seasonal change pattern but the highest value is still in May. The mean score pixels exhibit almost no seasonal change pattern with a peak in December where it is suggested that low sun angles introduce artifacts in the imagery.

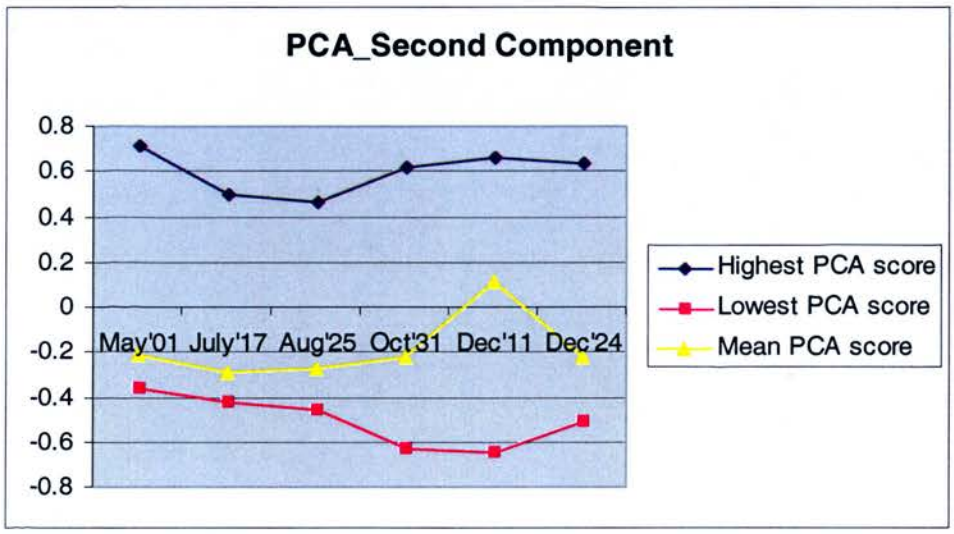

Figure 3.18: High, low and mean scores of the Second Principal Component showing the seasonality of the values through time.

These results indicate that seasonal change may be estimated using the values of the second component of principal analysis. Although the contribution of this component to the total variation is small (8.99%) in comparison to the contribution of the first

component (89.99%), it is possible to discriminate its information by using PCA and to characterize inter-annual variation.

In order to evaluate the ability of PCA to characterize the species from a phenological point of view, the pixel values of the second component analysis corresponding to the four species analyzed were extracted from the imagery and displayed as seen in figure 3.19.

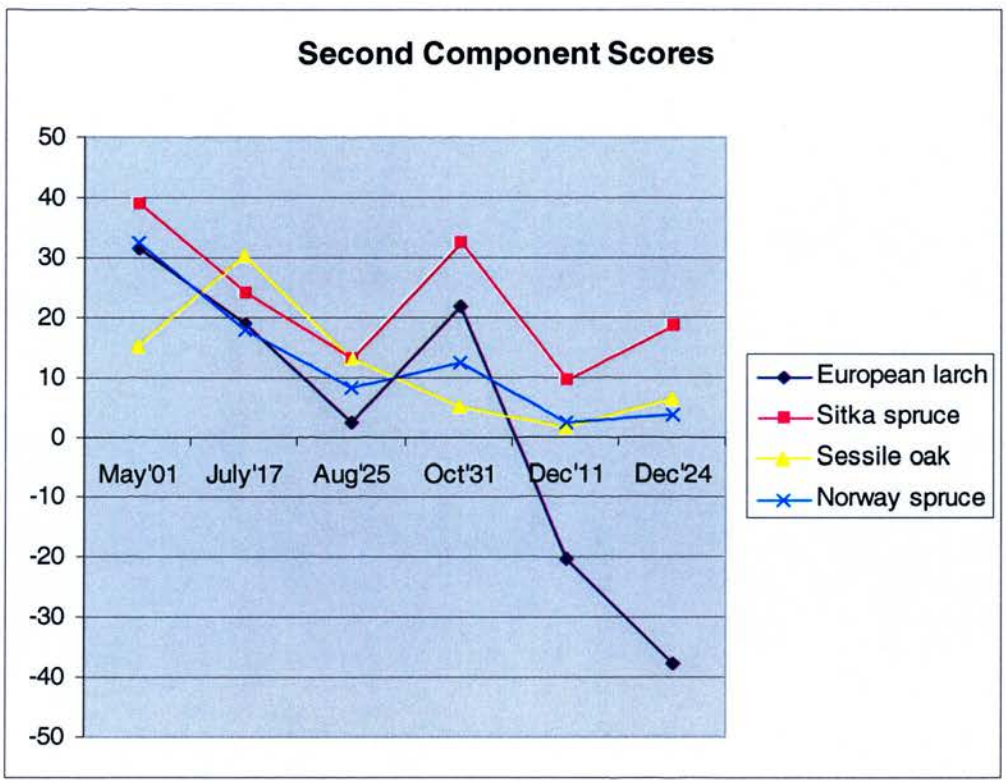

Figure 3.19: Second Principal Component scores for the tree species showing the seasonality of the values trough time.

As in the previous analysis using the raw band and NDVI data, Sitka spruce and Norway spruce show a similar seasonal pattern. Sessile oak exhibits the lowest second PC score in March, peaks with the highest score in the following image (July) and then decreases for the remainder of the growing season. On the other hand, European larch shows a similar pattern during the growing season to the other coniferous species but shows markedly lower, and negative PC2 scores in the winter scenes. As the reflectance of the stand is

influenced by the reflectance of the understorey, it is possible that the second component scores not only reflect the seasonality of the main species but that of the understorey vegetation as well. This might explain why two species (Sessile oak and European larch) that have a very similar NDVI values in May, exhibit quite different PCA second component scores.

In contrast with the NDVI pattern for the spruces with little variability through the year, the second PCA component shows greater variability for these species between dates. The range of values is also larger (0 - 40) which allows for a better discrimination accuracy. The greatest differentiation between species for the second PC on any single date was observed in October with Sitka spruce exhibiting the highest value and Sessile oak the lowest.

In general, it seems that PCA is able to capture better the subtle spectral differences among species than NDVI with October imagery showing the greatest amplitudinal differences among them. The second PC reflects the seasonal vegetation change patterns throughout the time shown in figure 3.18 which contributes 8.99% to the total variance in the dataset. Although further investigation is required, there is evidence to suggest a potential difference in PCA pattern between coniferous and broadleaved species (contrast Sessile oak to the other species) and between deciduous and evergreen coniferous species (e.g. December second PC scores for European larch in comparison to the spruce species). Overall, the evidence would suggest further investigation of PCA as a tool for multitemporal analysis of forest types, is warranted.

3.8 Discussion of the results

The use of ETM+ data in this forested environment was aimed at the study of the reflectance of four tree species that characterize the Aberfoyle area, and to the analysis of the effects that seasonal changes have on the reflectance responses of those species. The goal was to present a preliminary analysis on how spectral seasonality might affect the

relationship between vegetation indices such as NDVI and LAI and other derived forest parameters for these canopies.

One of the main constraints to the study was the limited number of images available for the seasonal characterization and the lack of ground information related to site conditions on the specific image acquisition dates. The temporal resolution of the Landsat satellite along with cloudy Scotland conditions resulted in the availability of just a few cloud-free scenes. Full utilization of phenological changes would require that the development of the canopy could be followed at a greater temporal frequency through the year, and that the imagery would be available at the right times. The latter requirement is rather difficult as the number of useable images is limited due to cloud cover.

Another limitation of this study is related to the lack of direct field measurements that enable the accuracy assessment of the satellite-derived results. Although the results achieved in this research offer an insight on the phenology of the species analysed in a local ecosystem, direct measurements of the temporal variability and differences between deciduous and coniferous canopies are required to validate seasonal patterns derived from remote sensing data. The measurement *in situ* of the spectral characteristics of the understorey can be used to reproduce the spectral signatures of the types of ground vegetation which are needed in simulating the reflectance spectra of the forest stands.

The accurate determination of the seasonal variations of the species reflectance through field measurements and Landsat imagery would form a reliable source for the validation of phenology derived from broader spatial and spectral resolution datasets and help to bridge the gap between large scale remote sensing and local measurements. Despite the large number of *in situ*, plot-level phenological measurements and satellite-derived phenological studies, there has been little success to date in merging these records temporally or spatially (Fisher *et al.* 2006). The main problems lay in the large spatial differences between the two methods and in the differences in phenological measures between local studies and broad scale measurements derived from satellite data. Recent

research (Fisher *et al.* 2006) has explored this issue by using a large series of Landsat scenes (57) to derive the phenology of an area in the United States. This study showed that the derivation of fine spatial scales of phenological variability through satellite imagery will require a rigorous processing of this data considering the following aspects: 1) proper spectral calibration between scenes, 2) account for forest and ground cover composition, 3) accurate knowledge of dates of phenological key processes, 4) temporal uncertainty imposed by compositing methodologies.

Atmospheric correction was restricted by the lack of atmospheric information related to ozone concentration and water vapour content in the atmosphere at the time of acquisition, which were required if a rigorous correction was to be carried out using the 6S atmospheric correction method. Instead, the image-based COST method was chosen as it uses the information contained in the imagery for the correction. A normalisation process using Pseudo Invariant Features was subsequently used to eliminate the residual errors. The difficulty of the PIF method laid in the selection of features whose reflectance properties do not change through time and which are also spectrally homogeneous targets. The results obtained after atmospheric correction and PIF normalisation showed that the reflectances values among datasets were comparable with the exception of winter dates. However, recent research (Paolini *et al.* 2006) has showed that the high levels of positive correlation between PIFS do not imply a successful radiometric normalisation. The analysis of the spectral variability of the PIFs through time showed significant deviations, which underlines the importance of a careful radiometric correction and of adequate calibration capabilities. Therefore, it is suggested that further research should make use of a methodology for the assessment of the normalisation process. Paolini *et al.* (2006) proposed the use of an algorithm for improved PIFs selection and the assessment of the quality of the radiometric corrections through the use of the Quadratic Difference Index. This method has been validated and achieved an accuracy of >80%.

Other aspects that made the analysis more complex was the high spatial variability in the spectral signatures for specific species and the difficulty in finding pure pixels

representing each species. Further analysis is required to establish the nature of variation in seasonal spectral reflectance within individual plots and species.

Registration of the ETM+ imagery to the OSGB coordinate system was carried out using Map to Image registration and Co-registration. The limitations to these processes were fundamentally in the availability of enough control points upon which to base the transformation between images. Most of the features selected were located in the surroundings of the study site, particularly in the Glasgow area where man made features were abundant. In order to achieve good control points distribution some natural features had to be selected mainly in the north part of the scenes. Nevertheless, registration accuracies of about 1 pixel were achieved.

The selection of the best subsets of bands or band transformations for the analysis of the temporal characteristics of species spectral reflectance and for discriminating and predicting forest attributes requires an understanding of the dominant radiometric interactions that take place within a ETM+ scene. In this way, bands 4,5,3 were chosen for the display of features although all raw ETM+ bands were analyzed in order to determine the species' seasonal reflectance trends in all wavelengths. Three different approaches were used to characterize the seasonal and inter-annual spectral variation among forest species. The first approach was to analyse raw band spectral reflectances. From this analysis it was found that Sessile oak exhibited the highest reflectance followed by European larch, Sitka and Norway spruce. This is in agreement with the common knowledge that coniferous forests are generally less reflective than deciduous forests, due primarily to the density of water versus air in the leaf internal structure and the contrasting geometries of the broadleaved and coniferous plant canopies.

Both spruce species showed more consistent spectral reflectance pattern with temporal variation except for the values observed for the December 11 image. The most representative band for the characterization of these species was band 4. In this band, there is an apparent increase in reflectance for these coniferous species of about 10%

between May and July followed by a decrease of about 5% between July and August. Between August and December reflectance slowly increased although values extracted from the winter imagery may be affected by low sun angles and other effects.

On the other hand, European larch and Sessile oak showed more marked temporal variations in spectral reflectance for bands 4, 5, and 7. The seasonal pattern for Sessile oak was much more defined and easy to explain than the trend observed for European larch, although both are likely to be influenced by reflectance contributions from the understorey vegetation. In both species a decrease in reflectance values after July was observed, which was more accentuated in the oak species (19%); European larch decreased by about 8%. The main difference in the seasonal trend between these species was after August where NIR reflectance values for Sessile oak continued decreasing while it kept increasing for European larch.

The band in which spectral discrimination amongst all the species was best appeared to be near infrared band 4 and the date of imagery that showed a maximum contrast among spectral reflectances was the July 2000 image. However, no single date was considered ideal for discrimination of the four species which suggests that optimal differentiation between the species will be achieved using a combination of two or three datasets covering their phenological cycles. It was also concluded that winter imagery exhibited the poorest performance due mainly to the effects of shadowing as a result of low sun angles and poorer signal to noise performance due to reduce light levels at this time. Good radiometric normalisation of the winter imagery could not been achieved. The often unusual values obtained from the winter imagery for some of the plots have been explained by the low sun angles and increasing shadows for some of the stands. Although further field investigation is required, other unusual values were explained by contributions from the understorey vegetation and soil background, as it maybe expected that the understorey phenology contributes to overall spectral responses particularly in the seasonal variation. In conclusion, a more extensive study to determine the effect of

phenological changes on the remotely sensed signal will require the use of a longer or more temporally intensive, sequence of images.

The second approach investigated was the use of a vegetation index (NDVI) to study seasonal variation in its values and differences between species. Vegetation indices are considered a means of deriving canopy biophysical variables such as Leaf Area Index (LAI), percent green cover, and photosynthetically active radiation (PAR). Satellite monitoring of vegetation phenology has often made use of vegetation index data such as NDVI because it is related to the amount of green leaf biomass (Lillesand & Keifer, 2000). Remote sensing data has been applied to the quantification of LAI, timber volume, and PAR but it has been acknowledged that the relationship between vegetation biophysical parameters and radiometric data collected by remote sensors is not a simple one. NDVI was analyzed in this work as a means of representation of the seasonal variations of the species under study.

Observations of the seasonal variation corresponding to each of the four species studied in the Aberfoyle area showed that seasonal variability in NDVI was characteristic of species type and was observed to increase in level by species in the following order: Sitka spruce, Norway spruce, European larch, and Sessile oak. Sitka spruce and Norway spruce NDVIs were relatively stable throughout the observed period, whereas distinct seasonal patterns were observed in European larch and Sessile oak. The varying solar zenith angles in the imagery complicated analysis of the seasonal differences of the forest stands and may also have influenced NDVI. For the spruces no significant differences were observed other than slight variation in the May and August scenes and possibly the December 11 scene (but low sun angles might play a significant role in this latter difference). The largest seasonal variations were observed in the Sessile oak NDVI. The lowest NDVI values observed for Sessile oak and Norway spruce have been explained by the low sun angles of the December imagery and the location of these plots on shadowed sites at the acquisition time. The largest difference in NDVI (of about 20%) between Sessile oak and Norway spruce (apart from the observed in the December 11 scene) was

observed in the October image, followed by a difference of approximately 15% in the May image. Both species exhibited same NDVI for the July and August scenes. Overall, variations in NDVI across the growing season for all species were less marked than seasonal patterns observed in the individual band reflectances.

PCA transformation was the third analysis used, showing that the second principal component was able to capture key intra-annual variations as well as spectral differences among species. The advantage of the PCA analysis is the considerable reduction of the data by capturing the majority of data variation in the fewest possible number of features. The Second Component was of particular importance and was able to portray species spectral responses in a way that could be associated with phenological changes. The relative measure of seasonal variation showed a more accurate depiction of species dynamics. Similarities in the shape of the second component scores were observed between the coniferous tree plots (European larch, Norway spruce and Sitka spruce) and the Sessile oak specie. As the reflectance of the stand is influenced by the reflectance of the understorey, it is possible that the second component scores not only reflect the seasonality of the main species but also that of the understorey vegetation. Because of that, a more in depth study and spectral characterization of the understorey vegetation in the Aberfoyle area is needed with the aim of quantifying the influence of the understorey in the stand spectral responses.

Overall, the results from the multitemporal analysis indicate that acquisition date can greatly affect the spectral response observed in remotely sensed scene for European larch and Sessile oak species while the lower variation in the seasonal pattern of the evergreen coniferous species would have a lower impact in the spectral values retrieved from ETM+ imagery and the subsequent estimation of biophysical parameters. In any case, the results suggest that image acquisition should be carefully considered to ensure maximum information content in remotely sensed data. Furthermore, the results suggest that no single time of year may be optimal for both the characterization of species (e.g. classification) and for the estimation of biophysical parameters, suggesting that the use of

data obtained at different times of the year may be most ideal. Further investigation into these implications is warranted.

From this study it can also be concluded that although the approaches used helped to characterize the four forest species, especially to discriminate between spruces, larch and the deciduous species oak, further work is needed in order to define an optimum approach to discriminate between spruce species (e.g. Sitka spruce and Norway spruce) where spectral responses are very similar. In general, the useful ranges of the indices were small, so a careful and accurate preprocessing of the imagery is required specially related to calibration and radiometric correction.

Chapter 4

LiDAR data analysis

4.1 Introduction

LiDAR is an acronym which stands for Light Detection and Ranging and is a technology that uses an Airborne Laser Scanning (ALS) system. The developments in the technique began in the 1970s and 1980s with the deployment of the early NASA's airborne system Atmospheric Oceanographic Lidar (AOL) and Airborne Topographic Mapper (ATM) (Flood 2001). Developments have been very rapid in the last decade or so, mainly due to improvements in the integrative use of kinematic GPS and inertial navigation systems (Baltsavias 1999). In 1994 LiDAR was first used as a method for the derivation of digital models (Petzold 1999) and its potential to pass through forest canopies was the original motivation to study laser systems for the purpose of generating digital terrain models (DTMs) in forest areas (Ackermann 1999, Luethy 2004), and to retrieve various forest parameters as a subsequent application. This technique can support both forest monitoring and management planning by providing information at tree level with an efficiency and precision that is difficult to achieve using conventional methods. Although Behera and Roy (2002) cite few users for the LiDAR technology 4 years ago, (USA (12), Canada (7), Japan (5), Australia (3), South Africa (1) and Europe (19 – Belgium, Germany, Norway, Russia, Sweden, The Netherlands, UK and Italy), new markets continually open up to take advantage of the high speed of data acquisition and low cost per measurement.

Because LiDAR data directly record information characterizing the physical structure of a forest (tree height, crown closure, crown size, etc.), they provide an opportunity to assess directly the three-dimensional structure of vegetation formations in ways that are not possible with other sensors (Campbell 2002). Although technologically complex, LiDAR provides a methodology that is accurate, timely, capable of operating in difficult terrain, and increasingly affordable (Jensen 2000). This is particularly important within

the forestry context, where both forest companies and governments are interested in estimating forest attributes to create and maintain up-to-date forest inventories at the lowest cost possible.

One of the unique properties of LiDAR is its ability to penetrate the vegetation canopy and to map the ground surface below. This has useful applications in measuring vegetation attributes useful for planning and reporting, which have been explored in several studies: LiDAR has proved to be capable of retrieving forest parameters such as basal area, biomass, stand volume (Lefsky *et al.* 1999, Nilsson 1996, Means *et al.* 1999, Means *et al.* 2000), and leaf area index (LAI) (Lefsky *et al.* 1999, Hagiwara *et al.* 2004). It also allows for the determination of forest structure (Blaschke *et al.* 2004, Zimble *et al.* 2003, Heurich 2004, Mcombs *et al.* 2003, Popescu 2003), and tree crown detection (Gougeon 2003, Brandtberg *et al.* 2003, Popescu 2003, Heurich and Weinacker 2004). St-Onge and Vepakomma (2004) assessed forest gap dynamics and growth using multitemporal LiDAR data. Hudak *et al.* (2002) researched on the integration of LiDAR and Landsat data for estimating and mapping forest canopy height.

LiDAR data combines both surface elevation and accurate planimetric coordinates, and processing algorithms, which can identify single trees or groups of trees in order to extract various measurements on their three-dimensional characteristics. Within forest inventory research, the main interest has focused on automatic measurement of tree height for different tree species and automatic delineation of tree crowns, because from crown diameter and tree height other important inventory parameters can be derived (Yu *et al.* 2004). For example, Nilson (1996) estimated tree heights and stand volume. Studies in conifer stands (Naesset 1997; Magnussen and Boudewyn 2000) have shown that stand height can be predicted with r^2 values of over 0.9 and timber volumes with r^2 values of 0.45 to 0.89. Persson *et al.* (2002) reported a standard error for the estimate of the height of individual trees of less than 1 m, and Brandtberg (2000) slightly more than 1 m. Clark *et al.* (2004) predicted sub-canopy elevation with 2.29 m accuracy in a tropical landscape.

The estimation of individual tree crown parameters is also possible with LiDAR data, although with less precision. This analysis has been attempted in many studies: St-Onge

and Vepakoma (2004) performed a manual delineation to assess forest gap dynamics; Holmgren and Persson (2004a) detected crown diameters in Finland with a root mean square error of 0.61 m; Brandtberg *et al.* (2003) estimated tree crowns in deciduous forest in North America obtaining low accuracies caused mainly by non-overlapping reference and test polygons; Næsset and Økland (2001) estimated tree crown properties in a boreal nature reserve where R^2 values of average height to the crown and average relative crown length were 0.71 and .60 respectively.

Thus the applications of LiDAR technology to forestry have been considerable and of great importance. The ability of LiDAR to map ground elevations even through dense canopies represents its main advantage over traditional techniques for forest mapping, such as photogrammetry, which can often only obtain elevations at the top of dense canopies.

Although LiDAR systems are now mature enough to allow its applicability to forest monitoring, the data processing algorithms necessary for the accurate retrieval of useful forest parameters, are still being developed and evaluated. More research is required to design a standard and automated procedure for the integration with multi- and hyperspectral optical imagery to improve various feature extraction tasks.

4.2 Objectives

The main objective in this chapter was to investigate multi-return LiDAR data to assess its potential for predicting tree heights and for the production of a Digital Canopy Model (DCM) for tree crown delineation within the CCF context and the UK forest scenario in general, where there are at the moment limited studies about the applicability of LiDAR for both coniferous and broadleaved species characterization and the potential of LiDAR in relation to plant densities. This included: the collection of LiDAR data over the existing ground plots in Aberfoyle, Scotland; the development of an algorithm for the extraction of ground elevation and tree heights from multiple return LiDAR data, and the production of Digital Terrain Model and Digital Surface Models (DSM) of the area under

study, followed by the comparison of the predicted LiDAR tree heights with the true tree heights. Further analysis in a following chapter will consist of the object oriented segmentation and classification for crown delineation.

4.3 The Laser System

LiDAR is an active remote sensing technology, which means that transmits and receives electromagnetic radiation (Thiel and Wehr, 2004) emitted from a laser source. LiDARs operate in the ultraviolet, visible and infrared region of the electromagnetic spectrum.

LiDAR, as its most basic level, is a laser altimeter that determines the distance from the instrument to the physical surface by measuring the time elapsed between a laser pulse emission and its reflected return signal. Multiplied by the speed of light, this time interval measures twice the distance to the target, thereby providing a measure of target elevation (Hudak *et al.* 2002).

4.3.1 The Airborne Laser Scanning (ALS) system

The major components of an ALS include (Baltsavias 1999) (figures 4.1 and 4.2):

- a laser range finder (LRF): which includes the laser, transmitting and receiving optics, the signal detector, amplifier, time counter and necessary electronic components;
- a computer, operating system and software for control of the on-line data acquisition;
- storage media for laser, GPS, INS, scanner and possibly image data;
- a scanner;
- GPS for navigation, possibly including radio links or antennas for receipt of real-time corrections and (excluding cases where attitude is estimated by multiple GPS antennas on the aircraft) an attitude (pitch, roll and heading of the aircraft) measurement system;
- platform and mounting of the system components;
- ground reference GPS station(s);

- software for mission planning, and various stages of postprocessing;
- Optionally, other sensors, especially video and digital CCD-cameras, photogrammetric aerial cameras, other sensors (thermal, multiespectral line CCDs, etc.);
- Optionally, temperature and humidity control.

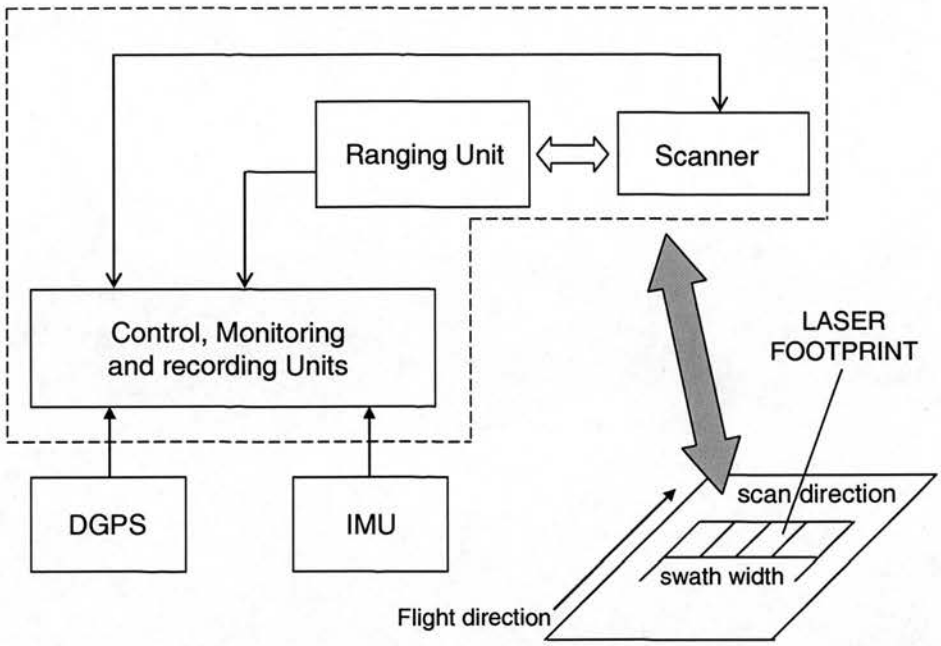

Figure 4.1: Typical ALS system (Wehr and Lohr 1999) showing the diverse components of the system and the graphic definition of terms such as laser footprint and swath width used in relation to LiDAR technology.

An important trend is towards programmability/selectivity of various parameters in order to allow more flexibility and adaptation to the requirements of different applications. Apart from flying speed and height, which can obviously vary, the following parameters are also variable in one or the other systems: scan angle, pulse rate, scan rate (often inverse proportionally related to scan angle), beam divergence, recording of first and/or last returns or multiple echoes per pulse, scanning pattern, and INS frequency. Other parameters, which depend on the previous ones like across and along track point spacing, swath width, point density, and area covered can also vary.

Other recent trends in LiDAR development and deployment include: higher flying height, higher pulse rate, recording of intensity and/or more than one echo per pulse, installation on multiple platforms, tighter integration of cameras and with higher resolution, wider selection of GPS receivers and inertial measurement units (IMU), smaller and lighter systems or components with less power requirements. The laser wavelength is often in the range of 1040 – 1060 nm (and for bathymetric lasers also 532 nm), while a few systems have a wavelength of approximately 900 or 1550 nm.

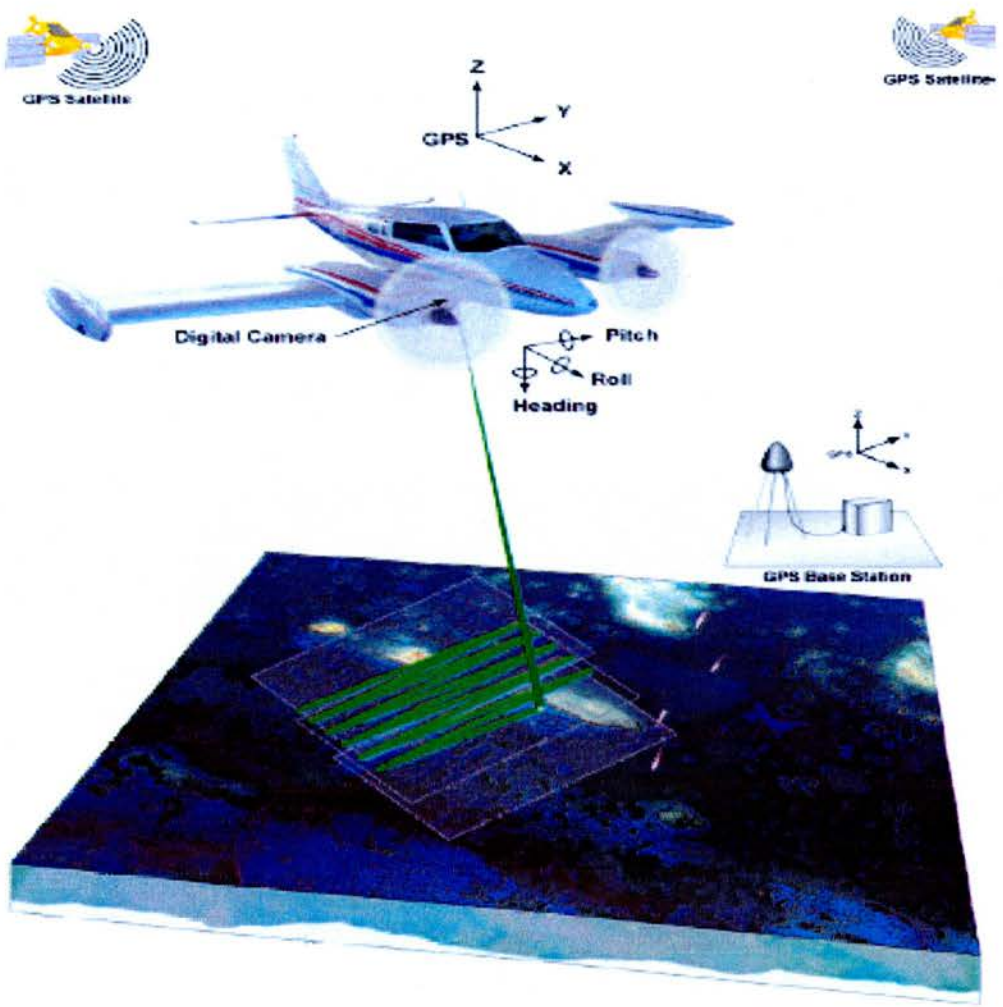

Figure 4.2: Typical components of an airborne LiDAR ranging system. These include the laser altimeter, instruments for precision navigation (aircraft position and attitude), and a down-looking digital photographic or video camera (Crane *et al.* 2002).

In range measurements with laser, two major ranging principles are applied: the pulse ranging principle, and ranging by measuring the phase difference between the transmitted and the received signal backscattered from the object surface.

For pulse ranging systems the range solution tells how far apart two targets have to be, so that they can be resolved as separate targets. Besides that, for each transmitted laser pulse several returns can be observed, from the treetops and from the ground. Therefore, today, airborne scanners typically discriminate between first and last laser return pulses. If the traveling times of multiple returns are measured, it is possible to resolve different elevation layers. The comprehensive sampling of a return signal is known as full wave detection (Thiel and Wehr 2004).

The phase difference method is applied with lasers that continuously emit light. These lasers are called continuous wave (CW) lasers. In current ranging laser systems, mostly pulsed lasers are used (Wehr and Lohr 1999) (figure 4.3).

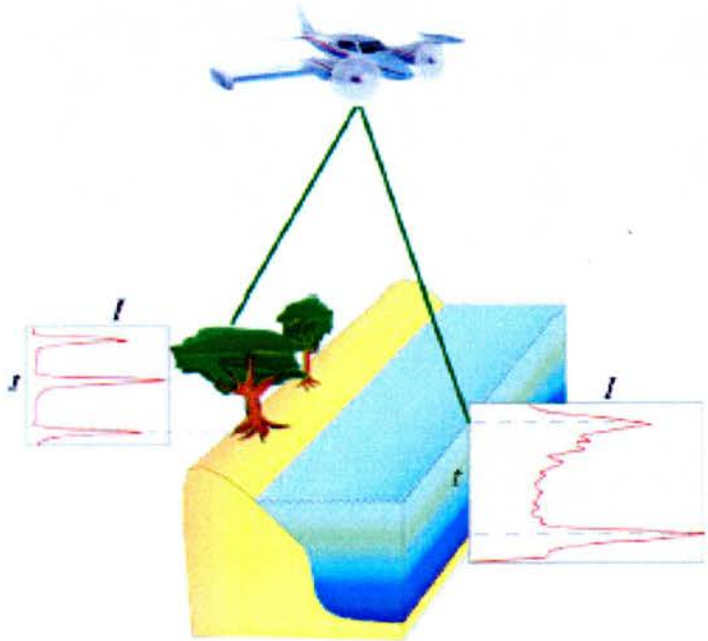

Figure 4.3: Full laser waveform digitization provides nearly continuous vertical (range) resolution (Crane *et al.* 2002).

The first generation of LiDAR sensors used for remote sensing of vegetation were designed to measure the range to the first surface intercepted by the laser, typically along singular transects defined by the flight line (Nilsson 1996). More advanced laser altimeters, imaging or scanning LiDARs, are capable of scanning the ground surface beneath the airborne platform, resulting in a true three-dimensional data set. Commonly, for such LiDAR sensors, the laser beam sample area or footprint, is relatively small, usually less than 1 m in diameter.

Naturally, the larger the spot diameter or footprint the greater the degree of target mixing. However, smaller is not necessarily better: the optimal spot size will be determined by the application at hand.

An alternative form of laser altimeter, known as surface LiDAR, utilizes the complete time-varying distribution of returned pulse energy, or waveform, that results from the reflection of a single pulse with a large footprint (up to 25 metres) (Popescu 2003).

Dubayah and Drake (2000) classified LiDAR systems for forestry applications according to three basic characteristics:

- their ability to record one or more returns
- the size of their footprints, ranging from a few centimetres (5-90 cm) to tens of metres (10-25 m) in diameter
- their sampling rate and scanning pattern

The main advantages of LiDAR technology can be summarized as follows:

- high accuracy up to the order of 10-15 cm in the vertical and 50-100 cm in the horizontal, according to commercial vendors. However, a number of studies have examined the vertical accuracy of LIDAR data, obtaining results that ranged from 3 to 100 cm, with the majority of the studies reporting from 7 to 22 cm (www.ctre.iastate.edu/mtc/papers/2002/Veneziano.pdf).
- it can be collected under a variety of environmental conditions, including low sun angle, cloudy conditions, and even darkness, resulting in expanded windows for data collection.

- capability of canopy penetration unlike passive techniques like photogrammetry
- high data density
- free of the need for ground control points making it an ideal method for inaccessible areas
- needs less time for data collection. However, because of the massive amount of point data acquired even in a single flight line, processing times depends on two factors: computing capacities and personnel skills (as LiDAR processing demands a large learning curve).

Today only pulsed laser systems are used for airborne laser scanning (Thiel 2004). The early non-pulsed systems had to separately collect the first and last pulses, but nowadays all systems are capable of recording simultaneously at least the first and last pulses, and some systems are even capable of recording multiple pulses, continuous waveforms and aerial photographs in parallel (Hyyppa *et al.* 2004).

4.3.2 The Optech ALTM 2033

The LiDAR data used in this study was acquired using the Optech ALTM 2033 system (figure 4.4). This is one of the most advanced instruments available, individually acquiring height data points at a rate of 33,000 per second, whilst flying at a height of up to 2,000 m above ground level. The main characteristics of the instrument are:

- at 850 m altitude it provides a point density of 1 m, a swath of 600 m and a typical height accuracy of +/- 15 cm (1 sigma)
- typical acquisition rates are 30-50 sq km per hour, depending on specification, allowing acquisition of hundreds of square km per day
- it can operate day or night (subject to safety considerations) and in weather that would preclude the acquisition of traditional aerial photography
- it provides simultaneous first- and last-pulse capability giving ranges to tree tops and to the ground in a single pass
- it is relatively compact and capable of flying on both fixed wing and helicopter platforms

- along with first and last returns, it provides a grey scale intensity image which helps with feature identification
- it offers flexibility in terms of its acquisition modes: high or low, narrow or broad viewing angles

Figure 4.4: Optech ALTM 2033 LiDAR system (Copyright 2005. Optech Inc.)

4.4 LiDAR for the retrieval of forest parameters

The information provided by LiDAR was first used for the derivation of digital elevation models, a field that has traditionally been one of the domains of photogrammetry. The two methods have aspects which can be compared (Ackermann 1999): both are highly automated, although photogrammetry still is to a lesser degree; their results are geometric and can reach similar accuracies; and with either method, extended areas can be covered, although flying time per unit area is much shorter for photogrammetry. On the other hand, there are essential differences between both methods: laser scanning is an active system, applicable even at night. LiDAR provides ground points in a certain pattern, which is primarily determined by the system design and only influenced to some extent by the geometry of the terrain surface and its cover. However, point density is an important parameter within the LiDAR systems as it might be crucial for detection of treetops, which is currently one of the main issues in this technology. The

photogrammetric points, measured automatically or interactively, may be arranged in a prefixed rigid pattern, but often they are arbitrarily selected, depending on image texture and features.

The first studies with LiDAR for forest inventory concentrated on using a profiling system for forest height, stand density, tree species and biomass estimation (Hyyppa *et al.* 2004). Holmgren and Persson (2004) carried out studies for the identification of species of individuals trees using an airborne laser scanner in the Scandinavian boreal forest. They used the structure and shape of tree crowns to differentiate between Norway spruce (*Picea abies* L. Karst) and Scots pine (*Pinus sylvestrys* L.). The classification accuracy was of 95% and crown base height estimations of individual trees were also evaluated ($r = 0.84$).

The characterization of vertical forest structure using LiDAR has been reported in several publications. Zimble *et al.* (2003) demonstrated that this variable could distinguish between two classes of vertical structure which were based on the median value between the minimum tree height variance observed in multistory plots (2.75 m), and the maximum tree height variance observed in single-story (1.21 m) plots. A small footprint, multi-return LiDAR system (AeroScan) was used for the data collection and the registered returns were processed with algorithms developed by EarthData Technologies. Clark *et al.* (2004) also estimated sub-canopy elevations and tree height in a tropical rain forest in Costa Rica. They estimated heights with a mean absolute error of 0.90 m ($r^2=0.97$) using the mean of LiDAR returns in the plot. As in other small-footprint LiDAR studies, they found that plot mean height was underestimated.

During the last 15 years several experiments have been carried out in order to determine tree heights by various airborne laser profiling and LiDAR systems (Nilsson 1996, Næsset 1997, Means *et al.* 1999, Lefsky *et al* 1999, Rieger 1999, Means *et al.* 2000, Zimble 2003). Naesset (1997) found that the maximum height value of laser canopy hits for a certain fixed area could be used to estimate the mean tree height. Later, Magnussen and Boudewyn (1998) showed that, for a given crown shape and a certain plot size, there

exists a certain quantile of the distribution of the canopy height of a plot that matches the tree height of interest or the mean height. Furthermore, other variables of the distribution of canopy heights such as the mean and median values, standard deviation divided by the mean (coefficient of variation), and various quantiles have been found to be correlated with mean tree height, dominant height and other biophysical properties (Nelson *et al.* 1997, Næsset 1997, Means *et al* 1999, Lefsky *et al* 1999, Means *et al.* 2000, Magnussen *et al.* 1999, Nelson 1997). In their Costa Rican study, Clark *et al.* (2004) found that individual tree heights were underestimated and had 3.67 m mean absolute errors.

The height estimate or vertical distribution of laser returns provides a basis to classify vegetation and to estimate other important canopy characteristics such as canopy cover and crown volume (foliage, trunk, branches). Since the vertical components of stands change with age, older stands can be characterized by canopy gaps. Estimation of canopy cover is made using the fraction of the LiDAR measurements that are considered to have been returned from the ground surface (Nelson 1984).

This chapter focused in the retrieval of tree height from LiDAR data. This forest structure parameter was chosen due to several reasons:

1. the proved success of LiDAR in retrieving tree height
2. the necessity of developing a Digital Canopy Model from LiDAR for the comparison with other remote sensing datasets
3. the importance of tree height as a parameter which is a function of species composition, climate and site quality, and can be used for land cover classification or in conjunction with vegetation indices. If coupled with species composition and site quality information, height serves as an estimate of stand age or succesional stages (Behera and Roy 2002).

4.5 Algorithms for processing airborne laser scanning data

The algorithms and details of the methods used to sort LiDAR data into returns from vegetation and terrain are the subject of few published papers. Most of the LiDAR

acquisitions are processed commercially using mostly complex algorithms implemented through proprietary software. One such algorithm is a method developed by Axelsson that has been implemented in the Terrascan software (Hyyppa 2004). The method consists of the development of a progressive TIN densification method where the surface is allowed to fluctuate within certain values, controlled by minimum description length, constrained split functions, and active contour models for elevation differences. Ground points are connected in a TIN. A sparse TIN is derived from neighborhood minima, and then progressively densified to the laser point cloud. In every iteration, points are added to the TIN, if they are within defined thresholds.

Kraus and Pfeifer (2001) developed an algorithm in which a rough approximation of the surface is computed first. Next, the residuals, e.g., the oriented distances from the surface to the measured points, are computed. The true terrain points are expected to have negative residuals, while the vegetation points are more likely to have small negative or positive residuals. Each (z) measurement is given a weight according to its distance value, which is the parameter of a weight function. The surface is then recomputed under the consideration of the weights. If an oriented distance is above a certain value, the point is classified as an off–terrain point and eliminated from the surface interpolation. This process of weight iteration is repeated until all gross errors are eliminated (a stable situation) or a maximum number of iterations is reached.

Other researchers have developed algorithms to extract bare-earth points from point clouds. Some elements identified in these algorithms are (Sithole and Vosselman 2004):

- Data structure: the output of a laser scanner survey is a cloud of irregularly spaced 3D points. Some filter algorithms work with the raw point cloud. Some others resample the point cloud into an image grid before filtering.
- Test neighborhood and the number of points filtered at a time: filters always operate on a local neighborhood. In the classification operation, two or more points are classified at a time into bare earth or vegetation. This classification can be done in three possible ways:

- Point to point: in these algorithms, two points are compared at a time. The discriminant function is based on the positions of the two points. If the output of the discriminant function is above a certain threshold, one of the points is assumed to belong to an object. Only one point is classified at a time.
- Point to Points: in these algorithms, neighboring points (of a point of interest) are used to solve a discriminant function. Based on the output of the discriminant function, the point of interest can then be classified. One point is classified at a time.
- Points to points: in these algorithms, several points are used to solve a discriminant function. Based on the discriminant function, the points can then be classified.

- Filter concept: every filter makes an assumption about the structure of bare-Earth points in a local neighborhood. For example, bare-Earth points in a localization must fit a given parametric surface. Four distinct concepts were observed:

  - Slope-based: in these algorithms the slope or height difference between two points is measured. If the slope exceeds a certain threshold, then the highest point is assumed to belong to an object.
  - Block-minimum: here the discriminant function is a horizontal plane with a corresponding buffer zone above it. The buffer zone defines a region in 3D space where bare-Earth points are expected to reside.
  - Surface based: in this case, the discriminant function is a parametric surface with a corresponding buffer zone above it.
  - Clustering/segmentation: the rationale behind such algorithms is that any points that cluster must belong to an object if their cluster is above its neighborhood.

- Single step vs. iterative: some filter algorithms classify points in a single pass while others iterate, and classify points in multiple passes. The advantage of a single step algorithm is computational speed but the classification by multiple passes is usually more accurate.

Sithole and Vosselman (2004) compared the capabilities of these algorithms finding that all of them perform well in smooth rural landscapes, but all produce errors in complex urban areas and rough terrain with vegetation. In general, algorithms that estimate local surfaces were found to perform best. None of the algorithms made use of the reflectance intensity. Only one of the algorithms made use of both the first and last pulse data; all other algorithms in the study only made use of the last pulse data.

Despite all of the efforts in the development of algorithms that provide an accurate classification between ground and vegetation or other features, there does not exist at the moment a methodology or standard strategy for its processing. Consequently, the characterization of the ground surface using LiDAR data, especially in forested areas, is still a major challenge. Current research is seeking to identify the best methods for automated identification and extraction of ground measurements (Petzold *et al.* 1999).

4.6 Data collection

For this study, the LiDAR data was acquired by the Natural Environmental Research Council, with an Optech ALTM 2033 scanner. The area under analysis, which encompasses the plots within the stands of interest, was flown at Aberfoyle in September 2002 at an altitude of 1000 m a.s.l. using a scan angle of 20°, with a point density of 4 returns per square metre and a beam divergence of 10 cm. LiDAR data for this project consisted of a list of X, Y, and Z coordinates of the first and last return pulses as well as of reflectance intensity, georeferenced to the Ordnance Survey Great Britain (OSGB) national grid. First return data more likely reflect from leaves or branches of trees while the laser pulses of the last return data sometimes reflect from the ground below the trees or between surface and ground.

A single LiDAR over-flight produces millions of measurements or coordinates in X, Y, Z. Figure 4.5 depicts a sample of raw LiDAR data (first return and last return) over a forested area.

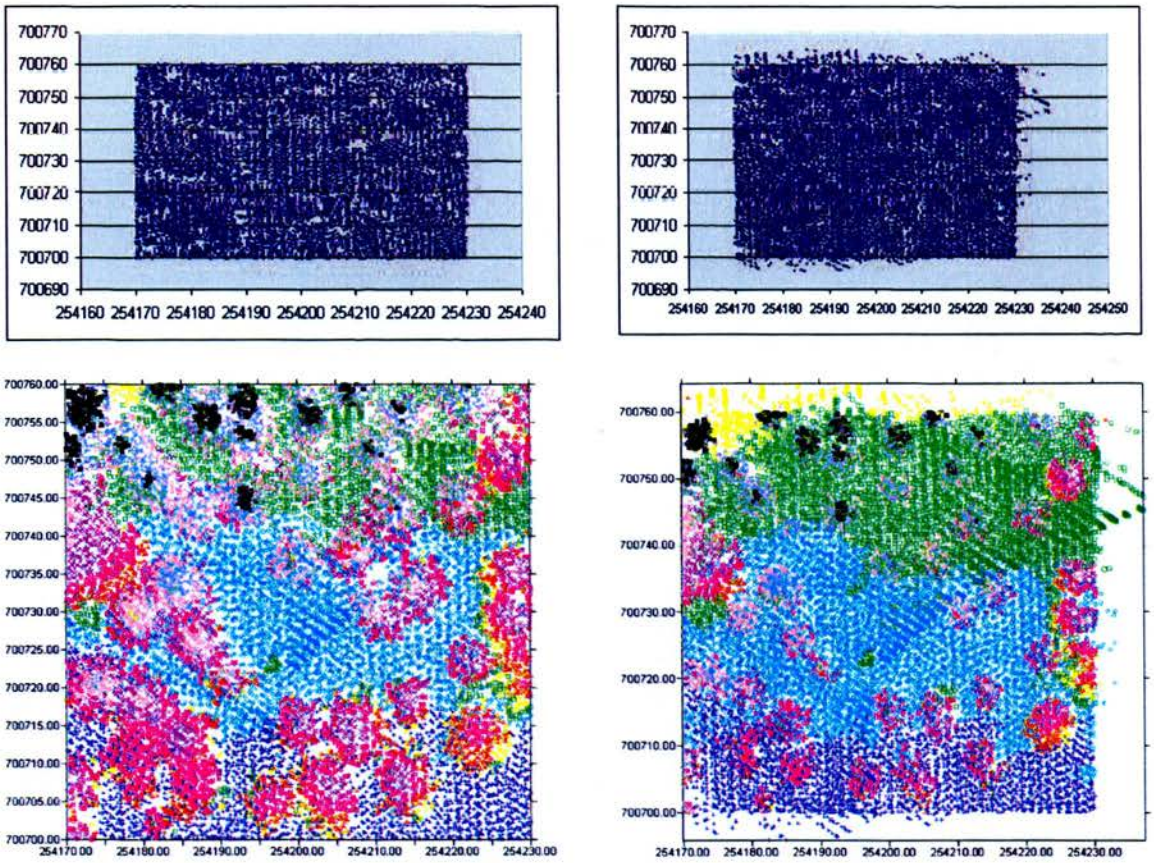

Figure 4.5: Raw LiDAR data over a sample plot. The figures on the left show the spatial distribution of the first laser return and the figures on the right, the spatial distribution of the last return. The figures at the top show the universe of laser points collected over the area and figures at the bottom show the same points classified by their height.

Figure 4.6 shows a 120 m profile of the distribution of last returns in which ground terrain is clearly characterized with top measurements up to approximately 16 m height. The measurements between the ground surface and the top of the canopy have to be removed in order to characterize the ground surface and the canopy surface. The discrimination between the ground measurements from measurements of vegetation and other structures can be difficult, especially if only a few measurements of the ground are made through the canopy. Figure 4.7 shows a profile of the first return and the last return for a forest area.

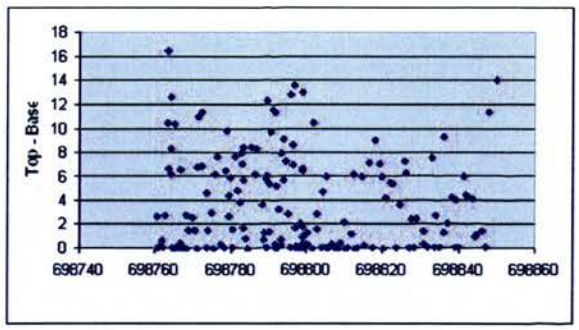

Figure 4.6: Profile of LiDAR measurements over a forested area.

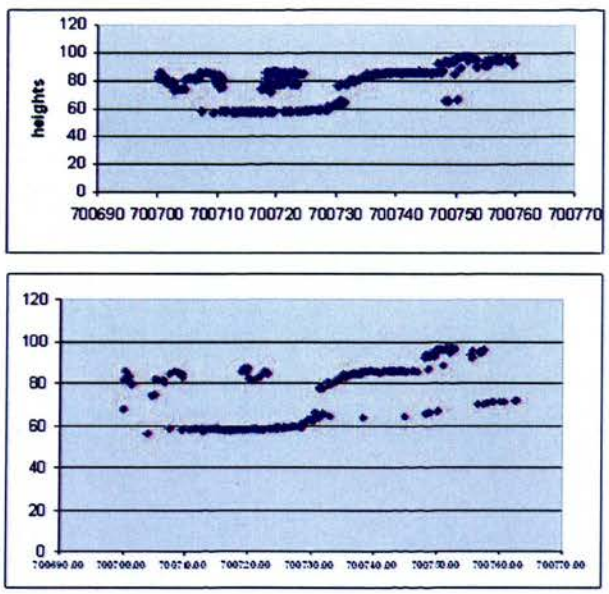

Figure 4.7: First (top) and last return (bottom) LiDAR measurements for a forested area.

4.7 Filtering process

A programme referred to as *Ground* (Appendix 1) was written in FORTRAN for the purposes of classification of points as belonging to the ground or vegetation, and also for the interpolation task in areas with low ground point registration. This classification task leads to the generation of the LiDAR DTM, which is key to the extraction of forest parameters. The flow chart for the algorithm developed is shown in figure 4.8.

The program works on the assumption that the lowest points in a point cloud must belong to the terrain. According to the classification made by Sithole and Vosselman (2004), the characteristics of the algorithm developed are as follows:

- Data structure: it works with the raw point cloud
- Tests neighborhood and the number of points filtered at a time: it operates locally performing a point by point classification
- Filter concept: the algorithm is slope based
- Single step vs. iterative: it classifies points in a single step

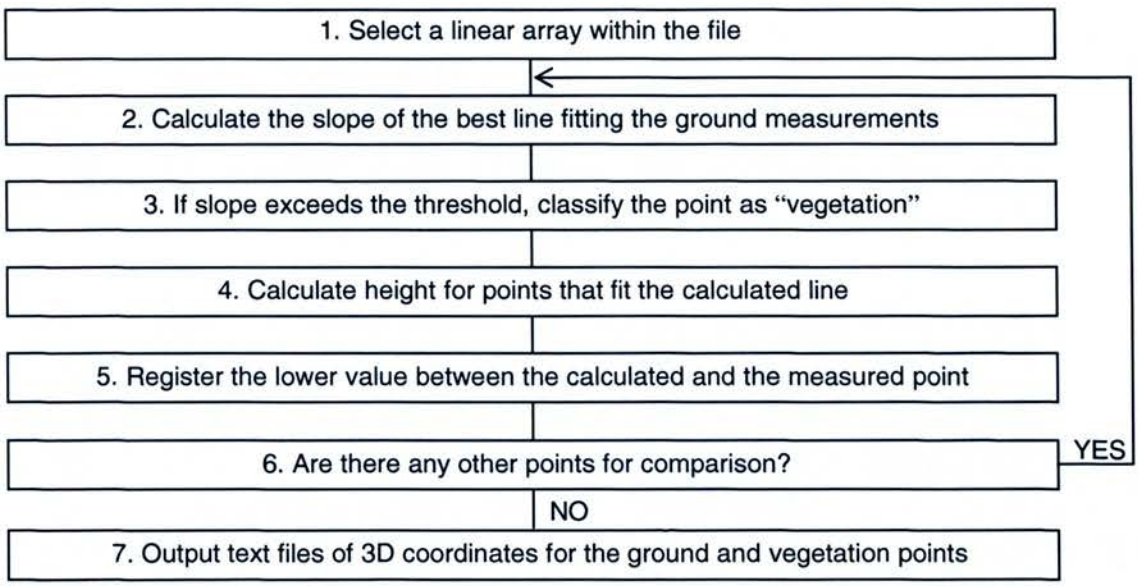

Figure 4.8: Flow chart for the development of the linear algorithm for the LiDAR DTM generation.

This programme read a file containing LiDAR data consisting of OSGB coordinates, heights, and signal intensity for first and last returns, and calculated a surface that approximates the ground height by two different methods: lineal (in two directions, North and East) and by area. It also calculated tree heights by the difference between a digital surface model representing the canopy top (generated through the interpolation of first returns corresponding to the top of the canopy layer) and the ground surface as previously estimated. Height differences are a key to separating the bare-Earth (ground surface) and

trees. Therefore, points significantly above their neighbours are assumed to be of vegetation. This assumption is valid for terrain that is flat or that presents smooth slopes, but becomes more difficult as the slope of the terrain increases.

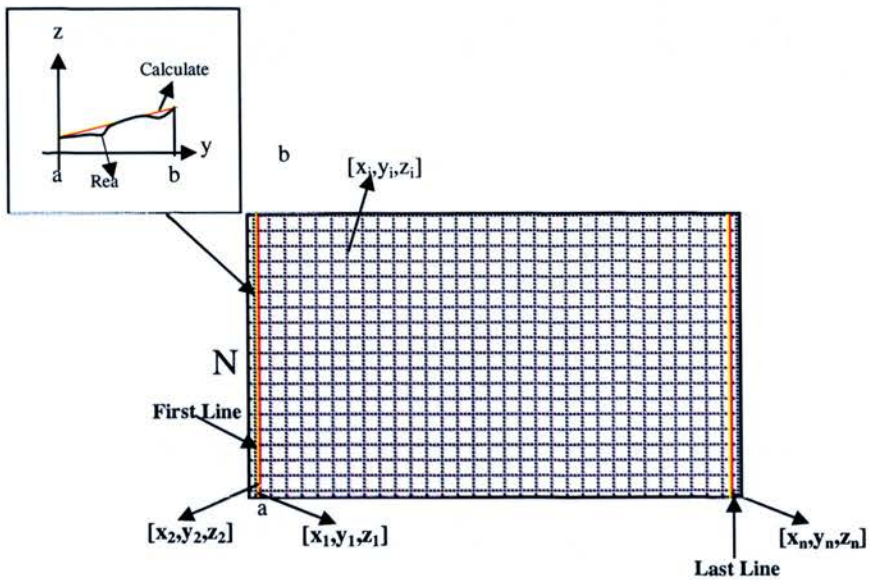

Figure 4.9: Linear regression method for the calculation of ground points.

The algorithm is based on a linear regression method and it assumes that a large height difference between two adjacent measurements is unlikely to be due to a change in the terrain topography, but more reasonably to the point belonging to the vegetation layer or other feature rather than the terrain. The algorithm calculates a line that fits the ground surface. For that, a linear section of a specified width of the data is selected in either North or East direction (figure 4.9). The accuracy of this calculation depends on the existence of enough data that represents the ground as well as its relatively even distribution. A condition obliges the calculated line to keep the raw values (ground values) when they are lower in height than the calculated ones. The result of this filtering process, consisting of the classified ground laser returns, was used to create a digital terrain model in Surfer (Version 6.02, Golden Software, Inc.). The grid resolution was 0.5 m and the interpolation method used was Kriging, which was already implemented in the software and which has been used in several studies as the interpolation method for LiDAR measurements to regular grids that produced the smallest residuals among others

such as inverse distance and triangulation (Lloyd and Atkinson 2002, Popescu *et al.* 2002).

The area method consisted of the selection of the minimum height measured in a defined area or window. This minimum value is then assigned to all the points within the area so that the ground surface is obtained through the calculations of these values for the entire plot (see figure 4.10 and 4.11). The flow chart of the algorithm is shown in figure 4.12.

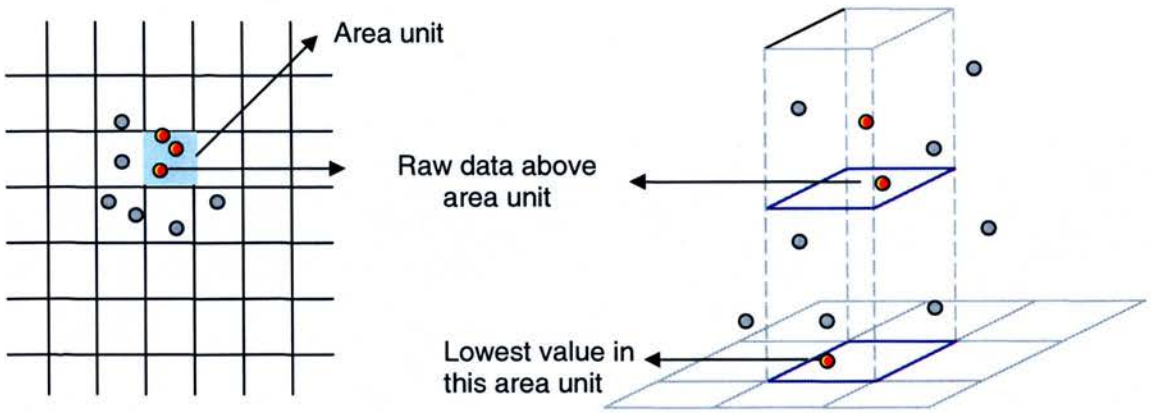

Figure 4.10: Area method for the classification of ground points.

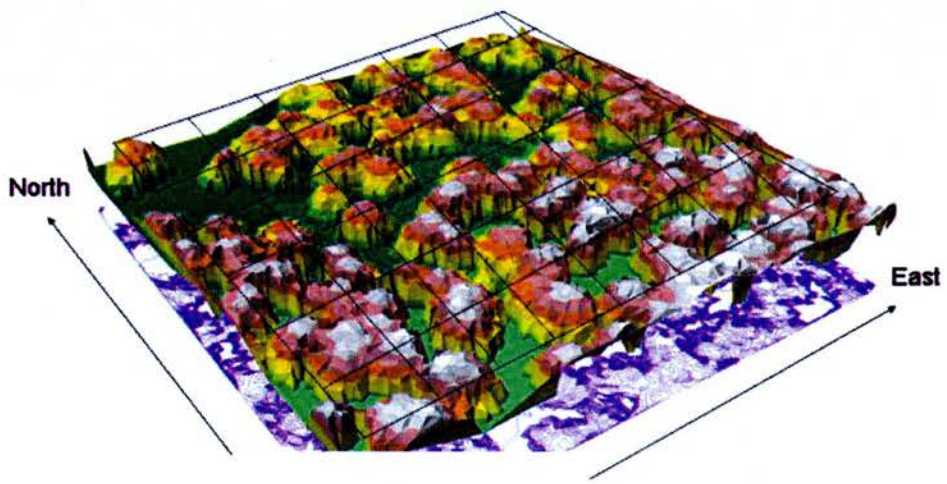

Figure 4.11: Three-dimensional view of the raw LiDAR data for one of the plots. An imaginary grid has been overlaid to depict the size of area considered by the interpolation method and which contains several laser hits corresponding either to the ground or the vegetation as shown in figure 4.8.

The first step after the algorithm is run is to read the data base for each file. These files are in .txt format and correspond to the first and last return of the laser signal.

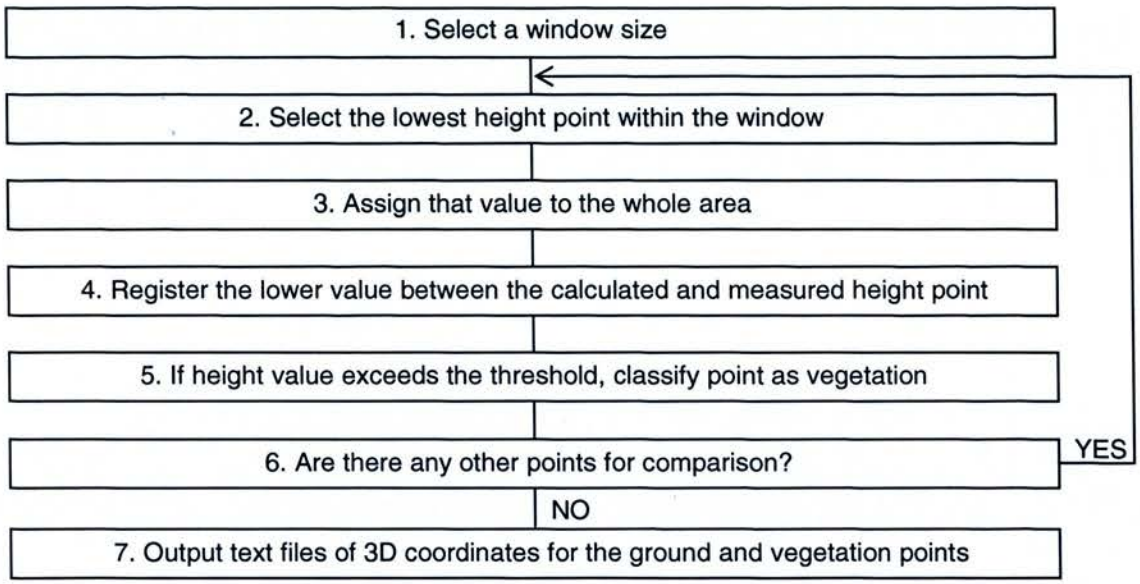

Figure 4.12: Flow chart of the area algorithm for the LiDAR DTM generation.

The programme read two files (first and last return) containing six values each: file, Plot_number, F_East (East coordinate for first return), F_North (North coordinate for First return), F_Elev (Height of the First return), and F_Int (Intensity of the First return) (table 4.1). The first field (file name) is alphanumeric, the second (Plot_number) is an integer, the following three (coordinates and elevation) are real and the last one (intensity) is an integer.

file	Plot_number	F_East	F_North	F_Elev	F_Int
Aberfoyle_p.osd	1	249659.94	698847.88	85.62	75
Aberfoyle_p.osd	1	249659.69	698848.31	85.77	67
Aberfoyle_p.osd	1	249659.38	698848.75	85.53	84
Aberfoyle_p.osd	1	249659.08	698849.19	85.5	84
Aberfoyle_p.osd	1	249658.91	698849.44	85.52	66
Aberfoyle_p.osd	1	249658.61	698849.88	85.51	70

Table 4.1: Example of first return file

The following step in the programme consists in the input of control parameters. These are:

- **Height control value**. This parameter allows the classification of points as belonging to the terrain or the vegetation layer and it is closely related to the expected maximum variation in the Z coordinate in a particular area. The tests performed with several parameter values (height differences between the expected highest point and the expected minimum point), produced the best results when a value of 3 m was used for this parameter. Other research has also used this value as a threshold for the classification task (Lim and Treitz 2004).

  The height value strongly depends on the topography of the terrain (and the acknowledgement of it by the operator) so that a sensible value can be used in the analysis. For the data studied in this research it was initially considered to be half of the difference between the maximum and the minimum ground height. No substantial variation in the results was noticed when the calculations were made in the direction of the minimum slope using different threshold values (e.g. 1m, 2m, 3m) which can be seen in figure 4.13. In this case, the area studied had a variation in the ground height of approximately 10m according to the data and verified in the terrain.

  The middle graph in figure 4.13 shows all the lines fitted to the ground data considering several values for the height parameter. It can be seen that all of them have a similar behaviour. In contrast, the bottom graph shows the results for the same analysis but in the maximum slope direction (North), which produced differences in the heights calculated.

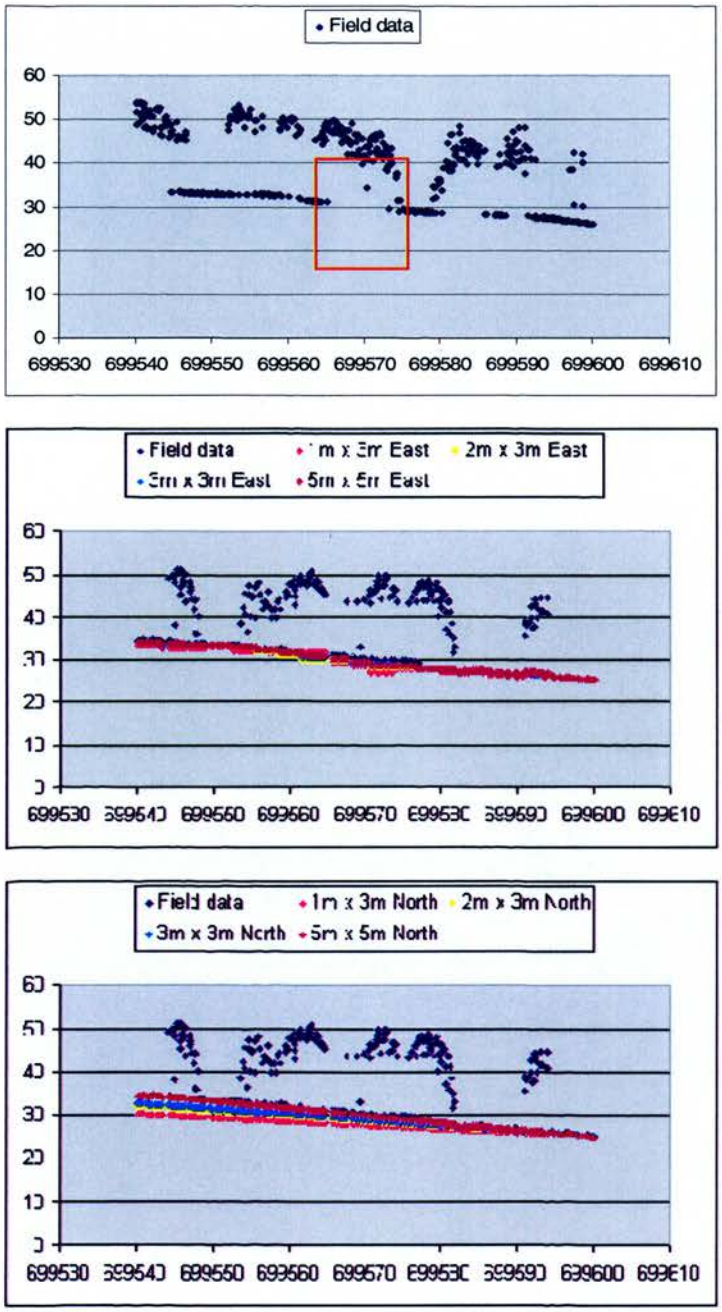

Figure 4.13: Generation of ground data points using the linear method. The top graph shows the raw LiDAR data. Note the lack of ground measurements delimited by the red box. The method is applied to the minimum slope (East direction, middle graph) and the maximum slope direction (North direction, bottom graph) using different values of the height parameter: 1m, 2m, 3m and 3m for the width of the line. It also shows the results when using the area method in 5m x 5m window size.

When the ground is not well characterized because of lack of LiDAR returns from the ground as in very dense stands (figure 4.14), the selection of the methods as well as the parameters has to be undertaken with the help of visualization tools such as Excel or Surfer. Others, like Blaschke *et al.* (2004), mapped the data set in a GIS as it is often claimed that 3d analysis and visualization for data processing provide better understanding of the phenomena under consideration. Some other studies have also pointed out the need for optical data fusion in the processing phase of LiDAR data in order to improve the selection of targets and for feature extraction tasks (Hudak *et al.* 2002, Popescu *et al.* 2002).

The problem lies in the fact that the few data points representing the ground are not very well distributed, as is shown within the red box in figure 4.14, and the calculation in the North direction results in a negative slope. The analysis in the other direction solves the problem. The figure also shows the results for the area method.

Finally, the parameter value that gave the best performance was 3m and the direction of the calculation was always assisted by prior visualization of the data in Excel (Microsoft Corporation 2003).

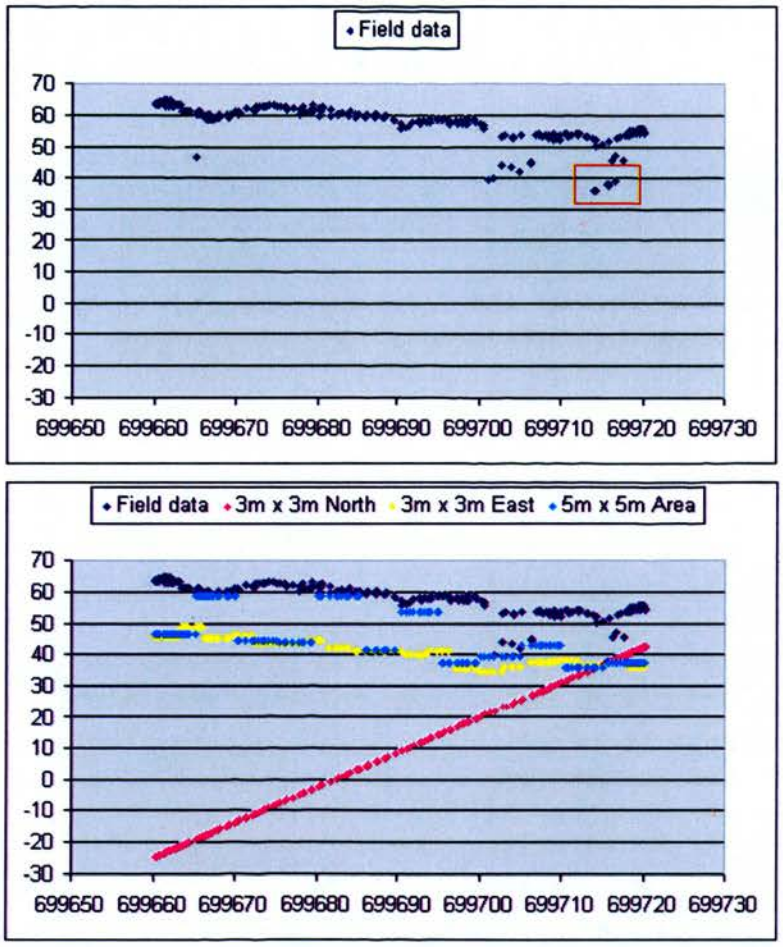

Figure 4.14: Linear and area method applied to a dense Norway spruce stand.

- **Width control value**. This parameter represents the maximum amplitude in the East or North coordinate to be considered (width parameter). This value controls the line width.

  The width parameter sets the amount of data to be taken into account in the calculation of the slope. The programme finds the best linear fit for all the points within the set range. The results of this calculation with different widths are shown in figure 4.15.

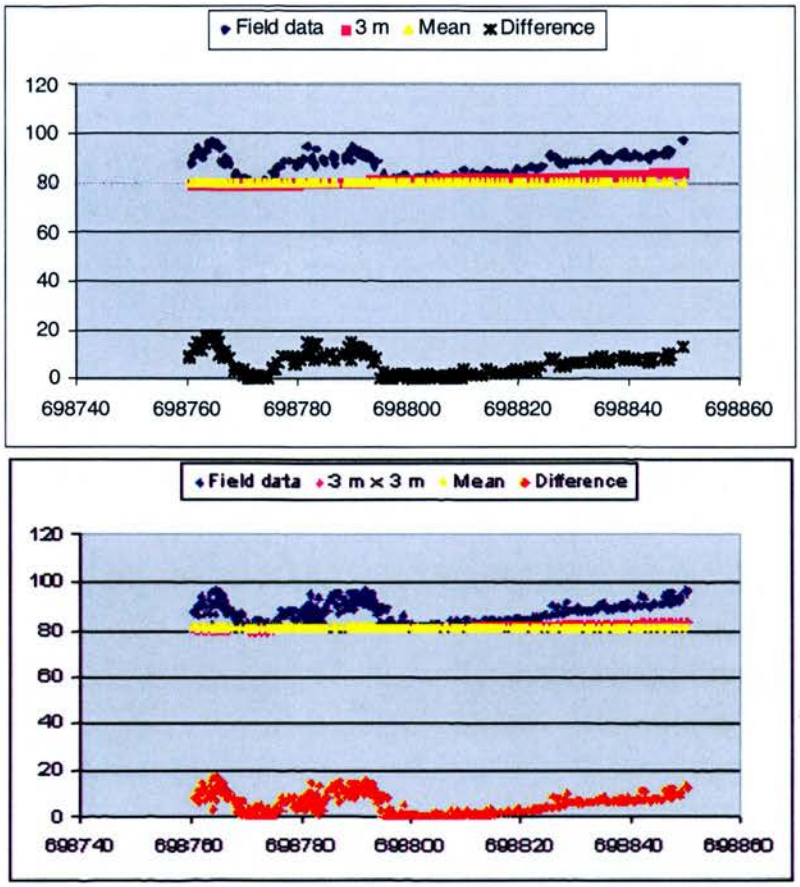

Figure 4.15: Line method with different width parameter values: 1m and 3m. The figure at the top shows the effect on the calculation of the ground heights (pink line), when a width parameter value of 1 m is considered. The figure at the top shows the effect on the calculation of the ground heights (purple line), when a width parameter value of 3 m is considered. The curve at the bottom of the figures (black and red) represents the difference between height values for the original data and calculated heights.

The visualization of these results in a shaded relief graph shows a vertical line effect when a width parameter equal to 1m is considered (figure 4.16a). This effect can be eliminated by the selection of a greater width for the analysis as for example 3m as is shown in figure 4.16b.

In plots when there is not enough ground data, or returns from the ground are not well distributed as shown previously in figure 4.14, consideration of a width parameter of 5m or more increases the quantity of data available to make the calculation of the slope allowing a better characterization of the terrain (figure 4.17).

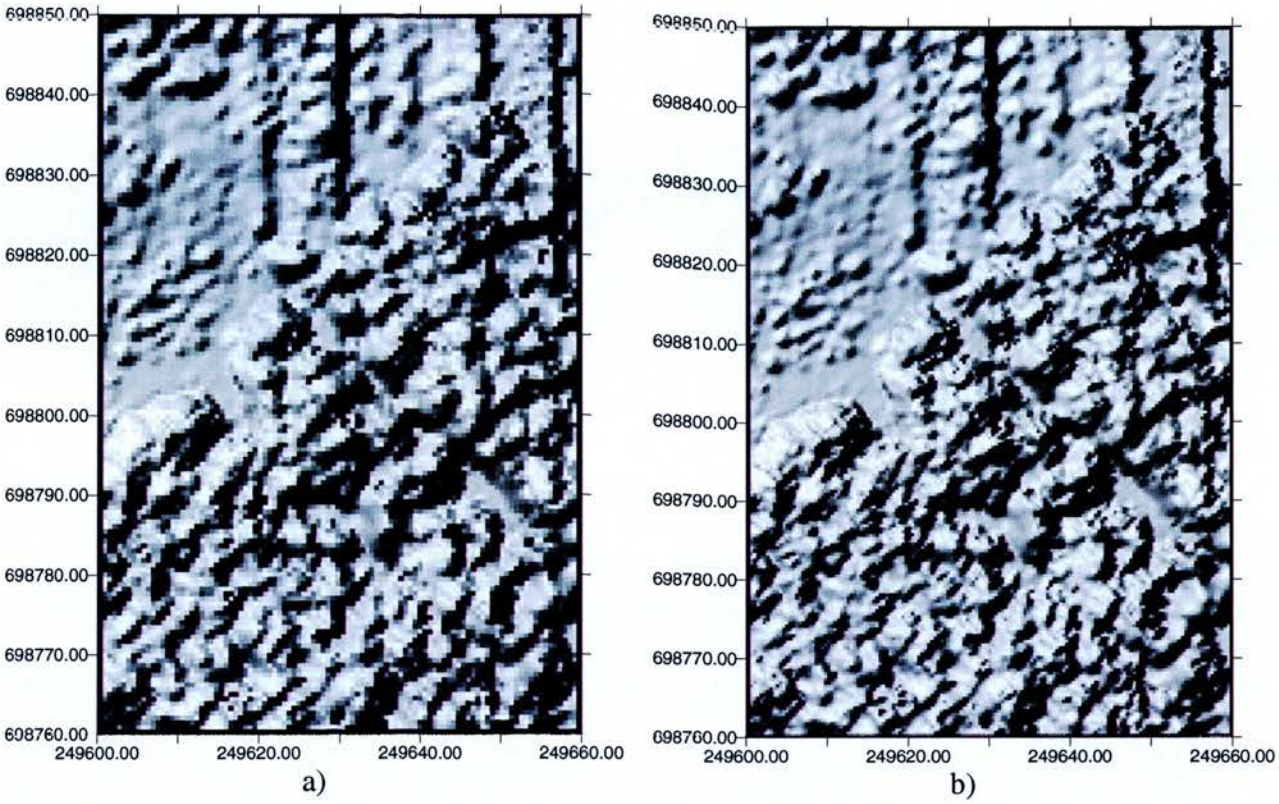

Figure 4.16: Linear method applied to a dense stand. A linear effect is produced when not enough data is considered for the calculations as shown in figure a). In figure b) the effect disappears by increasing the width parameter from 1m to 3m.

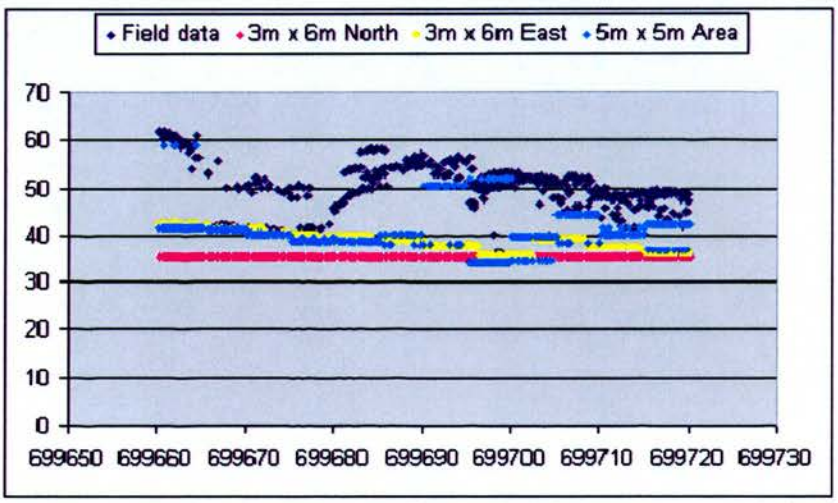

Figure 4.17: Linear method considering 3m for the height parameter and 6m for the width parameter. The best characterization of the ground surface is achieved with the linear method in the East direction. The area method (blue line) gave the poorest results.

- **The window size parameter:** this parameter is considered for the calculation using the area method. Figure 4.18 shows a section of the raw data for an area covered by Norway spruce stands.

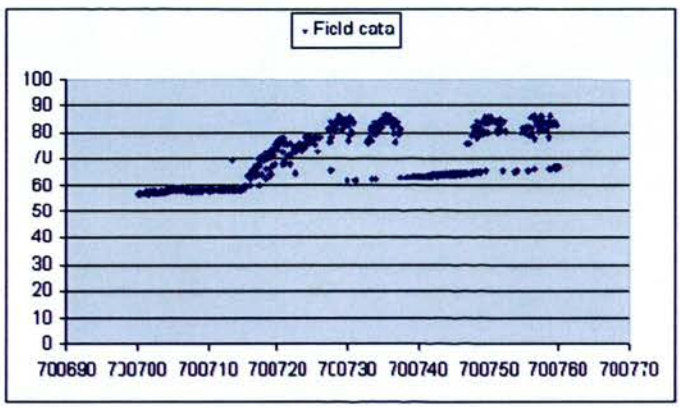

Figure 4.18: Raw data section from Norway spruce stand.

Figure 4.19 shows the calculated ground heights for this dataset (window size 1m x 1m) following the raw data. Ground height is in many areas overestimated when using the area method (blue dots) in comparison to the linear method in both North direction (red dots) and East direction (yellow dots). This is due to the combined effect of the small area considered and the lack of ground laser measurements; therefore it is unlikely that the size window considered contains at least one of the last returns.

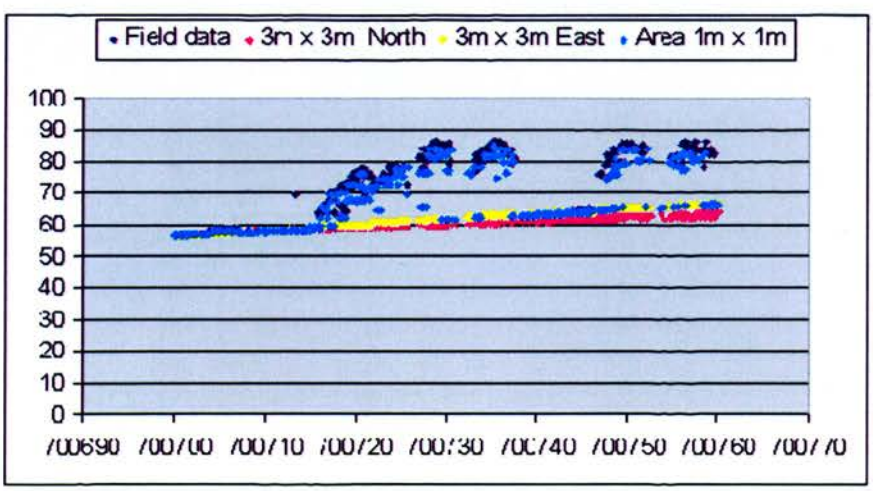

Figure 4.19: Area method 1m x 1m (blue dots) following the raw data. This is produced by the lack of ground returns within the window size considered for the calculation. The lineal method (pink and yellow lines) estimated better the ground heights.

Figures 4.20 and 4.21 show the distribution of the calculated ground heights by the area method considering areas of 3m x 3m and 5m x 5m, respectively. In figure 4.21 it can be seen that the 5x5m parameter produces nearly similar results as for the line method. However, problems occur when areas larger than 5m x 5m do not have any last returns within them so that the value taken as representative of the ground surface may actually represent the canopy (figure 4.22).

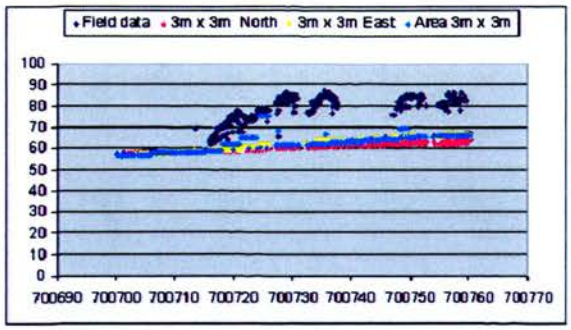

Figure 4.20: Area method window size 3m x 3m.

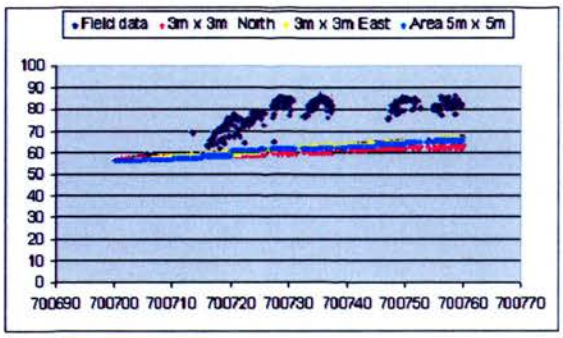

Figure 4.21: Area method window size 5m x 5m

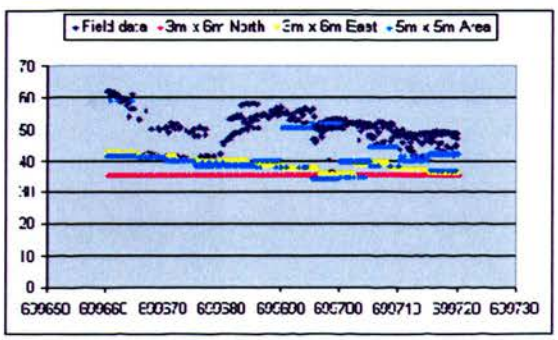

Figure 4.22: Area method applied to a very dense Norway spruce stand with a window size of 5m x 5m.

All the analyses for the evaluation of both the lineal and area methods, considering different values for height and width parameters, were performed on three different sections of the data plots: at the beginning, middle, and at the end of the plots, to cover for topographical variations that might be present. As the size of the plots was not too big (50 m x 50 m) and the stands were topographically nearly flat (with the exception of plot 6), the differences among the three analyses were mostly negligible but the visualization of the distribution of the data all over the plots helped to characterize the variation in the terrain. Figure 4.23 illustrates that analysis.

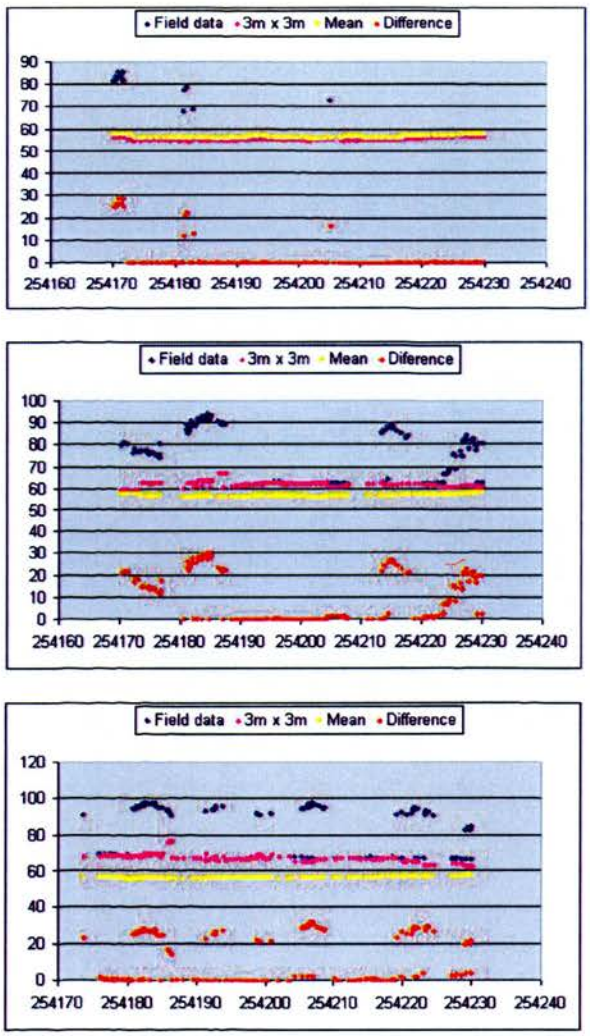

Figure 4.23: LiDAR data distribution for different sections of the selected field plot (plot 5 corresponding to the European larch species). The figure at the top shows a profile at the beginning of the plot, the one at the center is a profile at the middle of the plot, and the bottom figure a profile at the end of the plot, all of them at different heights.

4.8 Generation of the Digital Terrain Model (DTM)

Once the analyses using the linear and area method with different thresholds was carried out and evaluated, the linear method with parameters of 3m for both height and width of the line was chosen for the classification and interpolation of ground and vegetation points. A DTM was generated for each plot under study using Surfer (Version 6.02, Golden Software, Inc.) where the classified points were used to interpolate the DTM to a regular grid of 0.5 m resolution. Several methods such as Inverse Distance, Nearest Neighbour and Kriging were used to interpolate the DTM surface. The method of interpolation chosen was Kriging with linear variogram (which does not have a sill) and no anisotropy (as coordinates X and Y are plot in the same scale and there is no a preferred direction of lower or higher continuity between data points). This method and its respective parameters offered the closest visual correspondence with the topography of the studied plots. The DTM corresponding to the European larch (plot 5) is shown in figure 4.24.

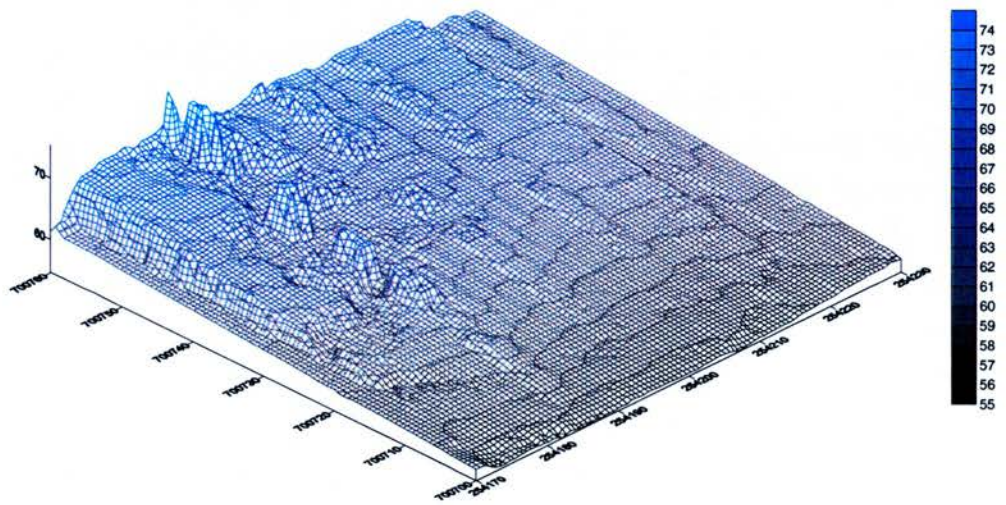

Figure 4.24: LiDAR DTM of the area that contains a 50m x 50m European larch plot 5 under study.

One of the main limitations of the LiDAR technique is the large size of the files that are generated (Morsdorf et al. 2004). The storage, distribution, interpolation, and analysis of LiDAR datasets, which frequently exceed a billion data points, present significant computational challenges. In this work only the data specific to each plot was analyzed,

therefore a DTM was built for every plot rather than for the total area for which LiDAR data was acquired. Every LiDAR plot file of 100 x 100 m analyzed consisted of approximately 30000 LiDAR "hits" or XYZ coordinate values. It was expected that data reduction to ease calculations did not affect the accuracy of the analysis but a method to reduce dataset size reliably is needed.

The derived LiDAR DTMs were compared to existing DTM and GPS ground control points. The main problem when comparing the results to another DTM was the fact that the existing DTM is based on measurements with a lower point density therefore a lower resolution. Thus, it is difficult to find a DTM that has a higher reliability, which could serve as a reference. The DTM that served as a comparison was at 10m resolution from Ordnance Survey.

All positions extracted from the LiDAR derived DTM were within the 10m accuracy of the OSGB DTM. A most precise comparison was performed against positions obtained with Global Positioning System (GPS) technology. The resulting LiDAR DTM was compared with 30 GPS points used for the location of the 6 plots (figure 4.26). For this comparison, elevation differences were calculated at these 30 point locations distributed over the study area. The GPS points for the location of the plots were collected with a Trimble Pro XL dual frequency receiver and were post-processed for ephemeris to correct for satellite positions. The list of three-dimensional coordinates of the points used for the comparison is given in table 4.2. The root mean square error (RMSE) of the elevation differences was less than 30 cm (when 18 points lying under short vegetation, gaps or roads as described in table 4.2 were considered) and was calculated using the following equation:

$$RMSE = \left(\sum (Z_l - Z_{GPS})^2 / n\right)^{0.5} \quad \text{.....[7]}$$

where: Z_l = the LiDAR elevation,

Z_{GPS} = the elevation of the GPS points,

n = the number of points compared.

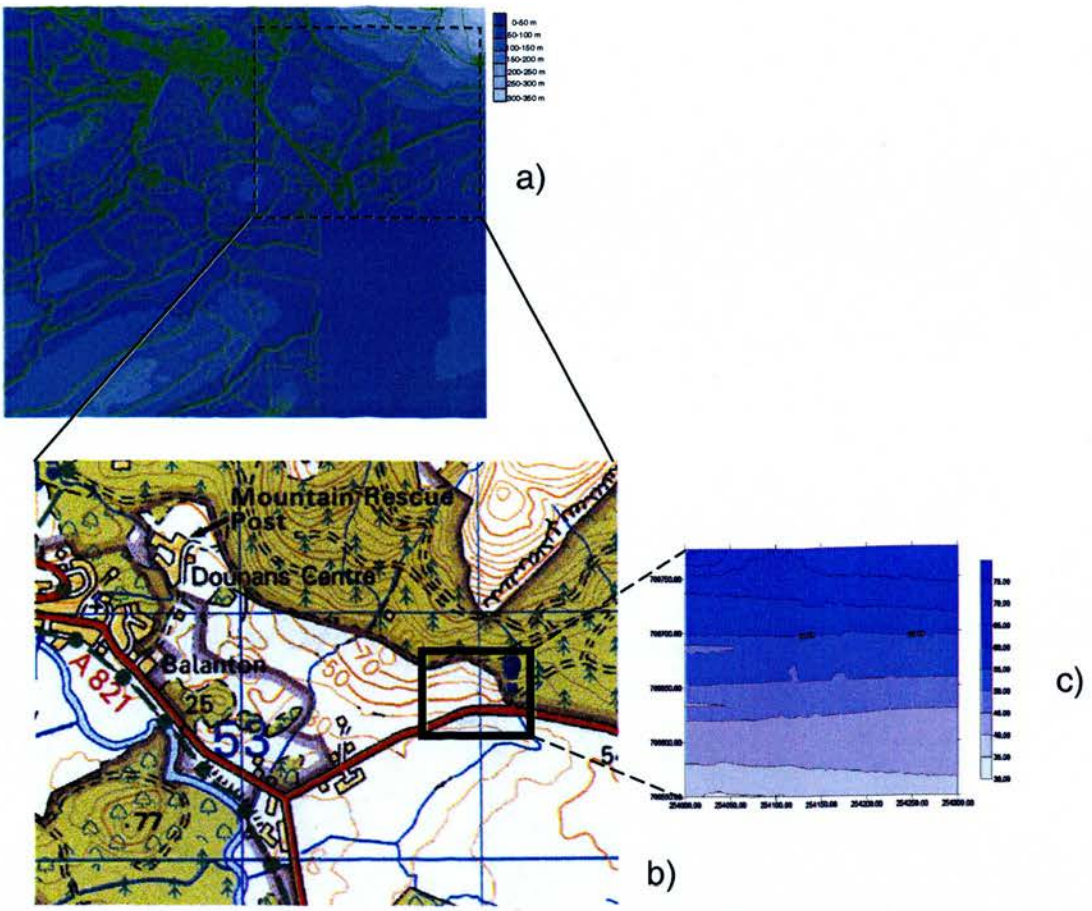

Figure 4.25: Ordnance Survey digital DTM a) of the Aberfoyle area showing in the black box the approximate location of the area in the topographic map b) and the LiDAR-derived DTM showed in c) for plot 5.

When all the points described in table 4.2 were included in the calculation, the RMSE was 2.1 m. The reasons behind these differences might be attributed at the difficulty of the laser hits to penetrate to the ground, as it can be seen in table 4.2 that the LiDAR height of most of the points lying under tall vegetation is higher than its correspondent GPS height.

Point Number	Field height (m)	LiDAR height - Field height (m)	Description
Plot 1			
1	32.53	0.08	road
2	54.86	-0.18	gap
3	42.34	-0.15	short vegetation
4	56.71	1.23	short vegetation
5	61.29	0.31	short vegetation
Plot 2			
6	28.94	0.15	short vegetation
7	36.75	-0.22	short vegetation
8	40.35	1.73	big trees
9	34.87	-0.24	short vegetation
10	36.49	-0.12	short vegetation
Plot 3			
11	20.94	-0.02	road
12	45.16	-0.48	gap
13	41.33	3.06	big trees
14	54.52	4.41	big trees
15	43.86	-0.29	short vegetation
Plot 4			
16	47.54	1.62	big trees
17	50.98	2.59	big trees
18	63.54	-0.04	gap
19	58.36	-0.23	short vegetation
20	45.76	0.27	short vegetation
Plot 5			
21	73.64	5.63	big trees
22	86.33	-0.17	gap
23	84.12	6.34	big trees
24	79.45	2.85	big trees
25	70.62	-0.51	road
Plot 6			
26	68.32	0.86	big trees
27	67.15	0.11	road
28	71.82	2.24	big trees
29	62.26	1.41	big trees
30	67.93	0.94	big trees

Table 4.2: Comparison between field heights obtained with GPS and LiDAR heights.

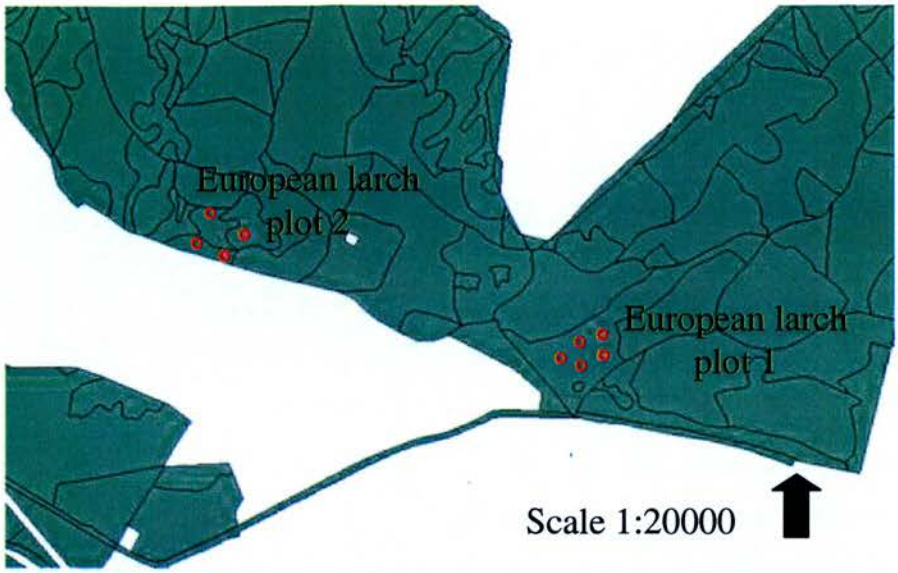

Figure 4.26: Extract of the Achray Sub Compartment Database from Forestry Commission showing the location of GPS measured control points (red dots) on two plots comprising the European Larch species.

It is also known that forest canopy affects the reception and positioning of GPS data. The dispersion of the positions estimated at the same point can be more than ten times greater than when operating in the open (Yoshimura and Hasegawa 2003; Sigrist et al. 1999). Foliage, as one of the three canopy components besides branches and trunks, plays a major role in signal reception and repeatability of GPS observations.

The largest single errors occurred in the European larch sample plots which are characterized by the tallest trees among the species studied and also by the location of these plots in terrain with slopes ranging from low (plot 5, 20%) to high (plot 6, 60%). It has been reported that in sloped terrain, planimetric and height accuracy derived from LiDAR data decrease (Kraus and Pfeifer 1998).

As the European larch plots were also less dense, these results suggest that even though a greater rate of laser hits are able to reach the ground, the topography of the terrain plays an important role. Considering the GPS performance again, it might be that tallest trees cause more interference to the GPS signal making the discrepancies found in these plots a product of a combined effect of topography and tree height. In general, the DTM

developed for each of the plots adjusted fairly well to the ground truth. However, it is recognized that LiDAR may not accurately map all features particularly well as, depending on point density, laser hits may well miss the very tops of trees but can also miss the very bottom of depressions or other terrain irregularities. The smoothing on the data through Kriging interpolation constitutes another important factor that hampers the accurate representation of ground features.

Figure 4.27 shows a LiDAR-derived DTM for the plot 6 using SURFER (Golden Software).

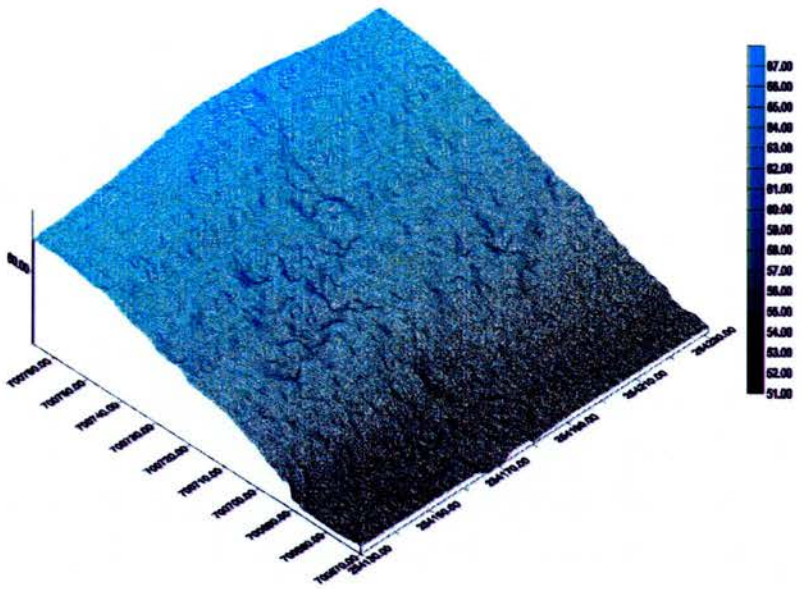

Figure 4.27: LiDAR derived DTM of a European larch sample plot in Aberfoyle.

4.9 Generation of the Digital Canopy Model (DCM)

The digital canopy model was computed as the difference between the digital surface model (DSM), representing the tops of the trees, and the digital terrain model (DTM). The digital surface model corresponds to the tree canopy hits or first return LiDAR points interpolated to a regular grid of 0.5 m and 1 m resolution using a Kriging interpolator (figure 4.28).

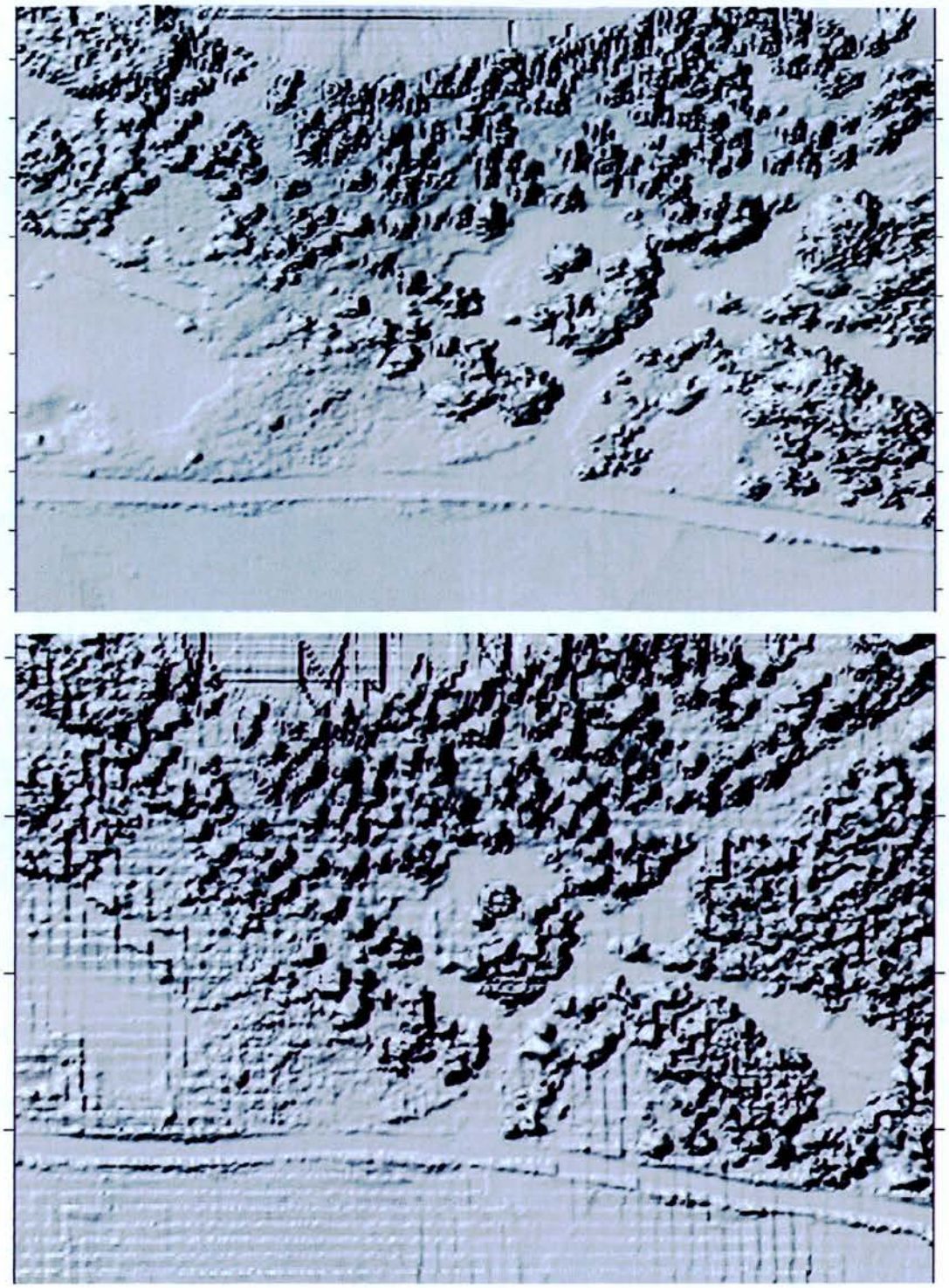

Figure 4.28: Digital canopy models 1 m resolution (a) and 0.5 m resolution (b) of a European larch plot 5 in Aberfoyle.

The resultant DCM at 1 m resolution was detailed enough to detect roads and clearly depicted trees and gaps in the segmentation process. Besides the additional benefit of requiring less computing time, the 1 m resolution grid was also a smoother digital canopy model, as opposed to a 0.5 m grid, as can be seen in figure 4.28. A spline smoothing process was applied to the data in order to get a better visual representation.

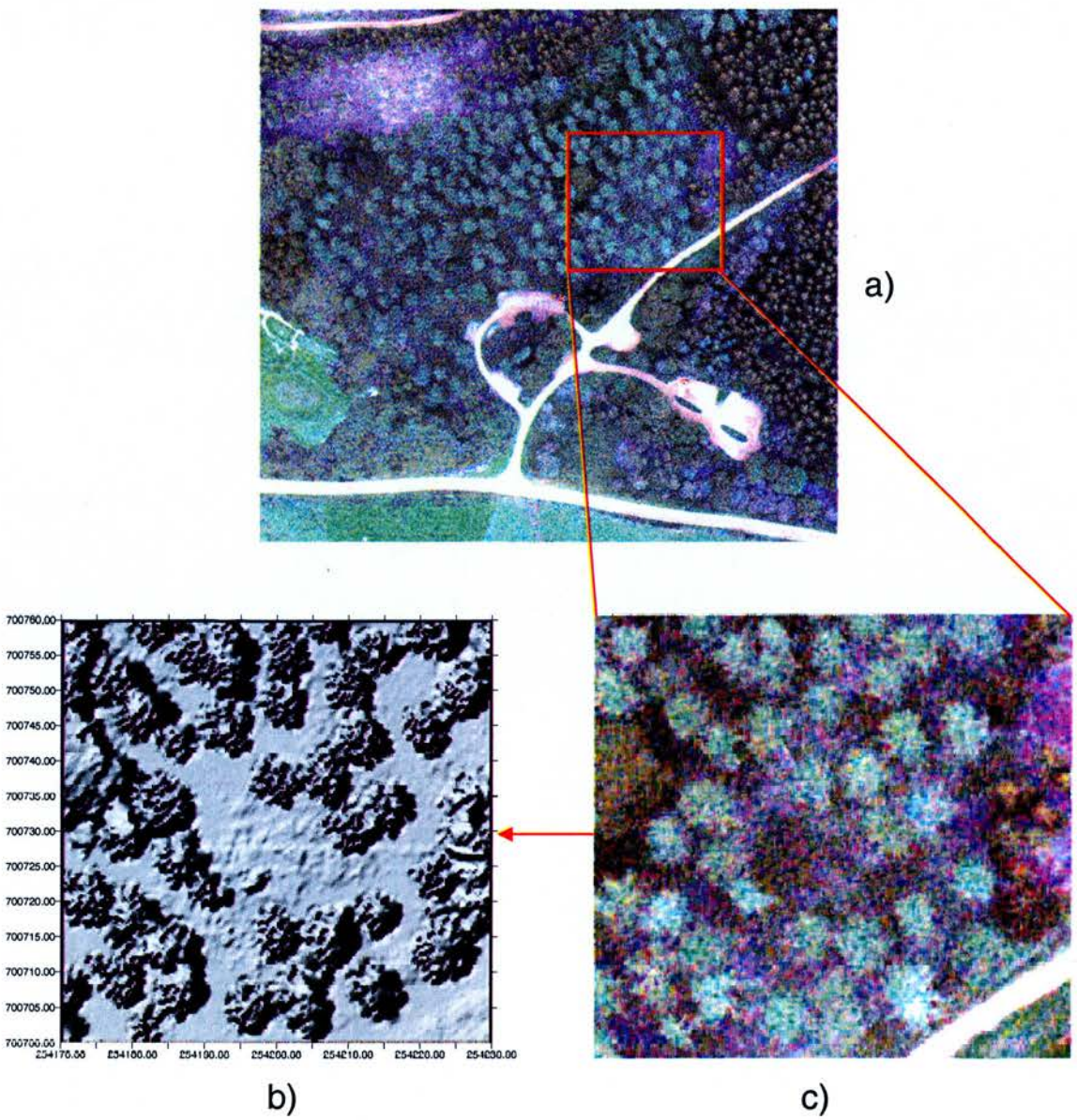

Figure 4.29: Orthophoto (a) and shaded relief view (b) of the LiDAR derived DCM for a European larch plot section within the red box in the orthophoto (c).

Figures 4.29 to 4.30 correspond to the orthophotograph, Digital Terrain Model, and LiDAR derived Digital Canopy Model for a European larch sample plot. The irregularities present to the Northwest of the plot correspond to an abrupt change of topography in that plot.

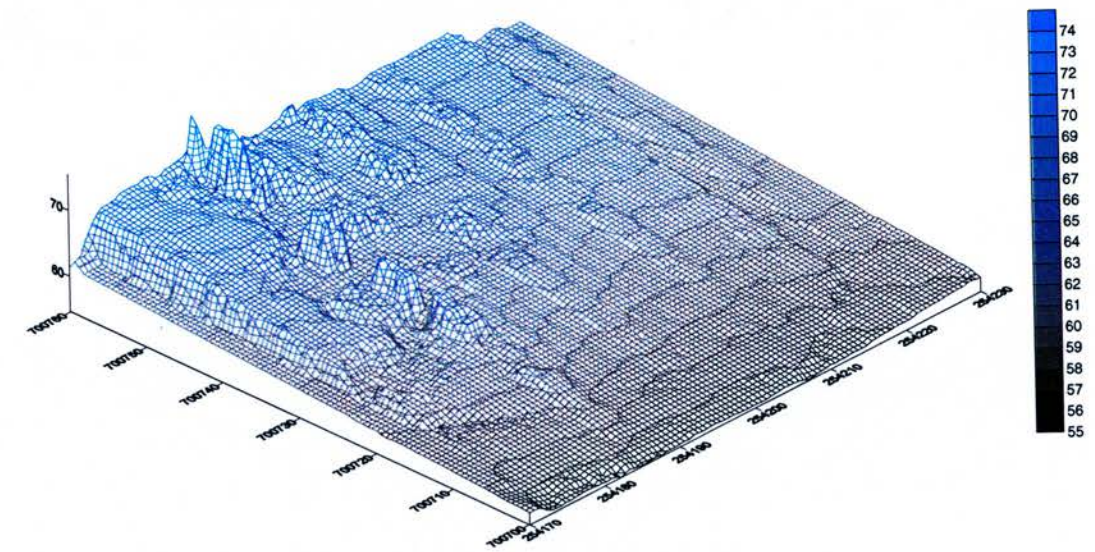

a)

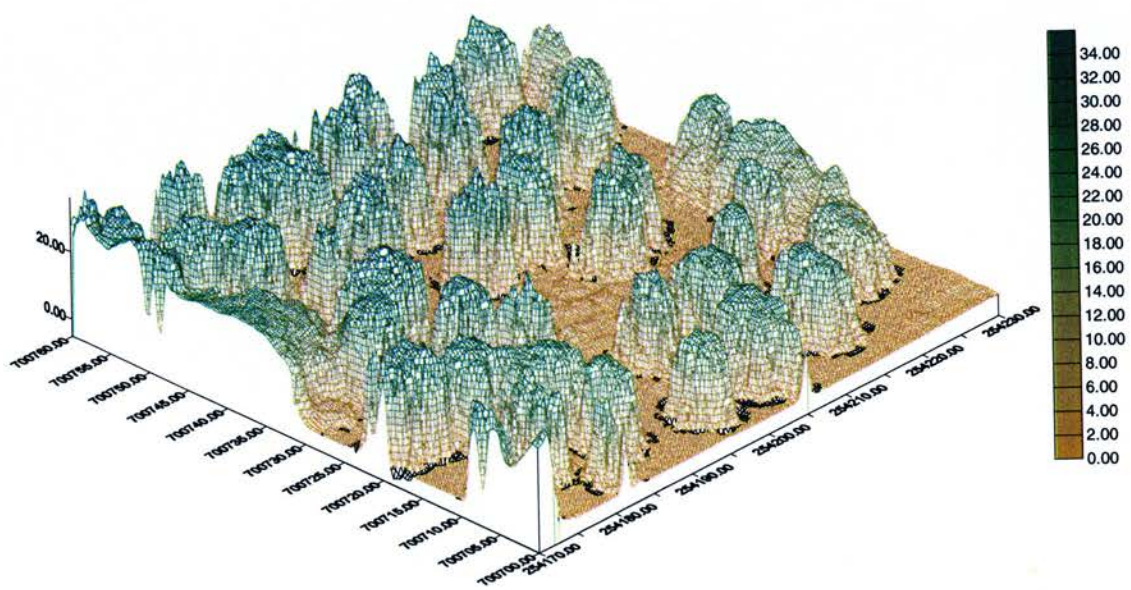

b)

Figure 4.30: LiDAR derived DTM (a) and DCM of a European larch plot 5 (b).

Another example of the DCM generated for a Norway spruce sample plot is shown in figure 4.31. Figure 4.32 shows the DCM's shaded relief view of another Norway spruce stand.

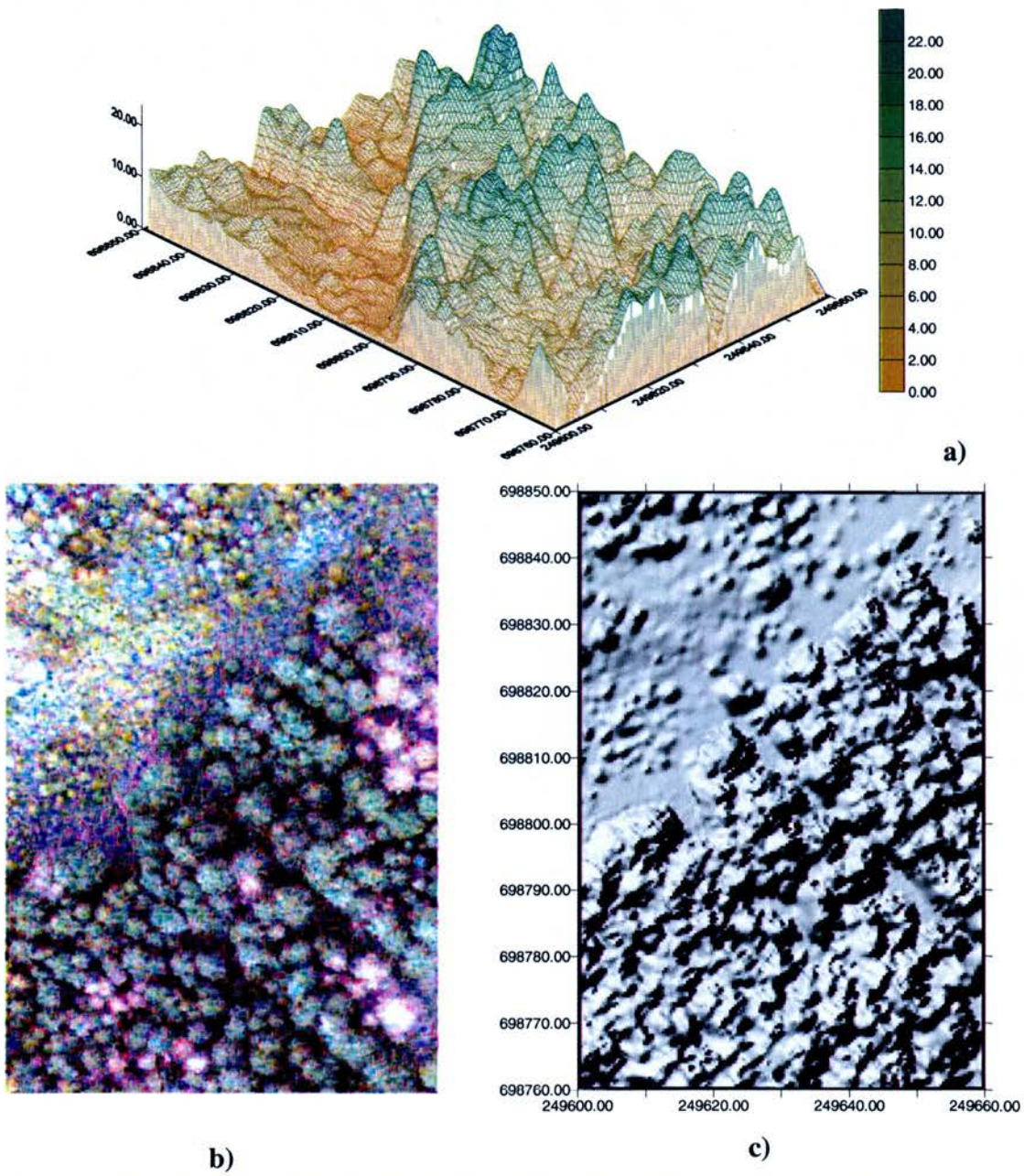

Figure 4.31: Shaded relief view of the DCM of a Norway spruce stand section in Aberfoyle. The density of the data allows both the identification of tree crowns and gaps of different sizes.

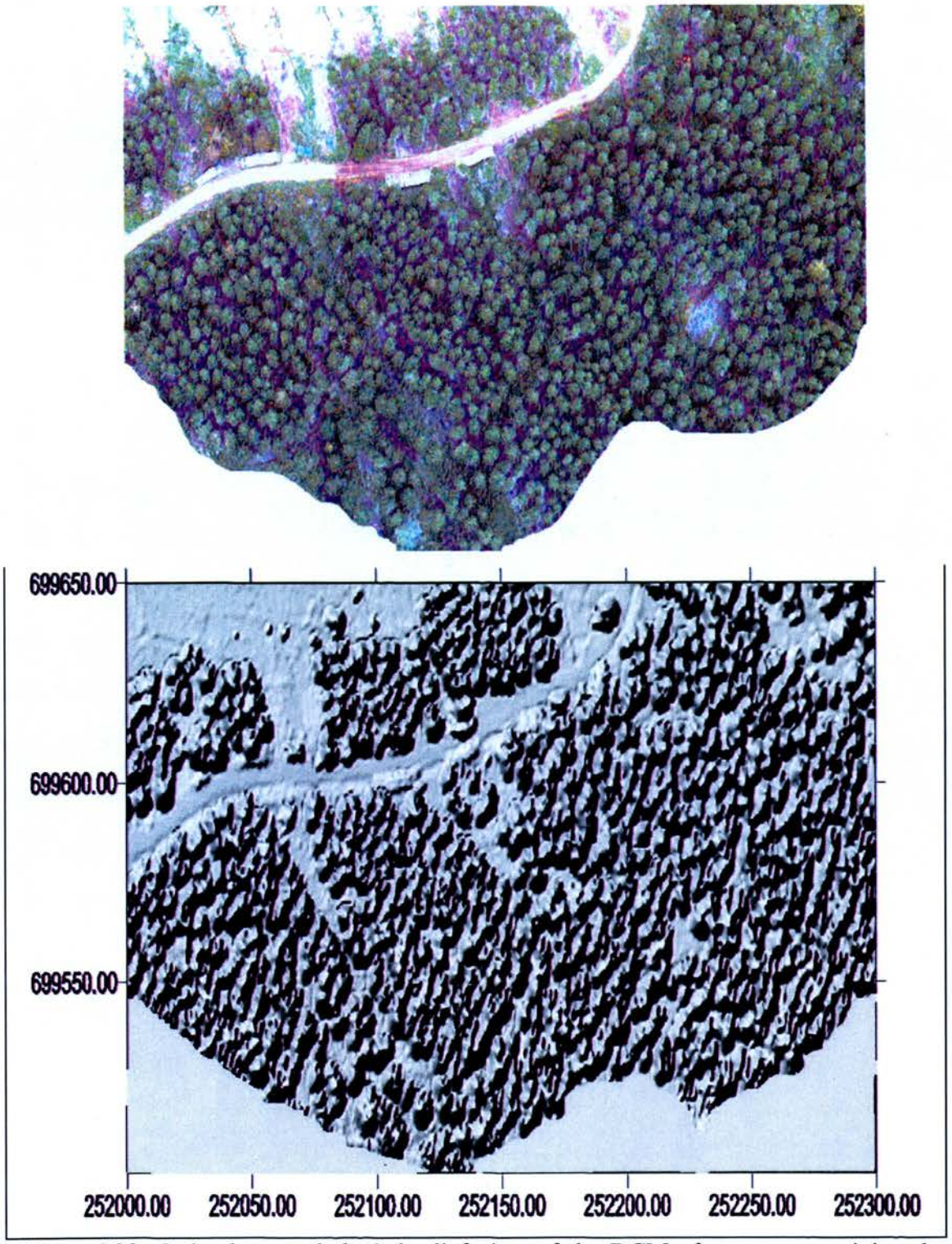

Figure 4.32: Orthophoto and shaded relief view of the DCM of an area containing the Norway spruce stand plot 2 in Aberfoyle.

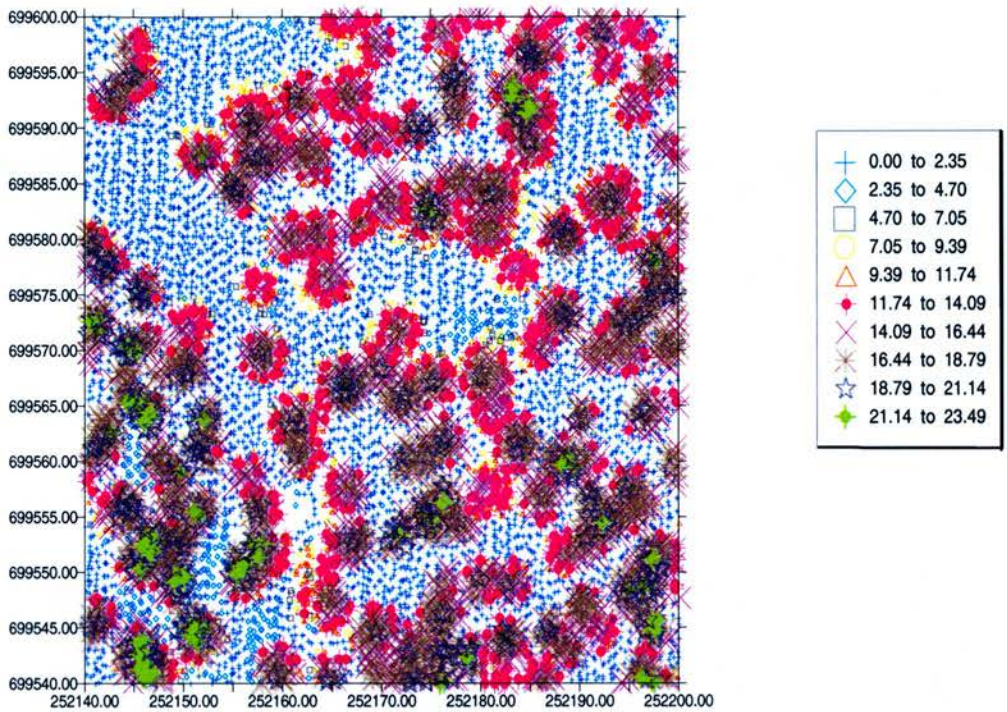

Figure 4.33: Vegetation heights derived from Optech ALTM LiDAR data, 60 m by 60m. The individual tree crowns are Norway spruce. The blue patches are clearcuts. Image brightness scales from blue for zero vegetation height to for trees up to 24 m tall, in 2-metre classes.

Figure 4.33 shows a two dimensional view of the LiDAR-derived heights for the Norway spruce plot 2, which corresponds to the red box in figure 4.32.

Mean tree height, as one of the most important stand characteristics in forest planning, was calculated for all sample plots in order to compare with their respective values obtained from the LiDAR derived canopy height model. Top tree heights were also compared (figure 4.34 and table 4.3).

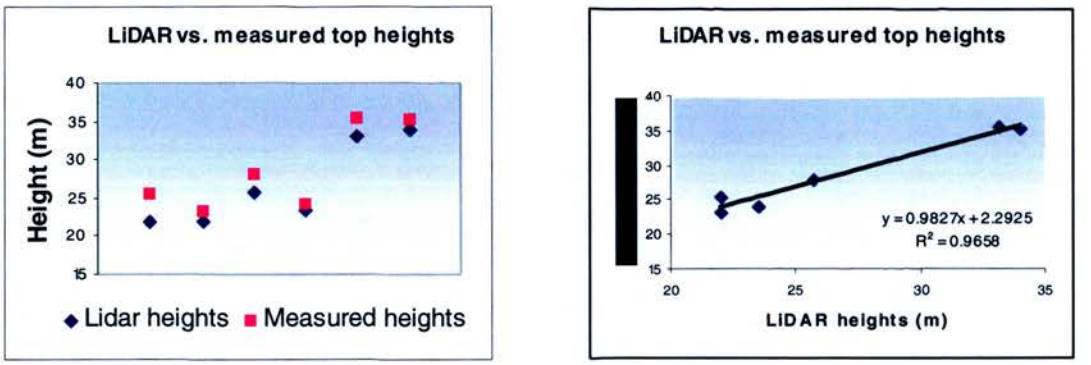

Figure 4.34: Comparison between top heights measured in the field and their respective values obtained from LiDAR.

The individual LiDAR heights of 85 trees were compared with their respective field measured heights. For this comparison, only trees whose position was easily identified on the orthophotographs were chosen. The position of each of these trees was marked on a paper copy of the orthophoto during fieldwork, and their coordinates extracted from the digital orthophoto in Erdas Imagine 8.7. Simultaneously, every tree was identified in the LiDAR derived DCM and their height extracted using the Grid Node Editor tool in Surfer 6.04 (figure 4.35).

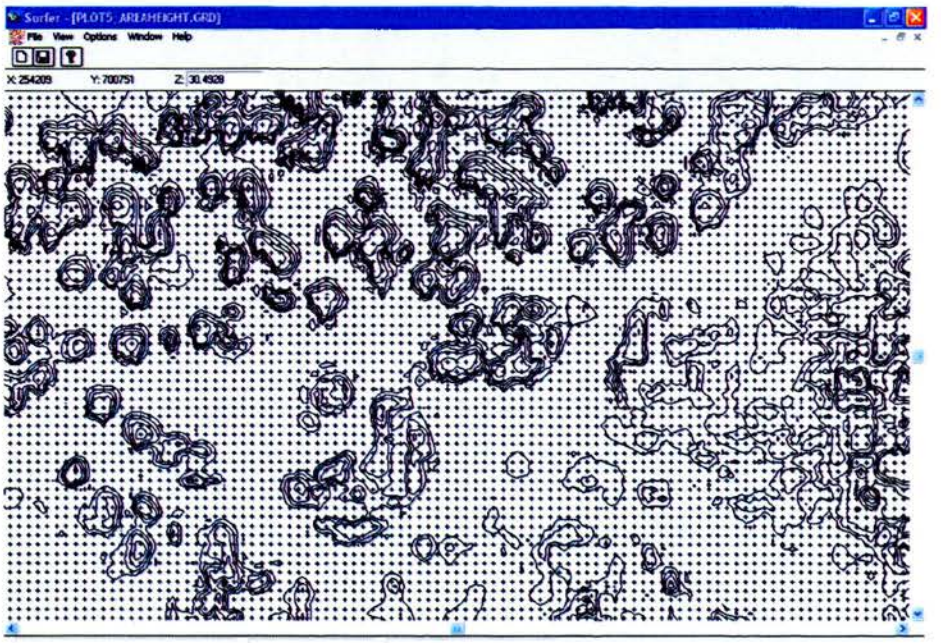

Figure 4.35: Grid node editor in Surfer 6.04 for LiDAR height extraction.

Statistic	Dbh (cm)	Height (m)	Crown width N (m)	Crown width E (m)
		Norway Spruce		
		Plot 1 (115 trees)		
Mean	99	19.83	5.23	5.08
Minimum	45	12.3	3	3.5
Maximum	73	25.4	8.5	7.2
Standard deviation	26.03	3.06	1.056	0.91
		Plot 2 (222 trees)		
Mean	72.83	18.1	2.84	3.416
Minimum	11	9.8	1.1	1
Maximum	182	23.2	5.2	6.1
Standard deviation	36.97	3.56	1.03	1.15
		Sessile oak		
		Plot 1 (168 trees)		
Mean	76.3	24.84	5.75	5.57
Minimum	25	18	2	2
Maximum	170	27	10.2	9.3
Standard deviation	26.75	2.71	2.06	1.75
		Plot 2 (174 trees)		
Mean	89.35	15.73	6.58	5.87
Minimum	35	9.1	3.35	2
Maximum	197	24	15	14
Standard deviation	29.93	3.40	2.88	2.84
		European larch		
		Plot 1 (45 trees)		
Mean	128.7	29.18	6.6	8.8
Minimum	18	14.5	4.5	4
Maximum	161	35.4	12.5	11.6
Standard deviation	27.32	3.58	1.8	1.61
		Plot 2 (83 trees)		
Mean	129.4	31.2	5.37	5.49
Minimum	78	26.4	3.2	3.1
Maximum	221	35.2	7.8	7.4
Standard deviation	37.47	2.17	1.1	1.07

Table 4.3: Descriptive statistics of the field inventory data for the species under study.

Initially, a paired t-test was performed to determine if these datasets were significantly different. With a mean LiDAR height of 27.69 m (variance = 13.32) and a mean field measured height of 29.18 m (variance = 10.58) the heights were different ($\alpha = 0.05$) with a t statistic equal to 10.6 and a critical t-value of 1.21.

Simple linear regression was then applied to the paired heights to determine the existence of a linear relationship. Figure 4.36 shows a plot of the relationship between LiDAR-based and field measured heights where the regression line is $y = 0.9501x$ and correlation coefficient of determination $r = 0.93$. Similar results have been reported, for instance Holmgren and Persson (2004) obtained $r = 0.84$ with a sample (n) of 135 trees; Clark et al. (2004) reported an $r = 0.97$ for mean LiDAR height with n=32; Heurich and Weinacker (2004) compared laser measured tree height versus field measured tree height for 857 trees and obtained $r = 0.98$. In the present study, LiDAR underestimated tree heights by an average of 1.49 m (table 4.4). The standard deviation of the LiDAR estimates was 3.64 and the mean standard error was 0.39.

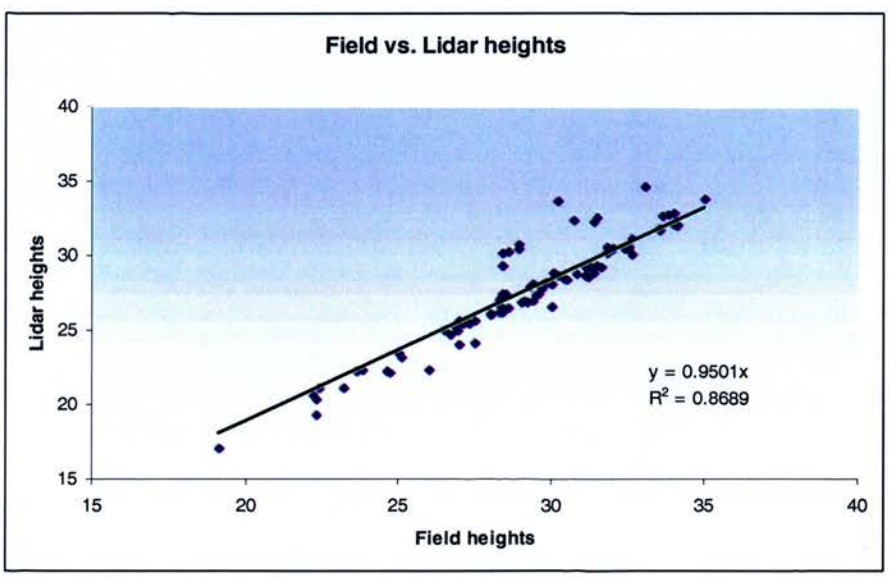

Figure 4.36: Comparison between tree heights measured in the field and their respective values obtained from LiDAR.

	N	Mean	Std. error mean	Std. dev.	Variance
Field height	85	29.18	0.35	3.25	10.58
LiDAR height	85	27.69	0.39	3.64	13.32
Difference	85	1.49	0.04	0.39	1.66

Table 4.4: Descriptive statistics of field measured height and LiDAR derived tree height, and the difference between field and LiDAR measurements.

This systematic underestimation of the tree height using the laser data was found for all plots with a maximum difference of 3.26 m and a minimum of 0.83 m. This result is due, according to this experience, mostly to two factors: 1) the LiDAR data processing: algorithms used for the creation of the DTM and DSM, the interpolation method, and the smoothing applied to get better visual representation of the tree canopy and 2) the uncertainty about the reliability of ground reference data, i.e. the measurement of field heights, which might not be very accurate. Brandtberg (2003) noted that the tree heights measured manually on the ground could be affected by random errors introduced by the field personnel. He concluded that in his research the ground reference heights caused a large proportion of the variance of the differences between ground reference and laser-based tree heights. Such an explanation might also apply to this study although the device used for the height measurement (Vertex II, © Haglöf Sweden AB) has been reported to provide great accuracy (Barron, 2001) even when used by people with little experience of tree measurement. However, Heurich and Weinacker (2004) have pointed out that it is especially difficult to get good height measurements for deciduous and very high trees in the field, as for both classes it is very hard to detect the shoots of the trees especially in the leaf-on period. Moreover the measurement angle becomes very steep for high trees, which can cause a large error.

Maltamo *et al.* (2004) suggest that the major cause of the LiDAR tree height underestimation is due to the fact that not always the laser hits do not necessarily hit the

very top of the tree crowns (figure 4.37). Therefore the DSM may not represent or include the highest possible values for height within the stand. As only the dominant tree layer is detected, suppressed trees may not be found and the detection of the shortest dominant trees and individual trees in tree groups is also difficult. Maltamo *et al.* (2004) also stated that even if laser scanning produces information of tree crowns and suppressed trees under the dominating tree layers, the current processing methods cannot utilise it effectively.

Figure 4.37: The laser pulses hit the trees usually missing the tree tops (Yu *et al.* 2004).

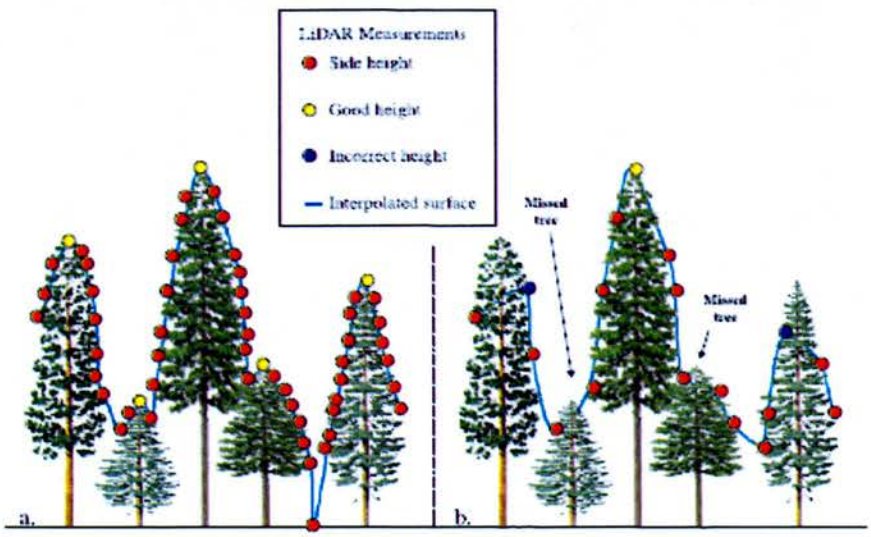

Figure 4.38: Influence of sampling density for the detection of true tree heights. (a) Accurate estimation of tree height due to small post spacing (<2.0m). (b) Less accurate estimate of tree height due to lower sampling density (≥2.0m) (Zimble *et al.* 2003).

Hyyppa (2004) and Lefsky *et al.* (2002) suggest several other reasons for height underestimation: sampling density (figure 4.38); the algorithm used to obtain the canopy height model; the amount and height of under vegetation; the algorithm used to calculate the digital terrain model; the sensitivity of the laser system and thresholding algorithms used in the signal processing as well as a pulse penetration into canopy; and the tree shape and tree species effect investigated by Nilson (1997). Maltamo *et al.* (2004) gave some other reasons as penetration in the foliage in addition to the time interval between field measurements and laser data acquisition.

Due to the fact that there are several sources of error and also that they cannot be considered separately but most likely interact, the exact causes of the underestimation of the tree heights are still unknown.

4.10 Discussion of results

The results of this analysis show that LiDAR is a technique that provides forest parameters and allow forest mapping in a reliable manner. Although the method of building the ground DTM and DCM for the sample plots in this study was relatively simple, it produced accuracies similar to those used by LiDAR companies using more sophisticated algorithms. This method could save time when greater accuracy is not needed, although a more accurate approach would almost certainly improve estimates.

Although this is one of a few studies to test LiDAR methods in the context of forestry in the UK, the retrieval of tree height proved to be highly successful, as has been reported in most LiDAR research projects. This has significant benefits for forest management and particularly for Continuous Cover Forestry, where the diversity of species and heights calls for intensive forest inventory. In order to use airborne laser scanning in standard forest inventories, the tree species as well as tree heights have to be extracted. The management of forests under or in transition to CCF may rely on the potential of LiDAR for the extraction of individual tree heights for its monitoring. However, little success has been reached related to species recognition, an area that needs further analysis.

The basic limitation of the LiDAR method, suggested by Ackermann (1999), is its blindness about the capture and identification of objects and object features, which translates in the forested environment analyzed in the inability to recognize species. This restriction was overcome in this study with the use of aerial photographs to support the filtering of laser pulses, and provided a much better understanding of the area and the forest stands and thereby improved the algorithm performance.

Further improvements are expected when filter algorithms start making use of additional information sources (Sithole and Vosselman 2004). Results and performance could be enhanced if image information would become an integral part of automated data processing. A fusion can be expected by the combination of LiDAR approaches with photogrammetry and multi-spectral data.

The main objective of this chapter was to produce the digital canopy models that will be used as input for segmentation and classification for tree crown detection and delineation. In order to achieve this, new algorithms for processing the data were required to be written. Three species were selected for the study, as they provide different scenarios for analysis and are representative of different light regimes. Deciduous plots were characterized for strong shadowing and very dense canopies, while spruce stands were more homogeneous but also dense. European larch sites were also homogeneous but of particular interest due to their location within the Regeneration Study Area described in chapter 2 and also for its particular topography. LiDAR, obtained at a point density of 4 returns per square metre, was able to map the differences between plots regarding tree density, gaps, topography, and most importantly, to provide high-resolution imagery for crown and gap delineation with considerable detail and accuracy.

Chapter 5

Object oriented analysis of tree crowns and forest gaps using LiDAR, ATM and aerial photography

5.1 Introduction

This chapter evaluates small foot-print multireturn LiDAR, multispectral Airborne Thematic Mapper (ATM) imagery and aerial photography acquired over an area covered with deciduous and coniferous stands in Aberfoyle, Scotland, for their ability to detect and delineate tree crowns. The study also evaluated the potential of a LiDAR-based object oriented approach to deciduous and coniferous forest classification. This analysis was carried out with the use of object oriented segmentation and classification analysis, performed separately on each dataset, followed by a combined analysis to investigate potential improvements on the results. In the segmentation process, an iterative segmentation and classification of the LiDAR and ATM imagery was performed until a good correspondence with aerial photography was achieved. Thus, the potential of LiDAR for mapping horizontal structure of forest stands alone or in combination with high spatial and spectral resolution data was thoroughly explored.

Specifics objectives included:

- Evaluation of the potential of digital aerial photographic data, multispectral ATM imagery, and LiDAR for crown delineation, based on object oriented approaches.
- Determination of the optimum segmentation result and
- Validation of the segmentation selection through comparison with reference data.

As was highlighted in the previous chapter, there exists a considerable body of research using LiDAR data for forestry applications and which have dealt mostly with the extraction of stand characteristics like tree height, basal area, stand volume, and stem density (e.g. Nilsson 1996, Lefsky *et al.* 1999, Means *et al.* 2000, Næsset 2002, Zimble *et*

al. 2003, Clark *et al.* 2004, Collins *et al.* 2004, Maltamo *et al.* 2004) as well as leaf area index and biomass (Hagiwara *et al.* 2004, Lim and Treitz 2004, Brandtberg *et al.* 2003). Diversity and species composition have also been studied with LiDAR (Blaschke *et al.* 2004, Holmgren and Persson 2004, Hill and Thomson 2005).

LiDAR data has been increasingly used for tree delineation in the last few years (Tiede *et al.* 2004; St-Onge and Vepakomma 2004; Brandtberg *et al.* 2003). The main advantage of the LiDAR- derived digital canopy models (DCMs) is that they are unaffected by non-uniform light intensity which means that they can be used to detect trees that would otherwise be in shadow; however, DCMs are often less precise than those derived from high resolution imagery and trees that are very close cannot be extracted (Mei and Durrieu 2004).

The renewed interest in sustainable management of forests, maintaining ecosystem diversity and resilience and protecting sensitive species while providing for a variety of ecosystem services of value to the community (Coates and Burton 1997) have demanded the consideration of the use of remote sensing techniques to provide information and parameters that help to understand and describe in a better way the complex processes occurring at stand level. Acquiring data on the distribution and species of individual tree crowns, crown sizes, crown closure, and canopy gaps would be a valuable contribution (Leckie *et al.* 2005). But these processes cannot be completely evaluated with the traditional methods of forest inventory and stand mapping, which can hardly deliver continuous information about different forest structures as is required by more ecological silvicultural systems such as CCF. Therefore, high resolution LiDAR and multispectral imagery, among other remote sensing sources of data, have been evaluated and researched for their potential to provide, alone and in combination, reliable and accessible information about traditional forest structure attributes and in the description of the three-dimensional character of the forest, especially at forest stand and tree levels (Bunting and Lucas 2006, Hill and Thomson 2005, Hudak *et al.* 2002, Tickle *et al.* 2001, Watt *et al.* 2004, Heurich *et al.* 2004, Bhogal *et al.* 2004). This information could not have been assessed before, but advances in technology now allow.

Along with improvements in spatial and spectral resolution of remote sensing data, more sophisticated algorithms for its processing have been developed in the last decade. Specifically for forest classification, object oriented techniques have been increasingly used for their advantages over traditional pixel based classification approaches, especially for its more realistic representation of the elements in the forest. A more in depth review of the object oriented classification method and its usefulness for tree mapping is given as follows.

5.2 Object oriented image segmentation and classification

The automatic classification of remotely sensed data is often an essential action within the image analysis process. Unfortunately, the high spatial resolution of advanced sensors increases the spectral within-field variability and therefore may decrease the classification accuracy of traditional per-pixel based methods (Schiewe *et al.* 2001), which use the radiometric information contained in the image bands. Ideally, pixels are expected to be more or less grouped in multispectral space in clusters corresponding to different land cover types (Price 1994).

A per pixel-based classification results in a thematic map with a label for each pixel of the class to which it has the highest strength of membership. This "hard" or "crisp" classification is based on conventional crisp set theory. A conventional classification of remotely sensed imagery models the study area as a number of unique, internally homogeneous classes that are mutually exclusive. However, these assumptions are often invalid, especially in areas where transition zones and mixed pixels occur. Most of geographical features are rarely internally homogeneous and mutually exclusive; therefore, classes can hardly ever be separated by sharp or crisp boundaries, in feature space as well as geographic space. Furthermore, complex relationships exist between spectral responses recorded by the sensor and the situation on the ground, where similar classes, pixels or objects show varied spectral responses and similar spectral responses may relate to dissimilar classes, pixels or objects. Moreover, remotely sensed images

contain many pixels where boundaries or sub-pixel objects cause pixel mixing, with several land covers occurring within a single pixel (Lucieer 2004).

The problems arising from a method that considers a pixel as the basic unit for the classification process can be solved with methods that are able to compose spatial entities (i.e. regions) which can be used as basic units in image analysis instead of single pixels. These regions can be determined with the help of image segmentation. Segmentation is defined by Pal and Pal (1993) as "a process of partitioning the image into some non-intersecting regions such that each region is homogeneous and the union of no two adjacent regions is homogeneous".

Thresholding, statistical classification, edge detection, and region growing are defined as the principal image segmentation approaches. Each method has advantages and disadvantages. For example, thresholding of image histograms is relatively straightforward, but disregards spatial information. On the other hand, statistical approaches take all image information into account, but ignore the spatial explicitness inherent in remote sensing imagery. Edge detection and region growing share the common disadvantage of subjective user input, while spatial information recognition is an advantage in both cases (van Aardt 2004).

The concept of image segmentation is not new but it has attracted lot of attention in recent years. Many new segmentation algorithms as well as applications have been developed, but not all of them lead to qualitatively convincing results while being robust and operational. One reason is that the segmentation of an image into a given number of regions is a problem with a large number of possible solutions (Blaschke and Strobl 2001).

Image segmentation methods are split into two main domains: knowledge driven (top down) methods and data driven (bottom up) methods. In the top down approach the user already knows what they wants to extract from the image but does not know how to

perform the extraction. By formulating a model of the desired objects, the system tries to find the best methods of image processing to extract them (Yan 2003).

Bottom-up methods perform a segmentation of the complete image. It groups pixels into spatial clusters that meet certain criteria of homogeneity and heterogeneity. Bottom-up methods can thus be seen as a kind of data abstraction or data compression. As with clustering methods, in the beginning the generated segments are only image object primitives. It is up to the user to determine what kind of real world objects the generated image objects represent. Yan (2003) lists the most common types of bottom-up approaches to image segmentation as follows:

- Global thresholding. In this kind of approach feature space is separated into subdivisions, and locally adjacent pixels of the same subdivision are merged. This method leads to results of relatively limited quality. Oversegmentation and undersegmentation (i.e., separation into units which are too small or merging regions that do not belong to each other), take place easily without good control of meaningful thresholds. Local contrasts are not considered or not represented in a consistent way and the resulting regions can differ widely in size.
- Region growing algorithms cluster pixels starting from a limited number of single seed points. These algorithms basically depend on the set of given seed points and often from a lack of control in the break-off criterion for the growth of a region.
- Texture segmentation algorithms. They typically obey a two-stage scheme: 1) in the modeling stage characteristic features are extracted from the textured input image and range from spatial frequencies. 2) In the optimization stage features are grouped into homogeneous segments by minimizing an appropriate quality measure. These methods are only applicable to a limited number of types of image data, texture types and problems. Texture often must be very regular to be recognized. Results can often not be achieved on any chosen scale.
- Knowledge-based approaches. These approaches try to incorporate knowledge derived from training areas or other sources into the segmentation process. These approaches mostly perform a per pixel-based classification, based on clustering in

a global feature space. Segments are produced implicitly after classification, simply by merging all adjacent pixels of the same class. In doing so these approaches are typically not able to separate different units or objects of interest of the same classification. Furthermore, the information on which the classification can act is typically limited to spectral and filter derivatives.

The multiresolution hierarchical approach developed by Baatz and Schäpe (2000) called the "fractal net evolution approach", is a bottom-up region growing technique that has been implemented in eCognition software (Definiens Imaging 2004). This approach is a move away from per pixel-based analysis, towards an object-based analysis, and multiple scales of objects can be explored within a single data set (Burnett and Blaschke 2003).

eCognition was chosen for the analysis carried out in this research because the segmentation results are robust, it has widespread availability, and adequate software support. This approach has been widely used for forestry applications such as automated tree detection (Heurich and Weinacker 2004, Tiede *et al.* 2004, Collins *et al.* 2004, Brandtberg *et al.* 2003), prediction of forest volume and biomass (van Aardt 2004) and for forest type classification (Shataee *et al.* 2004), showing good results specially for conifer forest stands but requiring further work in complex canopies like the ones characterized by deciduous species and mixed forest. All the reported forest classifications performed in eCognition have been more succesful than their per pixel-based counterparts.

The process and results of object oriented image analyses such as that which eCognition performs is carried out in methodological steps described by Burnett and Blaschke (2003) as: database building, segmentation, object relationship model building and classification, and quality assessment.

Database building involves the collation of all sources of information into a database of georeferenced survey, sample and auxiliary data. Segmentation is the key to the multi-scale approach of which the main objective is the extraction of meaningful objects, often

involving an iterative process searching for changes in image object heterogeneity/homogeneity. Object relationship model building includes assigning object relationships that are either automatically derived (such as mean spectral values, shape and distribution) or are semantic and require the knowledge of the expert, at least for training purposes. The subsequent body of relationships is needed to classify homogeneous objects. Finally, quality assessment is an essential component of the approach, both at the final stage and during of the preceding steps.

The following section aims to explain some of the concepts behind the object orientated segmentation procedures in eCognition.

5.3 Segmentation procedure in eCognition

According to Schiewe *et al.* (2001) segmentation is basically an automated procedure representing the way human eyes might recognize a group of pixels as individual objects. It divides the image into objects and in recognizing those objects, it follows the hypothesis that neighbouring image elements belong to the same class. This approach for classification avoids the problems of single mixed pixels and provides more parameters upon which to classify (texture, shape, neighbouring, distance, and direction) rather than the brightness normally used.

Multi-resolution segmentation is a basic procedure in eCognition for object-oriented image analysis. It is used to produce image object primitives as a first step for further classification and other processing procedures (Yan 2003). The segmentation rule is to create image objects as large as possible and at the same time as small as necessary.

The segmentation starts with one pixel objects. In numerous subsequent steps, smaller image objects are merged into bigger ones. Throughout this pair-wise clustering process, the underlying optimization procedure minimizes the weighted heterogeneity of resulting image objects. In each step, that pair of adjacent image objects is merged which stands

for the smallest growth of the defined heterogeneity. If the smallest growth exceeds the threshold defined by the scale parameter, the process stops (Yan 2003).

Throughout the segmentation procedure, the whole image is segmented and image objects are generated based upon several adjustable criteria of homogeneity in colour and shape. Adjusting the so-called scale parameter indirectly influences the average object size: a larger value leads to bigger objects and *vice-versa*. Additionally, the influence of shape as well as the image's bands on the object's homogeneity can be adjusted.

The process starts at the level of pixels and continues to consecutive levels. Each level is constructed based on its direct sub-objects, i.e., sub objects are merged into larger image objects. Merging is limited by the borders of super-objects; adjacent image objects cannot be merged when they are sub-objects of different super-objects (Rajapakse 2003).

5.4 Object oriented classification techniques

The meaningful primitive objects obtained through segmentation can be classified by two methods: Sample based classification using a nearest neighbour classifier and rule based classification using a membership function technique.

The nearest neighbour method classifies objects in a given feature space and with given training samples for the class of concern. The simple nearest neighbour classifier computes the Euclidean distance from the pixel to be classified to the nearest training data pixel in n-dimensional feature space and assigns it to that class. This process can yield useful results if the training data are well separated in feature space (Jensen 2005).

However, classes are often hard to define resulting in vagueness and ambiguity in a nearest neighbour-based classification scheme. Most, if not all geographical phenomena are poorly defined to some extent and, therefore, fuzzy set theory as an expression of concepts of vagueness can be an appropriate model for working with remotely sensed

imagery. To adapt to the fuzziness characteristic of many natural phenomena, fuzzy classification approaches have been proposed (Lucieer 2004).

Fuzzy clasification allows greater flexibility in comparison with binary theory which can only have two extreme values, and one pixel can only belong to one class. Fuzzy set theory allows a pixel to hold several non-zero membership grades for different information classes (Yan 2003).

Fuzzy classification is a technique that operates on fuzzy logic, a multi-valued logic quantifying uncertain statements. The basic idea is to replace the two Boolean logical statements "true" and "false" by the continuous range of [0,….,1], where 0 means "false" and 1 means "true" and all values between 0 and 1 represent a transition between true and false. Avoiding arbitrary sharp thresholds, fuzzy logic is able to approximate the real world in its complexity much better than the simplifying Boolean systems do; fuzzy logic can model imprecise human thinking and can represent linguistic rules (Benz *et al.* 2004).

Each class of a classification scheme formulated in eCognition contains a class description. Each class description consists of a set of fuzzy expressions allowing the evaluation of specific features and their logical operation. Three main processes or steps are involved in fuzzy classification implemented in eCognition. The first one is called "fuzzification" and it performs the conversion from a hard to a soft system. In this step a membership value is assigned to each feature of an object (e.g. shape, texture, spectral value) with a value between 0 and 1. The second step is the building of a fuzzy rule-base which is a combination of fuzzy rules. A fuzzy rule can have one single condition or can consist of a combination of several conditions that have to be fulfilled for an object to be assigned to a class. The last step is defuzzification. Here the fuzzy memberships are translated back into hard values in order to visualize classification results where maximum fuzzy membership degree of the class is used as the class value to be represented (eCognition User Guide 4, 2004).

In short, the output is twofold: a fuzzy classification with detailed information of class mixture and reliability of class assignement, and a final crisp classification where each object is assigned to only one class (or none, if assignment was not possible).

Previous experience has demonstrated that if a class can be separated into other classes by just a few features or only one feature, the application of membership is recommended otherwise the nearest neighbour method is suggested (Ivits *et al.* 2002).

5.5 Data characteristics

In order to investigate the usefulness of multispectral remote sensing in combination with LiDAR data for vertical and horizontal forest structure characterisation, an Airborne Thematic Mapper image and a LiDAR dataset were acquired for this study.

Due to its high spatial resolution, existing orthophotographs of the area were used as a visual aid in the classification process, and as a validation set for the segmentation and classification results from the object oriented approach, along with the data collected directly on the sample plots as described in chapter 2.

The main characteristics of the datasets used are outlined in table 5.1.

Data Set	Number of bands	Spectral Range	Horizontal Resolution
Aereal Photography	3	Visible	25 cm
ATM	11	Visible, near, short and thermal infrared	2 m
LiDAR	1	Ultraviolet, visible and infrared	1 m

Table 5.1: Main characteristics of the available datasets.

LiDAR data provide accurate 3D coordinates and detailed information on forest canopy vertical structure but over a limited spatial extent (Hudak *et al.* 2002) and less direct information on the object's geometrical shape. In contrast, high resolution imagery such as Airborne Themathic Mapper provides more detailed information on objects, such as spectral signature, texture, shape, although it cannot supply direct measurements of canopy height or estimates of tree diameter or timber volume as LiDAR data can (Hill

and Thomson 2005); therefore the combination of the two datasets should improve the results for segmentation and classification compared with the use of spectral response only.

The ideal situation for the forestry community would be to base its operational and strategic applications on just one data source, for instance LiDAR or multispectral data, with which technical and economical issues could be highly reduced. This implies the development of high resolution sensors that can contribute to a detailed analysis of forest structure on a tree level, along with the techniques for the processing of this high resolution data. However, despite great technical advances, there is still a lack of acceptable accuracies on information required routinely such as canopy cover, tree size (height and crown diameter), biomass, and crown volume, among others. The primary reason for this is that important characteristics of the land surface are tied to vertical structure which most remote sensing techniques have difficulty to retrieve (Dubayah *et al.* 2005). That is why LiDAR represents a breakthrough technology, providing direct measurement of the vertical dimension, but although being a relatively new technique, there is lack of expertise and a need for experiments that integrate field work and subsequent data analysis and the development of a methodology for the processing and evaluation of LiDAR products.

In the segmentation, the LiDAR points are resampled to raster form. After that it is possible to utilize the combination of the elevation attributes from LiDAR data and radiometric atributes from the image in the segmentation. The data with similar heights and spectral attributes are merged into a region. An advantage of this process is that image objects can be extracted from one data layer, and subsequently in the image analysis step those image objects are able to take into account the attributes of the other data layers (Syed *et al.* 2005).

In the classification, the object-based classification was used to separate the vegetation and no vegetation region and then the trees from the gaps. The attributes considered in the classification are: the elevation information from LiDAR data, the spectral

information from multispectral imagery ATM and orthophotography, the texture information from the high spatial aerial photography, and the shape of regions.

Spatial registration of LiDAR data, Airborne Thematic Mapper imagery and orthophotography were performed as data preprocessing to unify the datasets in the object coordinate system. A more detailed description of the data sets used in this chapter as follows.

5.5.1 LiDAR data

As described in chapter 4, LiDAR data was acquired on the 19th of September 2002, using and Optech ALTM2033 scanner. The LiDAR data consisting of a list of tridimensional coordinates for the first and last return of the laser signal, was used in the derivation of a Digital Terrain Model and a Digital Surface Model, and subsequently in the determination of a Digital Canopy Model (DCM) through the substraction of the Digital Terrain Model from the Digital Surface Model for each of the sample plots under study in the Aberfoyle area. The eCognition segmentation and classification algorithm was used to segment this LiDAR derived DCM along with the multiespectral imagery.

The original LiDAR data for every plot consisted in a list of coordinates X, Y, Z plus an intensity value for each hit, where Z represented the absolute measured LiDAR height referenced to the Transverse Mercator projection and the Ordnance Survey Great Britain 1936 datum. The LiDAR data used for the segmentation consisted of a list of coordinates per plot with approximately 50,000 laser hits, where the Z value corresponds to the calculated tree or ground height after LiDAR processing.

- Geometric correction: In spite of the high vertical and horizontal accuracy that characterizes LiDAR data, a shift of -7 m and -1 m in East and North directions, respectively, was found in comparison with coordinates taken from the orthophotography. This shift was corrected using the program Surfer (Golden Software) and the new geographical reference was checked again against aerial

photography, resulting in sub-metre accuracies. This process was followed by the subset of the large original datasets to make the data and workspace more manageable and to reduce data volume. This pre-processing was carried out using tools in Erdas Imagine 8.7.

5.5.2 Airborne Thematic Mapper (ATM) data

The platform used to collect imagery of the Aberfoyle area was a Dornier 228 (D-CALM) aircraft, operated by the UK's Natural Environment Research Council (NERC) Airborne Research and Survey Facility, on July 13, 2003. The image dataset contains eight north-south orientated flight lines of ATM imagery of the Queen Elizabeth II Forest Park collected at 11:49 am. From that set of eight images, two flightlines (03/021 and 03/023) contained the plots under study and therefore were chosen for the object-oriented segmentation and classification process, and are shown in figure 5.1.

The Daedalus 1268 ATM onboard the aircraft is a passive sensor designed to collect and record reflected and emitted radiation from the earth's surface. The radiation is separated into 11 spectral bands, some of which simulate the satellite-borne Landsat Thematic Mapper (table 5.2) and range from the visible blue to the thermal infrared. Channels 1–5 are in the visible, 6–8 are in the near-infrared, 9 and 10 are in the short wave infrared (SWIR), and band 11 is a thermal infrared band. The imagery was collected at 1200 m during uniform cloud-free conditions and the pixel resolution was 2 m. Further characteristics of the ATM instrument are presented in table 5.3.

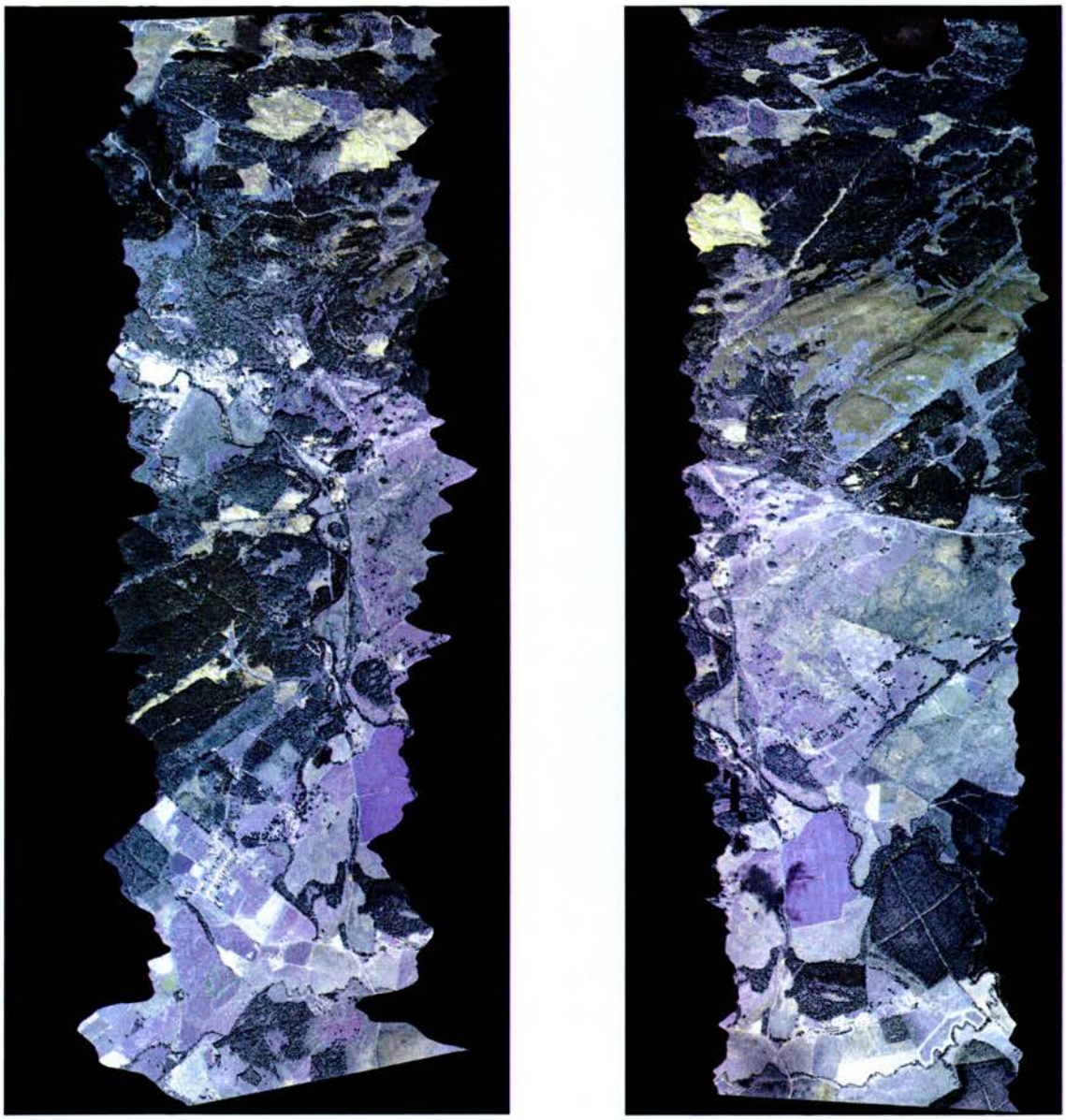

Figure 5.1: Airborne Thematic Mapper imagery 03/021 and 03/023 used in the analysis.

ATM Band	Spectral range (μm)	Equivalent Landsat TM band
1	0.42 - 0.45	
2	0.45 - 0.52	1
3	0.52 - 0.60	2
4	0.605 - 0.625	
5	0.63 - 0.69	3
6	0.695 - 0.75	
7	0.76 - 0.90	4
8	0.91 - 1.05	
9	1.55 - 1.75	5
10	2.08 - 2.35	7
11	8.5 - 13.0	6

Table 5.2: Band characteristics of the Daedalus 1268 Airborne Thematic Mapper instrument compared to those of the Landsat Thematic Mapper instrument.

Instantaneous Field Of View	**2.5 mrad**
Pixel swath	938
Digitised Field of View	90°
Scan Rate	12.5 , 25 and 50 Hz
Radiometric Resolution	16 bit
Temperature Reference	Two black-bodies for calibration of thermal channel

Table 5.3 Daedalus 1268 Airborne Thematic Mapper sensor parameters.

- Radiometric correction: The imagery was delivered processed to level 3B which means that radiometric calibrations algorithms had been applied by the producers and that the data had been mapped to a geographic coordinate system using onboard attitude and positional information with additional ground control point for precise location.

- Atmospheric correction: attempts were made to remove the spectral effects of the atmosphere, ensuring the recorded radiance was as close as possible to the actual radiance reflected from the ground surface. However, in the end atmospheric correction was not performed on the ATM dataset as it was considered not necessary as Mather (1999) states that atmospheric correction must be undertaken when: a) the ratio of pixel values between wavebands is required, b) measures of radiance are related to specific properties of features within the data and c) temporal comparison between datasets is required. None of these analyses were

needed for the research. Other studies on tree segmentation and classification with high resolution digital imagery have also not performed atmospheric correction (Hajeck 2005, Leckie *et al.* 2005).

- Geometric correction: the initial geometric correction was carried out with the program AZGCORR, an Airborne Remote Sensing Geocorrection Package designed by Azimuth Systems and provided by NERC ARSF. The purpose of the program is to adjust the image data to match true ground space in a known coordinate system. In order to apply the geometric correction to the image, information about the image pixel size and the number of lines defining the image was retrieved from the HDF file. A DEM grid of the area 10 m resolution was also added to the system, in order to improve geometric accuracy. The image was geocorrected and resampled to 1 m pixel size. Then Azexhdf program was used to convert the image corrected by Azgcorr into a BIL binary file.

However, even single flight lines of airborne data are difficult to rectify to a standard map series because of aircraft roll, pitch, and yaw during data collection (Jensen 2005). Therefore, further correction of the ATM imagery was necessary to remove geometric distortions remaining in the data following pre-processing by the NERC ARSF software, in order to get a dataset spatially registered to the LiDAR data for the segmentation analysis. This was achieved by registering the required sections of each ATM flight-line to the matching aerial orthophotographs by identifying 20 ground control points in both the aerial photography and in the imagery. A first order polynomial transformation was carried out and, in order to preserve the statistical properties of the data, the image was resampled with a nearest neighbor algorithm which assigns the brightness value closest to the specified x', y' coordinate to the output x, y coordinate (Jensen 2005). The accuracy of the correction was of RMSE 0.46 m. All these operations were performed using the tools for geometric correction implemented in Erdas Imagine 8.7 (figure 5.2).

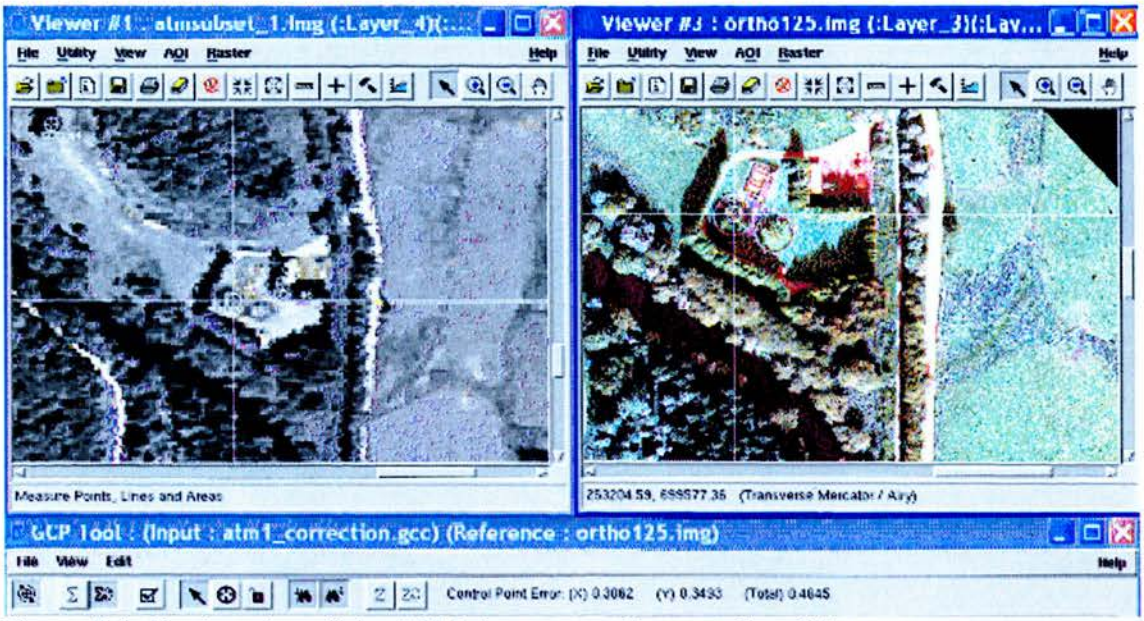

Figure 5.2: Registration of the ATM data to ortophotography of the area.

Band	1	2	3	4	5	6	7	8	9	10	11
1	1										
2	0.835	1									
3	0.785	0.911	1								
4	0.732	0.935	0.961	1							
5	0.754	0.931	0.961	0.991	1						
6	0.634	0.536	0.762	0.589	0.621	1					
7	0.535	0.432	0.681	0.503	0.524	0.970	1				
8	0.519	0.429	0.680	0.514	0.531	0.956	0.986	1			
9	0.513	0.609	0.793	0.753	0.759	0.757	0.766	0.806	1		
10	0.282	0.184	0.021	0.009	0.042	0.003	-0.061	-0.089	0.118	1	
11	0.406	0.573	0.646	0.692	0.697	0.378	0.326	0.350	0.638	-0.124	1

Table 5.4: Correlation matrix for the 11 ATM bands.

In order to reduce the size of the dataset, a selection of bands was undertaken. Visually, combinations of bands 5 (visible red), 7 (near-infrared), 9 (middle infrared), and 11 (thermal infrared) were best for species discrimination. To help with the band selection, a correlation matrix of each image was calculated using the tools in the Model Maker module implemented in Erdas Imagine 8.7 (table 5.4). The results indicated that these

bands are certainly no too highly correlated (0.326 to 0.766) therefore they contain most of the information needed for subsequent analysis.

5.5.3 Aerial ortophotography

Six high resolution (25 x 25 cm) digital colour ortophotographs scale 1:12500 encompassing the plots under study were accessed from the Forestry Commission (figures 5.3 and 5.4). The digital aerial photography was taken simultaneous to the LiDAR data in September 2002, at the end of the growing season. The data were georeferenced to the Ordnance Survey Great Britain 1936 system, Transverse Mercator projection, and due to its high resolution and planimetric accuracy, was used as a reference for the geometric correction of the other datasets, for visual identification of features of interest, and for the generation of vector files of manual tree crown delineations for comparison with the automatic tree crowns generated through segmentation with the eCognition algorithm.

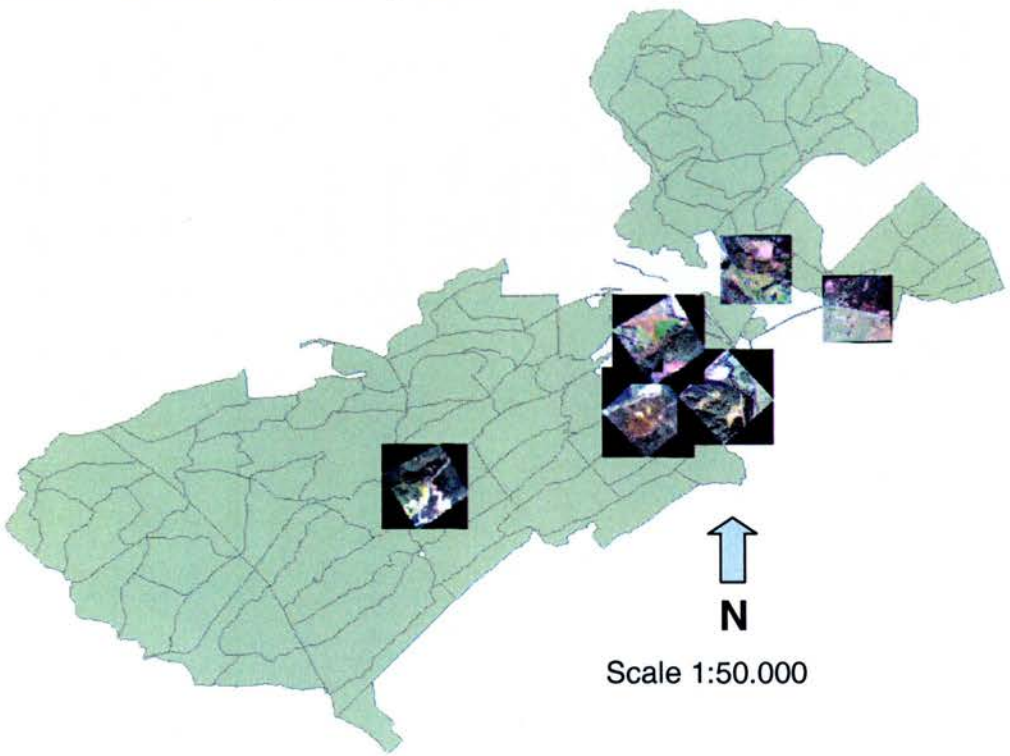

Figure 5.3: Relative position of digital colour orthophotographs used as a layer for segmentation and classification of forest species and for tree crown and gap delineation, overlaid onto the compartment database from the Forestry Commission.

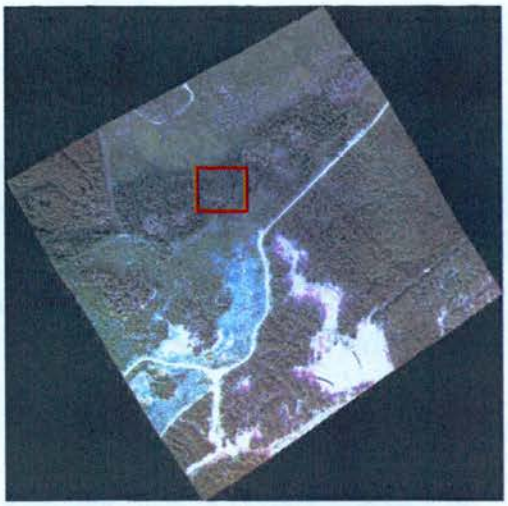

Norway spruce sample plot 1

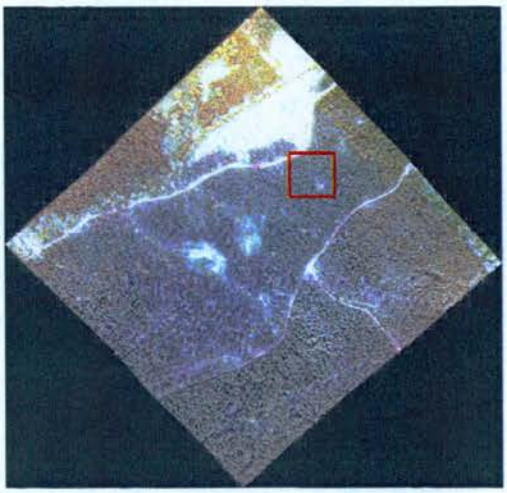

Norway spruce sample plot 2

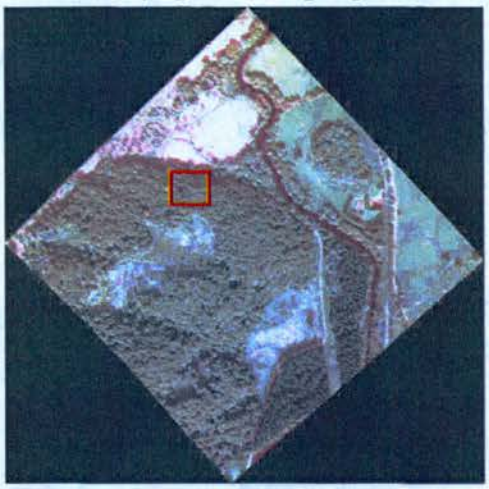

Oak sample plot 1

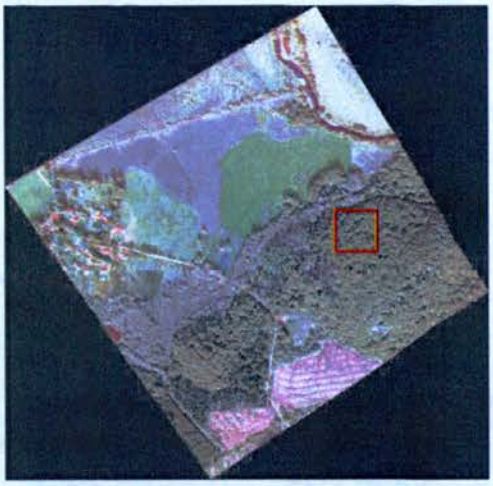

Oak sample plot 2

European larch sample plot

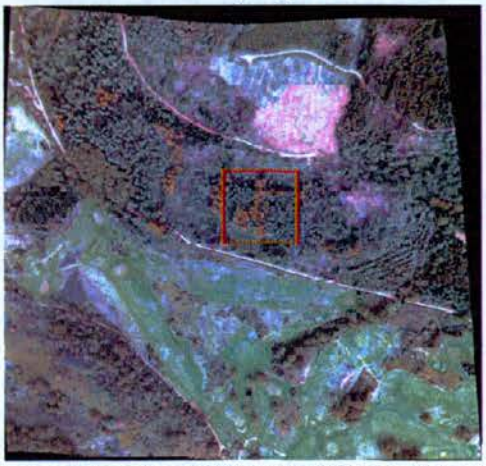

European larch and Douglas fir sample plot

Figure 5.4: Individual digital colour ortophotographs scale 1:125000 encompassing the sample plots denoted by red boxes.

5.6 Data preprocessing

Data import, geometric correction, atmospheric correction, georeferencing, clipping, and image enhancement were preprocessing tasks carried out in order to generate a consistent and accurate set of data to be used for the analysis. Filter tools were applied to some of the digital ortophotographs and ATM data to improve segmentation and classification in areas affected by shadows. For the remaining datasets, segmentation was carried out on raw bands. Further details about data preprocessing are included in following sections.

5.7 Manual crown delineation

As the digital aerial photography presented the best spatial resolution (25 cm), results from segmentation were compared visually and geometrically to this data set.

For the geometric comparison, manual delineation of features was performed on all digital ortophotographs containing the study area. Representative examples of this operation are shown in figure 5.5. Manual delineation was carried out in ArcGIS 9 (ESRI Inc. 2005) using the graphic tools and then each layer created was saved as a polygon shape file to enable *a posteriori* comparison with results obtained from classification. These shape files were considered as the ground reference.

Crown delineation of European larch and Norway spruce species (figure 5.5 a, b, c) was a straightforward task; the process was facilitated by the relative open canopy in the sample plots and the distinctive crown shape of the spruce and larch species. On the contrary, delineation of the deciduous species was more subjective due to the complexity of the deciduous crowns, the closed canopy, and the shadowing of wooden parts. The assignment of one canopy segment to a particular crown or to the contiguous one was a difficult task. All dominant trees within the plot could be detected but the trees distributed in the other canopy layers were more difficult to identify, with most of them dissapearing under the upper canopy layer.

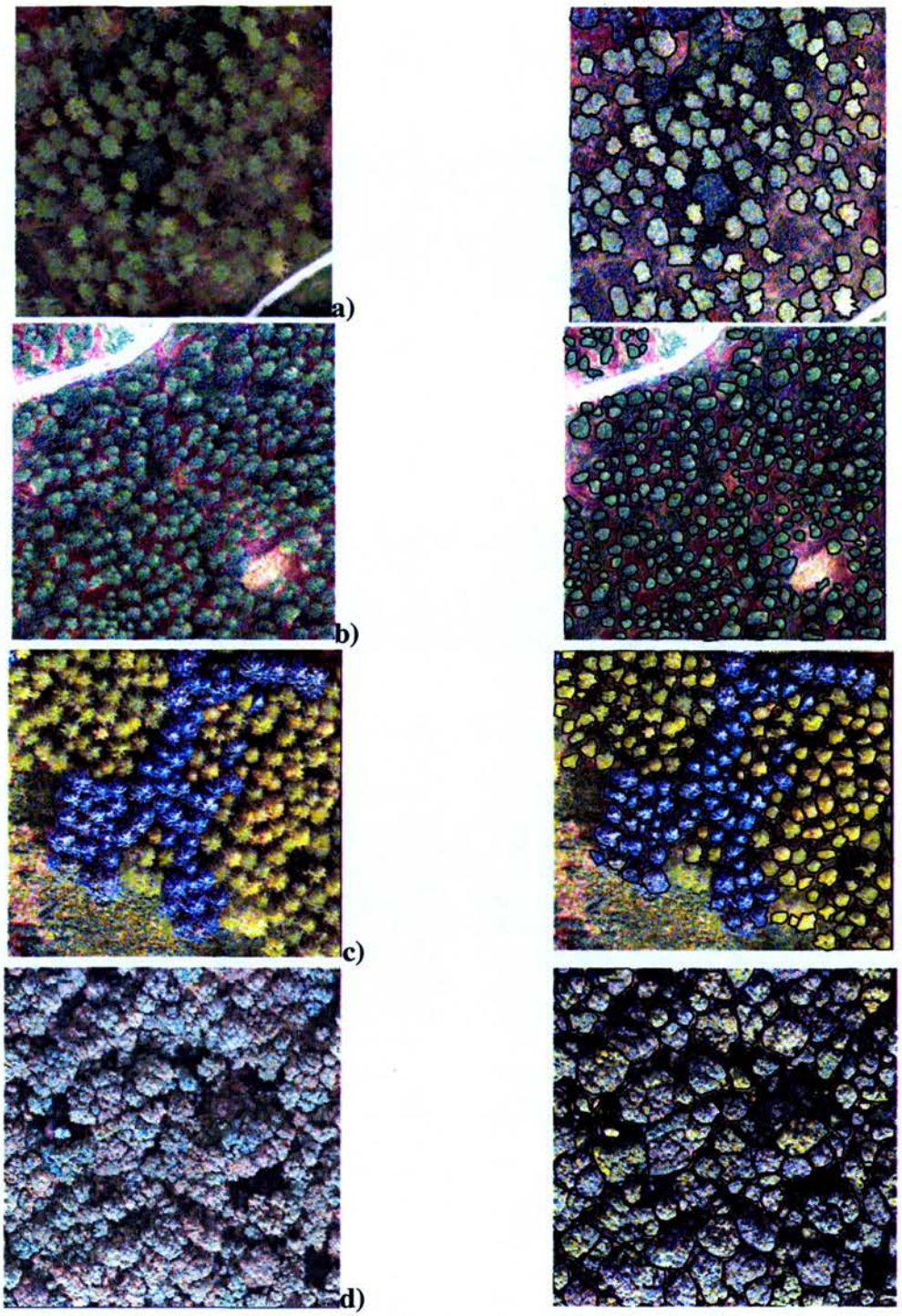

Figure 5.5: The first column show subsets of aerial photographs corresponding to European larch plot (a); Norway spruce plot (b); mixed European larch and Douglas fir sample plot (c); Oak sample plot (d), and their respective images in the second column showing the manually delineated crowns layer overlaid.

5.8 Segmentation and classification process

The segmentation and classification process was performed using the multiresolution, hierarchical algorithm implemented in eCognition in order to evaluate its ability for the detection of tree crowns and gaps with regard to variations in species and stand density, as well as the potential of the available datasets to deliver this information. The objective was to perform segmentation and classification on each dataset individually at first and then proceed to segmentation using a combination of aerial photography with LiDAR data and ATM data with LiDAR data to enable accuracy comparisons. A diagram of the methodology followed is shown in figure 5.6.

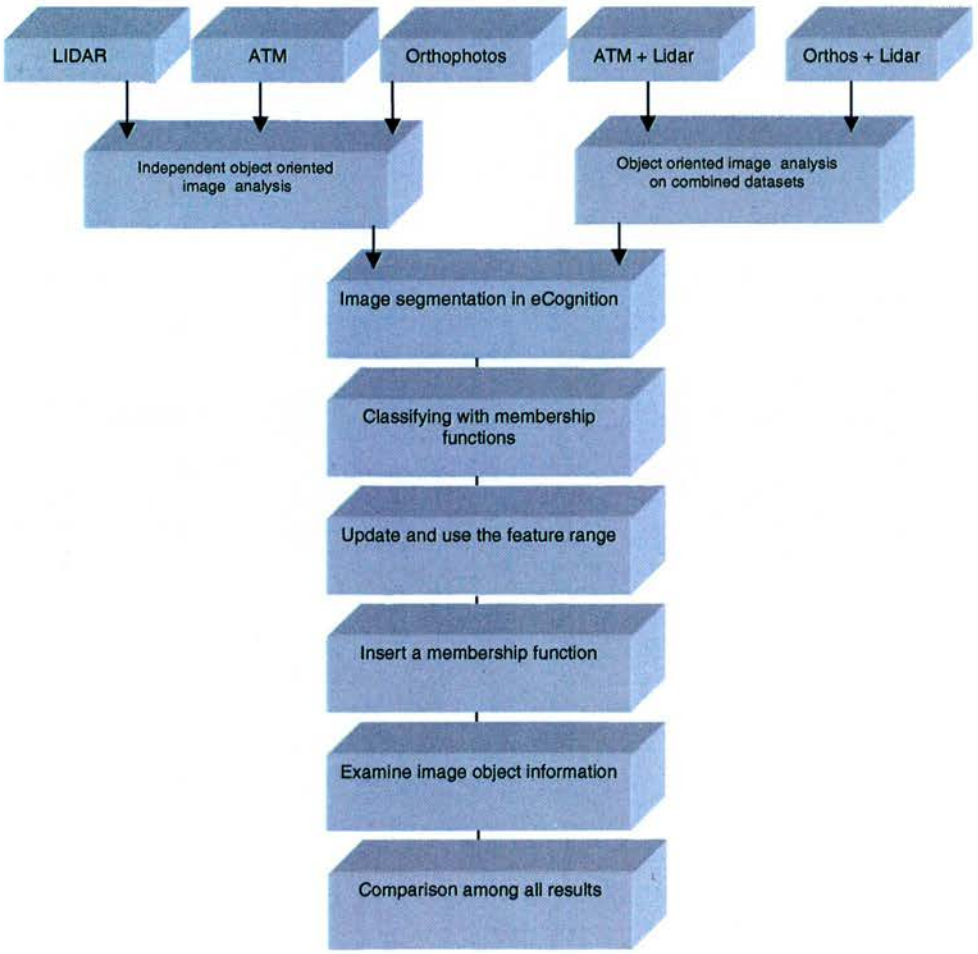

Figure 5.6: Methodology used in the segmentation and classification process.

The segmentation starts with the importation of data and the assignment of weights to the different layers that compose the imagery, followed by the assignment of values to the most important criteria considered by the oriented-objected algorithm, e.g., heterogeneity and homogeneity. These criteria are defined as follows (eCognition User Guide 4 2004):

- Heterogeneity: this criterion measures the maximum allowed heterogeneity of the resulting image objects; in other words, it determines the size of the image objects. It is expressed as the Scale Parameter.
- Homogeneity: this criterion is composed of three factors: colour, smoothness, and compactness. In most cases the colour criterion is the most important one for creating meaningful objects. The shape criterion, defined by smoothness and compactness factors, especially helps to avoid a "fractal" shaping of objects in strongly textured data. The colour criterion defines to which percentage the overall homogeneity is defined by the spectral values of the image layers as opposed to the Shape homogeneity criteria. Changing the weight for the colour criterion to 1 result in objects entirely optimized for spectral homogeneity. In addition to spectral information, object homogeneity can be optimized with regard to object shape, especially according to its smoothness or compactness. Large smoothness weights tend to yield more circular segments while large compactness weights tend to yield rectangular or square segments (Collins *et al.* 2004).

The assignment of the values is performed through an iterative data exploration process while developing the classification rule base. The quality of the classification depends mainly on the quality of the segmentation and the knowledge base. The segmentation is good if the objects represent the meaningful features to be classified. This can be achieved only if an appropiate combination of segmentation parameters (scale, colour, shape) is used to produce the most meaningful objects.

Two main principles for segmentation to be followed are (eCognition User Guide 4 2004):

- Always produce image objects at the largest possible scale which in turn still distinguish different image regions (as large as possible and as fine as necessary).
- Use as much colour criterion as possible and as much shape criterion as necessary to produce image objects of the best border smoothness and compactness. The reason for this rule is that the spectral information is ultimately the primary information contained in image data. Using too much shape criterion therefore can reduce the quality of segmentation result.

The knowledge base refers to the membership functions. An approach that is often taken is to perform a nearest neighbour classification first which produces very coarse results. This is then refined using membership functions. The use of membership functions requires the selection of the appropriate features to describe each class. These features can consist for instance, in a spectral range (Object Features/Layer Values/Mean/Brightness/Ratio); a certain area (Object Features/Shape/Generic Shape Feature/Area); or a certain context (Class Related Features/Relations to Neighbour Objects/Relative Border to).

After the selection of the appropriate features, a definition for them according to a membership function should be assigned. There are many functions to choose from and all of them are considered fuzzy, which as was mentioned before, means that the objects (created during segmentation) will be assigned to the class for which its membership is higher. Once a set of features for a class using membership functions is defined, it is refered to as a knowledge base for that class. Typically, the more membership functions used for one class the more defined that class is and the more refined the classification will be.

The eCognition software offers a great quantity of tools for the refinement of the classification. As an example, fine segmentations can be run on specific classes and then can be followed by segmentation-based classification; segments within the same class can be merged; nearest neighbour (NN) and fuzzy methods can be integrated and used for

a more complex classification. All these tools were used to a certain degree mostly with the purpose of obtaining non over-segmented objects which most closely matched the reference crowns, for instance, suitable features were used to extract gaps and road classes at a fine segmentation level and then segmentation based on classification was used to merge objects in the same class in a superior level; however, the goal in this project was to use a simple segmentation and classification protocol which could be used for the processing of all datasets with minor adjustments. The process is summarised in figure 5.7.

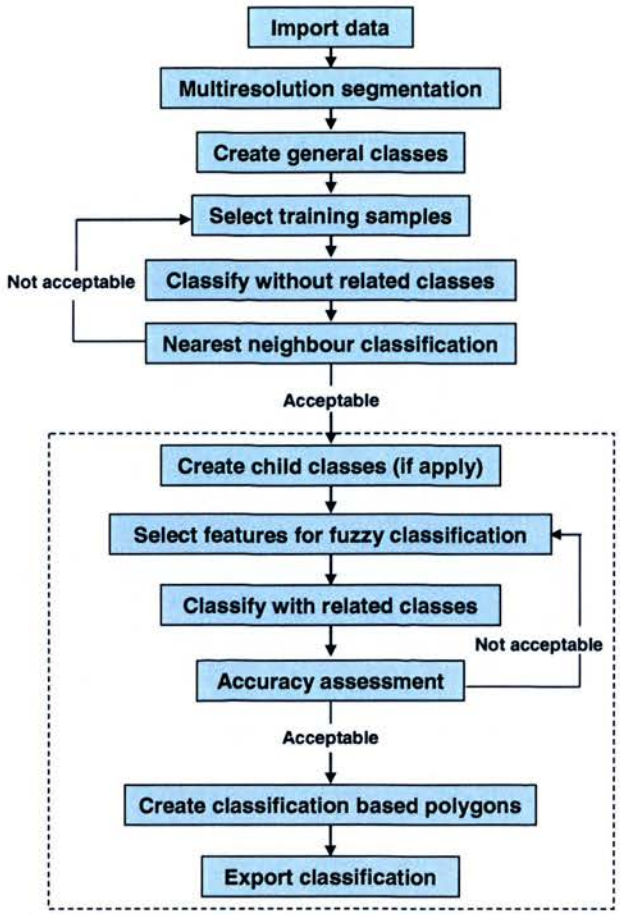

Figure 5.7: Processing flow in eCognition for the segmentation and classification of datasets.

Following classification, the accuracy assessment tools included in eCognition were used to check the quality of the classification and re-run the process to improve accuracy whenever results were not satisfactory. Two of these tools were evaluated: Classification

stability and Error matrix based on samples. These tools provide measures such as Overall accuracy, Producer's accuracy, User's accuracy, and the Kappa Index of Agreement (KIA) of which definitions are given as follows (Jensen 2005):

- Overall accuracy is determined by dividing the total correct observations (sum of the major diagonal) by the total number of observations in the error matrix.

- The user's accuracy is a measure of how well the classification performed in the field by categories (rows). The user's accuracy details errors of commission, which results when a pixel is committed to an incorrect class.

- The producer's accuracy is a measure of how accurately the image data was classified by category (columns). This measure details the errors of omission which results when a pixel is incorrectly classified into another category. The pixel is omitted from its correct class.

- The Kappa Coefficient is a discrete multivariate technique to interpret the results of a contingency matrix. The Kappa statistic K (equation 5.1) incorporates the off diagonal observations of the rows and columns as well as the diagonal to give a more robust assessment of accuracy than overall accuracy measures. It is a measure of agreement between the remote sensing-derived classification and the reference data as indicated by a) the major diagonal and b) the chance agreement, which is indicated by the row and column totals. Kappa values >0.80 represent strong agreement or accuracy between the classification map and the ground reference information. K values between 0.40 and 0.80 represent moderate agreement. K values <0.40 represent poor agreement.

$$k = \frac{N\sum_{i=1}^{k} x_{ii} - \sum_{i=1}^{k}(x_{i+} \times x_{+i})}{N^2 - \sum_{i=1}^{k}(x_{i+} \times x_{+i})} \quad \text{.....5.1}$$

After a good classification result was found, polygons corresponding to the crown and gap classes were created and saved as shape files along with their attributes (area, width, length), to enable comparisons with the reference data in a GIS.

5.8.1 Segmentation and classification of digital aerial photography

The orthophotographs were segmented based on the eCognition standard multi-resolution segmentation. Figures 5.8 to 5.12 show the segmentation results using different segmentation parameters.

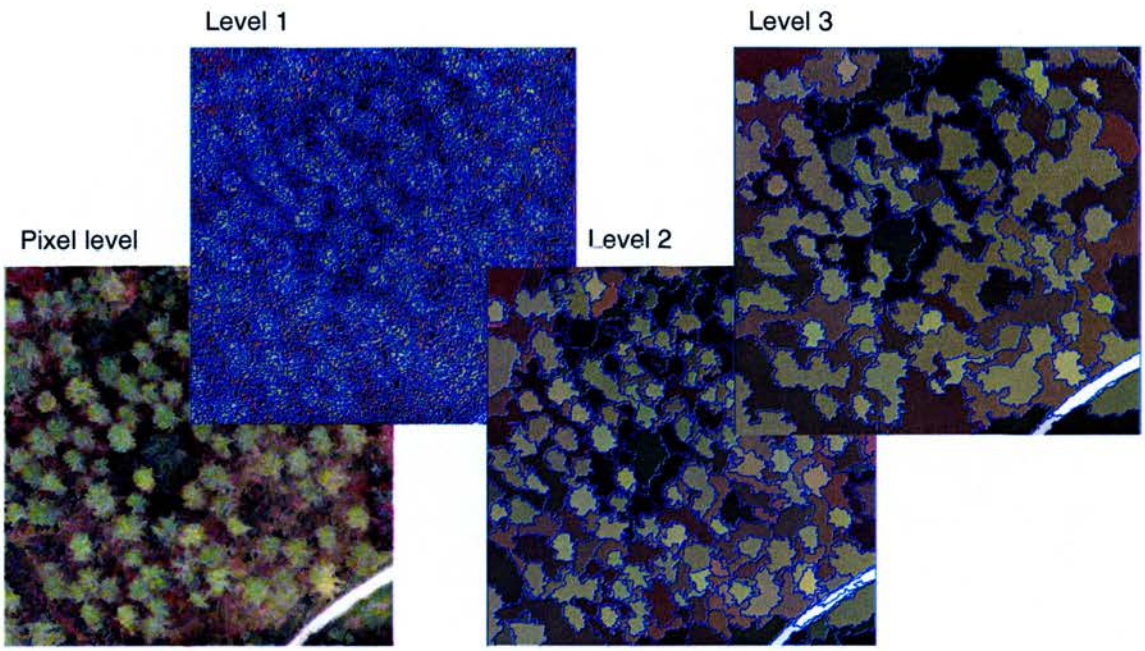

Figure 5.8: Hierarchical net of image objects derived from image segmentation level 1 (10 scale parameter), level 2 (50 scale parameter) and level 3 (90 scale parameter) in a European larch stand.

Along with the scale factor, the other parameters that influence the segmentation result are colour, shape, smoothness and compactness. The first stage in the analysis was to perform several trials for the segmentation with combinations of different values for each of these parameters. In this way, the best segmentation result was chosen by comparison among 25 trials which tested the segmentation algorithm for the following combination of parameter values:

- **Scale parameter**: this factor has no unit but controls the amount of spectral variation within objects and therefore their resultant size. The initial value for this parameter was set at 10 (large number of small segments) and was subsequently evaluated in increments of 10 to 110 (larger and fewer segments). These results were visually compared with the original imagery and the scale parameter that better adjusted to the size and number of the real objects was chosen. Visual comparison as a criterion for the selection of optimal segmentation output has been used in several works (Schiewe 2002, Schiewe *et al.* 2001), there is no standard method defined to date to aide in the selection of optimal scale. Small segmentation scales extract the objects well but produce a high quantity of segments which make the classification more difficult and takes more time. Larger scales can simplify the classification tasks reducing the number of objects but at the expense of the merging of objects that might not belong to the same class. Minimum and maximum values tested on a European larch sample plot for the scale parameter produced 6691 segments for a value of 10 and 89 segments for for a scale value of 110 (figures 5.10 and 5.11). It was considered unnecessary to test segmentation with values bigger than 110 as the output corresponding to this value was already not a good representation of meaningful objects.

- **Colour/shape parameter**: this parameter was evaluated for values ranging from 0.9:0.1 to 0.1:0.9 in all datasets. The assignment of large weight to shape homogeneity generally resulted in poor results (figure 5.11 c) and d)), where neighbouring tree crowns of the same colour were assigned to the same object. This output was expected as the algorithm developers (eCognition User Guide 4 2004) suggested. The effect of an increase in shape weight resulted in deviation from the colour information in which segments are smoother. However, small output differences between the use of Colour/Shape at 0.9:0.1 and 08:0.2 mean that the tree crowns were better represented by the last combination of values, as the former delivered more fragmented crowns. Therefore, the combination of values that gave best results, according to visual comparisons to the original imagery, was 0.8 for Colour and 0.2 for Shape (figure 5.12 d)). Smoothness and compactness were kept

constant at 08:0.2. These values were also kept constant during the analysis of the different datasets with some exceptions which will be explained as appropriate.

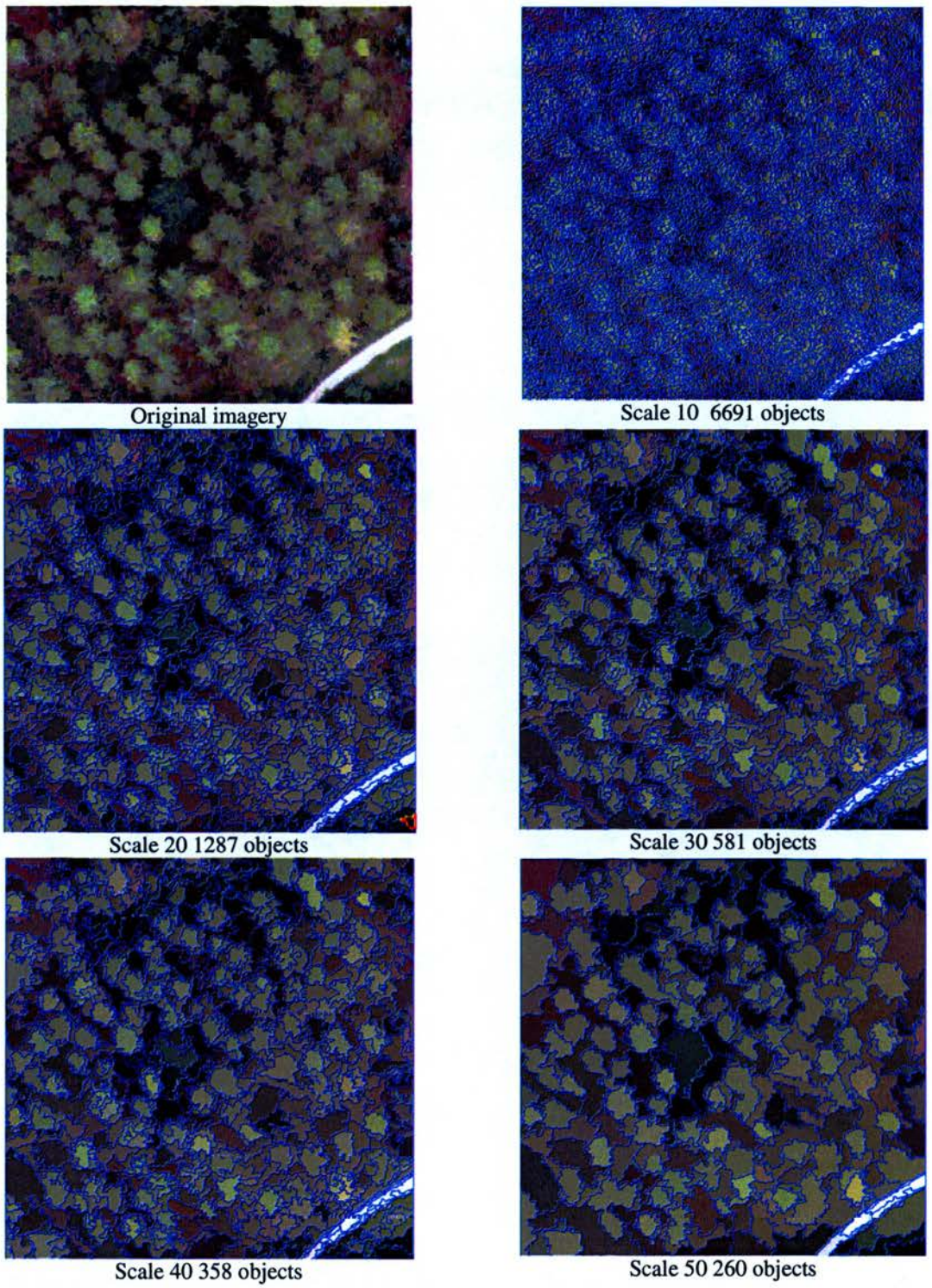

Figure 5.9: Results obtained from the segmentation process considering values for the scale parameter ranging from 10 to 50 for a European larch dataset.

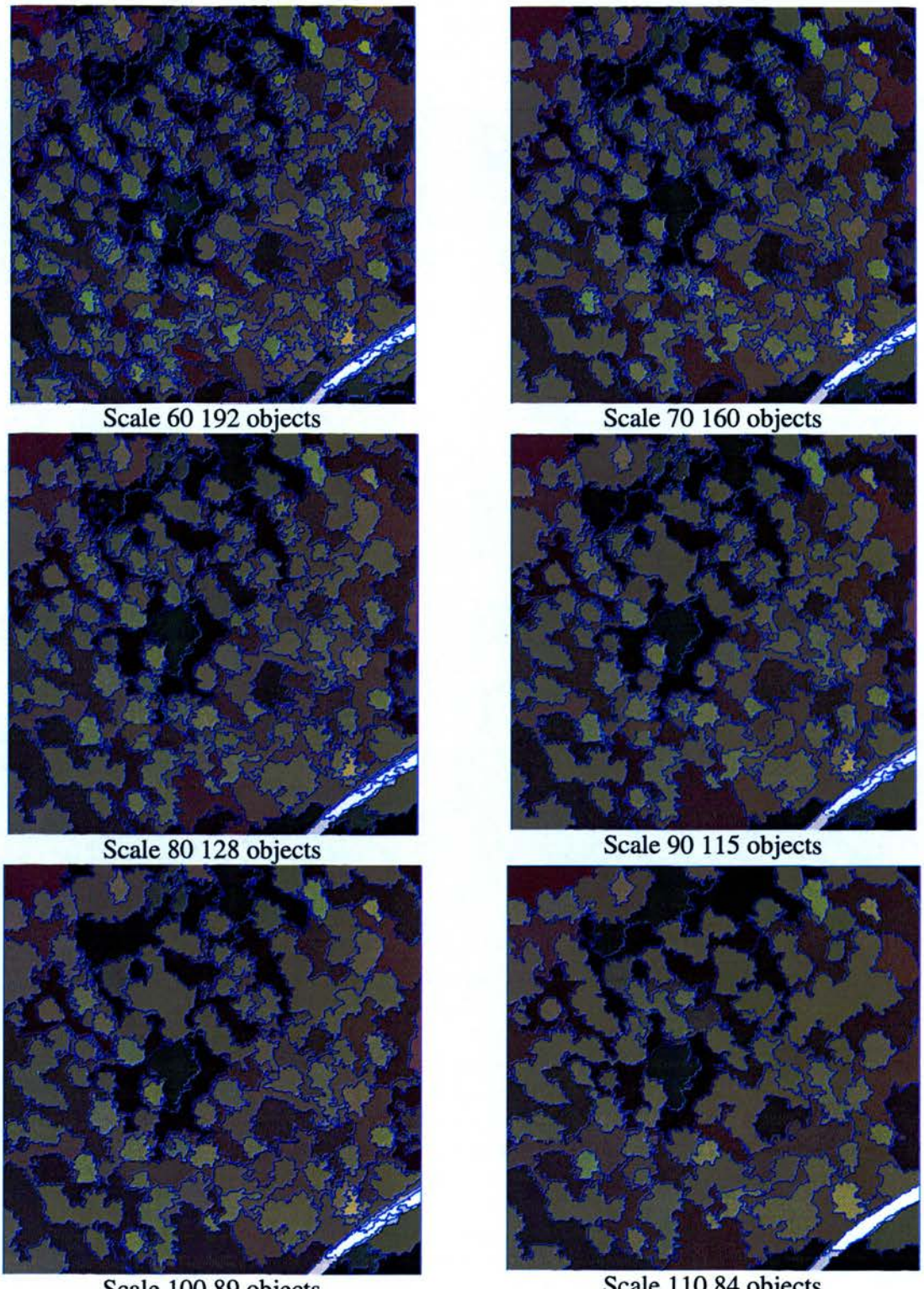

Figure 5.10: Results obtained from the segmentation process considering values for the scale parameter ranging from 50 to 100 for a European larch dataset.

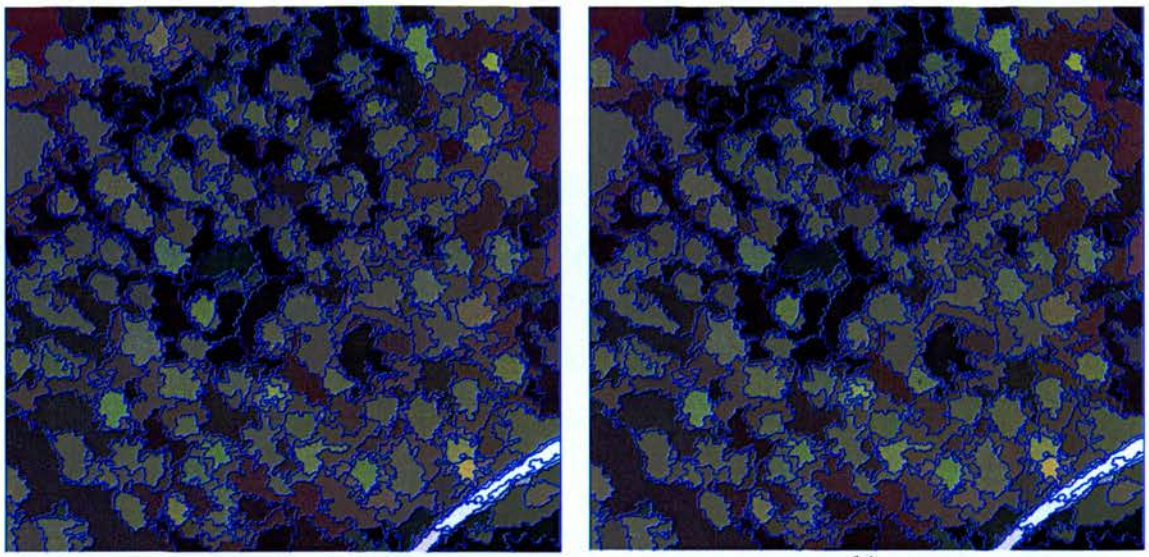

a)
Scale 50 Colour/shape 0.9:0.1
Compactness/smoothness 0.5:0.5
261 objects

b)
Scale 50 Colour/shape 0.7:0.3
Compactness/smoothness 0.5:0.5
262 objects

c)
Scale 50 Colour/shape 0.3:0.7
Compactness/smoothness 0.1:0.9
207 objects

d)
Scale 50 Colour/shape 0.1:0.9
Compactness/smoothness 0.5:0.5
112 objects

Figure 5.11: Results obtained from the segmentation process considering values for the scale parameter of 50 and varying values for Colour/shape and compactness/smoothness parameters, for a European larch dataset.

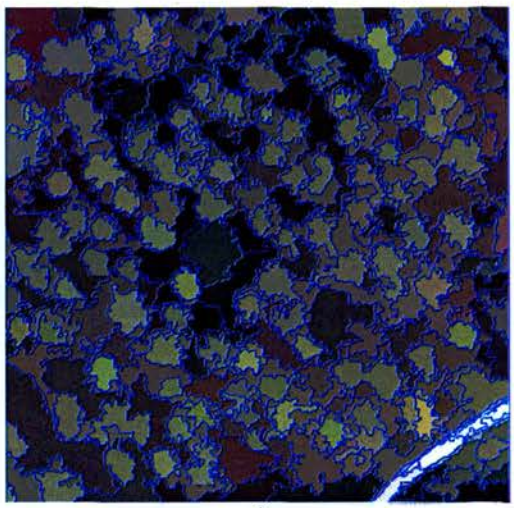

e)
Scale 50 Colour/shape 0.9:0.1
Compactness/smoothness 0.9:0.1
254 objects

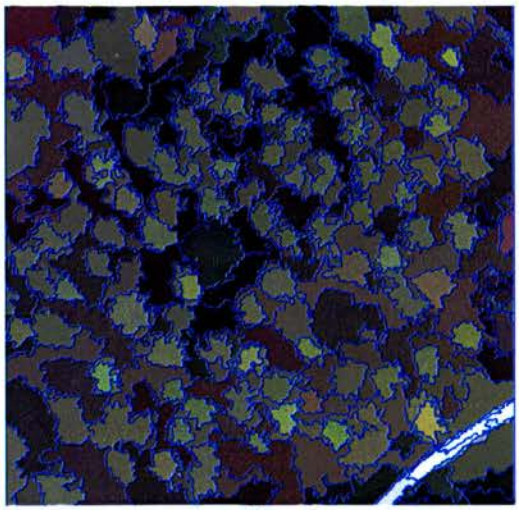

f)
Scale 50 Colour/shape 0.9:0.1
Compactness/smoothness 0.1:0.9
261 objects

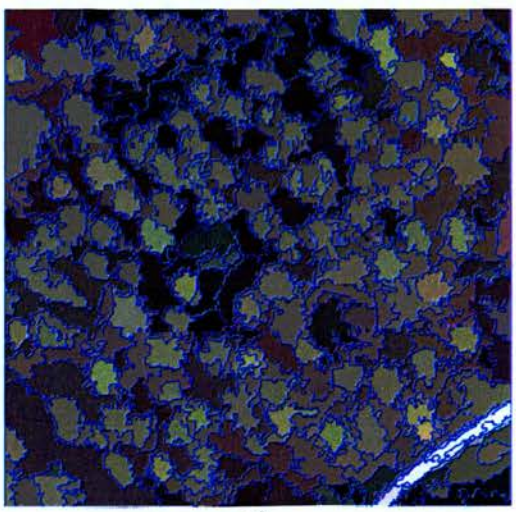

g)
Scale 50 Colour/shape 0.9:0.1
Compactness/smoothness 0.2:0.8
261 objects

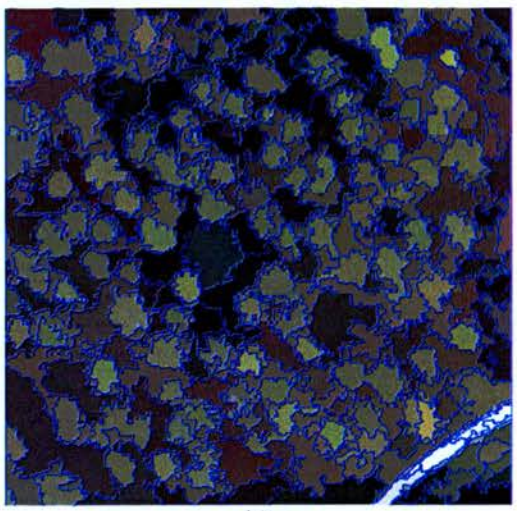

h)
Scale 50 Colour/shape 0.8:0.2
Compactness/smoothness 0.2:0.8
253 objects

Figure 5.12: Results obtained from the segmentation process considering values for the scale parameter of 50 and varying values for Colour/shape and compactness/smoothness parameters.

The weights for the three colour layers (R, G, B) that compose each digital aerial photograph were set equal for each layer. Nearest Neighbour (NN) and fuzzy classification were performed on each dataset. Based in the knowledge acquired during field work, samples were taken to enable NN classification and accuracy assessment of

the fuzzy classification. For the latter, different membership functions were used to produce the corresponding class description. Details of these functions are included in the following sections along with the depiction of the segmentation and classification process carried out on each sample plot dataset.

The following sections describe the analysis performed on each of the datasets.

- **Segmentation and classification of the dataset corresponding to the European larch sample plot.** By visual comparison to the original dataset, a scale parameter of 50 was selected because the segmentation result fitted the information class extraction best. Based on these parameters, the segmentation process was performed. Figure 5.13 shows the segmentation result. The maximum and minimum number of segments was 6431 for scale 10 and 89 for scale 100, respectively.

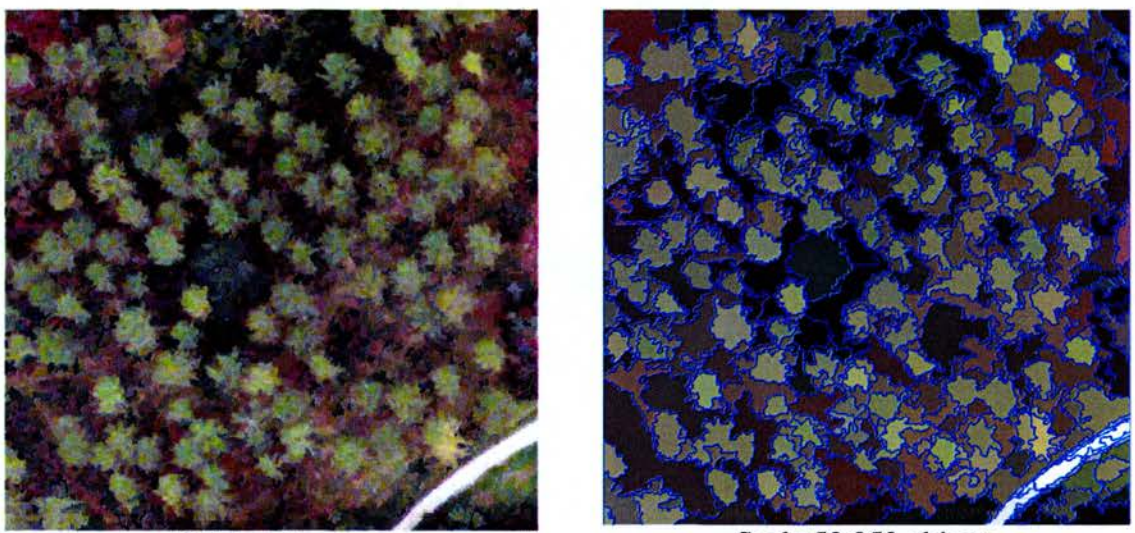

Original image Scale 50 253 objects

Figure 5.13: Results obtained from the segmentation process considering values for the scale parameter of 50 and Colour/Shape 0.8:0.2; Compactness/Smoothness 0.8:0.2, for a European larch dataset.

For the classification task four classes were created: Road, European larch, Understorey species, and Gaps. Fuzzy classification was performed on the dataset. The accuracy assessment in eCognition is carried out through the comparison of declared samples with the classified segments, therefore 10

samples of each category were taken (except for the road class for which just 2 samples were taken) for the building of the error matrix. For the fuzzy classification membership functions were declared. These memberships included the mean value of band 1, the mean of band 3, the ratio of band 1, and the standard nearest neighbour (table 5.5).

Classes	Feature	Range
Road	Mean band 3	190 - 255
European larch	Mean band 1	105 - 190
Other understorey species	Ratio band 1	0.30 – 0.33
Gaps	Standard Nearest Neighbor	10 samples

Table 5.5: Membership functions used for the fuzzy classification of the European larch dataset.

In a processing level 4, a segmentation based classification was performed in order to merge the segments in the class gaps and road (figure 5.14). New polygons for this class were created and exported to a shape file. The objective of this processing step was to retrieve all gap areas for further analysis in chapter 6.

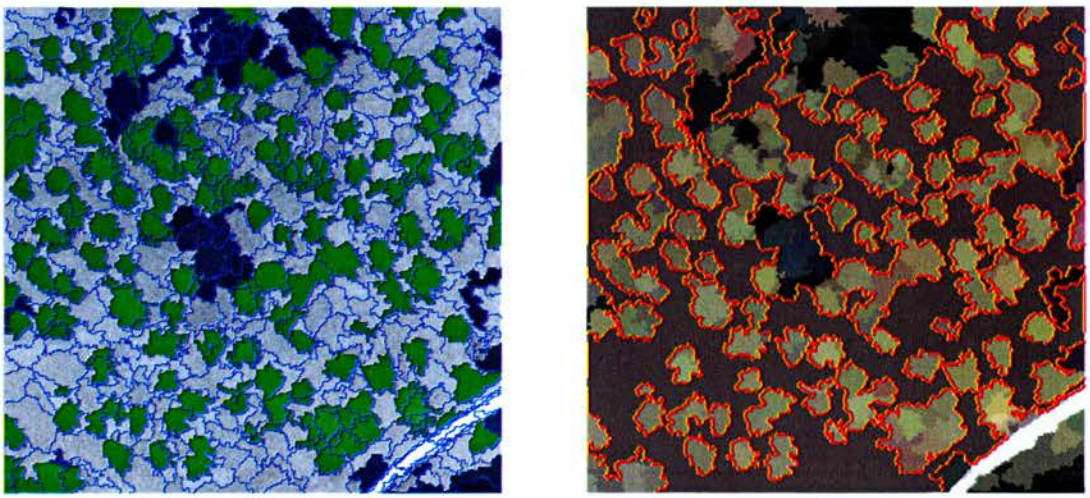

a) b)

Figure 5.14: Grey segments represent gaps in a) and brown segments delineated in red in the b) figure, represent the gap area after gap segments were merged.

The classification results corresponding to the fuzzy approach are shown in figure 5.15.

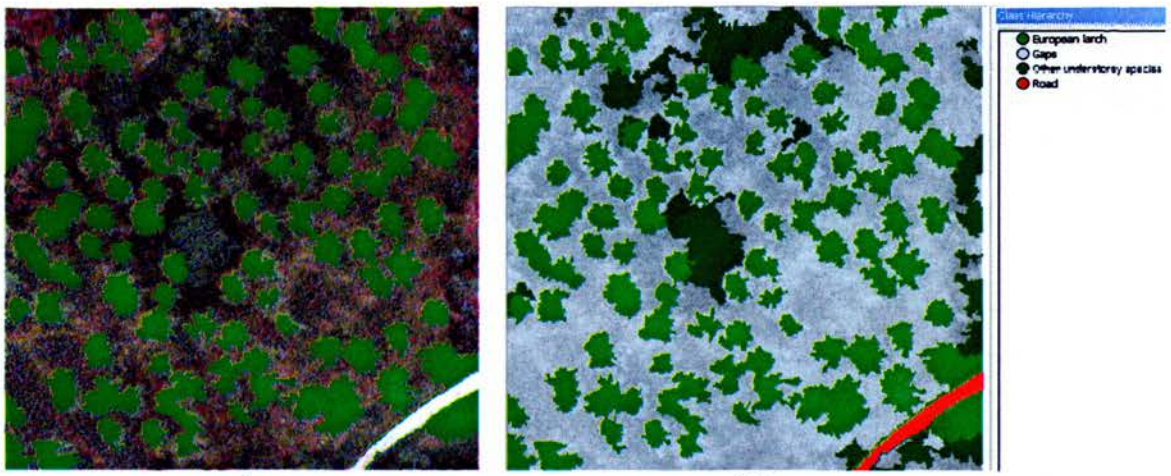

a) b)

Figure 5.15: First attempt to detect European larch species using fuzzy classification a) and final fuzzy classification of a European larch dataset b).

The results from the accuracy assessment are shown in table 5.6:

Class	Objects	Mean	Std. Deviation	Minimum	Maximum
Road	9	0.888	0.314	0	1
European larch	180	0.410	0.288	0	1
Gaps	335	0.883	0.170	0.106	1
Other understorey vegetation	47	0.433	0.369	0.033	1

Accuracy	Road	European larch	Gaps	Other understorey
Producer	0.875	1	0.916	0.777
User	1	0.941	0.733	0.933
Kappa per class	0.856	1	0.884	0.692
Totals				
Overall Accuracy	0.888			
Kappa	0.848			

Table 5.6: Fuzzy classification accuracy assessment of the European larch dataset.

Discussion of the results: Table 5.6 shows the classification stability computed over all image objects in the scene. The number under "Objects" indicates how many objects were classified in a certain class, for instance, 180 objects were classified as European

larch and have the European larch membership. "Mean" represents the mean value of the differences between the best and the second best classification membership values for each class. "Minimum" and "Maximum" are the minimum values and maximum values of the difference of the best and second best classification membership values for each class. From this table it can be noted that the road and gaps classes have the best classification stability both with a relatively high "Mean" value of 0.88. The European larch class exhibits the lower "Mean" value of 0.41.

The classification has an overall accuracy of 0.88 and a Kappa index of 0.84. There is thus strong agreement between the classification and the reference data.

The most important accuracy to be evaluated in this case is that of the classes of interest, e.g., European larch and gaps. These classes have Producer's accuracy of 1 and 0.91, respectively; User accuracies of 0.94 and 0.73, and Kappa coefficients of 1 and 0.88. The less accurate results for the gaps class are likely due to its high spectral heterogeneity. The objects grouped in this class represent several conditions of the ground layer, which for this plot can be bare soil or covered by grass or bracken, each of which has a particular spectral response. One solution to improve the classification could be to include more classes for these different features, but as the main objective is to quantify the total gap area, gap size and gap distribution, the effect of grouping all these features in one class or to declare a class for each one of them does not significantly affect the estimated values for these parameters.

- **Segmentation and classification of the dataset corresponding to the mixed European larch and Douglas fir sample plot.** By visual comparison to the original dataset, a scale parameter of 30 was selected because the segmentation result fitted the information class extraction best. Based on these parameters, the segmentation process was performed. Figure 5.16 shows the more representative segmentation results. The maximum and minimum number of segments were 6945 for scale 10 and 111 for scale 100, respectively.

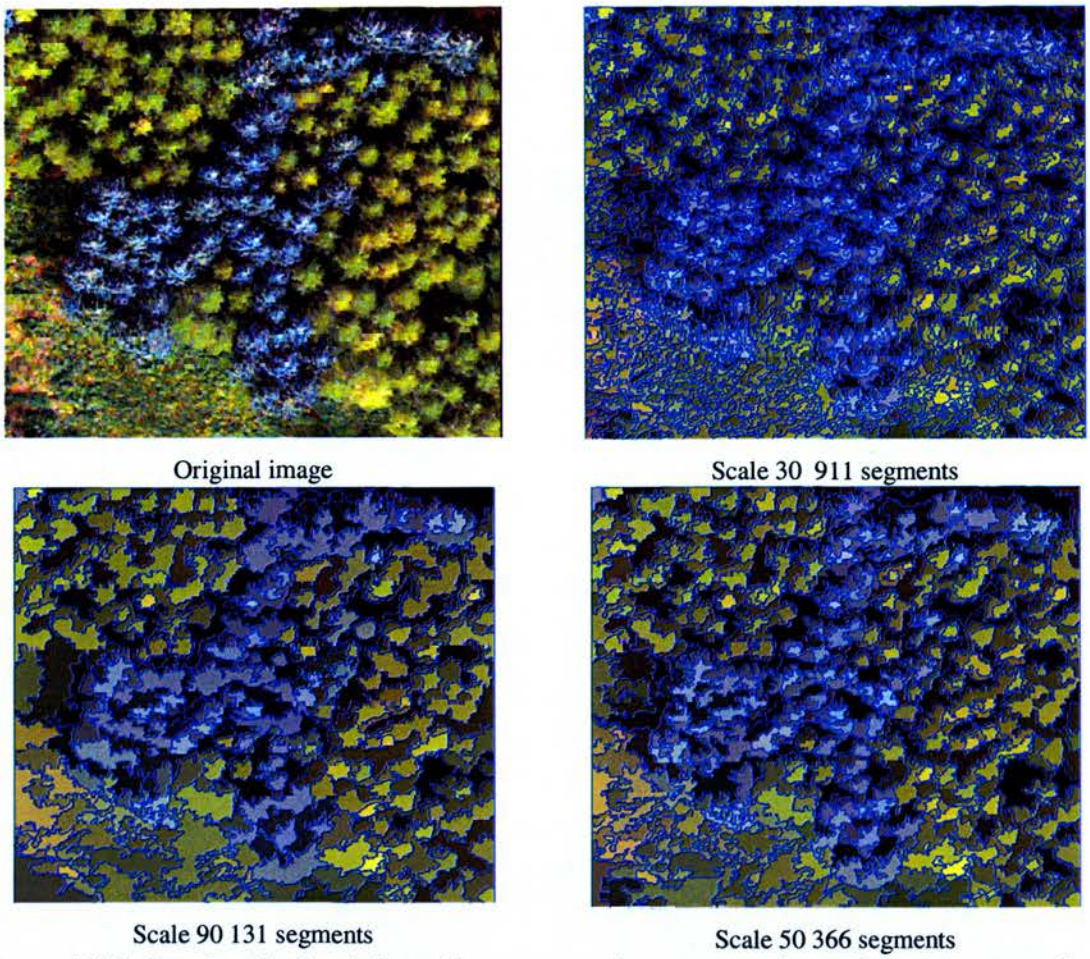

Figure 5.16: Results obtained from the segmentation process for scale parameter values ranging from 30 to 90 and the scale chosen for the final segmentation of 30 with values for parameters Colour/Shape and Compactness/Smoothness set at: 0.8:0.2

For the classification task two parent classes were created: Forested and Non forested areas. Within the Forested area class, three subclasses were defined, European larch, Douglas fir, and Gaps, in order to describe the features of interest. Fuzzy classification was performed on the dataset. To enable the accuracy assessment of the classification through the construction of the error matrix, 10 samples of each category were taken. For the fuzzy classification membership functions were declared. These memberships are different from the functions chosen for the European larch plot classification, due to the fact that the spectral characteristics of the mixed plot were best portrayed by the mean NDVI value, the mean value of the brightness, inverted similarity, and the standard nearest neighbour (table 5.7).

Classes	Feature	Range
Non forested area	Inverted similarity	
European larch	Standard nearest neighbour	10 samples
Douglas fir	Mean NDVI	-0.07 – 0.44
Gaps	Mean brightness	1.34 - 30

Table 5.7: Membership functions used for the fuzzy classification of a mixed European larch and Douglas fir dataset.

The results of the fuzzy classification are shown in figure 5.17. Results of the accuracy assessment are shown in table 5.8.

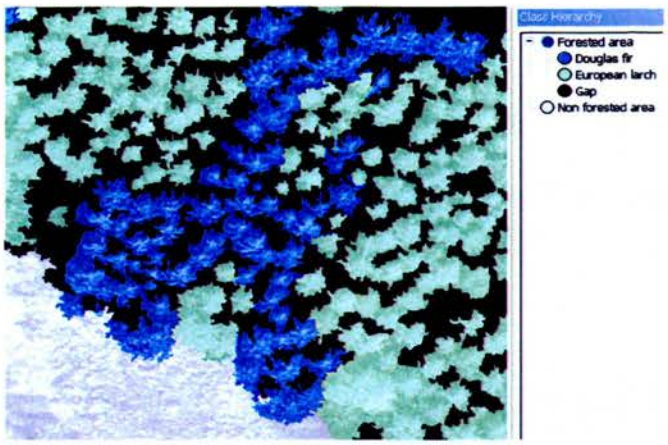

Figure 5.17: Fuzzy classification results for a mixed European larch and Douglas fir plot.

Class	Objects	Mean	Std. Deviation	Minimum	Maximum
European larch	373	0.406	0.211	0.023	0.955
Douglas fir	293	0.620	0.174	0.010	1
Gaps	137	0.554	0.185	0.029	0.691
Non forested area	108	0.475	0.285	0.017	1

Accuracy	European larch	Douglas fir	Gaps	Non forest
Producer	0.692	1	0.857	0.9
User	0.818	0.833	1	0.818
Kappa per class	0.6097	1	0.814	0.873
Totals				
Overall Accuracy	0.865			
Kappa	0.819			

Table 5.8: Fuzzy classification accuracy assessment for a mixed European larch and Douglas fir dataset.

Discussion of the results: Table 5.8 shows the classification accuracy assessment of the fuzzy classification for the mixed sample plot. The classification showed the lowest stability for the European larch and non forested classes which is mainly composed of shrub and herbaceous understorey vegetation. This problem was due to the spectral similarity between these two classes. The best classification stability result was achieved for the Douglas fir class (mean 0.6206) followed by the gap discrimination which also performed well (mean 0.5548).

The lowest Kappa index was for the European larch class (0.6097) and the highest for the Douglas fir class (1). European larch showed a lower producer's accuracy due to omission errors where some European larch segments were classified as non forest. Due to problems with shadows, there was a compromise during the classification and training of samples by which some small objects that actually belong to the European larch class were classified as gaps. These segments were obscured either by shadows or contamination from the darker gap pixels. For a more accurate classification, each tree class could be assigned more child classes that reflect the spectral variability within the species, for instance, shadowed part, healthy, unhealthy, etc. As a consequence of this compromise, an increase in gap area is expected. However, it is hypothesized that this increase is compensated for the within-crown gaps that are not being detected and classified as such.

Overall accuracy and Kappa index had high values were high (0.8653 and 0.8191 respectively), showing a strong agreement with the training samples. Separation of the European larch class from grass was a difficult task. The open area covered by herbaceous vegetation in the lower part of the image was classified by means of inverted similarity to the forest class with the initial classification being refined manually as the thresholds applied did not work satisfactorily and areas of non forest were often classified as forest. The European larch class was classified by the nearest neighbour method on the basis of 10 samples. A NDVI image (figure 5.18) was created in an attempt to discriminate grass from European Larch and Douglas fir species. However, the NDVI image was useful just for the separation of the Douglas fir from the rest of the classes.

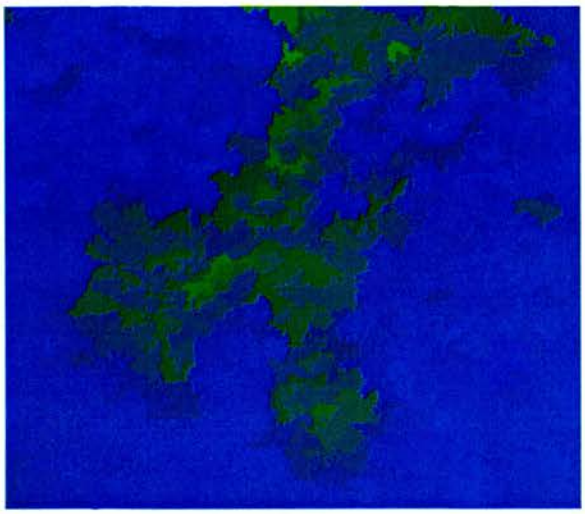

Figure 5.18: NDVI of the mixed Douglas fir and European larch sample plot.

- **Segmentation and classification of the dataset corresponding to a Norway spruce sample plot.** By visual comparison to the original dataset, a scale parameter of 30 was selected because the segmentation result fitted the information class extraction best. Based on these parameters, the segmentation process was performed. Figures 5.19 and 5.20 show the more representative segmentation results. The maximum and minimum number of segments were 3542 for scale 10 and 40 for scale 100, respectively.

  Comparing visually the images produced at scale 30 and 40 with the original dataset, it can be seen that scale 30 performed well enough in isolating most of the trees and that scale 40 merged the crowns that are close to each other, therefore the former scale value was chosen for the final segmentation. Furthermore, the characteristic circular shape of the spruce species constitutes an important discriminating factor that should be taken in account. For that reason, from the trials carried out testing different combination values for the colour/shape parameter, for this particular species the best results were obtained at colour: 0.6 and shape:0.4 and these values were used for the segmentation.

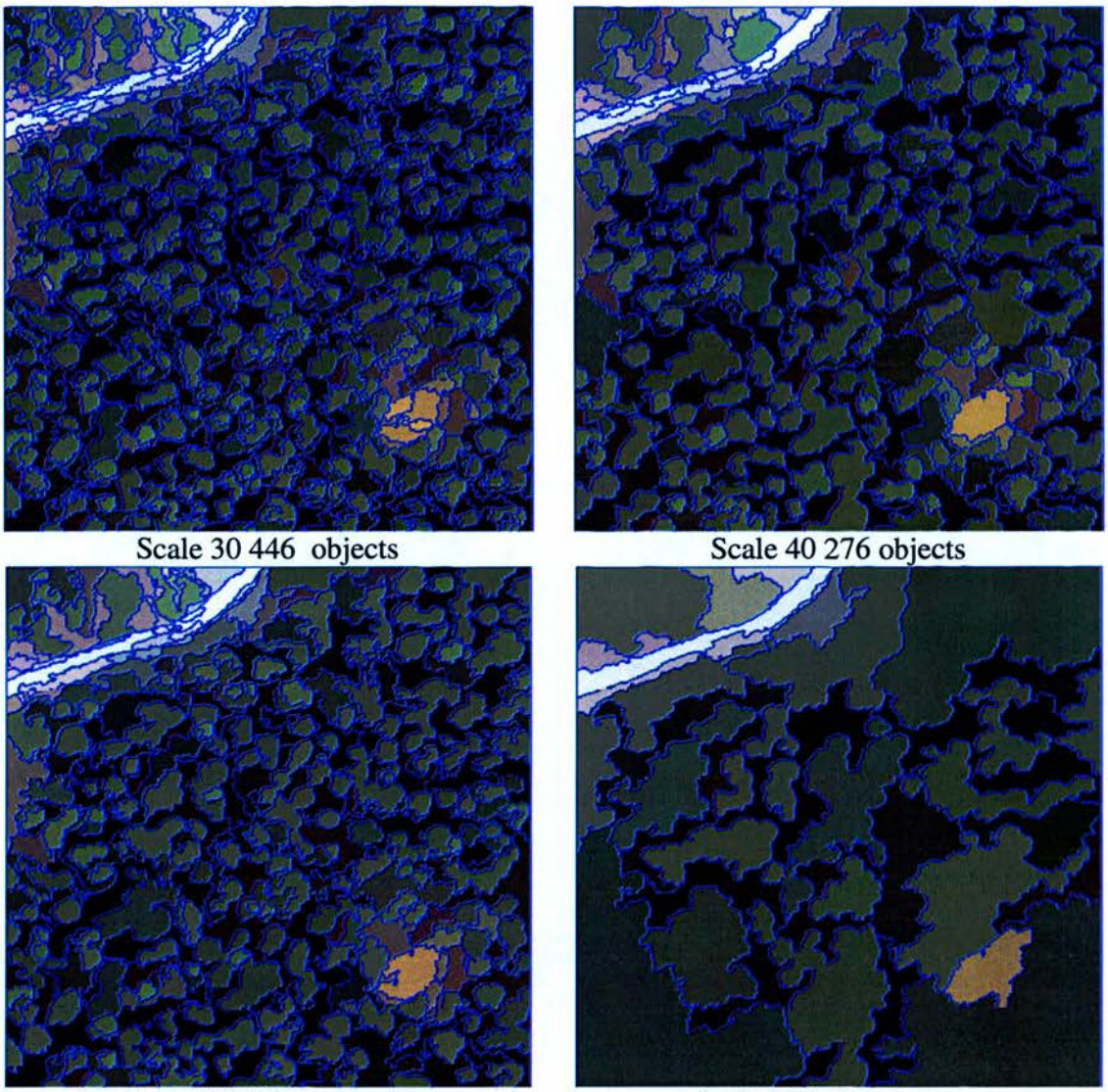

Figure 5.19: Results obtained from the segmentation process of a Norway spruce dataset considering values for the scale parameter of 30, 40, 50, and 100.

Another characteristic of the coniferous stands that makes them easier to classify is that they represent only a single-story crown canopy, as opposed to one having multiple sub-canopy layers which are often found in deciduous stands.

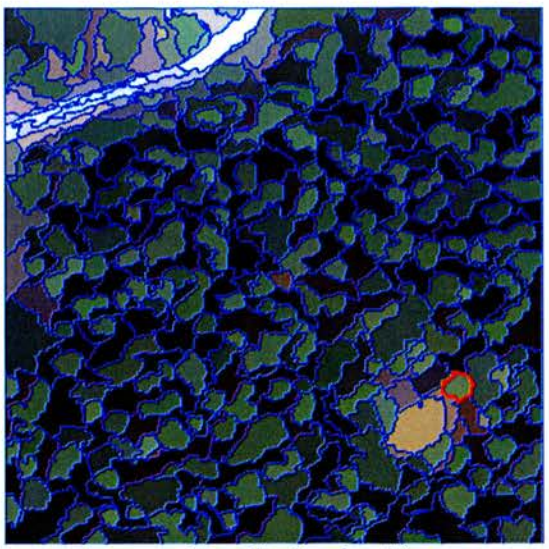

Figure 5.20: Best segmentation results obtained with parameter values of Scale 30, Colour/ Shape 0.6:0.4 and Compactness/Smoothness 0.8:0.2 for a Norway spruce plot.

For the classification task four classes were created: Norway spruce, road, gap/shadows, and gaps. Fuzzy classification was performed on the dataset. For the construction of the error matrix 10 samples of each category were taken, except for the road class which did not have as much segments and for which classification was performed with 6 samples. For the fuzzy classification membership functions were declared. These memberships included the mean brightness value to isolate the road and the gaps; the mean value of band 1 to classify the gap/shadow class; and the mean value of band 3 for the classification of Norway spruce (table 5.9).

Classes	Feature	Range
Norway spruce	Mean band 3	53 - 81
Gap/shadows	Mean band 1	11 - 27
Gaps	Mean brightness	102 - 105
Road	Mean brightness	161 - 247

Table 5.9: Membership functions used for the fuzzy classification of a Norway spruce stand.

The classification results corresponding to the fuzzy approach are shown in figure 5.21.

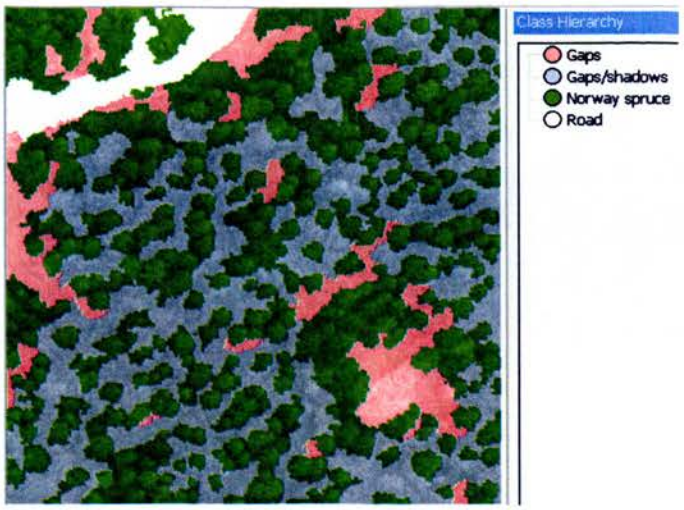

Figure 5.21: Fuzzy classification of Norway spruce dataset.

Results of the accuracy assessment are shown in table 5.10.

Discussion of the results: Table 5.10 shows the classification accuracy assessment of the fuzzy classification for the Norway spruce sample plot. The spectrally most differentiable class had the highest mean (road 0.6469) and the lowest value was for the Gaps class (mean 0.166).

Class	Objects	Mean	Std. Deviation	Minimum	Maximum
Norway spruce	228	0.315	0.121	0.011	0.566
Road	21	0.646	0.327	0.080	1
Gaps	41	0.166	0.150	0.010	0.772
Gaps/Shadows	110	0.273	0.182	0.002	0.710

Accuracy	Norway spruce	Road	Gaps	Gaps/Shadows
Producer	0.9	1	0.8	0.8
User	0.9	1	0.8	0.8
Kappa per class	0.866	1	0.733	0.733
Totals				
Overall Accuracy	0.875			
Kappa	0.833			

Table 5.10: Fuzzy classification accuracy assessment of the aerial photography, Norway spruce dataset.

Producer's accuracy was best for the Road class (1), followed by Norway spruce (0.866), Gaps and Gaps/shadows (both 0.733). Overall accuracy was high at 0.875 and the Kappa Index showed strong agreement between the classification and reference data (Kappa = 0.833). The classification accuracy for this plot is slightly lower than the one obtained for the classification of the European larch sample plot, mainly because the larch trees are well spaced which facilitates their identification, and also because the background offers a contrast for class identification; on the contrary, the Norway spruce plot is more dense making the crowns closer to each other, and apart from few very well identified gaps, shadowing effects make it more difficult to separate tree crowns, gaps, and shadows. The exclusion of the class Gaps/shadows will significantly improve the overall performance of the classification.

- **Segmentation and classification of the dataset corresponding to a Sessile oak sample plot.** By visual comparison to the original dataset, a scale parameter of 20 was selected because the segmentation result fitted the information class extraction best (figure 5.22).

  This particular sample plot presents problems with shadowed segments which get confused with gaps during the segmentation and classification. A visual analysis of the three bands that composed the digital dataset was carried out but no single band was able to discriminate between shadows, trees and gaps. To overcome this problem, a new set of images was generated in Erdas Imagine, where filters were used to maximize the texture and minimize the influence of shadow. A low pass filter with 3x3 window size, a high pass filter with 3x3 window size, a texture filter using variance and skewness options with 3x3 and 5x5 window size respectively, as well as the statistical filter option, were applied to generate the new images (figure 5.23).

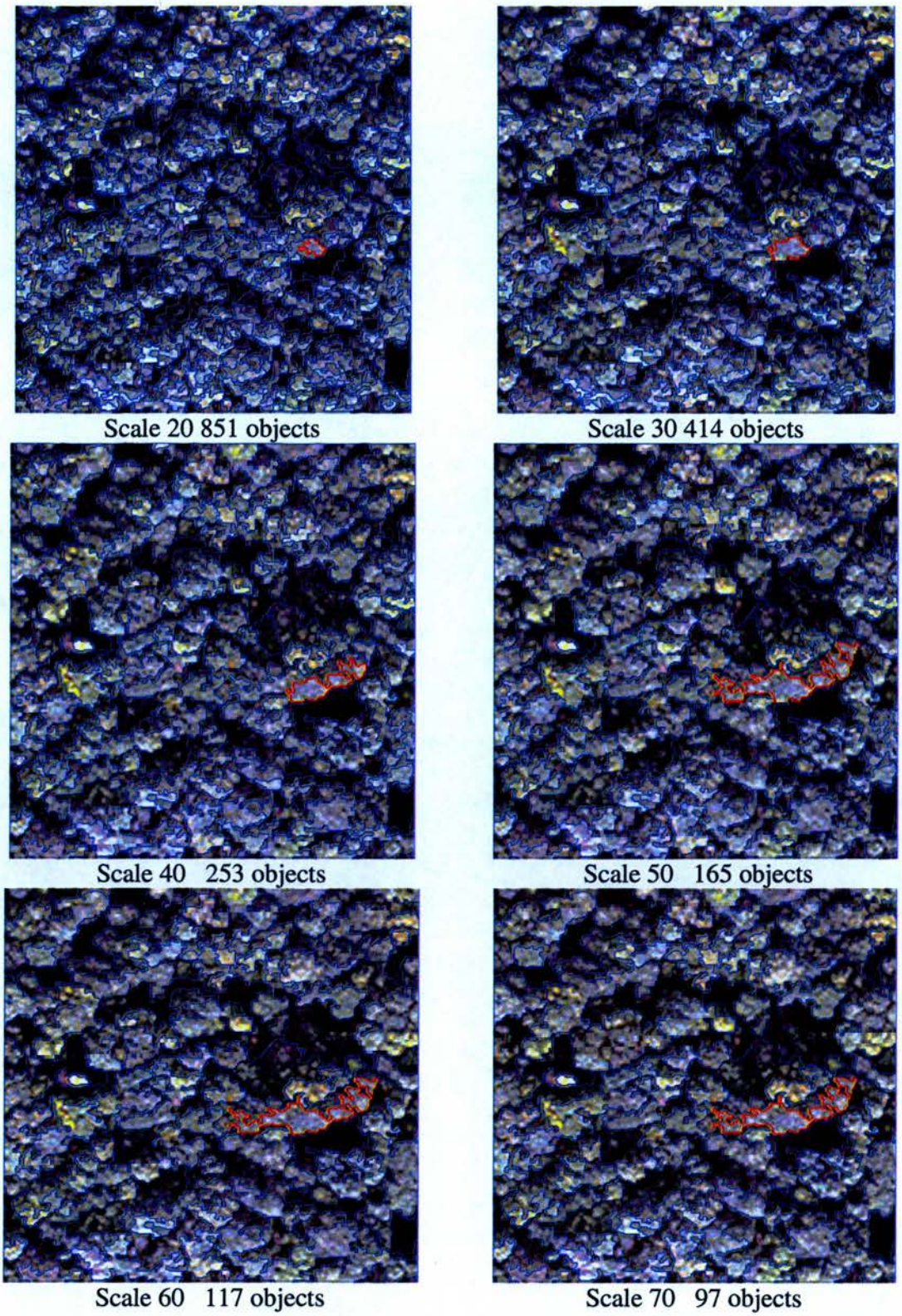

Figure 5.22: Results obtained from the segmentation process of a Sessile oak dataset considering values for the scale parameter of 20, 30, 40, 50, 60, and 70.

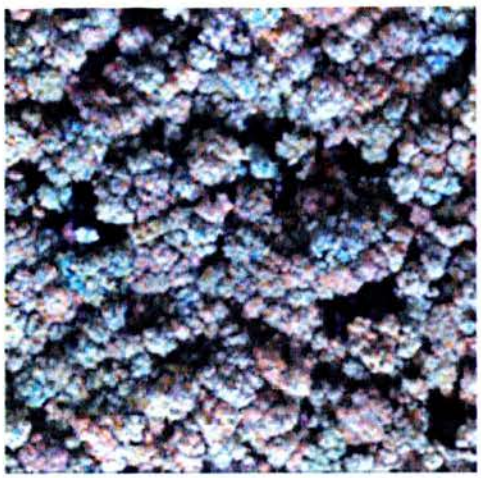

(a) Low pass filter 3x3 window size

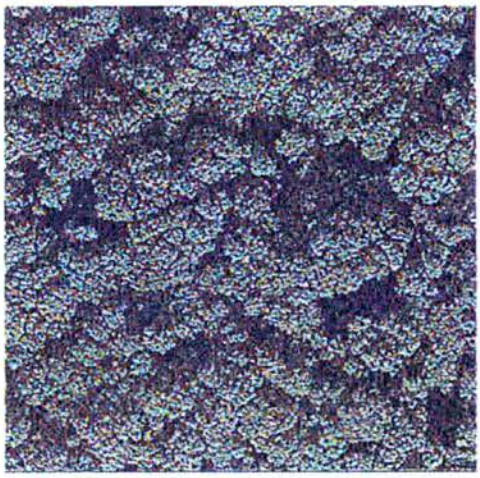

(b) High pass filter 3x3 window size

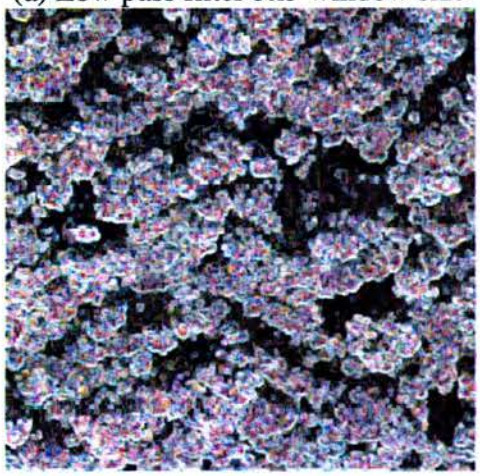

(c) Skewness 3x3 window size

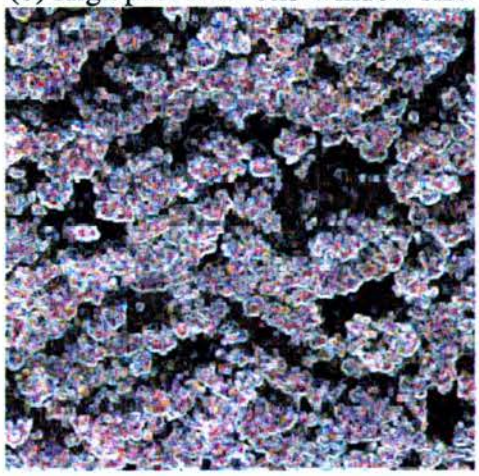

(d) Variance 3x3 window size

Figure 5.23: Imagery generated using a low pass filter (a), high pass filter (b), and texture filters using skewness (c) and variance (d) of an oak dataset.

The new set of images was visually compared to the original dataset in order to determine which represented a best separation between the trees and their shadowed parts. It was decided that the low pass filter produced the best discriminator and that this dataset was chosen for segmentation using parameters for: scale parameter of 20; colour 0.8 and shape 0.2; smoothness 0.2 and compactness 0.8. The combinations of these options provided a result in which tree crowns were highly segmented but it was nevertheless deemed as the best.

For the classification task two classes were created: Gaps and Sessile oak. For the purposes of accuracy assessment of the classification 10 samples of each category were taken. For the fuzzy classification membership functions were declared. These memberships included mean brightness to isolate the gaps and then inverted simmilarity to classify the trees (table 5.11).

Classes	Feature	Range
Gaps	Mean brightness	34.24 - 56
Sessile oak	Inverted similarity	56 – 248.28

Table 5.11: Membership functions used for the fuzzy classification of a Sessile oak stand.

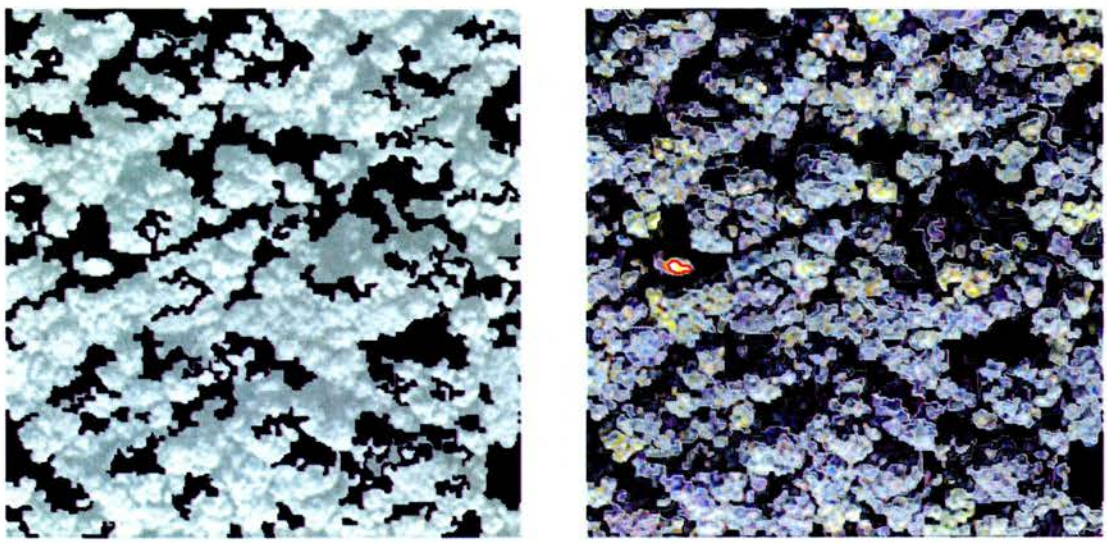

Figure 5.24: Fuzzy classification of a Sessile oak dataset. Final classification a) and segments of crown trees b).

Results of the accuracy assessment are shown in table 5.12.

Class	Objects	Mean	Std. Deviation	Minimum	Maximum
Sessile oak	671	0.81	0.209	0.050	0.994
Gaps	180	0.185	0.104	0.016	0.280

Accuracy	Sessile oak	Gaps
Producer	0.963	0.8
User	0.963	0.571
Kappa per class	0.904	0.762
Totals		
Overall Accuracy	0.863	
Kappa	0.760	

Table 5.12: Fuzzy classification accuracy assessment of a Sessile oak dataset.

Discussion of the results: Table 5.12 shows the classification accuracy assessment of the fuzzy classification for the oak sample plot. The classification showed good results for the two classes. The best result was achieved for the Sessile oak class with a producer's accuracy of 0.96 followed for the gaps class with 0.8. The overall accuracy was 0.86 and the Kappa Index (0.76) showed a strong agreement between classification and reference samples.

The main constraint for this classification, as mentioned before, was the shadowing of tree objects which could influence the estimation of the gap area. Also the gaps between and within-crowns were very difficult to extract, especially the detection of most of the within crown gaps would require a much more sophisticated segmentation and classification process.

5.8.2 Segmentation of ATM imagery

Figure 5.25 depicts the subsets of ATM containing the datasets used for segmentation and classification using the object oriented method implemented in eCognition.

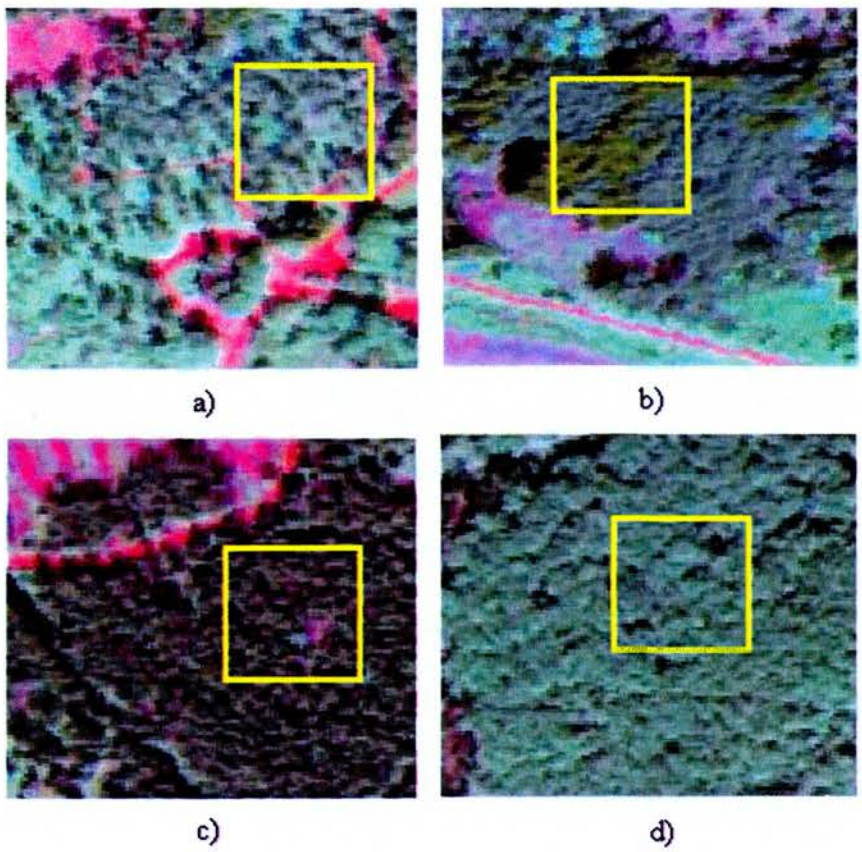

Figure 5.25: Subsets of ATM 5,7,9 band composites showing the location of the plots under study in the yellow boxes: European larch a); Mixed b); Norway spruce c); and Sessile oak d).

The segmentation and classification of these datasets followed the same procedure as for the aerial photography. The lower resolution of the data (resampled to 1 m), which also exhibits a high spectral variation among pixels, led to the use of small segmentation scales in the range of 20 to 30. An example of the type of crowns segmented and classified is shown in figure 5.26.

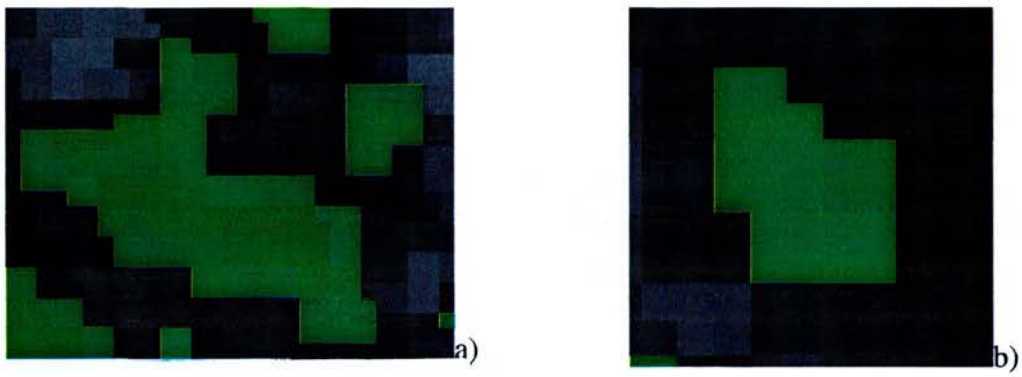

Figure 5.26: Multiple crowns a) and single crown b) of Sessile oak species in a segmented and classified ATM image; bands 5,7,9 composite.

Shading, obscuration, and merging of close crowns were also problems that affected the discrimination of individual trees. The segmentation and classification process followed the steps planned for all the datasets and the accuracy evaluation was carried out firstly within the eCognition program through the matrix error build with the training samples, and secondly through the comparison of tree crown polygons derived from the object oriented analysis against the manually delineated ground reference data.

- **Segmentation and classification of the ATM dataset corresponding to the European larch sample plot.** By visual comparison to the original dataset, a scale parameter of 30 was selected because the segmentation result fitted the information class extraction best. This segmentation scale generated 12822 segments. The values for the Colour/shape parameter and the Compactness/smoothness parameter were set at 0.8:0.2 and 0.5:0.5, respectively.

  For the classification task three classes were created: Gaps, Road, and European larch. Fuzzy classification was performed on the dataset. For the purposes of accuracy assessment of the classification samples of each category were taken. For the fuzzy classification membership functions were declared. These memberships included layer features using spectral characteristics to discriminate between classes (table 5.13).

Classes	Feature	Range
Gaps	Mean brightness	5000-6100
European larch	Mean brightness	2800-4000
Road	Mean band 5	3200 - 5500

Table 5.13: Membership functions used for the fuzzy classification of the European larch plot.

Figure 5.27 shows the final results of the classification.

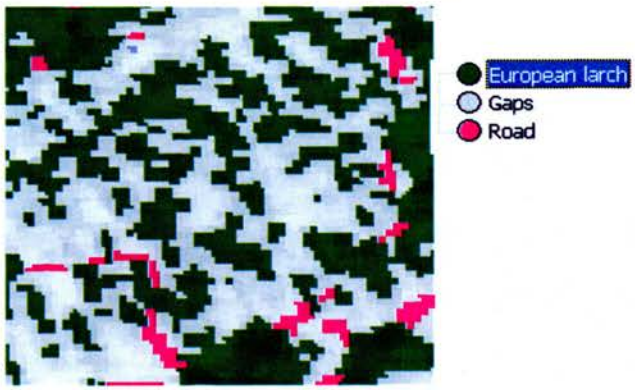

Figure 5.27: Fuzzy classification results for the European larch sample plot ATM dataset.

Results of the accuracy assessment based on the best classification result are shown in table 5.14.

Class	Objects	Mean	Std. Deviation	Minimum	Maximum
European larch	4284	0.84	0.216	0.51	0.996
Gaps	8233	0.463	0.185	0.631	0.927
Road	305	0.39	0.071	0.422	0.503
Accuracy	**European larch**		**Gaps**	**Road**	
Producer	0.95		1	0.181	
User	1		0.5	1	
Kappa per class	0.906		1	0.139	
Totals					
Overall accuracy	0.756				
Kappa	0.620				

Table 5.14: Fuzzy classification accuracy assessment of the ATM European larch dataset.

Discussion of results: Overall accuracy of the classification (0.756) was about 15% lower than that obtained with aerial photography. This result was expected due to the lower resolution of the data and the increasing difficulty for the visualization and selection of training samples. However, from table 5.14 it can be seen that the class with lowest accuracy was that of the Road, which was often misclassified either as gaps or European larch. The removal of this class or the use of a more sophisticated approach to separate spectrally the class road with a mask from the forest, could highly improve the accuracy of the classification.

The kappa index for this classification is low but it is again influenced by the misclassification of the road class; nevertheless, it is high enough for the classification to be rated as in good agreement with the reference samples.

- **Segmentation and classification of the ATM dataset corresponding to a mixed sample plot.** By visual comparison to the original dataset, a scale parameter of 20 was selected because the segmentation result fitted the information class extraction best. This segmentation scale generated 4640 segments. The values for the Colour/shape parameter and the Compactness/smoothness parameter were set at 0.8:0.2 and 0.5:0.5, respectively.

  For the classification task three classes were created: European larch, Douglas fir, and Gaps. Fuzzy classification was performed on the dataset. For the purposes of accuracy assessment samples of each category were taken. For the fuzzy classification membership functions were declared. These memberships included the mean of spectral bands and the nearest neighbour (table 5.15).

Classes	Feature	Range
European larch	Nearest neighbour	10 samples
Douglas fir	Mean band 9	430 - 780
Gaps	Mean band 9	220 - 350

Table 5.15: Membership functions used for the fuzzy classification of a mixed sample plot.

Figure 5.28 shows the final results of the classification.

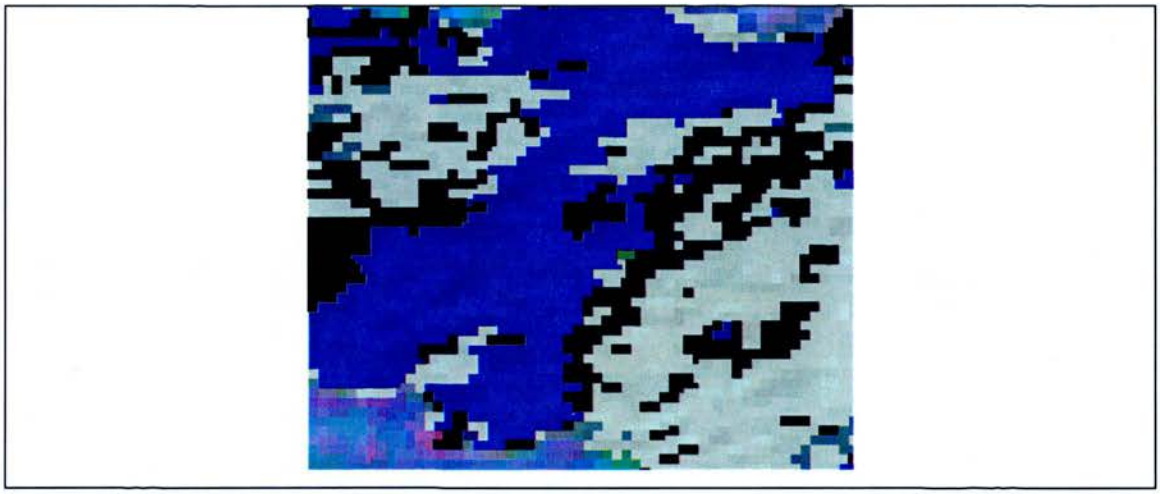

Figure 5.28: Fuzzy classification results for ATM imagery containing a mixed stand of European larch and Douglas fir species.

Results of the accuracy assessment are shown in table 5.16.

Class	Objects	Mean	Std. Deviation	Minimum	Maximum
European larch	2825	0.759	0.157	0.673	0.863
Douglas fir	1347	0.525	0.311	0.486	0.966
Gaps	468	0.675	0.202	0.542	0.748

Accuracy	European larch	Douglas fir	Gaps
Producer	1	0.7	0.6
User	0.769	0.6364	1
Kappa per class	1	0.5263	0.5
Totals			
Overall accuracy 0.766			
Kappa 0.650			

Table 5.16: Fuzzy classification accuracy assessment of the ATM mixed European larch and Douglas fir dataset.

Discussion of results: Overall accuracy (0.766) of the classification of this data set is in the range of the previous ATM classifications. Again, classification of the Gaps class obtained the lowest accuracy with producer's accuracy of 0.6 compared to 1 for the European larch and 0.7 for the Douglas fir class. The Kappa index was 1 for the European larch , 0.52 for the Douglas fir, and 0.5 for the Gaps class. It is noted that European larch was classified by means of nearest neighbour, the straightforward way for classification in eCognition. It was found that when the objects subject to classification have a more or less homogeneous spectral response, i.e. without large spectral variations within and between objects in the same class, the nearest neighbour method provides a reliable method for classification.

- **Segmentation and classification of the ATM dataset corresponding to a Norway spruce sample plot.** By visual comparison to the original dataset, a scale parameter of 30 was selected because the segmentation result fitted the information class extraction best. This segmentation scale generated 3361 segments. The values for the Colour/shape parameter and the Compactness/smoothness parameter were set at 0.8:0.2 and 0.5:0.5, respectively.

  For the classification task three classes were created: Norway spruce, Gap/shadows, and Gaps. Fuzzy classification was performed on the dataset. For the purposes of accuracy assessment samples of each category were taken. For the fuzzy classification membership functions were declared. These memberships included the mean of spectral bands and the nearest neighbour (table 5.17).

Classes	Feature	Range
Norway spruce	Nearest neighbour	15 samples
Gap/shadows	Mean maximum difference	3.0 – 3.4
Gaps	Mean maximum difference	1.8 – 2.0

Table 5.17: Membership functions used for the fuzzy classification of a Norway spruce sample plot.

Figure 5.29 shows the final results of the classification.

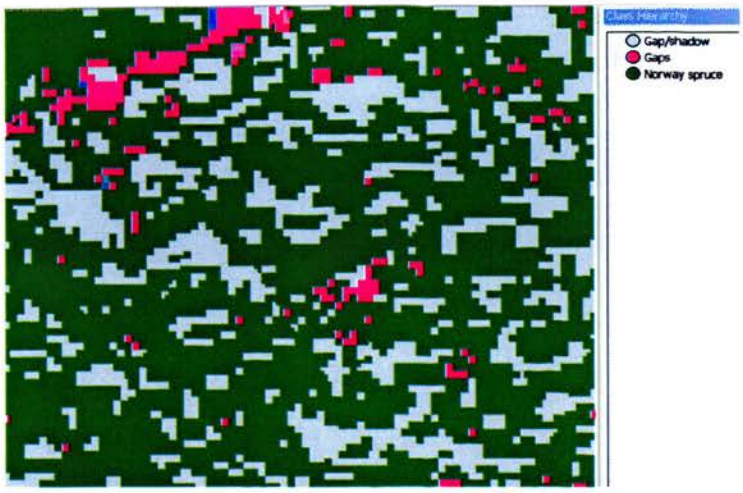

Figure 5.29: Fuzzy classification results for the Norway spruce sample plot ATM dataset.

Results of the accuracy assessment are shown in table 5.18.

Class	Objects	Mean	Std. Deviation	Minimum	Maximum
Norway spruce	2447	0.981	0.093	0.589	1
Gap/shadow	745	0.670	0.148	0.332	0.507
Gaps	169	0.471	0.266	0.364	1
Accuracy	**Norway spruce**		**Gap/shadow**		**Gaps**
Producer	0.916		0.692		0.785
User	0.785		0.750		0.846
Kappa per class	0.870		0.555		0.678
Totals					
Overall accuracy	0.794				
Kappa	0.692				

Table 5.18: Fuzzy classification accuracy assessment result for a Norway spruce ATM dataset.

Discussion of results: The overall accuracy for this classification was 0.794 and the Kappa index was 0.692 showing a moderate agreement with the trained samples. Producer's accuracies varied from 0.916 for the Norway spruce class to 0.692 for the Gap/shadow class. Kappa index per class showed similar values with 0.870 for the Norway spruce class, 0.678 for the Gap class and 0.555 for the Gap/shadow class, the latter being the poorest classified class.

- **Segmentation and classification of the ATM dataset corresponding to the Sessile oak sample plot.** By visual comparison with the original dataset, a scale parameter of 20 was selected because the segmentation result fitted the information class extraction best. This segmentation scale generated 8276 objects. The values for the Colour/shape parameter and the Compactness/smoothness parameter were set at 0.8:0.2 and 0.5:0.5 respectively.

  For the classification task two classes were created: Gaps and Sessile oak. Fuzzy classification was performed on the dataset. For the purposes of accuracy assessment classification samples of each category were taken. For the fuzzy classification membership functions were declared. These memberships included layer features using spectral characteristics to discriminate between classes but shape features were also included to aid in the classification (table 5.19).

Classes	Feature	Range
Gaps	Mean band 9	223 - 354
Sessile oak	Mean band 9	500 - 950

Table 5.19: Membership functions used for the fuzzy classification of the European larch plot.

Figure 5.30 shows the final results of the classification.

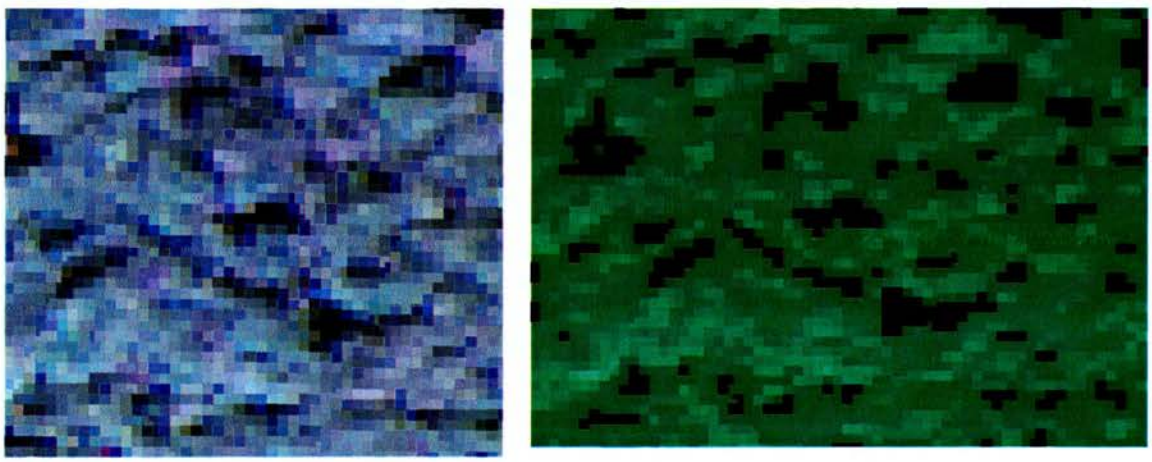

Figure 5.30: ATM composite of bands 5,7,9 showing the oak plot under study and its respective classification by means of fuzzy logic. Oak tree pixels are shown in green and gap pixels in black.

Results of the accuracy assessment based on the best classification result are shown in table 5.20.

Class	Objects	Mean	Std. Deviation	Minimum	Maximum
Sessile oak	484	0.508	0.031	0.452	0.98
Gaps	7792	0.729	0.026	0.66	1
Accuracy	**Sessile oak**		**Gaps**		
Producer	0.933		0.692		
User	1		1		
Kappa per class	0.866		0.546		
Totals					
Overall Accuracy	0.821				
Kappa	0.693				

Table 5.20: Fuzzy classification accuracy assessment of the Sessile oak ATM dataset.

Discussion of the results: Although it represents a very complex mature canopy of trees more than 100 years old, this dataset was relatively easy to classify as the only distinction to be made was between trees and gaps. The gap class in this dataset is characterised by very dark colour which spectral reflectance is very distinctive in band 9. The tree crowns are characterised by a spectral range, with the highest values denoting the top of the trees. However, the part of the trees obscured by shadows was often misclassified as gaps and therefore the accuracy of the classification was affected by this fact. The detection of within-crown gaps was particularly difficult and a compromise was made in which segments exhibiting a part of gap and a part of shadowed or obscured trees were assigned to a higher height class (i.e., belonging to a tree) if the tree part of the segment was greater than the gap part of the segment. As a consequence, total gap area derived from this dataset will be smaller than its actual counterpart in the ground reference dataset.

Nevertheless, the overall accuracy was 0.82, just slightly lower than that of the obtained through aerial photography (0.86). The Kappa index (0.69) was again lower than its counterpart for aerial photography (0.76) but it is still in good agreement with

the trained samples. The Sessile oak class had a higher producer's accuracy and Kappa index (0.93 and 0.86, respectively) than the Gaps class (0.69 and 0.54, respectively).

5.8.3 Segmentation of LiDAR derived DCM

The LiDAR-derived DCM of each plot was used as input for the eCognition segmentation and object-oriented classification algorithm. As the LiDAR data lacks significant information about fine scale texture, the only feature available for segmentation and classification is height.

- **Segmentation of the LiDAR dataset corresponding to the European larch sample plot.** The segmentation was carried out considering the following parameters: scale 4, Colour/ Shape: 0.8:0.2 and Compactness/Smoothness: 0.5:0.5, which were selected after an exhaustive process of trial-error due to their closest fitting when visually compared to the referenced data The segments were classified using a fuzzy classification. For the accuracy evaluation samples were taken on the "mean" object feature in height classes at 5 metre intervals from 0 m to >30 m.

Accuracy	**0 - 5**	**5 - 10**	**10 - 15**	**15 - 20**	**20 - 25**	**25 - 30**	**>30**
Producer	1	0.9	0.7	0.777	0.727	0.9	1
User	1	1	0.875	0.636	0.666	0.9	1
Kappa per class	1	0.885	0.661	0.736	0.670	0.883	1
Totals							
Overall accuracy	0.857						
Kappa	0.833						

Table 5.21: Fuzzy classification accuracy assessment of the European larch LiDAR dataset.

Discussion of the results: The accuracy of the classification according to the Overall and Kappa index is in strong agreement with the referenced samples. Overall accuracy was 0.857 and the Kappa index of agreement was 0.833. These accuracy values are higher than the ones obtained using the ATM dataset (0.756 and 0.620,

Overall accuracy and Kappa index respectively) but lower that their counterparts obtained through the use of aerial photography (0.888 and 0.848). The best classified classes were the ones corresponding to the low and top heights. There is no apparent explanation for the misclassification of certain classes, but they did not significantly affect the overall accuracy.

- **Segmentation of the LiDAR dataset corresponding to the mixed sample plot.** The segmentation was carried out on the basis of the following parameters: scale 4, Colour/Shape: 0.8:0.2 and Compactness/Smoothness: 0.5:0.5. Figure 5.31 a) shows the results of the segmentation procedure. The segments were classified using a fuzzy classification. For the accuracy evaluation a number of 10 samples per class were compared to the objects classified using the "mean" object feature in height classes at 5 metre intervals from 0 m to >30 m.

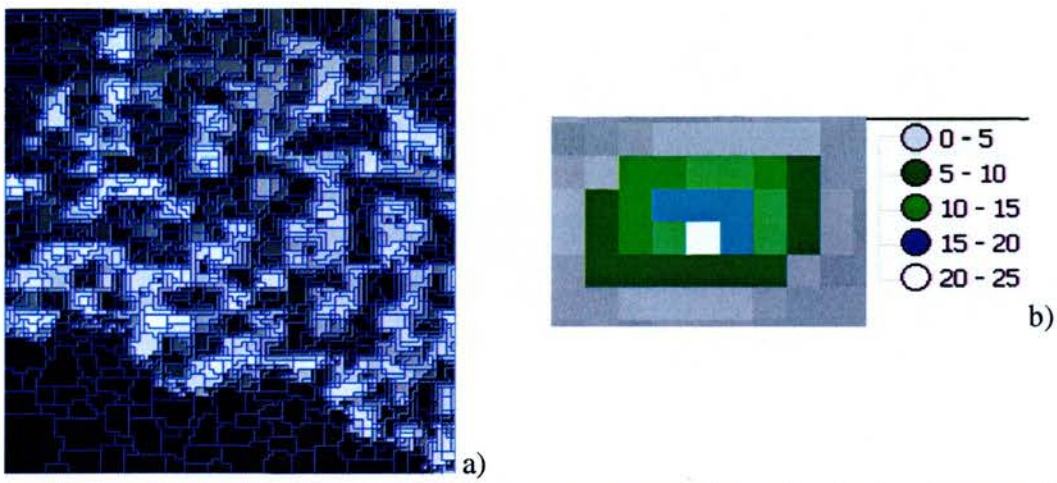

Figure 5.31: Whole stand segmentation a) and segmentation of a single European larch crown b) extracted from the classification of the LiDAR dataset corresponding to a mixed (European larch and Douglas fir) sample plot with overlaid eCognition segments.

The accuracy assessment of the classification is shown in table 5.22.

Accuracy	**0 - 5**	**5 - 10**	**10 - 15**	**15 - 20**	**20 - 25**	**25 - 30**	**>30**
Producer	1	0.75	0.666	0.666	0.75	1	1
User	0.75	1	1	0.666	1	0.666	0.75
Kappa per class	1	0.710	0.633	0.614	0.710	1	1
Totals							
Overall accuracy	0.818						
Kappa	0.788						

Table 5.22: Fuzzy classification accuracy assessment of the mixed species LiDAR dataset.

Discussion of the results: Overall accuracy for this classification (0.81) is lower than for the dataset corresponding to the European larch plot (0.92). When comparing to the classification of this plot using different datasets, the overall accuracy obtained with LiDAR is higher than that obtained using the ATM data (0.766) and lower than that yield by the aerial photography classification (0.865). Kappa index of 0.78 is also significantly higher than that of the ATM classification (0.650) and lower than the Kappa index value obtained using aerial photography (0.819). The lower accuracy obtained in this classification in comparison to the accuracy values of the European larch stand, might be explained by the increase in tree density, the mix of species against a pure stand, and also for the different topographic characteristics of this plot which exhibit a slope of ±60° in comparison with the relatively flat terrain in which the European larch stand lies. The best classified classes were again the ones corresponding to the low and top heights.

- **Segmentation of the LiDAR dataset corresponding to the Norway spruce sample plot.** The segmentation was carried out considering the following parameters: scale 2, Colour/Shape: 0.8:0.2 and Compactness/Smoothness: 0.5:0.5. Figure 5.32 shows the results of the segmentation procedure. The segments were classified using a fuzzy classification. For the accuracy evaluation a number of 10 samples per class were compared to the objects classified using the "mean" object feature in height classes at 5 meter intervals from 0 to 25.

Figure 5.32 shows the segmentation result of the corresponding LiDAR dataset.

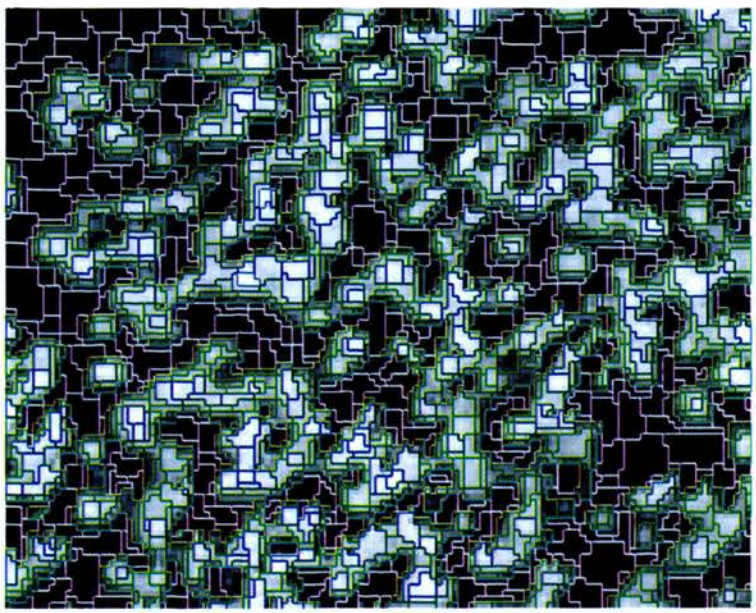

Figure 5.32: Segmentation of the LiDAR dataset corresponding to a Norway spruce sample plot.

The following table (5.23) shows the classification accuracy assessment results:

Accuracy	**0 - 5**	**5 - 10**	**10 - 15**	**15 - 20**	**20 - 25**
Producer	1	0.8	0.833	1	1
User	1	1	0.714	0.6	1
Kappa per class	1	0.752	0.75	1	1
Totals					
Overall accuracy	0.809				
Kappa	0.752				

Table 5.23: Fuzzy classification accuracy assessment of the Norway spruce LiDAR dataset.

Discussion of the results: Overall accuracy of the classification was 0.809 and Kappa index was 0.752. These values are higher in comparison to those obtained using ATM data (0.794 and 0.692) but lower than those obtained through aerial photography (0.875 and 0.833). Lower and highest height classes were the best classified. This might be explained as a consequence of the medium density of the plot where trees were well separated and because of the typical shape of the trees with one crown top clearly defined for most of the trees.

- **Segmentation of the LiDAR dataset corresponding to the Sessile oak sample plot.** The segmentation was carried out considering the following parameters: scale 7, Colour/ Shape: 0.8:0.2 and Compactness/Smoothness: 0.5:0.5. . Figure 5.33 shows the results of the segmentation procedure. The segments were classified using a fuzzy classification. For the accuracy evaluation 10 samples per class were compared to the objects classified using the "mean" object feature in height classes at 5 metre intervals from 0 m to 25 m.

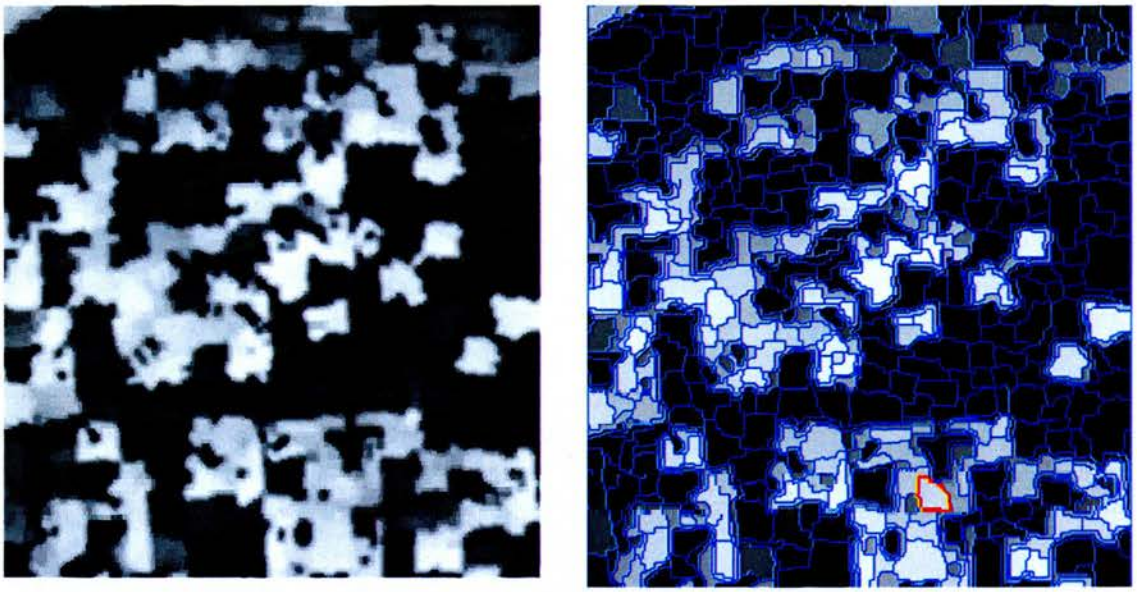

Figure 5.33: Segmentation of the LiDAR dataset corresponding to a Sessile oak sample plot.

Table 5.24 shows the classification accuracy assessment result:

Accuracy	**0 - 5**	**5 - 10**	**10 - 15**	**15 - 20**	**20 - 25**
Producer	0.666	0.8	0.666	1	0.8
User	0.666	0.8	0.666	0.666	0.8
KIA per class	0.604	0.728	0.604	1	0.728
Totals					
Overall accuracy	0.736				
KIA	0.664				

Table 5.24: Fuzzy classification accuracy assessment of the Sessile oak LiDAR dataset.

Discussion of the results: Overall accuracy of the classification was 0.736 and Kappa index was 0.664. These values were lower in comparison to those obtained using ATM data (0.821 and 0.693) and aerial photography (0.863 and 0.760). Lower accuracies in comparison with the other plots might be explained by the complexity of the hardwood canopy accompanied by a high tree density. Discrimination of single trees was very difficult due to the canopy appearance as a continuous surface in which several crowns are merged. The class height with better producer accuracy was between 15 – 20 m and the classes with lower accuracy were the ones corresponding to 0 - 5 m and 10 -15 m. The class 0 – 5 m height best corresponded to gaps.

5.8.4 Segmentation and classification of the aerial photography and LiDAR data

In this segmentation analysis, the three bands of the aerial photographs and the DCM with the height information about the plots were used as input for the eCognition process. In order to emphasize the height information contained in the DCM, a high weight (5) was assigned to the DCM layer. The selection of this weight was performed empirically through a process of trial and error.

The classification process was carried out in much the same way as for the aerial photography dataset alone but now the information about height allowed a better discrimination of non forested areas including gaps (figure 5.34).

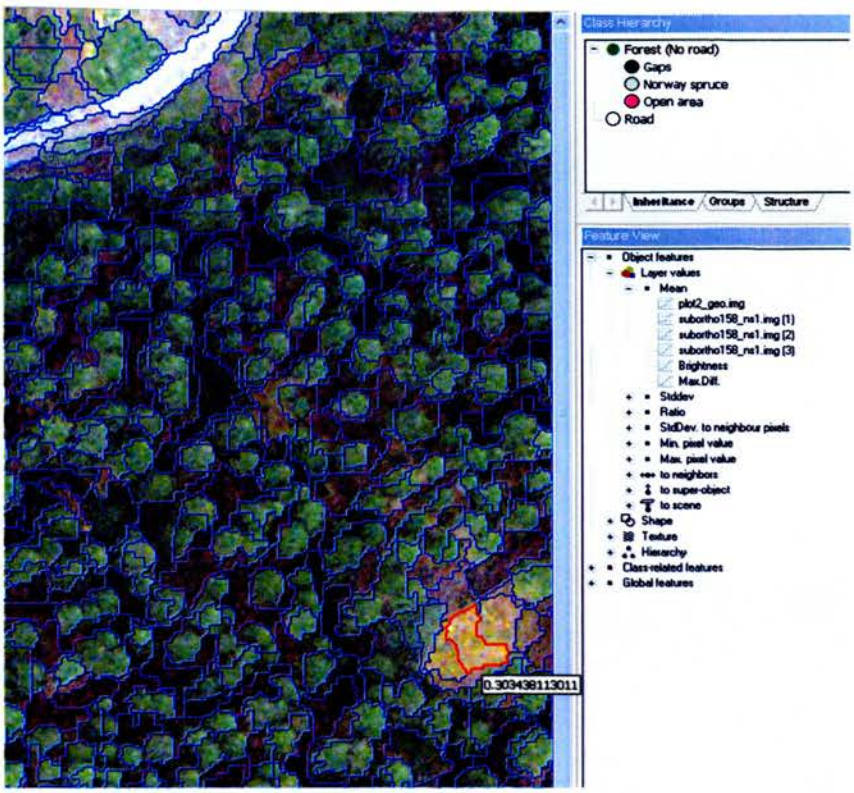

Figure 5.34: Aerial photograph and LiDAR (background) datasets with eCognition segments overlaid, corresponding to a Norway spruce plot. Note the segment delineated in red depicting a sunlit understory material visible and its correspondent height value in the LiDAR derived DCM band.

The accuracy assessment results for the classifications corresponding to the different plots are shown in tables 5-25 to 5.28.

Accuracy	European larch	Gaps	Road
Producer	1	0.90	1
User	0.937	1	1
Kappa per class	1	0.878	1
Totals			
Overall accuracy	0.975		
Kappa	0.960		

Table 5.25: Fuzzy classification accuracy assessment of a LiDAR and aerial photography dataset for European larch.

Accuracy	European larch	Douglas fir	Gaps
Producer	0.923	1	0.875
User	0.923	1	0.875
Kappa per class	0.867	1	0.831
Totals			
Overall accuracy	0.935		
Kappa	0.901		

Table 5.26: Fuzzy classification accuracy assessment of a LiDAR and aerial photographic mixed European larch and Douglas fir dataset.

Accuracy	Norway spruce	Gap/shadow	Gaps	Road
Producer	0.88	0.88	1	1
User	1	1	1	1
Kappa per class	0.815	0.815	1	1
Totals				
Overall accuracy	0.952			
Kappa	0.932			

Table 5.27: Fuzzy classification accuracy assessment result for a LiDAR and aerial photographic Norway spruce dataset.

Accuracy	Sessile oak	Gaps
Producer	0.882	0.900
User	0.937	0.818
Kappa per class	0.711	0.831
Totals		
Overall Accuracy	0.888	
Kappa	0.766	

Table 5.28: Fuzzy classification accuracy assessment of a LiDAR and aerial photographic Sessile oak dataset.

Discussion of the results: On the basis of comparison to the reference samples, the classification results performed well for all plots. The best classification results were for the European larch plot with a producer's accuracy of 0.975 and KIA 0.96, and the lower classification accuracy was for the oak plot with producer accuracy of 0.86 and KIA 0.72. Overall, accuracies were lower than the obtained using aerial photography and higher than the obtained using ATM data. All classifications were in good agreement with the

reference samples. The addition of the height LiDAR data was particularly useful when separating non-forest areas (herbaceous vegetation) from the forested areas which was a problem during the segmentation of the aerial photography alone due to the spectral similarity of some tree species to open areas with grass, as in the European larch and mixed plots. Discrimination between gaps and shadowed parts of trees was also aided by the LiDAR information.

5.8.5 Segmentation and classification of the multispectral and LiDAR data

In the multi-resolution segmentation process, the influence of the DCM and the multi-spectral bands on object generation was controlled by layer weight, scale parameters, the amount of colour and shape factors. Again, the LiDAR layer was assigned a high weight (weight = 5) in comparison with the multispectral bands 5, 7, 9 (weiht = 1). Note that eCognition assign weights to internally sum to 1.

The accuracy assessment results for the classifications corresponding to the different plots are shown in tables 5.29 to 5.32.

Accuracy	European larch	Gaps	Road
Producer	1	0.875	1
User	0.928	1	0.909
KIA per class	1	0.805	1
Totals			
Overall accuracy 0.948			
KIA 0.922			

Table 5.29: Fuzzy classification accuracy assessment of a LiDAR and ATM European larch dataset.

Accuracy	European larch	Douglas fir	Gaps
Producer	0.818	1	0.92
User	0.9	1	0.857
KIA per class	0.75	1	0.88
Totals			
Overall accuracy	0.921		
KIA	0.882		

Table 5.30: Fuzzy classification accuracy assessment of a LiDAR and ATM mixed European larch and Douglas fir dataset.

Accuracy	Norway spruce	Gap/shadow	Gaps	Road
Producer	1	0.777	0.75	1
User	0.92	0.777	0.857	1
KIA per class	1	0.697	0.685	1
Totals				
Overall accuracy	0.882			
KIA	0.837			

Table 5.31: Fuzzy classification accuracy assessment result for a LiDAR and ATM Norway spruce dataset.

Accuracy	Sessile oak	Gaps
Producer	0.866	0.80
User	0.866	0.80
KIA per class	0.666	0.814
Totals		
Overall Accuracy	0.845	
KIA	0.666	

Table 5.32: Fuzzy classification accuracy assessment of a LiDAR and ATM Sessile oak dataset.

Discussion of the results: Again note that for all plots the classifications are more accurate than on the basis of ATM data alone. However, the addition of aerial photography data to the classification did not represent a significant improvement over LiDAR data on its own. The best classification results were for the European larch plot with a producer accuracy of 0.948 and KIA 0.922, and the lower classification accuracy was for the oak plot with producer accuracy of 0.845 and KIA 0.666. The lower

resolution of the multispectral dataset complicated the segmentation and classification process, tree crown details were diluted and was difficult to make a judgement about the quality of the segmentation.

5.8.6 Results summary

Table 5.33 present the overall and Kappa accuracies values obtained for all the classifications per species and per dataset.

Species	European larch		Mixed		Norway spruce		Sessile oak	
Dataset	**Overall**	**Kappa**	**Overall**	**Kappa**	**Overall**	**Kappa**	**Overall**	**Kappa**
Aerial Ph.	0.888	0.848	0.865	0.819	0.875	0.833	0.863	0.760
ATM	0.756	0.620	0.766	0.650	0.794	0.692	0.821	0.693
LiDAR	0.857	0.833	0.818	0.788	0.809	0.752	0.736	0.664
LiDAR+ Aerial Ph.	0.975	0.960	0.935	0.901	0.952	0.932	0.888	0.766
LiDAR+ ATM	0.948	0.922	0.921	0.882	0.882	0.837	0.845	0.666

Table 5.33: Overall and Kappa accuracies values obtained trough object oriented segmentation and classification per species and per dataset.

Best classification results were obtained through the combination of aerial photography and LiDAR data for all species. This is explained by the high resolution of aerial photography (25 cm) in comparison with 1 m spatial resolution of multispectral data. The inclusion of the LiDAR dataset increased classification accuracies of both aerial photography and ATM datasets although in different proportions (Table 5.34). The results also indicated that the LiDAR data performed less accurately than aerial photography but better than ATM data.

Species	LiDAR + AP - AP	LiDAR + ATM - ATM	Difference
European larch	0.087	0.192	0.027
Mixed species	0.07	0.155	0.014
Norway spruce	0.077	0.088	0.07
Sessile oak	0.025	0.024	0.043

Table 5.34: Comparison of differences in classification accuracy between Aerial Photography (AP) and Airborne Thematic Mapper (ATM) datasets after inclusion of the LiDAR data.

The largest increases in classification accuracy for aerial photography datasets with the addition of height information was for European larch (8.7%), followed by Norway spruce (7.7%), the mixed plot (7%) and lastly the Sessile oak (2.5%) species. Similarly for the ATM datasets, the highest improvement was for the European larch plot (19.2%), followed by the mixed plot (15.5%), the Norway spruce (8.8%) and the Sessile oak dataset (2.4%). The results seem to indicate that the problems arising in classifications of optical data such as aerial photography or multispectral data such as ATM due to spectral similarities between classes can be resolved by the introduction of height information through LiDAR. However, the benefit of this addition still depends on density of the stand and distance between trees, as the most obvious factors influencing the classification in this study, and which are probably also species dependent. In their tree crown delineation using high resolution imagery, Mei and Durrieu (2004) noted that the results concerning tree segmentation were "stand dependant"; Tiede *et al.* (2004) also reported that tree detection and delineation results vary with canopy age, density, and dominance structure. Other factors to be considered are related to the accuracy of the LiDAR derived DCM itself which is also affected by topography and density of the stand, so that in stands with more gaps and greater distances between trees a better penetration of the laser hits occur and DCM accuracies are expected to be higher. Besides that, algorithms used for interpolation and generation of continuous surfaces could produce excessive smoothness of the terrain and/or canopy features, which might also influence the accuracy of the results.

All classifications were found to be more accurate when aerial photography plus LiDAR against ATM plus LiDAR were used, although the differences in accuracy were small (ranging from 1.4% to 7%). However, these classifications were run on a limited area, just big enough to include the sample plots (50 m x 50 m), and the stands examined were pure stands (European larch, Norway spruce, Sessile oak) or a two species stand as in the case of the mixed plot (European larch and Douglas fir) and all plots contained trees of the same age and which were more or less regularly distributed. These plot characteristics and the ultimate goal of the study, lead to relatively simple classifications considering just a few classes and run just over the sampled area. When forest stands comprise several species and of diverse tree ages over large areas, segmentation and classification accuracies are expected to be lower; for example, Collins *et al.* (2004) found the eCognition procedure for extracting image objects inadequate. They analyzed LiDAR and multispectral data (0.3 m resolution) on seven species obtaining an overall classification result of 0.3211 and attributed the poor results to the intermingled nature of hardwood tree crowns in high density areas which hampered the potential of eCognition to recognize individual tree crowns.

5.9 Validation of classification against manual delineation

The results of the object-oriented classification performed in eCognition were compared to the manually delineated tree shape files considered as the ground reference data. The number and size of detected trees were analyzed for each selected plot and compared to 40 manually delineated individual crowns per plot derived from the aerial photography. The layers were compared in vector format. Among the strategies used in other studies for the assessment of matching between automatic and manually delineated tree crowns, two were considered as potentially useful for this analysis. One, developed by Leckie *et al.* (2005), considers 20 categories of overlaps between the polygons and the other, developed by Mei and Durrieu (2004), establishes seven types of overlaps. After a first accuracy assessment using both methodologies, the one designed by Mei and Durrieu (2004) was found to be more adapted to the purpose of this thesis, more understandable

and easier to use, and therefore it was chosen for segmentation accuracy assessment (figure 5.35). The categories of overlap are defined as follows:

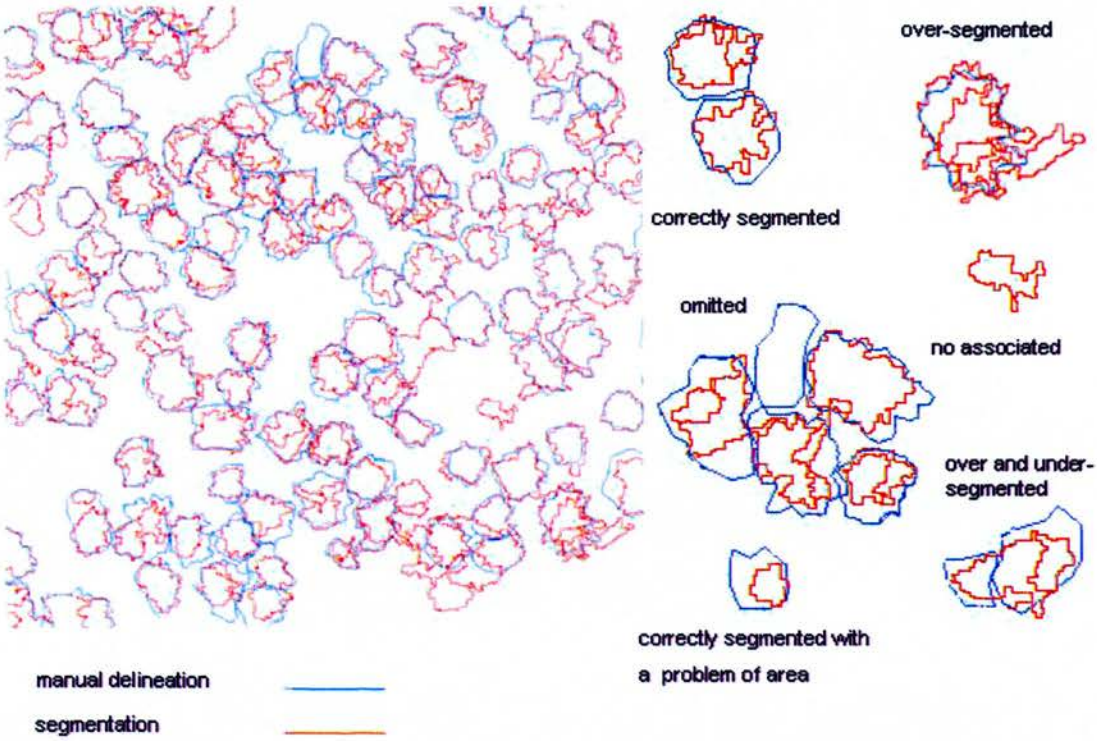

Figure 5.35: Comparison between reference crowns (manual delineation - blue) and eCognition generated crowns (red) over the European larch plot. Note the different types of overlaps observed, displayed on the right.

- Well identified tree occur when there is a one-to-one correspondence (only one segment associated with one ground delineation and viceversa), or with a tolerance of two pixels between both boundaries and with an overlap area greater than 80% of the delineated tree area.
- Over-segmented trees occur when more than one segment is associated with one ground delineation.
- Under-segmented trees indicates that a segment includes significant part (>10%) of more than one tree.

- Trees that are both over-segmented and under-segmented, which means that among the several segments associated with the ground delineation at least one is common to two or more trees.
- Trees that are well identified but with an overlap area <80% of the delineated tree area; omitted trees; and finally segments not associated with a tree (commission errors).

The results of the spatial comparison between the eCognition segmentation method and the ground reference dataset are presented in tables 5.35 to 5.39. The comparison was performed for the individual and combined datasets (aerial photography, ATM, LiDAR, aerial photography + LiDAR, ATM + LiDAR), and for the different sample plots (European larch, Norway spruce, Sessile oak, Mixed plot).

	Aerial Photography							
	European larch		**Mixed**		**Norway spr.**		**Sessile oak**	
	# trees	**%**	**# trees**	**%**	**# trees**	**%**	**# trees**	**%**
Trees correctly segmented	25	62.5	14	35	12	30	1	2.5
Trees correctly segmented with a problem of area	0	0	3	7.5	1	2.5	2	5
Trees over-segmented	12	30	8	20	14	35	8	20
Trees under-segmented	0	0	0	0	0	0	0	0
Trees over- and under-segmented	3	7.5	15	37.5	13	32.5	28	70
Trees omitted	0	0	0	0	0	0	1	2.5
Extra segments	2	5	3	7.5	3	7.5	3	7.5
Correct (segmentation +area)	25	62.5	17	42.5	13	32.5	3	7.5

Table 5.35: Comparison between eCognition extracted crowns and ground reference data for the aerial photography datasets.

	Airborne Thematic Mapper							
	European larch		**Mixed**		**Norway spr.**		**Sessile oak**	
	# trees	**%**	**# trees**	**%**	**# trees**	**%**	**# trees**	**%**
Trees correctly segmented	12	30	9	22.5	8	20	1	2.5
Trees correctly segmented with a problem of area	3	7.5	2	5	2	5	0	0
Trees over-segmented	0	0	4	10	5	12.5	0	0
Trees under-segmented	0	0	0	0	0	0	0	0
Trees over- and under-segmented	25	62.5	24	60	23	57.5	38	95
Trees omitted	0	0	1	2.5	2	5	1	2.5
Extra segments	5	12.5	7	17.5	6	15	9	22.5
Correct (segmentation +area)	15	37.5	11	27.5	10	25	1	2.5

Table 5.36: Comparison between eCognition extracted crowns and ground reference data for the ATM imagery.

	LiDAR							
	European larch		**Mixed**		**Norway spr.**		**Sessile oak**	
	# trees	**%**	**# trees**	**%**	**# trees**	**%**	**# trees**	**%**
Trees correctly segmented	18	45	10	25	7	17.5	1	2.5
Trees correctly segmented with a problem of area	6	15	0	0	3	7.5	0	0
Trees over-segmented	0	0	0	0	0	0	0	0
Trees under-segmented	0	0	0	0	0	0	0	0
Trees over- and under-segmented	14	35	29	72.5	27	67.5	37	92.5
Trees omitted	2	5	1	2.5	3	7.5	2	5
Extra segments	4	10	4	10	3	7.5	8	20
Correct (segmentation +area)	24	60	10	25	10	25	1	2.5

Table 5.37: Comparison between eCognition extracted crowns and ground reference data for the LiDAR datasets.

	Aerial Photography + LiDAR							
	European larch		**Mixed**		**Norway spr.**		**Sessile oak**	
	# trees	**%**	**# trees**	**%**	**# trees**	**%**	**# trees**	**%**
Trees correctly segmented	28	70	19	47.5	18	45	3	7.5
Trees correctly segmented with a problem of area	0	0	0	0	2	5	3	7.5
Trees over-segmented	0	0	0	0	0	0	0	0
Trees under-segmented	0	0	0	0	0	0	0	0
Trees over- and under-segmented	12	30	21	52.5	20	50	33	82.5
Trees omitted	0	0	0	0	0	0	1	2.5
Extra segments	2	5	4	10	3	7.5	5	12.5
Correct (segmentation +area)	28	70	19	47.5	20	50	6	15

Table 5.38: Comparison between eCognition extracted crowns and ground reference data for the aerial photography and LiDAR datasets combined.

	Airborne Thematic Mapper + LiDAR							
	European larch		**Mixed**		**Norway spr.**		**Sessile oak**	
	# trees	**%**	**# trees**	**%**	**# trees**	**%**	**# trees**	**%**
Trees correctly segmented	13	32.5	12	30	14	35	3	7.5
Trees correctly segmented with a problem of area	4	10	2	5	3	7.5	0	0
Trees over-segmented	0	0	0	0	0	0	0	0
Trees under-segmented	0	0	0	0	0	0	0	0
Trees over- and under-segmented	23	57.5	25	62.5	21	52.5	3	7.5
Trees omitted	0	0	1	2.5	2	5	1	2.5
Extra segments	4	10	5	12.5	6	15	10	25
Correct (segmentation +area)	17	42.5	14	35	17	42.5	3	7.5

Table 5.39: Comparison between eCognition extracted crowns and ground reference data for the ATM and LiDAR datasets combined.

Discussion of the results: Almost all ground reference crowns in each plot were identified, with most of them falling in the category of "over and under-segmented". The best match between ground reference and automatic segmentation was for the European larch plot using aerial photography with LiDAR (28 out of 40 trees were accurately delineated equivalent to 70%), followed by aerial photography (62.5%), LiDAR (60%), ATM with LiDAR (42.5%) and ATM (37.5%). The low accuracy obtained with ATM data on its own is explained by the low spatial resolution (2 m) of this dataset. Other studies for crown delineation, such as the carried out by Leckie *et al.* (2005), have reported that 50 – 60% of trees had a good match between manual and automated crown delineation, using CASI multispectral imagery of 70 cm resolution.

Good crown delineation accuracies were highly related to low density and high distances between trees in the stands. Of the plots under study, the European larch is the least dense and with a distance between trees of ± 4 m, followed by the Norway spruce and the mixed plot (European larch and Douglas fir) both of them being of medium density and with space between trees of 2 m, and finally the Sessile oak plot with the higher density and irregular spatial distribution of the trees. For example, accurate delineation reached 70% for the European larch plot where trees are well spaced and isolated but very low (15%) for the complex and dense canopy of the sessile oak plot. Also within plots where shadows or a poor contrast between understorey and overstorey exists, delineation accuracies are low.

For the sessile oak plot, a homogeneous stand with high density and trees close to each other, the accuracies were low. It was difficult to achieve good crown isolation on the oak plot mainly because of the different crown sizes which required different scales for segmentation. Thus, to isolate the smaller crowns using eCognition, it is unavoidable to over-segment the larger tree crowns. Even the isolation of tree crowns for manual delineation on the high spatial resolution aerial photographs was a difficult task.

Most of the trees were over-segmented. Considering that there were few omissions (less than 3 trees per plot), the accuracy of the classification could be assessed considering the

quantity of trees that were detected, without regard of the degree of segmentation of each crown. According to that, accuracies could be much higher as most of the trees were effectively detected (all over 90%). Omissions mainly occurred because of shadowing effects over the tree crowns. There were also some extra segments (up to 10 segments in one plot or 25%) generated usually on the borders of trees with gaps and in dark areas.

5.10 Summary

This chapter explored how well the object oriented method implemented in eCognition performed for segmentation and classification of tree crowns for diverse species and structure, using three different sources of data at various spatial and spectral resolutions. The approach used in this analysis was experimental as several combinations of values for the parameters scale, colour/shape and smoothness/compactness were investigated. It is clear that for a dataset that is being segmented and classified, the assignment of different parameter values will produce different results. The methodology for such assignment of parameter values it has not been yet standardized, which introduces a certain degree of subjectivity within the analysis. In general, small scale values and more weight for the colour parameter gave the best results. The level of optimization needed to obtain meaningful results could be considered high although sophisticated functions and tools implemented within the software not were used in their totality. The determination of the number of levels to use and the parameter values was complex and time-consuming. Different levels of aggregation were applied and the use of functions such as classification-based segmentation was useful as the software tends to the over-segmentation of the features.

In general, it was found that this method of classification, although complex in the assignment of segmentation parameters, produces results that greatly matched the ground referenced data.

Two results were analyzed with respect to the accuracies obtained: first, the accuracy assessment of the classifications for which overall values between 0.845 and 0.945 were

obtained, and second, the assessment of the match between segmented crowns and manual delineation for which accuracies ranged between 37.5% to 70%.

Best accuracies were for the European larch species in a low density plot and highly spaced trees, and lowest accuracies corresponded to the Sessile oak species in a high density plot and with less distance between trees. Shadowing between and within crowns and spectral similarities between under- and overstorey components were a major problem especially for the classification of dense plots (Norway spruce and sessile oak). This fact emphasize the data acquisition time as an important variable to consider in order to take full advantage of spatial and spectral data characteristics of the species under study and to maximize the contrast between under- and overstorey.

The spectral information from aerial photography, ATM and tree height data derived from LiDAR used as input for object oriented segmentation and fuzzy classification provides useful information for forest inventory and monitoring. The combination of LiDAR height data with multispectral imagery allowed species classification with accuracies close to those obtained using aerial photography. Crown delineation, however, was limited especially in complex canopies and high density stands where LiDAR data produced a continuous canopy where individual crowns were difficult to detect, and in which the spatial resolution of the ATM data was not sufficient to allow crown isolation.

Although the eCognition fuzzy classifications provide good results and offer a way to fully explore the increasing spatial and spectral resolution of the remote sensing techniques, its use on a daily basis within the forestry community is hampered by some disadvantages:

1. The use of the software requires highly skilled personnel.
2. Considerable effort is invested on the setting up of segmentation parameters.
3. Every dataset needs a different parameters value to be found for the segmentation process to produce meaningful results.
4. The software tends to 'over-segment' bright areas, which affects the recognition and extraction of some vegetated species.

5. The processing of large datasets, for instance a full Landsat scene, requires at least 3 hours of processing time.
6. The cost per license is high (~ £10000).

The datasets evaluated in this research for segmentation purposes correspond to even-aged, single species plots. The diversity in species, ages, sizes, and crown shapes introduced by CCF will make the segmentation and classification processes in eCognition very complex.

The comparison of the eCognition results with other segmentation packages commercially available such as Erdas Imagine, SPRING, and InfoPack, could help in the identification of a cost-effective tool.

Chapter 6

Canopy cover and light interception underneath a forest

6.1 Introduction

The forest light environment greatly affects stand regeneration, structure, and productivity. A variety of methods have been used to measure incoming radiation at different spatial and temporal scales (Englund *et al.* 2000), including hemispherical photography, spherical densiometry, and light sensors coupled to dataloggers. Light sensors are the most accurate source of light estimates beneath a forest canopy but they are expensive and endure high maintenance costs (Inoue 2004). These groun-based methods are also generally time consuming, the equipment can be expensive and cumbersome, and the measurements are dependant on the weather (Brown *et al.* 2000).

It is expected that the increase in resolution and dimensionality of remotely sensed data could help in the development of predictive models for forest dynamic that are needed for forest management. Such data could therefore provide the ecological detail missed by the other sensors and techniques (Levin 1992), for instance, the ecological relationships beneath a forest canopy. Such relationships are related spatially to the pattern of canopy gaps and sunlight penetration (Silbernagel and Moeur 2001).

Studies of canopy gaps have contributed significantly to our understanding of the role of small-scale disturbances in forest ecosystems, but have been little used by foresters for predicting ecosystem response to silvicultural systems (Coates and Burton 1997). Gap distribution and size are aspects that play a vital role within forest dynamics. Canopy gaps are a natural feature of the forest and important for the regeneration of plant species; thus, trees and gaps define the forest (van Dam 2001). The size of the gap is of particular importance, since research has shown that differences in size of gaps result in differences in species composition of the next cycle (Whitmore 1989). Gap size, position within a gap or distance from a gap edge may all be just as

important as the gap/non-gap distinction at a site location, but it is really the point-specific irradiance input or (conversely) canopy closure that is most predictive of tree growth, plant phenology, nitrogen mineralization, suitability as insect habitat and myriad other ecological processes (Coates and Burton 1997).

Although a LiDAR-based horizontal structural characterisation of forests has been carried out in several studies (Hill and Thomson 2005, Leckie *et al.* 2005, Heurich and Weinacker 2004, St. Onge and Vepakomma 2004), the description of gap sizes and their spatial distribution has been approached in more traditional ways, mainly using ground-based data such as hemispherical photography and scene simulation. Considering that the spatial structure of canopy trees is highly related to the amount of sunlight intercepted by the canopy, objective estimates of canopy openness and gap distribution can aid in the construction and interpretation of understorey light and forest dynamics models, and provide empirical knowledge of canopy structure for woodland management (Silbernagel and Moeur 2001).

6.2 Objectives

In this chapter the main objective was to investigate the potential of LiDAR for the characterization of the horizontal structure of the forest stands, and analyse its usefulness for the derivation of the light environment within each stand in the context of the Continuous Cover Forestry concept. The results were validated against hemispherical photography measurements carried out in the sample plots.

Specific objectives were:

- The assessment of the potential of LiDAR for the estimation of canopy openness.
- The analysis of the relationship between LiDAR-derived canopy openness for light interception estimation and hemispherical photography measurements by species.
- Determination of the utility of LiDAR derived light interception estimation in relation to species' climate regimes.

The proportion of canopy openness derived from the LiDAR data was compared with its corresponding values calculated from upward-looking hemispherical photography and these results were used to determine light interception. The potential of LiDAR for mapping horizontal structure of forest stands and derived light interception estimation was demonstrated and these results linked to findings about the species' climate regimes to evaluate the natural regeneration potential of the sites.

6.3 Hemispherical photography

Hemispherical photography provides an upward-looking view of all or part of the sky. Typically hemispherical images are acquired with either a standard film camera or a digital camera fitted with a hemispherical (fisheye) lens pointed upward (Hemiview User Manual 1999). After classification, hemispherical photographs provide a detailed map of sky visibility and obstruction. In turn, solar radiation regimes and canopy characteristics can be inferred from this map of sky geometry. In the case of plant canopies, a hemispherical photograph can be interpreted as a map of the directions of canopy openings relative to the location from which the photograph is taken. Commonly used estimates derived from hemispherical photography include canopy openness (VisSky), gap fraction, and gap light index. Hemispherical photography is also used for the determination of leaf area index (LAI) at high sampling rates or for large areas through the measurement of the gap fraction (van Gardingen *et al.* 1999). The relationship between canopy openness and LAI is logarithmic, so small differences in low levels of VisSky will produce large differences in LAI.

Although hemispherical photography is one of the most precise methods, as with other remote sensing techniques there are a number of problems associated with it. The most significant problem is that it does not consider light transmission and reflection from leaves or layers of leaves (Roxburgh and Kelly 1995). The technique assumes that all and any leaves completely block the passage of light. Reflection and transmission may also be affected by leaf orientation relative to sun angle. In the digitised image, canopy areas are assigned to either black (completely blocked) or white (clear sky). This may introduce errors in darker areas where a significant proportion of the total light arrives via reflection or partial transmission through a

complete canopy layer. Hemispherical systems also assume that the canopy above the photograph is a single layer. Usually, these problems do not introduce unacceptable errors; therefore hemispherical photography is a useful technique for measuring percentage canopy openness, gap formation and closure, and other physical properties of plant canopies. Indirect measurements of the light environment can be compared against direct measurements using light sensors coupled to dataloggers which give the most accurate measures.

Other disadvantages in the use of hemispherical photography lie in the difficulty to maintain the equipment in good working order during prolonged field use. The camera, lens, computer and image analysis software that are required are also expensive. At present, image processing and analysis are time consuming and rapid assessments of understorey illumination at a large number of points are not possible. Hence the necessity to explore alternative techniques such as LiDAR, which may allow a more rapid and spatially extensive acquisition of information about light interception.

6.3.1 Hemispherical photography acquisition

A total of 48 hemispherical photographs were taken at 16 sample points selected randomly within the plots (4 sample locations per plot, 8 pictures per plot), using a digitally operated camera Coolpix 995 (Nikon Corporation, Tokyo, Japan) with an exclusive fish-eye lens. The acquisition of hemispherical pictures was carried out in May 2003 on still and overcast days because it was the predominant sky condition of the area and also due to the difficulties in determining vegetation edges in photographs taken on sunny days or under skies with patchy clouds. It was assumed that canopy openings did not change significantly between the time of acquisition of LiDAR data (September 2002) and the acquisition of the hemispherical photography.

Camera and lens were placed on a tripod at 1.3 m above the ground. The camera was oriented north and levelled each time that a photograph was taken. At each sampling point in the forest, 2 pictures were taken: one with exposure compensation zero and the other with this value set to -1. For all plots, the underexposed picture always

showed the most detail and greatest contrast and, as such, was used for further processing (figure 6.1).

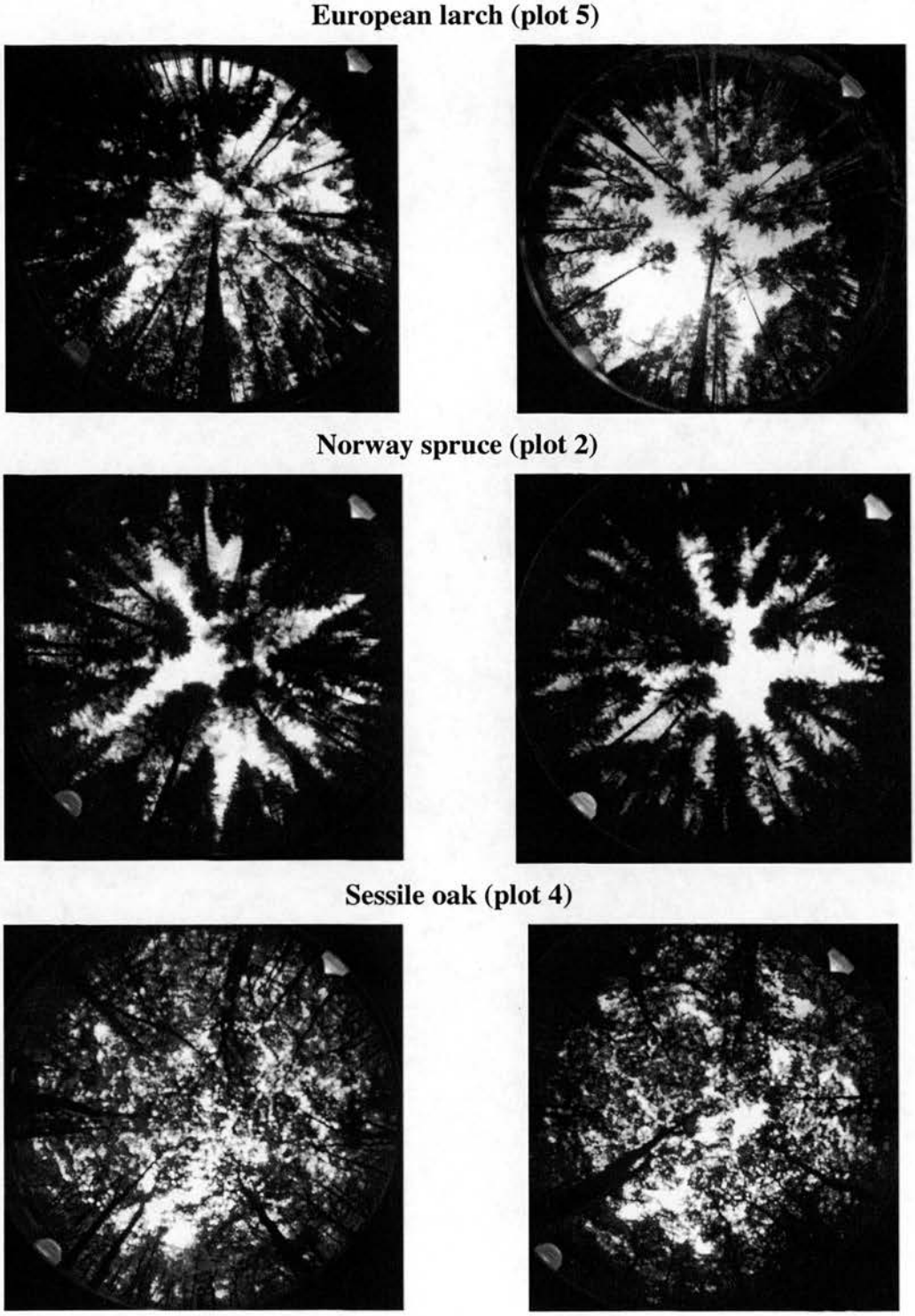

Figure 6.1: Hemispherical pictures of the three species analyzed. The figure shows two randomly selected pictures of each species which were taken above the understorey at 1.3 m from the ground.

6.3.2 Hemispherical photography processing

The hemispherical photographs in digital format were processed using the HEMIVIEW 2.1 software package (Delta-T Devices, UK). The analysis with this software required a number of stages. First, a lens correction function was applied to remove lens distortions and the image was then classified into visible and obscured sky elements. This classification was undertaken using an interactive brightness threshold, which allowed the development of a sky/non-sky mask on the computer screen.

The threshold to classify pixels into 'sky' and 'canopy' was set separately for each photograph. When a suitable threshold value was established, the following Hemiview variables were calculated, using the 'uniform overcast sky' setting (Steven and Unsworth 1980): canopy openness (VisSky, i.e. the proportion of the image not obstructed by canopy); indirect site factor (ISF, or the proportion of diffuse radiation transmitted through the canopy); direct site factor (DSF, or the proportion of direct beam radiation transmitted through the canopy); and Global site factor (GSF, or total transmittance through the canopy). Values for the VisSky parameter range from 0 to 1, with 0 representing complete sky obstruction, and 1 representing open sky.

Most studies have used an interactive thresholding of hemispherical photography (e.g. Machado and Reich 1999; Englund *et al.* 2000; Frazer *et al.* 2001; Hale 2001, 2003; Hale and Edwards 2002). However, it is known that this method introduces bias as the interactive thresholding depends on the observers' subjectivity (Englund *et al.* 2000). To reduce this subjectivity, the calculations were undertaken separately on all photographs on two occasions over different weeks. Regression of the two sets of measurements confirmed the high degree of consistency between them ($R^2 = 0.99$); therefore, one set of measurements was used for the subsequent calculations. These values of canopy openness derived from the hemispherical photography (table 6.1) were also used as the standard against which the LiDAR assessment method was compared.

Label	VisSky	ISF	DSF	GSF
hemis1_oak1	0.223	0.314	0.285	0.302
hemis2_oak1	0.215	0.311	0.181	0.257
hemis3_oak1	0.150	0.230	0.150	0.197
hemis4_oak1	0.160	0.228	0.259	0.241
hemis5_oak2	0.175	0.251	0.235	0.244
hemis6_oak2	0.147	0.212	0.142	0.183
hemis7_oak2	0.148	0.212	0.241	0.224
hemis8_oak2	0.146	0.214	0.222	0.217
hemis9_ns1	0.134	0.195	0.173	0.186
hemis10_ns1	0.155	0.250	0.183	0.222
hemis11_ns1	0.156	0.244	0.169	0.213
hemis12_ns1	0.148	0.212	0.241	0.224
hemis13_ns2	0.185	0.253	0.284	0.266
hemis14_ns2	0.165	0.253	0.321	0.281
hemis15_ns2	0.165	0.250	0.078	0.178
hemis16_ns2	0.173	0.246	0.278	0.259
hemis17_el1	0.185	0.297	0.120	0.223
hemis18_el1	0.226	0.294	0.311	0.301
hemis19_el1	0.173	0.213	0.212	0.212
hemis20_el1	0.219	0.307	0.337	0.319
hemis21_el2	0.190	0.276	0.182	0.237
hemis22_el2	0.269	0.385	0.459	0.416
hemis23_el2	0.277	0.384	0.503	0.433
hemis24_el2	0.260	0.357	0.382	0.367

Table 6.1: Variables obtained from the analysis of the hemispherical photography for the measurements made within each plot. VisSky represents the canopy openness, ISF (Indirect Site Factor), DSF (Direct Site Factor), and GSF (Global Site Factor).

6.4 LiDAR-derived canopy openness

In contrast to canopy cover, canopy openness is defined as the proportion of the sky hemisphere that is not obscured by vegetation when viewed from a single point (Jennings, Brown & Sheil 1999). Canopy openness can be measured using hemispherical photographs (Rich 1990). In order to assess the capacity of LiDAR to estimate canopy openness of three contrasting forest species and stand densities, one variable of the laser pulse measurements was evaluated. This variable corresponds to

the percentage of ground hits. In contrast, percentage of canopy hits has been found to be the best estimator of canopy cover (Ritchie et al. 1992), so it was expected that the inverse variable matched the indirect measurements of canopy openness.

Most studies attribute the error in the estimation of canopy cover to poor georeferencing between ground-based measurements and acquired remotely sensed data. In this study, validations of the corresponding locations of hemispherical photography acquisitions within the LiDAR datasets were performed for average plot measurements. This study explored the relationship between the information extracted from LiDAR data and canopy openness estimated from each hemispherical photograph, georeferenced within decimetres, therefore reducing the errors due to mis-registration.

To begin with the LiDAR estimations, the radius covered by the hemispherical picture at a determined height has to be calculated in order to extract LiDAR returns in the surroundings of the hemispherical picture acquisition point. Although hemispherical photograph variables can be measured at several zenith angles, it is considered that the zenith angle of approximately 57.3° provides robust estimates as this angle is nearly independent of the inclination angles from the canopy elements (Jonckheere *et al.* 2005). The percentage of ground hits in the vicinities of each of the hemispherical picture acquisitions was calculated assuming that all laser pulses with a height of <3m were understorey and ground hits. The radius covered by the photograph at a particular height is tan(57.3°) * height, which gives a radius of influence of approximately 5 m for a 3 m height. The total of ground hits was then divided between the total laser hits within the radius considered. Table 6.2 shows the ground hit percentage values per sample point compared to the VisSky data obtained from the hemispherical photography.

Label	VisSky	Ground hits (%)
hemis1_oak1	0.223	32.4
hemis2_oak1	0.215	26.2
hemis3_oak1	0.150	18.7
hemis4_oak1	0.160	15.6
hemis5_oak2	0.175	24.1
hemis6_oak2	0.147	18.5
hemis7_oak2	0.148	16.4
hemis8_oak2	0.146	17.8
hemis9_ns1	0.134	16.9
hemis10_ns1	0.155	18.3
hemis11_ns1	0.156	19.3
hemis12_ns1	0.148	17.5
hemis13_ns2	0.185	17.2
hemis14_ns2	0.165	18.4
hemis15_ns2	0.165	19.6
hemis16_ns2	0.173	19.8
hemis17_el1	0.185	19.7
hemis18_el1	0.226	24.1
hemis19_el1	0.173	19.0
hemis20_el1	0.219	22.2
hemis21_el2	0.190	23.4
hemis22_el2	0.269	28.8
hemis23_el2	0.277	30.2
hemis24_el2	0.260	29.5

Table 6.2: Comparison of VisSky canopy openness measurements obtained from the hemispherical photography compared to percentage ground hit information obtained from the LiDAR data.

The following graphs show typical examples of the distribution of total LiDAR hits in the surroundings of the hemispherical photography acquisition points for each species.

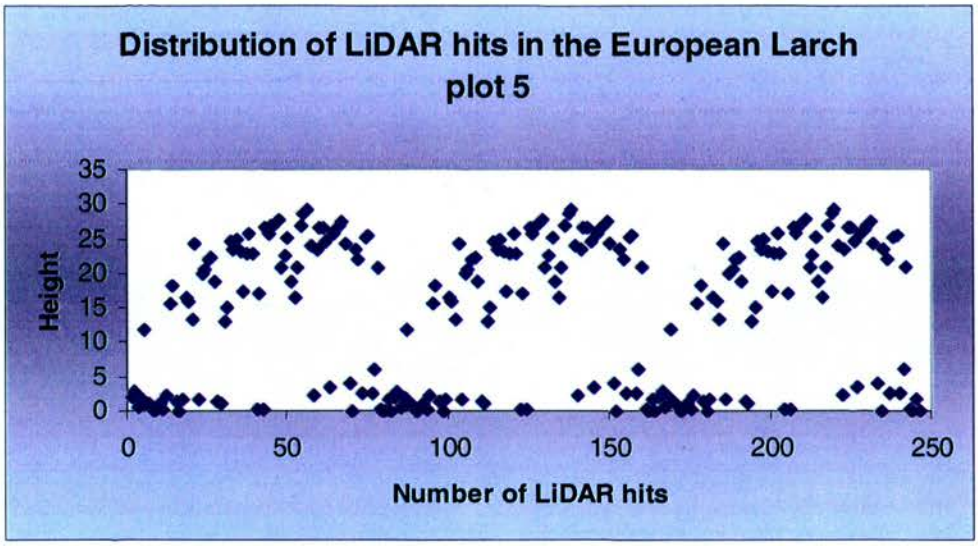

Figure 6.2: Two-dimensional distribution of LiDAR hits within a 5 m radius of the hemispherical photography acquisition point, for European Larch plot 5.

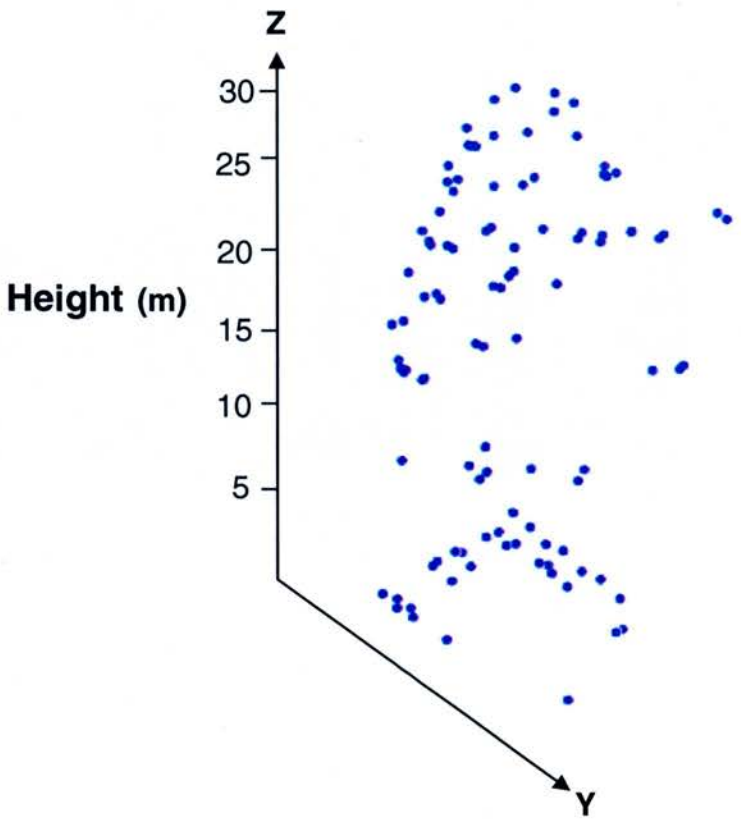

Figure 6.3: Three-dimensional distribution of laser hits for the European larch species for a section of the data shown in figure 6.2.

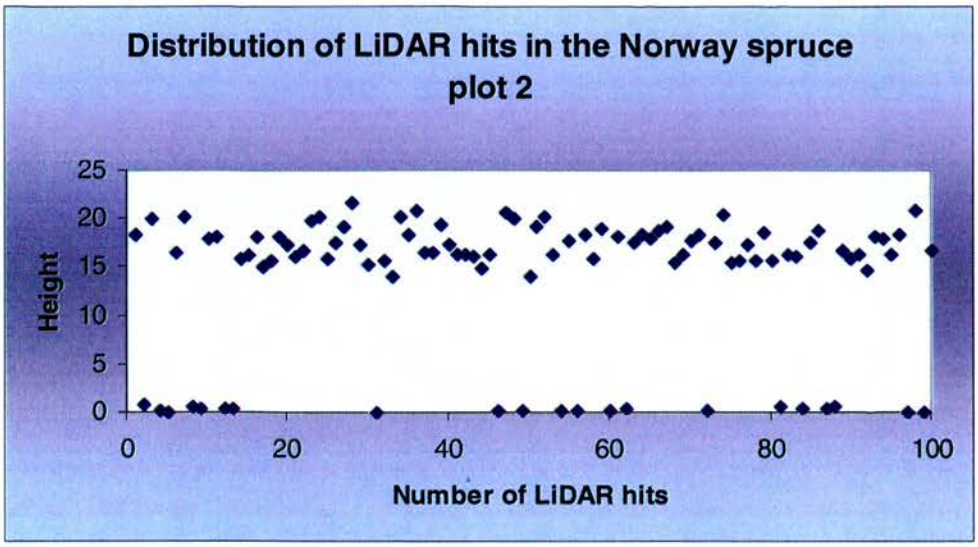

Figure 6.4: Two-dimensional distribution of LiDAR hits within a 5 m radius of the hemispherical photography acquisition point for Norway spruce plot 2.

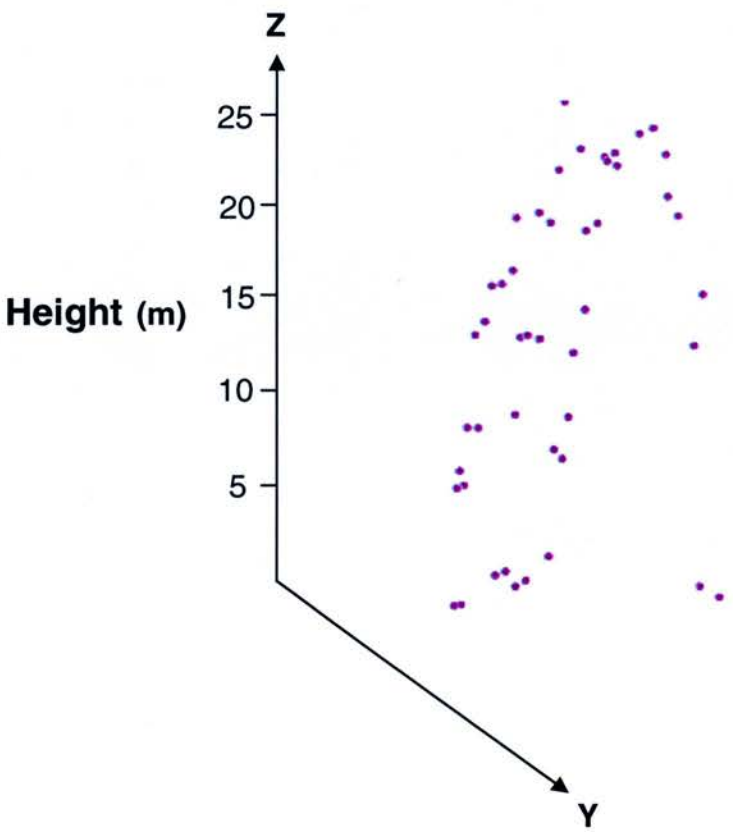

Figure 6.5: Three-dimensional distribution of laser hits for the Norway spruce species for a section of the data shown in figure 6.4.

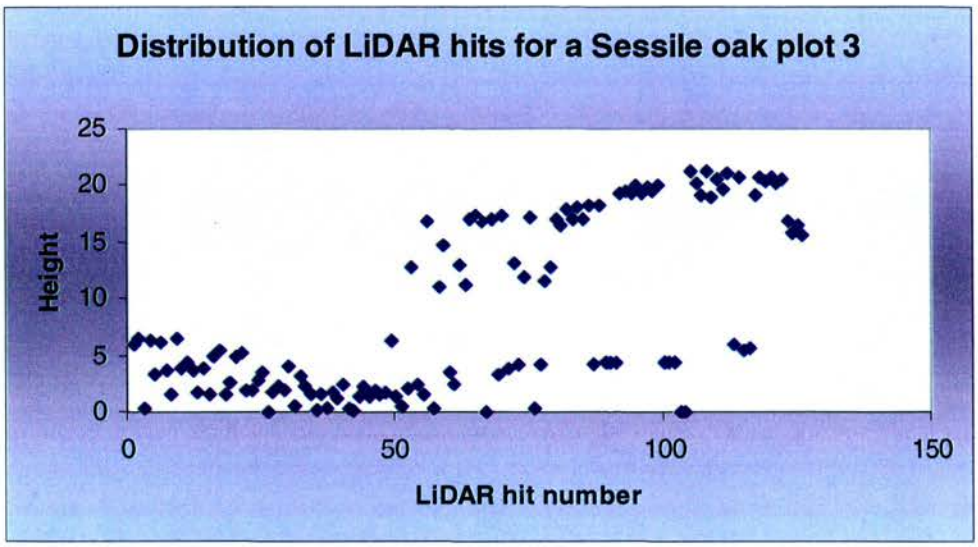

Figure 6.6: Two-dimensional distribution of LiDAR hits within a 5 m radius of the hemispherical photography acquisition point for Sessile oak plot 3.

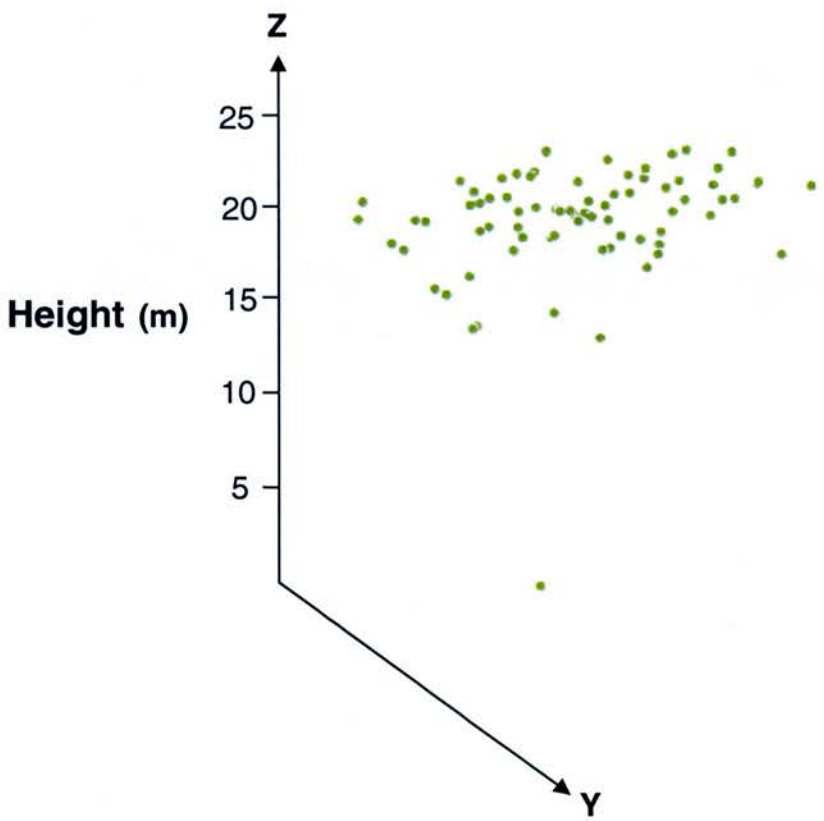

Figure 6.7: Three-dimensional distribution of laser hits for the Sessile oak species for a section of the data shown in figure 6.6.

The high correlation between VisSky and LiDAR percentage of ground hits for the species combined suggests that light environment in forested canopies can generally be predicted (figure 6.8).

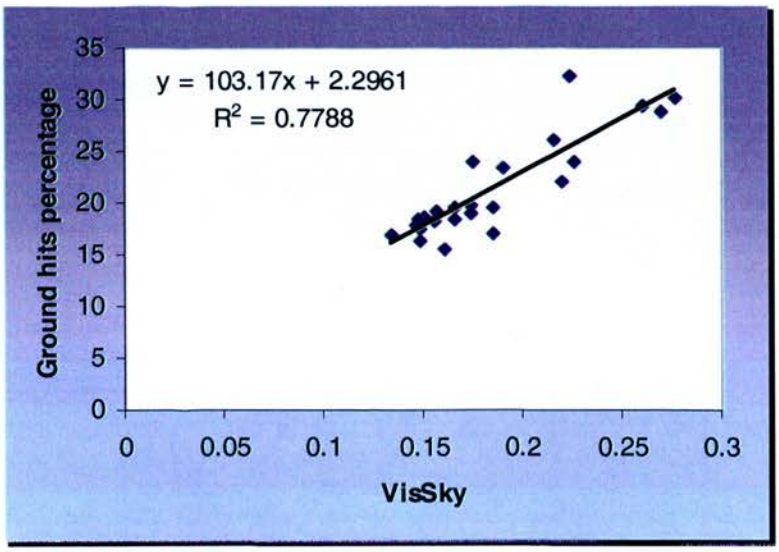

Figure 6.8: Correlation between ground hits percentage and VisSky for all the data in table 6.2.

Canopies with low transmittance have associated low canopy openness. Canopy openness can therefore be used as a light environment estimator. It is expected that the probability of light transmittance will vary as a function of vegetation density. Specifically, the probability of light transmittance is expected to be high where canopy gaps are present and low where vegetation density is high (Todd *et al.* 2003).

The relationships between the LiDAR derived estimates of canopy openness and VisSky estimates were examined for each forest type (figure 6.9).

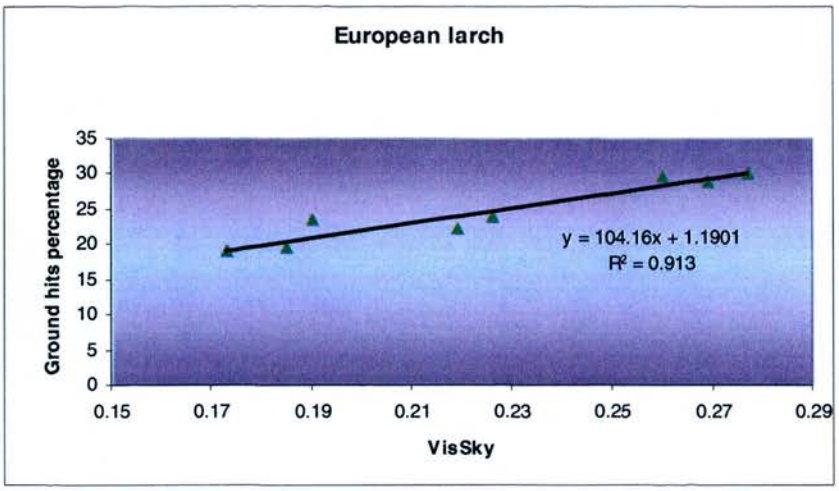

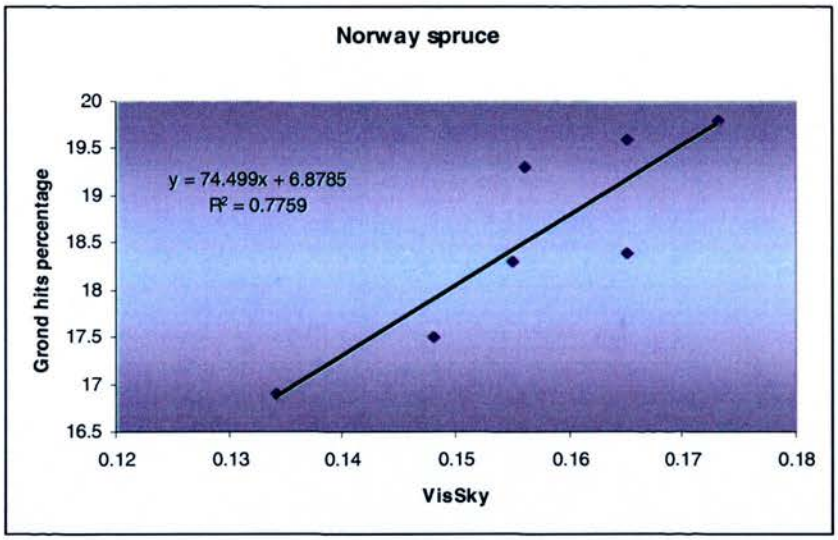

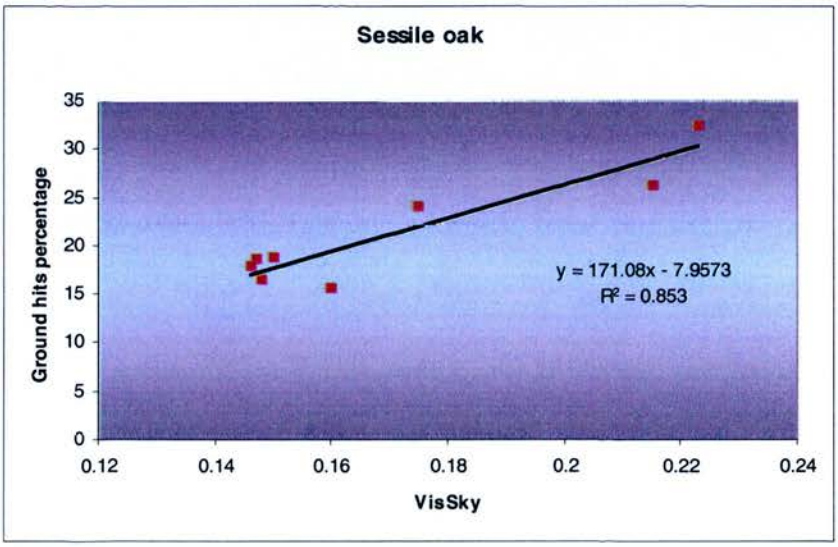

Figure 6.9: Correlation between LiDAR ground hits percentage and VisSky for European larch, Norway spruce, and Sessile oak species, respectively.

Overall, European larch species showed the strongest relationship among the three species investigated. This might be explained by the fact that these plots had the lowest stand density and larger distance between trees which gave not only a generally more open canopy but which also allowed a better laser pulse penetration.

Sessile oak species also showed a good agreement but with a somewhat bimodal distribution of data points. The poorer estimation in the Norway spruce plots was probably due to the larger foliage and branch clumping of this species in comparison with the others and the lower range of canopy openness values found.

Correlations between LiDAR ground hits percentage and Indirect Site Factor showed also good agreement (figure 6.10). In contrast, poor correlations were found with Direct Site factor (figure 6.11) and Global Site Factor (figure 6.12) suggesting that ground hits percentage is not as good an estimator of these canopy variables.

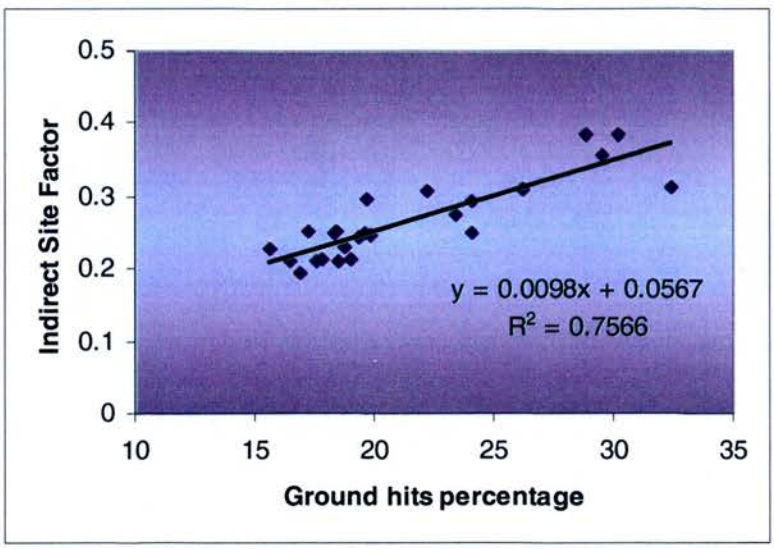

Figure 6.10: Correlation between ground hits percentage and Indirect Site factor for the three species.

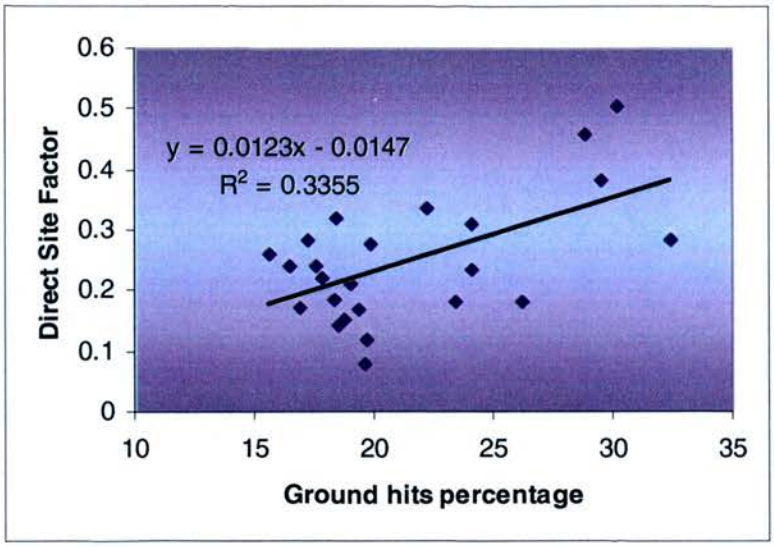

Figure 6.11: Correlation between ground hits percentage and Direct Site factor for the three species.

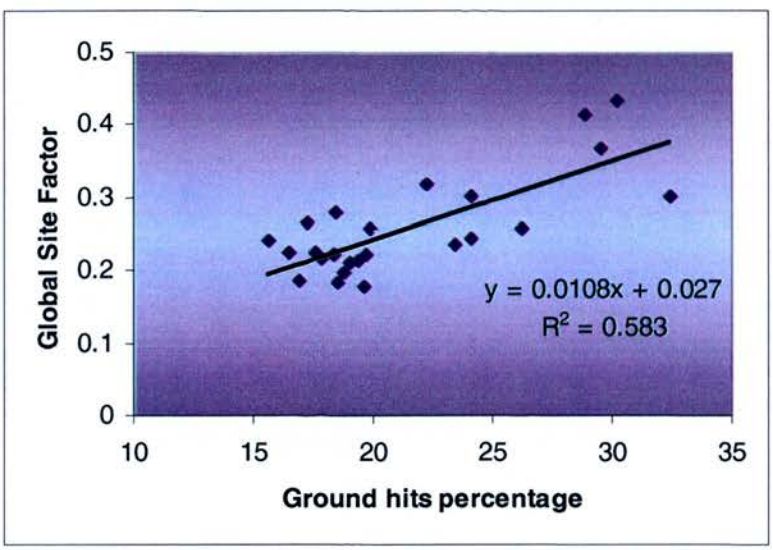

Figure 6.12: Correlation between ground hits percentage and Global Site factor for the three species.

6.5 LiDAR-derived canopy cover

Forest canopy cover, frequently defined as the percent area occupied by the vertical projection of tree crowns, is a commonly used concept in forestry and of wide interest in both scientific studies and political decisions. Other synonymous terms often used include canopy closure, crown closure or crown cover; however, there is no commonly accepted precise definition for the concept.

Nowak *et al.* (1996) reviewed four different methods that can be used to estimate tree cover from aerial imagery: Visual (ocular) estimation; dot grid method; line intercept or transect method; and digital image analysis methods. Of these, the dot grid and digital image analysis methods are probably the most useful for many forestry purposes.

The dot grid estimation method is an easy, accurate, and relatively rapid way for the determination of canopy cover (Carreiras *et al.* 2006). A dot grid is simply a set of dots, symbols, or intersecting grid lines that is superimposed over an image (figure 6.13). Tree canopy cover is estimated by counting the number of dots that that fall on tree crowns compared with the total number of dots in the area sampled. Tree canopy cover can then be calculated from the following formula:

% canopy cover = 100 x (dots falling on tree canopy/total number of dots within sampled area)

This method was carried out to evaluate comparisons of canopy cover estimated from LiDAR imagery and from aerial photography, due to the fact that the method is simple and frequently used.

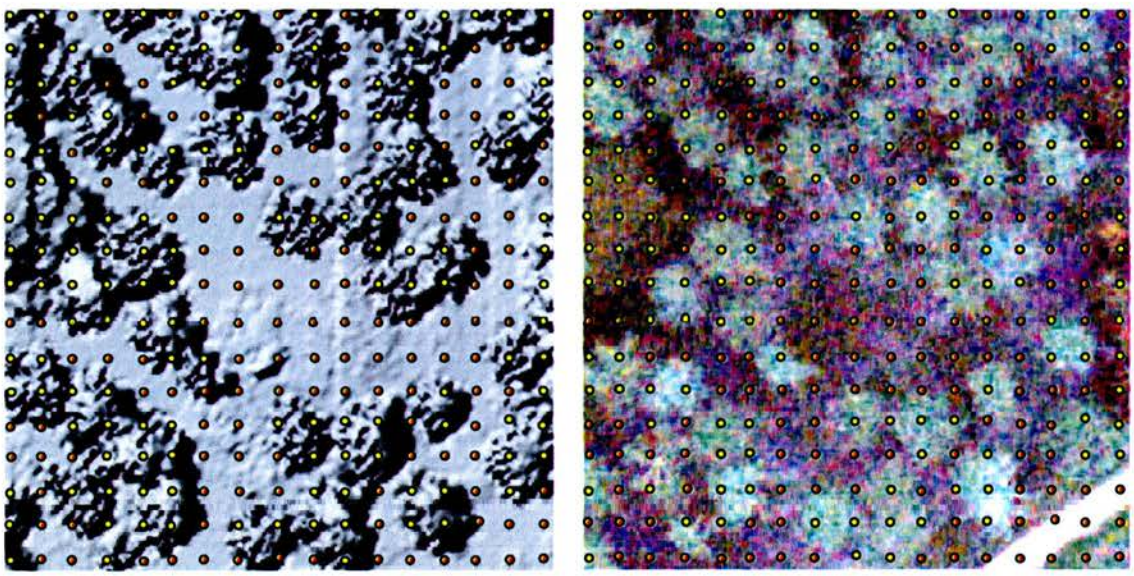

Figure 6.13: LiDAR derived DCM and corresponding aerial photograph of European larch sample plot 5 with overlaid grid used for conventional canopy cover calculation. Yellow dots represent grid points overlaid on tree crowns and red dots grid points overlaid on the understorey.

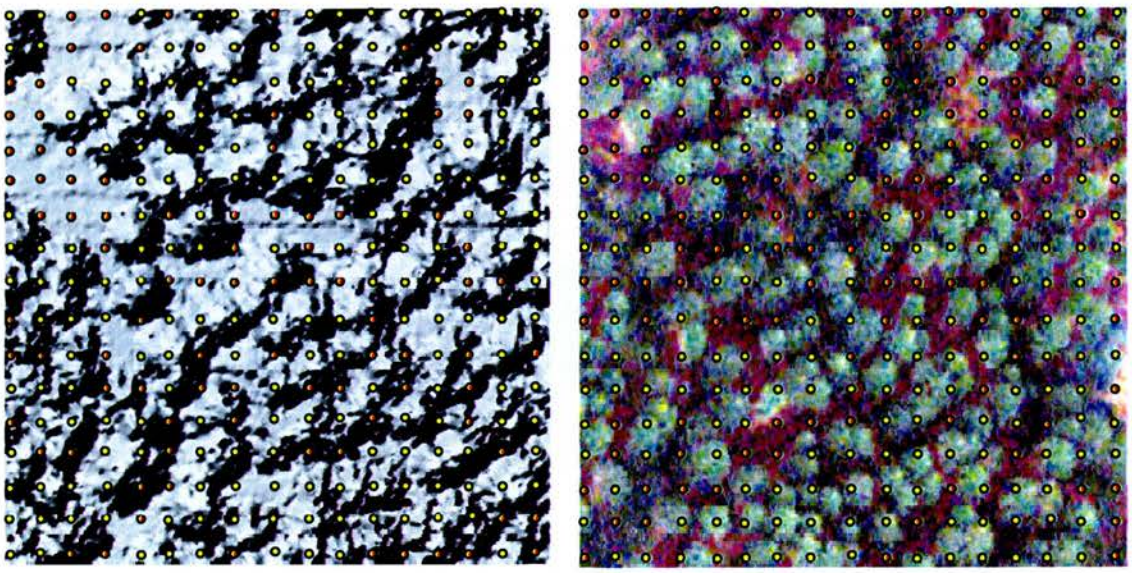

Figure 6.14: Lidar derived DCM and corresponding aerial photograph of Norway spruce sample plot 2 with overlaid grid used for canopy cover calculation. Yellow dots represent grid points overlaid on tree crowns and red dots grid points overlaid on the understorey.

The results of these calculations showed a high level of agreement between the methods (table 6.3). The maximum differences found were for Norway spruce (6.6%) and the minimum for European larch (5.1%). The results suggest that LiDAR data can be used to calculate canopy cover for typical UK species with similar accuracies.

	Canopy Cover estimations (%)	
Sample plot	**LiDAR**	**Aerial Photography**
European larch	50.8	45.7
Mixed species	82.4	76.1
Norway spruce	68.9	62.3
Sessile oak	91.7	85.2

Table 6.3: Comparison between canopy cover estimations obtained from aerial photography and LiDAR imagery for four different sample plots, using the dot grid method.

Digital image analysis techniques were also evaluated. As a result of the eCognition segmentation performed with the objective of crown detection and delineation (chapter 5), segments classified as trees and gaps were stored along with their area

size. Therefore, the sum of the area of the classified tree segments divided by the total plot area is equivalent to the canopy cover percentage. Similarly, the addition of the area of the gap classified segments divided by the total plot area represents canopy openness.

The canopy cover and canopy openness estimates obtained from both LiDAR-derived imagery and aerial photography are given in table 6.4. Again, the two methods are in close agreement.

Sample	LiDAR		Aerial Photography	
plot	Canopy Cover	Canopy Openness	Canopy Cover	Canopy Openness
Plot 1 Norway sp	65.5	22.7	68.7	25.3
Plot 2 Norway sp	70.3	23.3	72.5	19.4
Plot 3 Sessile oak	82.2	16.8	86.1	10.6
Plot 4 Sessile oak	83.6	14.9	89.5	8.2
Plot 5 European l	53.5	32.7	49.2	35.6
Plot 6 European l	76.4	22.3	81.4	17.2

Table 6.4: Comparison between canopy cover and canopy openness estimations obtained from aerial photography and lidar imagery for all sample plots, using the object-oriented classification method.

The comparison shows that LiDAR has the potential to provide accurate estimates of canopy cover and canopy openness, but that errors can still influence the results due to misclassification in both methods. In the case of the classification of the LiDAR segments through the object-oriented method, shadowed segments corresponding to trees were often misclassified. On other occasions, for instance during the segmentation and classification of the Sessile oak species, shadowed tree segments with reflectance values similar to those of gaps were often classified as the latter class, leading to a larger canopy openness value for these plots, in comparison to the results obtained using aerial photography.

This study demonstrates that LiDAR is capable of detecting gaps that occur naturally within the stand or as a result of the inter-tree distance, which are vital for light penetration. Given that CCF is a silvicultural system that aims for the use of natural regeneration as its main restocking method, the consideration of this technique to

assess the light environment under a forest canopy in an extensive and reliable way is an important one. Furthermore, this assessment can be linked to other decision support tools to allow, for instance, the exploration of the impact of different stand management regimes (Hale *et al.* 2004).

6.6 Discussion of the results

As a predictive tool, small-footprint LiDAR can be used to obtain accurate information on the horizontal characterization of forest structure and light transmittance within forest canopies, specifically for the prediction and monitoring of the VisSky variable which is an important indicator of light environment.

Differences in canopy structure and organization likely affect the variability of ground penetration of laser hits and also the variability of depths to which light from different angles can penetrate. Although there was a significant difference in the light conditions between the plots analyzed, relationships between regeneration occurrence and light environment could not be established due to the effect of other variables on natural regeneration such as vegetation competition and browsing. It is known that the increase in light penetration results in the thickness of the herb layer and the consequent reduction in germination success. In contrast, poor light penetration levels inhibit the production and growth of seedlings. As was reported in chapter two, the presence of regeneration was confirmed in only two plots, one of European larch species and the other of the Norway spruce species.

The main advantage of the use of the digital image analysis approach lies in the creation of permanent maps of tree canopy characterization that may be incorporated into a GIS and/or used to show how and where tree canopy characteristics change over time. The use of the LiDAR technique could provide estimations of canopy openness that could be associated with light penetration for the monitoring of minimum light requirements for the forest species. Manson *et al.* (2004) found that for conifer species, minimum light requirements increased from 10 to 30 per cent of full light with decreasing shade tolerance. They reported a clear trend in all species for the seedlings to be found in open conditions and for growth and survival to decline

progressively from wide towards narrow spacings (i.e. from higher to lower light levels).

Although the use of LiDAR data has great advantages it also has some limitations. The analysis carried out in this project has been developed on relatively small sample plots instead of the entire forest stand, thus sampling errors can still be important. Additional research may therefore consider applying the methodology of this study over larger spatial extents with variations in topography. This study has also been carried out on relatively uniform forest types so further research is necessary to consider areas with other and more variable vegetation cover. These studies are challenging as they will have to consider the effect of multiple species and multiple canopy architectures.

Future research will also probably make use of fine spatial resolution derived from LiDAR sensors with greater data densities. The detailed information within the LiDAR height profiles may also allow vegetation clumping and the size and distribution of canopy gaps to be evaluated. Recent studies on light dynamics within forests have focused on the spatial location and size of gaps within forest canopies (Chen *et al.*, 1997, Canham *et al.*, 1999). These studies have suggested that measures of vegetation clumping will provide greater accuracy in predictions of light transmittance within closed-forest environments. By characterizing the spatial distribution of vegetation clumping and indirect paths of light penetration through geometrical optical modelling, greater correspondence may be obtained between fine spatial resolution predictions of forest structure from LiDAR.

Chapter 7

Conclusions and recommendations

7.1 Introduction

Several remote sensing techniques have been explored in this work with the objective of gaining an understanding of their potential utility for the retrieval of forest parameters in general and particularly for the description of the structural attributes of stands composed by up to four species (Sitka spruce, Norway spruce, European Larch, Sessile oak) typically grown in the Scotland's managed forest. Specific stands of these species were chosen for study as some were being managed or in transition to the continuous cover silvicultural system and were expected to yield results relevant to ascertain the potential benefits of remote sensing methods for monitoring stands under full CCF management.

The remote sensing techniques investigated ranged from both airborne and satellite based passive optical remote sensing methods (aerial photography, ATM and Landsat ETM+ data) to active LiDAR techniques. The inclusion of the vertical dimension for the retrieval of forest structure, which is traditionally provided by field sampling, was possible thanks to the use of the LiDAR technology, which, along with the broad spatial coverage afforded by the other techniques, particularly aerial photography, provided a detailed and reliable characterization of forest stands.

Through a number of related studies on the above datasets this project is the first to investigate the utility of remote sensing methods for monitoring forests in transition to, and managed under the continuous cover forestry system in the UK context. Specific studies focussed on:

7.2 The influence of seasonal change on surface reflectance properties of common forest species

Despite the extremely large body of literature that exists which has focussed on exploring the relationship between key forest parameters and optical reflectance properties, there are very few studies which have explored the influence of seasonal phenologically related changes in reflectance on the relationships derived. This study sought to investigate variations in seasonal reflectance from common UK forest species using a temporal sequence of moderate resolution Landsat TM datasets over Aberfoyle obtained during 2000 and 2001. Such knowledge can also contribute to improved methods of forest classification, where knowledge of different species phenologies could be utilised and to an understanding of the influence of seasonal change on change detection if images are acquired at different times of the year.

Despite only a range of cloud free scenes being available, the results of the study indicated that the Landsat ETM+ data used in this study, once suitably processed, were sensitive enough to track the general vegetation phenology trajectory of deciduous forest species in Aberfoyle and that these were different from evergreen coniferous canopy types. Coniferous species showed generally similar spectral behaviours between them suggesting that other methods are required to further differentiate, and so classify them to species level.

Full utilization of phenological changes would require that the development of any canopy could be followed through the year, and that imagery would be available at the right times. This study has highlighted that the latter requirement may be difficult to achieve in high latitudes where the number of useable images may be limited due to cloud cover. The influence of changing sun angle on the responses observed also warrants further investigation. However, other research has highlighted that spectral contributions of the understorey may significantly alter the signal received from the overstorey, particularly at certain times of the year. This has direct consequences for CCF because the opening-up of canopies will be required to allow for regeneration to be successful in Scottish managed forests, especially for shade intolerant species such as Sessile oak. For the use of single images, a period when there is maximum spectral contrast between the overstorey and the understorey should be selected for the image

acquisition, as it appears clear that the understorey effect will increase as overstorey density decreases.

Despite warranting further investigation, the overall results of the phenological study showed that image acquisition date can significantly affect the spectral response observed in certain forest species which may impact the spectral values retrieved from ETM+ imagery and any subsequent estimation of biophysical parameters. Thus, image acquisition dates need to be carefully selected to ensure maximum information content in remotely sensed data. Further work is required to define an optimum approach to discriminate between spruce species (e.g. Sitka spruce and Norway spruce) where spectral responses are very similar and of the utility of different indices and methods to investigate the phenological response.

7.3 LiDAR data for the estimation of tree height

Within the CCF context and within the UK forest scenario in general, there is a lack of studies exploring the potential of LiDAR data for species characterization and estimation of plant structural attributes. In this study, multi-return, high density (4 hits per square metre) LiDAR data was assessed for its ability to determine tree heights and for the production of a Digital Canopy Model (DCM) for tree crowns for subsequent tree crown delineation. The research was hampered by the availability of software tools for the processing of such data; in order to proceed, relatively straightforward but effective algorithms for processing the data were required to be written. Despite the simplicity of the tools developed to generate the ground DTMs and DCMs, they were shown to produce accuracies similar to the reported in other works with the use of more sophisticated algorithms. Further development in LiDAR processing tools is clearly required as are their general widespread availability.

Although this is one of a few studies to test LiDAR methods in the context of forestry in the UK, the retrieval of tree height proved to be highly successful for the three species selected for study covering a range of different canopy types and light regimes. The method was also able to map accurately the differences between plots to identify tree density, gaps, topography, and most importantly, to provide high-

resolution imagery for crown and gap delineation with considerable detail and accuracy. This has significant implications for forest management under the Continuous Cover Forestry regime, where the diversity of species and heights calls for intensive forest inventory and where LiDAR shows considerable potential.

The selection of the season within which to conduct LiDAR surveys is also an important one; dense ground vegetation and leaf-on conditions make it difficult to detect the ground surface. Leaf-off conditions are desired if a "bald-earth" DEM is the main purpose of a LIDAR survey. However, winter acquisitions may present the problem of variable snow depth. Thus the spring and autumn time periods may present the best periods for optimum LiDAR data acquisition. Of these periods, spring has the added benefit of reduced shrub and understorey vegetation height as a result of possible flattening by the winter snow pack (Webster 2005).

7.4 Estimation of forest structural attributes from a range of RS methods

Comparisons among estimates of forest structural variables derived from remote sensing to measurements obtained in the field (large tree maximum canopy height, mean canopy height, and canopy openness) were carried out. The information from LiDAR, ATM, and aerial photography were combined in an attempt to improve the accuracy of the estimates. The results of the study indicated that LiDAR is the best single data type for estimating canopy height and for the retrieval of individual tree crowns. The addition of ATM data improved estimates either only marginally or not at all. The combination of LiDAR and aerial photography yielded the most accurate results, where it was evident that LiDAR data needs to be combined with high spatial resolution optical sensor data to compensate for lack of fine texture information in the LiDAR data.

The integration of spectral information from aerial photography and canopy height data from LiDAR into an object-oriented classification produced highly meaningful results for the forested environment under study. The resultant thematic classes contained information on species composition and structure, which, when combined with additional information, could reflect the underlying processes of vegetation succession and woodland management. Results showed that the final result of crown

detection could have good accuracy (between 0.84% and 0.94%) for broadleaves and coniferous species. Crown delineation accuracies, in comparison with manually delineated crowns from aerial photography, decreased mainly due to over-segmentation of larger crowns.

7.5 Estimates of canopy openness and light environment from RS data

The production of information about canopy gaps is important for CCF objectives where stand density and light transmittance are key variables in the conversion of the even-aged stand to a CCF silvicultural system. This project has shown that LiDAR data can be used to produce high-resolution maps of canopy cover/canopy openness since a good correlation was found with parameters retrieved from hemispherical photography ($r = 0.78$). The differences between ground-based estimations of canopy properties and LiDAR estimations could be attributed, at least in part, to the different point and angle of view of the hemispherical photography versus the LiDAR data. Hemispherical photography registers the canopy from a ground point looking upwards, whereas LiDAR scans the canopy from above. Therefore, there were areas seen in the hemispherical photographs, but obscured in the Lidar data, and vice versa. In addition, LiDAR results highly depend of the density of the measurements and on the transformations performed on the data, so departures from ground measurements were expected. This study indicates that each forest species has a unique laser penetration rate.

As a predictive tool, small-footprint LiDAR can thus be used to obtain information on the horizontal characterization of forest structure and light transmittance within forest canopies. The maps produced from such data could be used in the process of scaling up variables related to light environment from the point or local scale to the larger scale.

7.6 Overall conclusions

The results of this research, which focused in the evaluation of the potential of several remote sensing techniques for the retrieval of information of value to managing the

transition from traditional forest silvicultural systems to CCF, have highlighted the following aspects:

- Phenologically-induced seasonal responses in reflectance from vegetation canopies may significantly affect the ability to retrieve forest structural attributes from optical remotely sensed data, particularly for deciduous forest species. Under Continuous Cover Forestry, the role of contributions from the understorey in contributing to seasonal reflectance may be significant but required further investigation. The band in which spectral discrimination amongst all the species was best appeared to be near infrared band 4 and the date of imagery that showed a maximum contrast among spectral reflectances was the July 2000 image. However, no single date was considered ideal for discrimination of the four species which suggests that optimal differentiation between the species will be achieved using a combination of two or three datasets covering their phenological cycles.

- LiDAR data has the potential to play a key role in forest inventory under CCF through its capabilities to produce high-resolution imagery for tree height, crown and gap delineation with considerable detail and accuracy.

- The accuracies of estimates of canopy variables and for species recognition for stands under CCF will be optimally derived using a combination of LiDAR and very high spatial resolution optical remote sensing techniques. Digital photography may suffice as the optical tool where textural content, as opposed to spectral information may be the key information required.

- LiDAR data can be used to accurately monitor the light environment across CCF. The use of LiDAR in combination with other high resolution optical remote sensing product is desirable as it takes advantage of high vertical resolution from LiDAR and spectral/spatial resolution from other dataset, for instance, aerial photography.

- The use of object oriented approaches for segmentation and classification of forest stands proved to be successful for relatively homogeneous stands with

low to medium density. The application of this approach could be useful for monitoring the transition of even-aged stands to CCF. However, disadvantages related to the complexities of the processing and analysis of datasets using the methodology implemented in eCognition could affect its use as a daily tool to aid forest managers. Besides, further research is needed to test the potential of object oriented techniques on fully established CCF stands.

7.7 Limitations and problems of the research

As discussed above, the short time series and limited availability of cloud-free Landsat ETM+ imagery for the Aberfoyle region, limited the phenological study. Further research may also improve the accuracy results implementing a methodology to overcome the difficulties found in the radiometric normalisation of the imagery.

The lack of standardised methods for LiDAR processing and analysis is a major limitation to future LiDAR studies. Most of LiDAR applications have used proprietary software for the processing of the laser measurements. This has cost implications, as there are just a handful of programs available. In this study, it was necessary to invest significant time developing methods to read, process and visualize the data. However, once this problem was overcome, the process of obtaining individual tree measurements was repeatable and efficient. LiDAR data presents a simple format and its processing using basic appropriate algorithms could provide estimations accurate enough for many applications.

Data acquisition has also cost issues. Since field inventories constitute the major part of forest mapping costs, the interest is to reduce this cost through the combination of traditional field inventories and remote sensing methods. Although the cost of acquiring and processing ETM+ imagery is relatively minimal, the cost of acquiring and the time invested in the processing of LiDAR and ATM data is not. The correction and analysis of Landsat ETM+ data was also not trivial, requiring computing power, time, and expertise.

7.8 Future research

Additional research may consider applying the methodology of this study over larger spatial extents and in areas with other and/or variable vegetation cover. Extending these findings to larger areas is challenging due to the consideration of multiple species and multiple architecture effects. The evaluation of forest dynamics could also be assessed if multi-date data sets are available.

The detailed spectral characterization of forest species and understorey vegetation commonly found in the Scottish managed forest will certainly improve the mapping of species using remote sensing. Similarly, the investigation of vegetation clumping and indirect paths of light penetration making use of the LiDAR fine resolution can provide better estimates.

References

Ackermann, F. (1999). "Airborne laser scanning - present status and future expectations". ISPRS Journal of Photogrammetry & Remote Sensing 54: 64-67.

Ager, A. and K. Owens (2004). Characterizing meadow vegetation with multitemporal Landsat Thematic Mapper remote sensing. Research Note PNW-RN-544. USA, United States Department of Agriculture. Forest Service.

Ahl, D., S. Gower, *et al.* (2006). "Monitoring spring canopy phenology of a deciduous broadleaf forest using MODIS". Remote Sensing of Environment 104: 88-95.

Almeida-Filho, R. and Y. Shimabukuro (2002). "Digital processing of a Landsat TM time series for mapping and monitoring degraded areas caused by independent gold miners, Roraima State, Brasilian Amazon". Remote Sensing of Environment 79: 42-50.

Asner, G. (1998). "Biophysical and biochemical sources of variability in canopy reflectance". Remote Sensing of Environment 64(3): 234-256.

Atkinson, P. and D. Emery (1999). "Exploring the relation between spatial structure and wavelength: implications for sampling reflectance in the field". International Journal of Remote Sensing 20(13): 2663-2678.

Baltsavias, E. P. (1999). "Airborne laser scanning: existing systems and firms and other resources. ISPRS Journal of Photogrammetry & Remote Sensing". ISPRS Journal of Photogrammetry & Remote Sensing 54: 164-198.

Barnes, B., D. Zak, *et al.* (1998). Forest Ecology. 4th edition, John Wiley & Sons.

Basham, A., J. Pinder, *et al.* (1997). "A comparison of Landsat Thematic Mapper and SPOT multi-spectral imagery for the classification of shrub and meadow vegetation in northern California, USA". International Journal of Remote Sensing 18(18): 3719-3728.

Behera, M. and P. Roy (2002). "Lidar remote sensing for forestry applications: the Indian context". Current Science 83(11): 1320-1328.

Benz, U., P. Hofmann, *et al.* (2004). "Multi-resolution, object-oriented fuzzy analysis of remote sensing data for GIS-ready information". ISPRS Journal of Photogrammetry & Remote Sensing 58: 239-258.

Bishop, A. and N. Coops (1996). Remote sensing of forest vegetation. Canberra, CSIRO Division of Wildlife and Ecology.

Blaschke, T. and J. Strobl (2001). "What's wrong with pixels? Some recent developments interfacing remote sensing and GIS". http://www.definiens-imaging.com/down/.

Blaschke, T., D. Tiede, *et al.* (2004). "3D landscape metrics to modelling forest structure and diversity based on laser scanning data". International Archives of Photogrammetry, Remote Sensing and Spatial Information Sciences XXXVI-8/W2: 129-132.

Brandtberg, T., T. Warner, *et al.* (2003). "Detection and analysis of individual leaf-off tree crowns in small footprint, high sampling density lidar data from the eastern deciduous forest in North America". Remote Sensing of Environment 85: 290-303.

Brockhaus, J. and S. Khorram (1992). "A comparison of SPOT and Landsat TM data for use in conducting inventories of forest resources". International Journal of Remote Sensing 13(16): 3035-3043.

Brokaw, N. (1985). "Gap-phase regeneration in a tropical forest". Ecology 66(3): 682-687.

Brown, N., S. Jennings, *et al.* (2000). "An improved method for the rapid assessment of forest understorey light environments". Journal of Applied Ecology. Advances in applied ecological techniques 37: 1044-1053.

Bunting, P. and R. Lucas (2006). "The delineation of tree crowns in Australian mixed species forests using hyperspectral Compact Airborne Spectrographic Imager (CASI) data". Remote Sensing of Environment 101(2): 230-248.

Burnett, C. and T. Blaschke (2003). "A multi-scale segmentation/object relationship modelling methodology for landscape analysis". Ecological Modelling 168: 233-249.

Campbell, J. B. (2002). Introduction to remote sensing. London, Taylor & Francis.

Canty, M., A. Nielsen, *et al.* (2004). "Automatic radiometric normalization of multitemporal satellite imagery". Remote Sensing of Environment 91: 441-451.

Carreiras, J., J. Pereira, *et al.* (2006). "Estimation of tree canopy cover in evergreen oak woodlands using remote sensing". Forest Ecology and Management 223: 45-53.

Chamberlain, J., R. Bush, *et al.* (2000). Managing national forests of the Eastern United States for non-timber forest products. Proceedings, XXI IUFRO World Congress 2000, Forests and Society: The Role of Research.

Chavez, P. (1996). "Image based atmospheric corrections - Revisited and improved". Photogrammetric Engineering & Remote Sensing 62(9): 1025-1036.

Chavez, P. S. (1988). "An improved dark-object substraction technique for atmospheric scattering correction of multispectral data". Remote Sensing of Environment 24: 459-479.

Chen, J. and J. Cihlar (1996). "Retrieving leaf area index of boreal conifer forests using Landsat TM images " Remote Sensing of Environment 55(2): 153-162.

Cihlar, J., H. Ly, *et al.* (1996). "Land cover classification with AVHRR multichannel composites in Northern environments". Remote Sensing of Environment 58: 36-51.

Clark, M., D. Clark, *et al.* (2004). "Small-footprint lidar estimation of sub-canopy elevation and tree height in a tropical rain forest landscape". Remote Sensing of Environment 91: 68-89.

Coates, K. and P. Burton (1997). "A gap-based approach for development of silvicultural systems to address ecosystem management objectives". Forest Ecology and Management 99: 337-354.

Cobby, D., D. Mason, *et al.* (2001). "Image processing of airborne scanning laser altimetry data for improved river flood modelling". ISPRS Journal of Photogrammetry & Remote Sensing 56: 121-138.

Cohen, W. and T. Spies (1992). "Estimating structural attributes of Douglas-Fir/Western Hemlock forest stands from Landsat and SPOT imagery". Remote Sensing of Environment 41: 1-17.

Collins, C., R. Parker, *et al.* (2004). "Using multispectral imagery and multi-return lidar to estimate tree and stand attributes in a southern bottomland hardwood forest". ASPRS 2004 Annual Conference Proceedings.

Congalton, R. (1991). "A review of assessing the accuracy of classifications of remotely sensed data". Remote Sensing of Environment: 3735-3746.

CSIRO. (1995). "Remote sensing of forest vegetation, Batemans Bay NSW Australia". 2004, from http://www.ffp.csiro.au/nfm/mdp/bbproj/atcor.htm.

Danson, F. and P. Curran (1993). "Factors affecting the remotely sensed response of coniferous forest plantations
" Remote Sensing of Environment 43(1): 55-65.

Du, Y., P. Teillet, *et al.* (2002). "Radiometric normalisation of multitemporal high-resolution satellite images with quality control for land cover change detection". Remote Sensing of Environment 82: 123-134.

Dymond, C., D. Mladenoff, *et al.* (2002). "Phenological differences in Tasseled cap indices improve deciduous forest classification". Remote Sensing of Environment 80: 460-472.

Elvidge, C. and Z. Chen (1995). "Comparison of broad-band and narrow-band red and near-infrared vegetation indices". Remote Sensing of Environment 54: 38-48.

Englund, S., J. O'Brien, *et al.* (2000). "Evaluation of digital and film hemispherical photography and spherical densiometry for measuring forets light environments". Canadian Journal of Forest Research 30: 1999-2005.

Fallah-Adl, H., J. JaJa, *et al.* (1995). Efficient algorithms for atmospheric correction of remotely sensed data. Proceedings of the 1995 ACM/IEEE conference on Supercomputing (CDROM) - Article No. 12, California, United States

Flood, M. (2001). "LiDAR activities and research priorities in the commercial sector". International Archives of Photogrammetry and Remote Sensing XXXIV-3/W4: 5.

Forestry_Commission (2003). National Inventory of Woodland and Trees, Inventory Report Forestry Commission.

Forestry_Commission (2005). GB Public opinion on forestry: 37 pp.

Franklin, J. (1986). "Thematic Mapper Analysis of Coniferous Forest Structure and Composition". International Journal of Remote Sensing 7(10): 1287-1301.

Furley, P. (1998). History and destiny of middle american forests: the inheritors of the Mayan landscape. Human activities and the tropical rainforest. Past, present and possible future. Geo-Journal Library
Kluwer Academic Publishers. 44: 101-132.

Fyfe, S. (2003). "Spatial and temporal variation in spectral reflectance: Are seagrass species spectrally distinct?" Limnology and Oceanography 48((1, part 2)): 464-479.

Gemmell, F. (1995). "Effects of Forest Cover, Terrain, and Scale on Timber Volume Estimation with Thematic Mapper Data in a Rocky Mountain Site". Remote Sensing of Environment 51: 291-305.

Gemmell, F. (1999). "Estimating coniferous forest cover with Thematic Landsat Mapper" Remote Sensing of Environment 69: 105-121.

Gemmell, F. and D. Goodenough (1992). Estimating Forest Volume from TM data: The Importanceof Scale and Accuracy of Forest Cover Data. Remote Sensing from Research to Operation University of Dundee. .

Gemmell, F., J. Varjo, *et al.* (2001). "Estimating forest cover in a boreal forest test site using thematic mapper data from two dates " Remote Sensing of Environment 77: 197-211.

Gilabert, M., S. Gandia, *et al.* (1996). "Analyses of spectral-byophysical relationships for a corn canopy". Remote Sensing of Environment 55: 11-20.

Gilabert, M., J. Gonzalez-Piqueras, *et al.* (2002). "A generalized soil-adjusted vegetation index". Remote Sensing of Environment 82: 303-310.

Hagiwara, A., J. Imanishi, *et al.* (2004). "Estimating leaf area index in mixed forest using an airborne laser scanner". International Archives of Photogrammetry, Remote Sensing and Spatial Information Sciences XXXVI-8/W2: 298-300.

Hajek, F. (2005). Object-oriented classification of remote sensing data for the identification of tree species composition. Proceedings of ForestSat 2005 conference, Boras, Sweden.

Hale, S. (2001). "Light regime beneath Sitka spruce plantations in northern Britain: preliminary results " Forest Ecology and Management 151(1-3): 61-66.

Hale, S. (2003). "The effect of thinning intensity on the below-canopy light environment in a Sitka spruce plantation " Forest Ecology and Management 179(1-3): 341-349.

Hale, S. (2004). "Managing light to enable natural regeneration in British conifer forests". Information Note 63. Forestry Commission: 6.

Hale, S. and N. Brown (2005). "Use of the canopy-scope for assessing canopy openness in plantation forests " Forestry 78(4): 365-371.

Hale, S. and C. Edwards (2002). "Comparison of film and digital hemispherical photography across a wide range of canopy densities " Agricultural and Forest Meteorology 112: 51-56.

Hale, S., P. Levy, *et al.* (2004). "Trade-offs between seedling growth, thinning and stand stability in Sitka spruce stands: a modelling analysis " Forest Ecology and Management 187(1): 105-115.

Hall, F., D. Strebel, *et al.* (1991). "Radiometric rectification: toward a common radiometric response among multidate, multisensor images". Remote Sensing of Environment 35: 11-27.

Hanewinkel, M. (2001). "Economic aspects of the transformation from even-aged pure stands of Norway spruce to uneven-aged mixed stands of Norway spruce and beech " Forest Ecology and Management 151(1-3): 181-193.

Hardy, J., R. Melloh, *et al.* (2004). "Solar radiation transmission through conifer canopies". Agricultural and Forest Meteorology 126: 257-270.

Hart, C. (1995). "Alternative silvicultural systems to clear cutting in Britain: a review". Forestry Commission Bulletin No. 115.

Heurich, M. and H. Weinacker (2004). "Automated tree detection and measurement in temperate forests of Central Europe using laserscanning data". International Archives of Photogrammetry, Remote Sensing and Spatial Information Sciences XXXVi-8/W2: 198-203.

Hibberd, B. (1991). "Forestry Practice". Forestry Commission handbook No.6. Forestry Commission.

Hill, R. and A. Thomson (2005). "Mapping woodland species composition and structure using airborne spectral and LiDAR data". International Journal of Remote Sensing 26(17): 3763-3779.

Hirosawa, Y., S. Marsh, *et al.* (1996). "Application of standardized principal component analysis to land-cover characterisation using multitemporal AVHRR data". Remote Sensing of Environment 58: 267-281.

Hoffhine, E. and S. Sader (2002). "Detection of forest harvest type using multiple dates of Landsat TM imagery". Remote Sensing of Environment 80: 385-396.

Holmgren, J. and T. Jonsson (2004b). "Large scale airborne laser scanning of forest resources in Sweden". International Archives of Photogrammetry, Remote Sensing and Spatial Information Sciences XXXVI-8/W2: 157-160.

Holmgren, J. and A. Persson (2004a). "Identifying species of individual trees using airborne laser scanner". Remote Sensing of Environment 90: 415-423.

Howard, H. (1991). Remote sensing of forest resources. Theory and application. London.

Hu, B., K. Inannen, *et al.* (2000). "Retrieval of Leaf Area Index and Canopy Closure from CASI Data over the BOREAS Flux Tower Sites " Remote Sensing of Environment 74(2): 255-274.

Huang, C., B. Wylie, *et al.* (2001). Derivation of a Tasselled Cap transformation based on Landsat 7 at-satellite reflectance. Sioux Falls, USA, USGS EROS Data Center 10.

Hudak, A., M. Lefsky, *et al.* (2002). "Integration of lidar and Landsat ETM+ data for estimating and mapping forest canopy height". Remote Sensing of Environment 82: 397-416.

Huete, A., K. Didan, *et al.* (2002). "Overview of the radiometric and biophysical performance of the MODIS vegetation indices". Remote Sensing of Environment 83: 195-213.

Hyde, P., R. Dubayah, *et al.* (2006). "Mapping forest structure for wildlife habitat analysis using multi-sensor (LiDAR, SAR/InSAR, ETM+, Quickbird) synergy " Remote Sensing of Environment 102(1-2): 63-73.

Hyyppa, J., H. Hyyppa, *et al.* (2004). "Algorithms and methods of airborne laser scanning for forest measurements". International Archives of Photogrammetry, Remote Sensing and Spatial Information Sciences XXXVI-8/W2.

Inoue, A., K. Yamamoto, *et al.* (2004). "Effects of image quality, size and camera type on forest light environment estimates using digital hemispherical photography". Agricultural and Forest Meteorology 126: 89-97.

Ivits, E., B. Koch, *et al.* (2002). "Landscape connectivity studies on segmentation based classification and manual interpretation of remote sensing data". eCognition User Meeting. Retrieved from the world wide web ww.definiens.com/pdf/um2002/papers/ivits_full.pdf

Jensen, J. (2005). Introductory Digital Image Processing. A remote sensing perspective. New Jersey, Pearson Prentice Hall

Jensen, J., F. Qiu, *et al.* (1999). "Predictive modeling of coniferous forest age using statistical and artificial neural network approaches applied to remote sensor data". International Journal of Remote Sensing 20(14): 2805-2822.

Jensen, J. R. (2000). Remote sensing of the environment. An earth resource perspective. USA, Prentice Hall.

Jiang, H., J. Strittholt, *et al.* (2004). "The classification of late seral forests in the Pacific Northwest, USA using Landsat ETM+ imagery". Remote Sensing of Environment 91: 320-331.

Jonckheere, I., B. Muys, *et al.* (2005). "Derivative analysis for In Situ high dynamic range hemispherical photography and its application in forest stands". IEEE Geoscience and remote sensing letters: 1545-1598.

Joseph, G. (2000). "How well do we understand Earth observation electro-optical sensor parameters?" ISPRS Journal of Photogrammetry & Remote Sensing 55: 9-12.

Karpouzli, E. and T. Malthus (2003). "The empirical line method for the atmospheric correction of IKONOS imagery". International Journal of Remote Sensing 24(5): 1143-1150.

Kaufman, Y. (1989). The atmospheric effect on remote sensing and its correction Chapter 9 in Optical Remote Sensing, technology and application. Wiley.

Kodani, E., Y. Awaya, *et al.* (2002). "Seasonal patterns of canopy structure, biochemistry and spectral reflectance in a broad-leaved deciduous Fagus crenata canopy". Forest Ecology and Management 167: 233-249.

Kraus, K. and N. Pfeifer (2002). Advanced DTM generation from Lidar data. International Archives of Photogrammetry, Remote Sensing and Spatial Information Sciences, Annapolis, USA.

Kuusk, A., M. Lang, *et al.* (2004). "Simulation of the reflectance of ground vegetation in sub-boreal forests " Agricultural and Forest Meteorology 126(1-2): 33-46.

Kuusk, A., T. Nilson, *et al.* (2002). "Angular distribution of radiation beneath forest canopies using a CCD-radiometer". Agricultural and Forest Meteorology 110: 259-273.

Lauver, C. and J. Whistler (1993). "A hierarchical classification of Landsat TM imagery to identify natural grassland areas and rare species habitat". Photogrammetric Engineering & Remote Sensing 59: 627-634.

Leblon, B., L. Gallant, *et al.* (1996). "Effects of shadowing types on ground-measured visible and near-infrared shadow reflectances". Remote Sensing of Environment 58: 322-328.

Leckie, D., F. Gougeon, *et al.* (2005). "Automated tree recognition in old growth conifer stands with high resolution digital imagery". Remote Sensing of Environment 94: 311-326.

Lefsky, M. A., W. B. Cohen, *et al.* (1999). "Lidar remote sensing of the canopy structure and biophysical properties of Douglas-fir western hemlock forests". Remote Sensing of Environment 70: 339-361.

Levin, S. (1992). "The problem of pattern and scale in ecology". Ecology 73(6): 1943-1967.

Lieffers, V., C. Messier, *et al.* (1999). "Predicting and managing light in the understory of boreal forests". Canadian Journal of Forest Research 29: 796–811.

Lillesand, T. (1990). Chapter 13. Remote Sensing and Geographic Information systems. Introduction to Forest Science. Second edition. Y. a. Giese: 277-299.

Lim, K. and P. Treitz (2004). "Estimation of aboveground forest biomass using airborne scanning discrete return lidar in Douglas-Fir". International Archives of Photogrammetry, Remote Sensing and Spatial Information Sciences XXXVI-8/W2: 149-152.

Lloyd, C. and P. Atkinson (2002). "Deriving DSMs from LiDAR data with kriging" International Journal of Remote Sensing 23(12): 2519 - 2524.

Lucieer, A. (2004). Uncertainties in segmentation and their visualisation. The Netherlands, University of Utrecht. PhD Thesis: 197.

Luethy, J. and H. Ingensand (2004). "How to evaluate the quality of airborne scanning data". International Archives of Photogrammetry, Remote Sensing and Spatial Information Sciences XXXVI-8/W2: 313-317.

Magnussen, S. and P. Boudewyn (1998). "Derivations of stand heights from airborne laser scanner data with canopy-based quantile estimators". Canadian Journal of Forest Research 28: 1016-1031.

Magnussen, S., F. Gougeon, *et al.* (1999). "Predicting tree heights from a combination of lidar canopy heights and digital stem counts " Remote Sensing and Forest Monitoring Conference Proceedings.

Malcolm, D., W. Mason, *et al.* (2001). "The transformation of conifer forests in Britain - regeneration, gap size and silvicultural systems". Forest Ecology and Management 151: 7-23.

Mallinis, G., N. Koutsias, *et al.* (2004). "Forest parameters estimation in a European mediterranean landscape using remotely sensed data". Forest Science 50(4): 450-460.

Maltamo, M., K. Eerikainen, *et al.* (2004). "Estimation of timber volume and stem density based on scanning laser altimetry and expected tree size distribution functions". Remote Sensing of Environment 90: 319-330.

Malthus, T., J. Suarez-Minguez, *et al.* (2002). Review of remote sensing in commercial forestry. Edinburgh, Forestry Commission.

Martinez, B., J. Melia, *et al.* (2002). "An optimized burned area detection method based on the GESAVI". Forest Fire Research & Wildland Fire Safety: 1-11.

Maselli, F., G. Chirici, *et al.* (2005). "Estimation of Mediterranean forest attributes by the application of k-NN procedures to multitemporal Landsat ETM+ images". International Journal of Remote Sensing 26(17): 3781-3796.

Mason, W. (1999). "What is continuous cover forestry?" Forestry Commission Information Note 29. Forestry Commission.

Mason, W., C. Edwards, *et al.* (2004). "Survival and early seedling growth of conifers with different shade tolerance in a Sitka spruce spacing trial and relationship to understorey light climate". Silva Fenicca 38(4): 357-370.

Mason, W. and G. Kerr (2001). Transforming even-aged conifer stands to continuous cover management. Forestry Commission Information Note 40. Edinburgh, Forestry Commission.

Mason, W., G. Kerr, *et al.* (2005). Continuous cover forestry in British conifer forests. Forest Research Annual Report and Accounts 2003-2004, Forest Enterprise: 38-53.

Mather, P. (1999). Computer processing of remotely sensed images: An introduction. Chichester, John Wiley and Sons.

McCombs, J., S. Roberts, *et al.* (2003). "Influence of fusing lidar and multispectral imagery on remotely sensed estimates of stand density and mean tree height in a managed Loblolly Pine plantation". Forest Science 49(3): 457-466.

McDonald, A., F. Gemmell, *et al.* (1998). "Investigation of the utility of spectral vegetation indices for determining information on coniferous forests". Remote Sensing of Environment 66: 250-272.

McElhinny, C., P. Gibbons, *et al.* (2005). "Forest and woodland stand structural complexity: Its definition and measurement". Forest Ecology and Management 218: 1-24.

Means, J., S. Acker, *et al.* (2000). "Predicting forest stand characteristics with airborne scanning lidar " ISPRS Journal of Photogrammetry & Remote Sensing 66(11): 1367-1371.

Means, J., S. Acker, *et al.* (1999). "Use of large-footprint scanning airborne lidar to estimate forest stand characteristics in the western cascades of Oregon". Remote Sensing of Environment 67: 298-308.

Mei, C. and S. Durrieu (2004). "Tree crown delineation from digital elevation models and high resolution imagery". International Archives of Photogrammetry, Remote Sensing and Spatial Information Sciences XXXVI-8/W2.

Morsdorf, F., E. Meier, *et al.* (2004). "Lidar based geometric reconstruction of boreal type forest stands at single tree level for forest and wildland fire management". Remote Sensing of Environment 92: 353-362.

Mussche, S., R. Samson, *et al.* (2001). "A comparison of optical and direct methods for monitoring the seasonal dynamics of Leaf Area Index in deciduous forests". Silva Fennica 35(4): 373-384.

Myneni, R. and G. Asrar (1994). "Atmospheric effects and spectral vegetation indices". Remote Sensing of Environment 47(3): 390-402.

Naesset, E. (1997). "Determination of mean tree height of forest stands using airborne laser scanner data". ISPRS Journal of Photogrammetry & Remote Sensing 52: 49-56.

Naesset, E. (2002). "Predicting forest stand characteristics with airborne scanning laser using a practical two-stage procedure and field data". Remote Sensing of Environment 80: 88-99.

Naesset, E. and T. Okland (2002). "Estimating tree height and tree crown properties using airborne scanning laser in a boreal nature reserve". Remote Sensing of Environment 79: 105-115.

Naumburg, E. and L. DeWald (1999). "Relationships between Pinus ponderosa forest structure, light characteristics, and understorey graminoid species presence and abundance". Forest Ecology and Management 124: 205-215.

Nel, E., C. Wessman, *et al.* (1994). "Digital and visual analysis of thematic mapper imagery for differentiating old growth from younger Spruce-Fir stands". Remote Sensing of Environment 48: 291-301.

Nelson, R. (1997). "Modeling forest canopy heights: The effects of canopy shape". Remote Sensing of Environment 16(60): 327-334.

Ngeh, C. (1989). Effects of land clearing methods on a tropical forest ecosystem and the growth of Terminalia ivorensis (A. Chev.). Geography, The University of Edinburgh. PhD Thesis: 194.

Nicholls, F. (1999). "The value of understory vegetation". Land for Wildlife Note(7): 1-2.

Nilson, T. and A. Kuusk (2004). "Improved algorithm for estimating canopy indices from gap fraction data in forest canopies". Agricultural and Forest Meteorology 124: 157-169.

Nilson, T. and U. Peterson (1994). "Age dependence of forest reflectance: Analysis of main driving factors". Remote Sensing of Environment 48(3): 319-331.

Nilsson, M. (1996). "Estimation of tree heights and stand volume using an airborne lidar system". Remote Sensing of Environment 56: 1-7.

Nowak, D., R. Rowntree, *et al.* (1996). "Measuring and analyzing urban tree cover " Landscape and Urban Planning 36(1): 49-57.

Odenweller, J. and K. Johnson (1984). "Crop identification using Landsat temporal spectral profiles". Remote Sensing of Environment 14: 39-54.

Oesten, G. and A. Roeder (2002). Management von Forstbetrieben. Germany, Verlag.

Oetter, D., W. Cohen, *et al.* (2001). "Land cover mapping in an agricultural setting using multiseasonal Thematic Mapper data " Remote Sensing of Environment 76(2): 139-155.

Pal, N. and S. Pal (1993). "A review on image segmentation techniques". Pattern Recognition 26(9): 1277-1294.

Parker, G., M. Lefsky, *et al.* (2001). "Light transmittance in forest canopies determined using airborne laser altimetry and in-canopy quantum measurements". Remote Sensing of Environment 76: 298-309.

Pekkarinen, A. (2004). Image segmentation in multi- source forest inventory Forestry. Vantaa, Finnish Forest Research Institute. PhD: 37.

Peñuelas, J., J. Gamon, *et al.* (1994). "Reflectance indices associated with physiological changes in Nitrogen and water limited sunflower leaves". Remote Sensing of Environment 48: 135-146.

Pereira, M. and A. Setzer (1993). "Spectral characteristics of fire scars in Landsat 5 TM images of Amazonia". International Journal of Remote Sensing 14(11): 2061-2078.

Perry, C. and L. Lautenschlager (1984). "Functional equivalence of spectral vegetation indices". Remote Sensing of Environment 14: 169-182.

Persson, Å., J. Holmgren, *et al.* (2002). "Detecting and measuring individual trees using an airborne laser scanner". Photogrammetric Engineering & Remote Sensing 68(9): 925-932.

Peters, C., A. Gentry, *et al.* (1989). "Valuation of an Amazonian rainforest " Nature 339: 655-656.

Petrie, M. (1999). "Natural regeneration: principles and practice". Land for wildlife No.8.

Petzold, B., P. Reiss, *et al.* (1999). "Laser scanning – surveying and mapping agencies are using a new technique for the derivation of digital terrain models". ISPRS Journal of Photogrammetry & Remote Sensing 54: 95-104.

Pommerening, A. (2006a). "Transformation to continuous cover forestry in a changing environment". Forest Ecology and Management 224: 227-228.

Pommerening, A. (2006b). "Evaluating structural indices by reversing forest structural analysis". Forest Ecology and Management 224: 266-277.

Pommerening, A. and S. Murphy (2004). "A review of the history, definitions and methods of continuous cover forestry with special attention to afforestation and restocking". Forestry 77: 27-44.

Popescu, S., R. Wynne, *et al.* (2002). "Estimating plot-level tree heights with lidar: local filtering with a canopy-height based variable window size " Computers and Electronics in Agriculture 37(1-3): 71-95.

Popescu, S., R. Wynne, *et al.* (2003). "Measuring individual tree crown diameter with lidar and assessing its influence on estimating forest volume and biomass". Canadian Journal of Remote Sensing 29(5): 564-577.

Price, J. (1994). "How unique are spectral signatures? ". Remote Sensing of Environment 49: 181-186.

Price, K., X. Guo, *et al.* (2002). "Optimal Landsat TM band combinations and vegetation indices for discrimination of six grasslands types in eastern Kansas". International Journal of Remote Sensing: 1-12.

Price, M. and C. Price (2006). "Creaming the best, or creatively transforming? Might felling the biggest trees first be a win-win strategy?" Forest Ecology and Management 224: 297-303.

Pulliainen, J., M. Engdahl, *et al.* (2003). "Feasibility of multi-temporal interferometric SAR data for stand-level estimation of boreal forest stem volume " Remote Sensing of Environment 85(4): 397-409.

Qi, J., F. Cabot, *et al.* (1996). "Biophysical parameter estimations using multidirectional spectral measurements". Remote Sensing of Environment 54: 71-83.

Qi, J., A. Chehbouni, *et al.* (1994). "A Modified Soil adjusted Vegetation Index". Remote Sensing of Environment 48: 119-126.

Rautiainen, M. (2005). "The spectral signature of coniferous forests: the role of stand structure and leaf area index". Dissertationes Forestales 6: 54.

Rautiainen, M., P. Stenberg, *et al.* (2004). Mapping of LAI using optical satellite images. IUFRO Conference Modeling Forest Production, Vienna.

Rautiainen, M., P. Stenberg, *et al.* (2004). "The effect of crown shape on the reflectance of coniferous stands". 89(1): 41-52.

Reforesting Scotland (2006). "Rural alternatives". http://www.reforestingscotland.org/projects/rural_alternatives.php.

Rieger, W., O. Eckmullner, *et al.* (1999). Laser-scanning for the derivation of forest stand parameters. Mapping surface structure and topography by airborne and spaceborne lasers, La Jolla, USA.

Ripple, W., S. Wang, *et al.* (1991). "A preliminary comparison of Landsat Thematic Mapper and SPOT-1 HRV multispectral data for estimating coniferous forest volume". International Journal of Remote Sensing 12(9): 1971-1977.

Rondeaux, G., M. Steven, *et al.* (1996). "Optimization of soil-adjusted vegetation indices". Remote Sensing of Environment 55: 95-107.

Roxburgh, J. and D. Kelly (1995). "Uses and limitations of hemispherical photography for estimating forest light environments". New Zealand Journal of Ecology ©New Zealand Ecological Society 19(2): 213-217.

Sader, S., M. Bertrand, *et al.* (2003). "Satellite Change Detection of Forest Harvest Patterns on an Industrial Forest Landscape". Forest Science 49(3): 341-353.

Schabel, H. and M. Pecore (1997). Silviculture on Wisconsin's Menominee Indian Reservation is it a Dauerwald? . Proceedings, XI World Forestry Congress, Antalya, Turkey.

Schiewe, J. (2002). "Segmentation of high-resolution remotely sensed data - Concepts, applications and problems". http://www.definiens-imaging.com/down/.

Schiewe, J., L. Tufte, *et al.* (2001). "Potential and problems of multi-scale segmentation methods in remote sensing " http://www.definiens-imaging.com/down/

Schlerf, M., C. Atzberger, *et al.* (2005). "Remote sensing of forest biophysical variables using HyMap imaging spectrometer data". Remote Sensing of Environment 95: 177-194.

Schott, J., C. Salvaggio, *et al.* (1988). "Radiometric scene normalization using pseudoinvariant features". Remote Sensing of Environment 26: 1-16.

Shataee, S., T. Kelenberger, *et al.* (2004). "Forest types classification using ETM+ data in the North of Iran. Comparison of object-oriented with pixel-based classification techniques". XX ISPRS Congress Natural Resources 55(3).

Sica, R. (2005). "Exploring the atmosphere with lidar". http://pcl.physics.uwo.ca/pclhtml/introlidar/introlidarf.html.

Sigrist, P., P. Coppin, *et al.* (1999). "Impact of forest canopy on quality and accuracy of GPS measurements". International Journal of Remote Sensing 20(18): 3595-3610.

Silbernagel, J. and M. Moeur (2001). "Modeling canopy openness and understory gap patterns based on image analysis and mapped tree data". Forest Ecology and Management 149: 217-233.

Sithole, G. and G. Vosselman (2004). "Experimental comparison of filter algorithms for bare-Earth extraction from airborne laser scanning point clouds". ISPRS Journal of Photogrammetry & Remote Sensing 59: 85-101.

Spanner, M., L. Pierce, *et al.* (1990). "The seasonality of AVHRR data of temperate coniferous forests: relationship with Leaf Area Index". Remote Sensing of Environment 33: 97-112.

Staenz, K., J. Secker, *et al.* (2002). "Radiative transfer codes applied to hyperspectral data for the retrieval of surface reflectance". ISPRS Journal of Photogrammetry & Remote Sensing 57: 194-203.

Sterba, H. and T. Ledermann (2006). "Inventory and modelling for forests in transition from even-aged to uneven-aged management". Forest Ecology and Management 224: 278-285.

St-Onge, B. and C. Vega (2003). "Combining stereo-photogrammetry and lidar to map forest canopy height". International Archives of Photogrammetry, Remote Sensing and Spatial Information Sciences XXXIV-3/W13.

St-Onge, B. and U. Vepakomma (2004). "Assessing forest gap dynamics and growth using multi-temporal laser scanner data". International Archives of Photogrammetry, Remote Sensing and Spatial Information Sciences XXXVI-8/W2: 173-178.

Syed, S., P. Dare, *et al.* (2005). Automatic classification of land cover features with high resolution imagery and lidar data: an object oriented approach. Proceedings of SSC2005 Spatial Intelligence, Innovation and Praxis: The national biennial Conference of the Spatial Sciences Institute, Melbourne.

Teillet, P., K. Staenz, *et al.* (1997). "Effects of spectral, spatial and radiometric characteristics on remote sensing vegetation indices of forested regions". Remote Sensing of Environment 61: 139-149.

Thiel, K. and A. Wehr (2004). "Performance capabilities of laser scanners - An overview and measurement principle analysis " International Archives of Photogrammetry, Remote Sensing and Spatial Information Sciences XXXVI-8/W2.

Tiede, D., C. Burnett, *et al.* (2004). Delineation of individual trees with eCognition 3.0 using LiDAR and multispectral imagery. 3rd International eCognition User Meeting, Munich, Germany.

Todd, K., F. Csillag, *et al.* (2003). "Three-dimensional mapping of light transmittance and foliage distribution using lidar". Canadian Journal of Remote Sensing 29(5): 544-555.

Triepke, J., C. Brewer, *et al.* (2005). "Mapping forest plant associations in Northwestern Montana (USA)". http://www.definiens-imaging.com/documents/um2005/index.html.

Trotter, C., J. Dymond, *et al.* (1997). "Estimation of timber volume in a coniferous plantation forest". International Journal of Remote Sensing 18(10): 2209-2223.

UKWAS (2000). Certification standard for the UK woodland assurance scheme. Edinburgh, Forestry Commission.: 43 pp.

Universidad_de_Calgary. (2004). "Remote sensing applied to vegetation classification". 2004, from http://ucalgary.ca/geog/Virtual/Remote%20Sensing/rsveg.html.

Ustin, S., L. Duan, *et al.* (1994). Seasonal changes observed in AVIRIS images of Jasper Ridge, California. Proceedings International Geoscience and Remote Sensing Symposium IGARSS '94.

van Aardt, J. (2004). An Object-Oriented Approach to Forest Volume and Aboveground Biomass Modeling using Small-Footprint Lidar Data for Segmentation, Estimation, and Classification. Forestry. USA, Virginia Polytechnic Institute and State University. PhD Dissertation.

van Dam, O. (2001). Forest filled with gaps. Effects of gap size on water and nutrient cycling in tropical rain forest. The Netherlands, University of Utrecht. PhD: 207.

Veneziano, D., R. Souleyrette, *et al.* (2003). "Integration of light detection and ranging technology with photogrammetry in highway location and design". www.ctre.iastate.edu/mtc/papers/2002/Veneziano.pdf.

Vermote, E., D. Tanre, *et al.* (1997). "Second Simulation of the Satellite Signal in the Solar Spectrum, 6S: An Overview". IEEE Transactions on Geosciense and Remote Sensing 35(3): 675-686.

Verstraete, M., B. Pinty, *et al.* (1996). "Potential and limitations of information extraction on the terrestrial biosphere from satellite remote sensing". Remote Sensing of Environment 58: 201-214.

Vieira, I., A. Silva, *et al.* (2003). "Classifying successional forests using Landsat spectral properties and ecological characteristics in eastern Amazonia". Remote Sensing of Environment 87: 470-481.

Vogelmann, J. and T. DeFelice (2003). "Characterisation of intra-annual reflectance properties of land cover classes in southeastern South Dakota using Landsat TM and ETM+ data". Canadian Journal of Remote Sensing 29(2): 219-229.

Wagner, W., C. Eberhofer, *et al.* (2004). "Robust filtering of airborne laser scanner data for vegetation analysis". International Archives of Photogrammetry, Remote Sensing and Spatial Information Sciences XXXVI-8/W2.

Watt, P., D. Donoghue, *et al.* (2004). "Predicting forest height from Ikonos, Landsat and lidar imagery". International Archives of Photogrammetry, Remote Sensing and Spatial Information Sciences XXXVI-8/W2: 228-231.

Watt, P., D. Donoghue, *et al.* (2005). Using airborne light detection and ranging (LiDAR) to identify and monitor the performance of plantation species mixtures. ForestSat 2005, Finland.

WCED (1987). Brundtland report. Our Common Future. http://www.srds.ndirect.co.uk/sustaina.htm, World Commission on Environment and Development

Webster, T. (2005). The application of high-resolution LiDAR DEM data to landscape evolution: An example from the Fundy Basin, Nova Scotia, Canada Earth Sciences. Halifax, Dalhousie university. PhD Thesis: 216.

Whitmore, T. (1989). "Canopy gaps and the two major groups of forest trees". Ecology 70(3): 536-538.

Wild, P. and M. Weidenbach (1998). "German forestry review". http://www.landconsult.de/markus/foram/home/germany.html.

Wilson, E. and S. Sader (2002). "Detection of forest harvest type using multiple dates of landsat TM imagery". Remote Sensing of Environment 80: 385-396.

Wolter, P., D. Mladenoff, *et al.* (1995). "Improved forest classification in the Northern Lake States using multi-temporal Landsat imagery". Photogrammetric Engineering & Remote Sensing 61: 1129-1143.

Yorke, M. (2001). "Some misconceptions concerning the management of continuous cover forestry in the UK: perceived barriers to implementation". http://www.forestryandtimber.org/downloads/ccf0304.doc.

Yoshimura, T. and H. Hasegawa (2003). "Comparing the precision and accuracy of GPS positioning in forested areas". Journal of Forest Research 8(3): 147-152.

Young, R. and R. Giese (1990). Introduction to forest science. Second edition. USA, John Wiley and Sons.

Yu, X., J. Hyyppa, *et al.* (2004). "Effects of flight altitute on tree height estimation using airborne laser scanning". International Archives of Photogrammetry, Remote Sensing and Spatial Information Sciences XXXVI-8/W2: 96-101.

Yu, X., J. Hyyppa, *et al.* (2004). "Automatic detection of harvested trees and determination of forest growth using airborne lidar scanning". Remote Sensing of Environment 90: 451-462.

Zimble, D., D. Evans, *et al.* (2003). "Characterizing vertical forest structure using small-footprint airborne lidar". Remote Sensing of Environment 87: 171-182.

Appendix 1: Regression equations for Landsat ETM+ data normalisation

Regression equations per band for the normalisation of image acquired on 17.07.2000 with respect to the reference image 25.08.2000

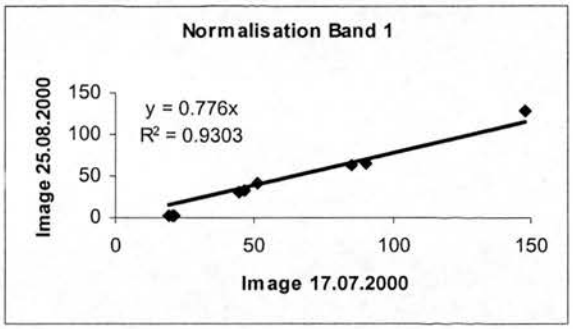

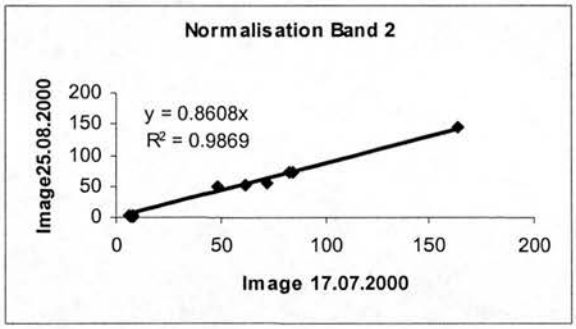

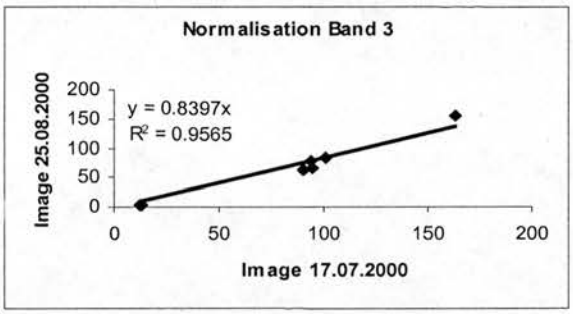

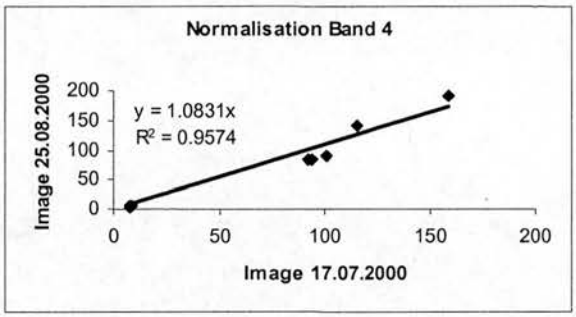

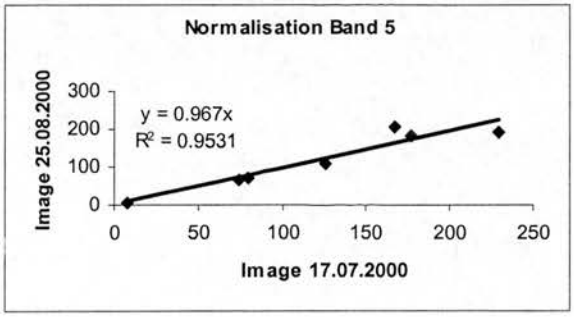

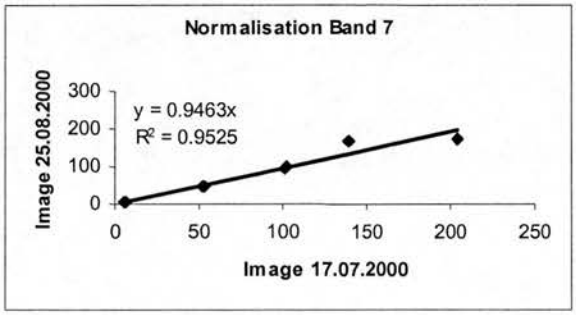

Regression equations per band for the normalisation of ETM+ image acquired on 24.12.2000 with respect to the reference image 25.08.2000

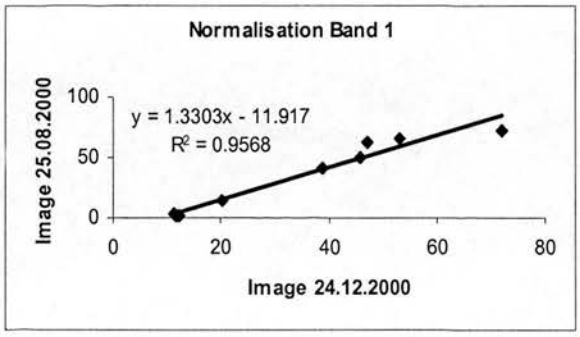

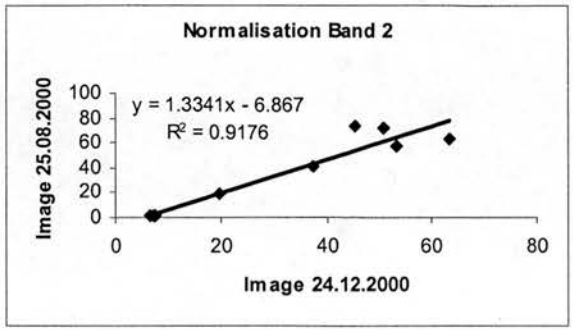

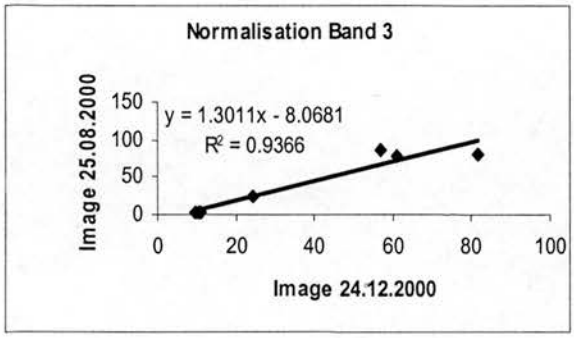

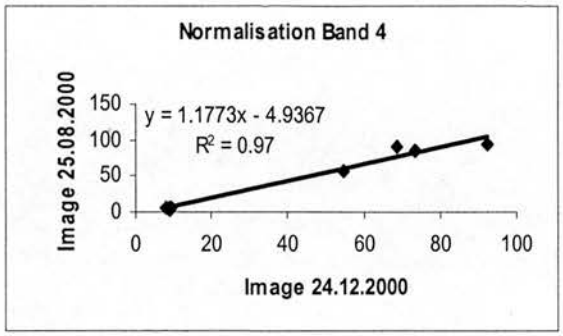

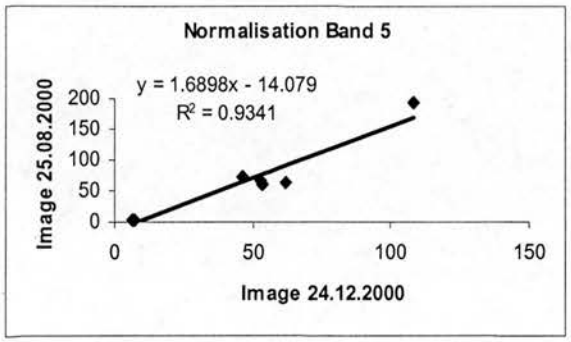

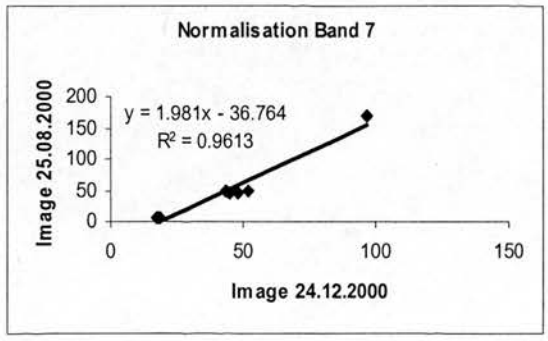

Regression equations per band for the normalisation of the ETM+ image acquired on 01.05.2001 with respect to the reference image 25.08.2000

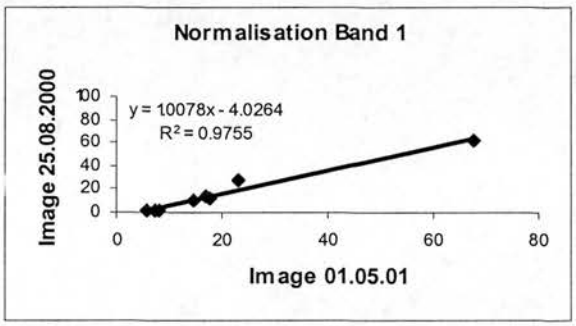

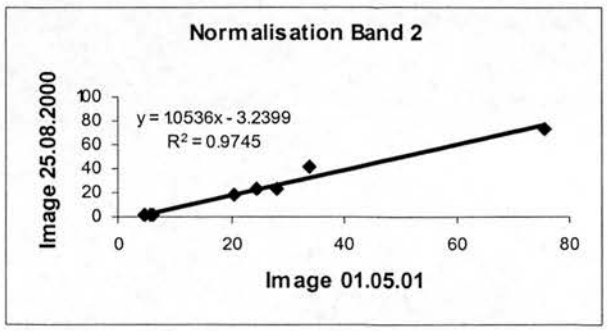

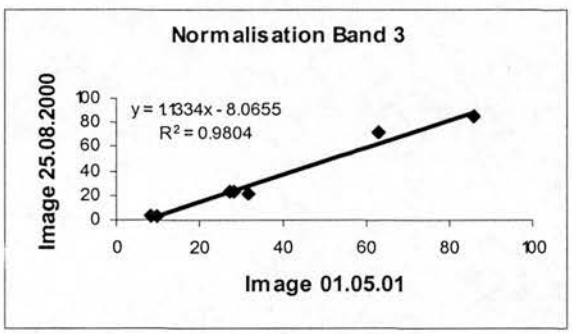

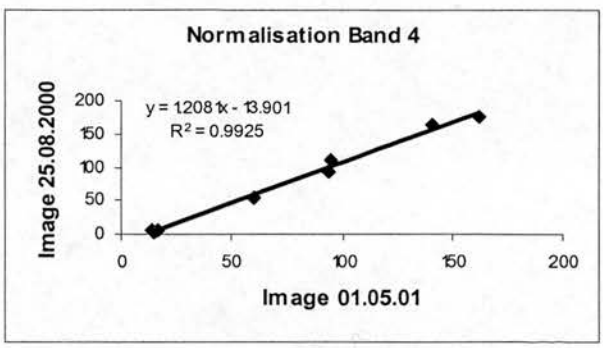

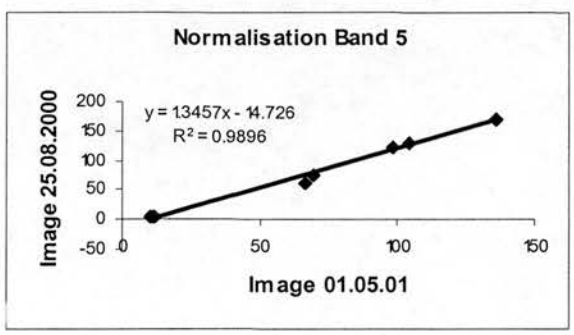

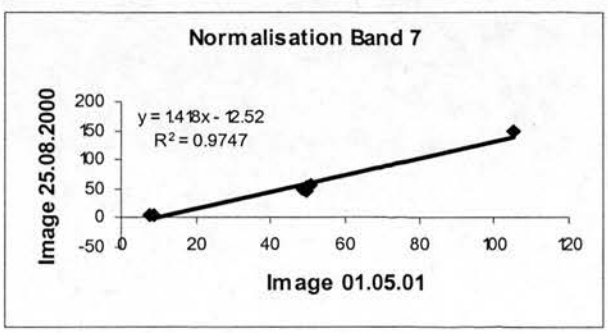

Regression equations per band for the normalisation of ETM+ image acquired on 31.10.2001 with respect to the reference image 25.08.2000

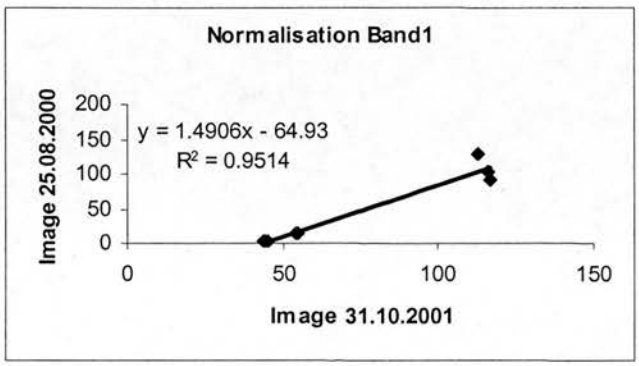

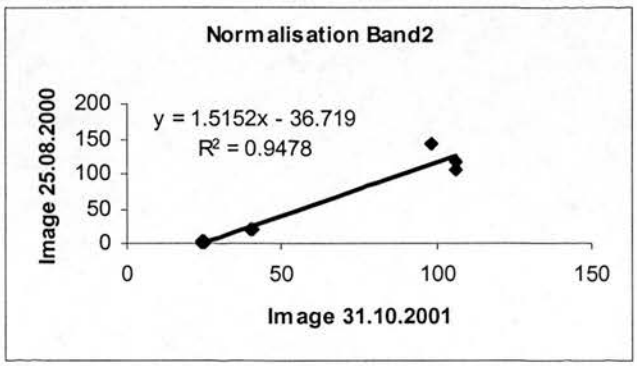

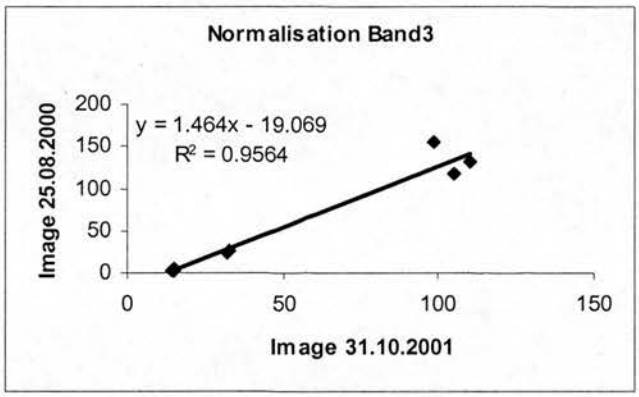

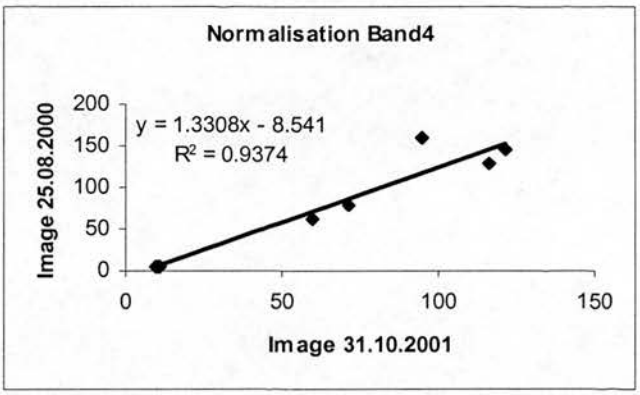

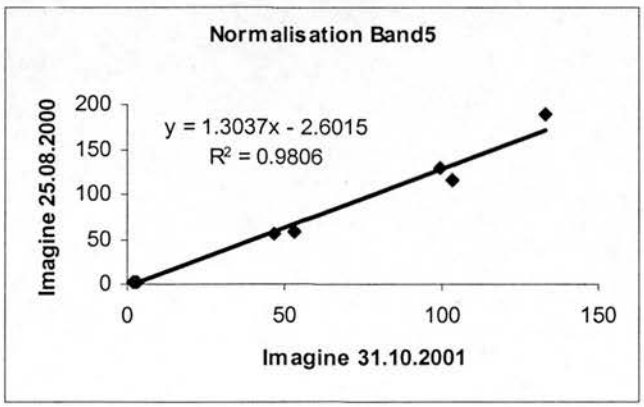

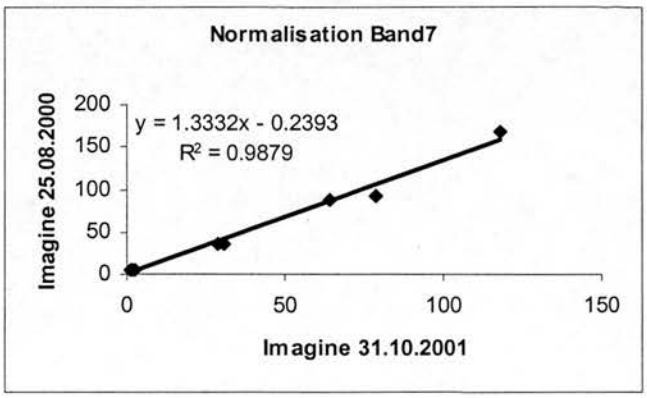

Regression equations per band for the normalisation of ETM+ image acquired on 11.12.2001 with respect to the reference image 25.08.2000

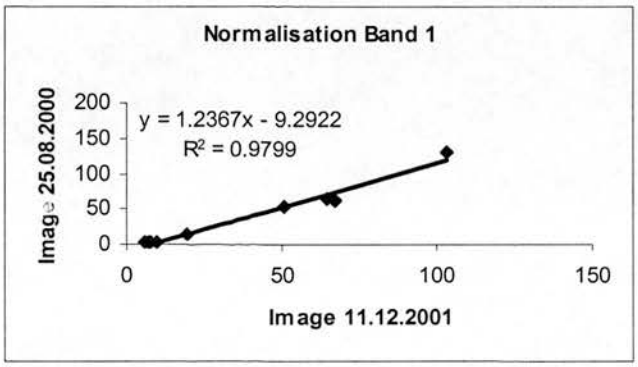

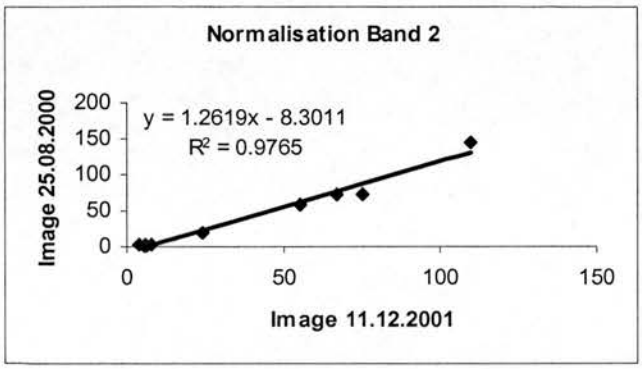

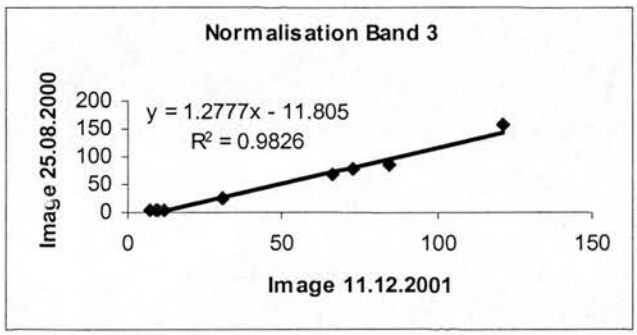

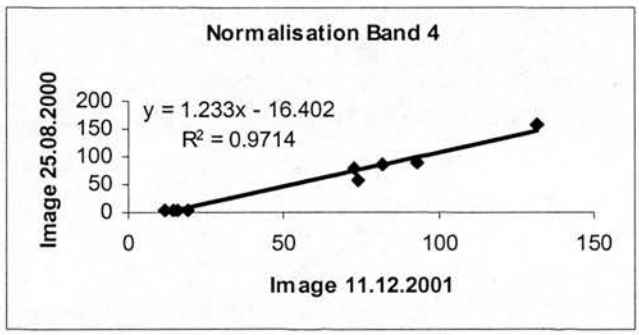

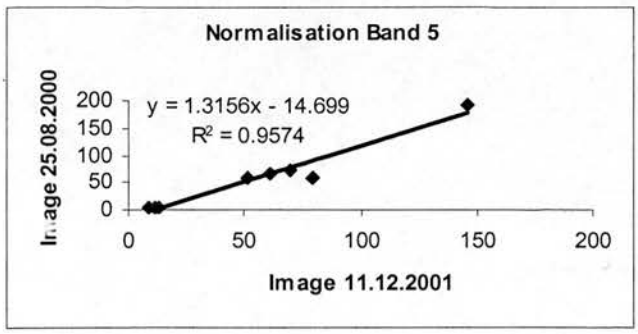

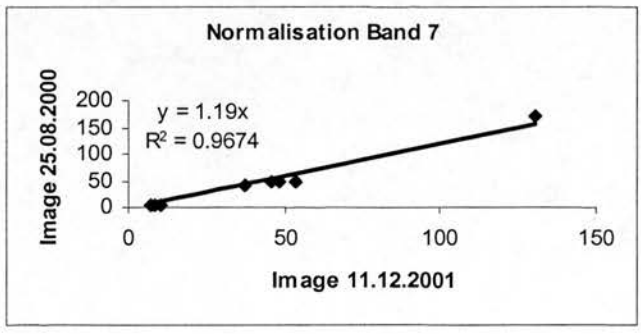

APPENDIX 2: programme *GROUND*

```
C
C
C This program read a file containing LiDAR (Light detecting and ranging
C data) consisting of OSGB coordinates, heights, and signal intensity
C for first and last return and calculates a surface that approximates
C the ground. It also calculates tree heights as the difference between
C the Digital Canopy Model created from the first return laser hits
C (corresponding to the canopy top) and the ground surface and the
C ground surface previously estimated.
C
C The program read two files (first and last return) containing six
C values each: fileid, Plot_number, L_East, L_North, L_Elev and L_Int:
C The first field is alphanumeric, the second is an integer, the
C following three are real and the last one is an integer.
C
C The program sort the data out to construct an array and in this way to
C ease the calculations and control of the results.
C
C Author: Gloria Patricia Olaya Gonzalez
C Date: June 6, 2004
C
C

      parameter (vect=99999,value=9999)
      integer i,j,k,l,m,r,plot,num2,num1,const,s,z,t
      character*40 inputfile1,inputfile2,outfile
      character*30  filename,list
      real*8 xo1(vect),yo1(vect),zo1(vect),mean,y
      real*8 xo2(vect),yo2(vect),zo2(vect),percen
      real*8 xxo1(vect),yyo1(vect),zzo1(vect)
      real*8 xxo2(vect),yyo2(vect),zzo2(vect)
      real*8 txo2(value),tyo2(value),tzo2(value),tco2(value)
      real*8 txo1(value),tyo1(value),tzo1(value),tco1(value)
      real*8 ctxo2(value),ctyo2(value),ctzo2(value),ctco2(value)
      real*8 fctxo2(vect),fctyo2(vect),fctzo2(vect),fctco2(vect)
      real*8 ftxo2(vect),ftyo2(vect),ftzo2(vect),ftco2(vect)
      real*8 ftxo1(vect),ftyo1(vect),ftzo1(vect),ftco1(vect)
      real*8 ptxo2(value),ptyo2(value),ptzo2(value)
      real*8 arr2,a,b,fmean(vect),minyo2,minxo2,min,maxyo2,maxxo2
      real*8 error1,error2,cmean(vect),area
      real*8 count1(vect),count2(vect),kk
      real*8 fmeanf(vect),fctzo2f(vect),ftxo2f(vect),ftyo2f(vect)
      real*8 ftzo2f(vect),ftzo1f(vect)
      real*8 axo2(vect),ayo2(vect),azo2(vect),aco2(vect)
      real*8 aaxo2(vect),aayo2(vect),aazo2(vect),aaco2(vect)
      real*8 faaxo2(vect),faayo2(vect),faazo2(vect),faaco2(vect)
      real*8 axo1(vect),ayo1(vect),azo1(vect),aco1(vect)
      real*8 aaxo1(vect),aayo1(vect),aazo1(vect),aaco1(vect)
      real*8 faaxo1(vect),faayo1(vect),faazo1(vect),faaco1(vect)

      call system('clear')
      call system('ls -l *.dat')
      write (*,'(A)')
      write (*,'(A)')
      write (*,'(A)') 'Input file name with [[ first return ]]:'
      read  (*,'(A)') inputfile1
      write (*,'(A)')
      write (*,'(A)') 'Input file name with [[ last return ]]:'
```

```
 read  (*,'(A)') inputfile2
 write (*,'(A)')
 write (*,'(A)') 'Output file name:'
 read  (*,'(A)') outfile

 open (unit=10, file=inputfile1, status='old')
 open (unit=20, file=inputfile2, status='old')
 open (unit=30, file=outfile, status='unknown')
 open (unit=40, file='accept.dat', status='unknown')
 open (unit=50, file='reject.dat', status='unknown')

 if(inputfile1.eq.inputfile2) then
    call system('clear')
    write (*,'(A)') '*********************************************'
    write (*,'(A)') '*********************************************'
    write (*,'(A)') '***            [[[ ERROR  ]]]               ***'
    write (*,'(A)') '***                                         ***'
    write (*,'(A)') '*** The files are equal, at least in name ***'
    write (*,'(A)') '*********************************************'
    write (*,'(A)') '*********************************************'
    stop
 endif

 write (*,'(A)')
 write (*,'(A)')'The maximum difference in height:'
 read (*,*) error1
 write (*,'(A)')
 write (*,'(A)')'The maximum difference in coordinate:'
 read (*,*) error2
 write (*,'(A)')
 write (*,'(A)')'The area [bxb], b:'
 read (*,*) area

 if(area.le.0) then
    call system('clear')
    write (*,'(A)') ' ************************************ '
    write (*,'(A)') ' ************************************ '
    write (*,'(A)') ' ***         [[[ ERROR  ]]]         *** '
    write (*,'(A)') ' ***                                *** '
    write (*,'(A)') ' ***  The area has to be positive  *** '
    write (*,'(A)') ' ***     and greater than zero     *** '
    write (*,'(A)') ' ************************************ '
    write (*,'(A)') ' ************************************ '
    stop
 endif

 call system('clear')
 write (*,'(A)') ' ************************************************
**************** '
 write (*,'(A)') ' ************************************************
**************** '
 write (*,'(A)') ' **                    [[[ First method ]]]
*           ** '
 write (*,'(A)') ' **  Fitting data to a straight line using linear
* regression  ** '
 write (*,'(A)') ' **              in the East and North direction
*           ** '
 write (*,'(A)') ' ************************************************
**************** '
 write (*,'(A)') ' ************************************************
**************** '
```

```
      write (*,'(A)') ' **                    [[[ Second method ]]]
     *            ** '
      write (*,'(A)') ' **             Fitting the data to a region usin
     *g           ** '
      write (*,'(A)') ' **                       the area method
     *            ** '
      write (*,'(A)') ' ************************************************
     ***************** '
      write (*,'(A)') ' ************************************************
     ***************** '
      write (*,'(A)')
      write (*,'(A49)') '          <o><o><o> PLEASE WAIT <o><o><o>'

      read(10,*,err=20) list,list,list,list,list,list
      do i=1,vect
         read (10, *, err=20)filename,plot,xxo1(i),yyo1(i),zzo1(i),
     *        num1
      enddo

 20   continue

      read(20,*,err=30) list,list,list,list,list,list
      do j=1,vect
         read (20, *, err=30)filename,plot,xxo2(j),yyo2(j),zzo2(j),
     *        num2
      enddo

      call sort(const,xo1,yo1,zo1,count1)
      call sort(const,xo2,yo2,zo2,count2)
      minxo2=xo2(1)
      maxxo2=xo2(const)

      s=1
      i=1
      r=0
      z=0
      do while (i.lt.const)
         arr2=xo2(i)
         k=0

         do j=i,const
            if(abs(xo2(j)-arr2).le.error2) then
               k=k+1
               r=r+1
               txo2(k)=xo2(j)
               tyo2(k)=yo2(j)
               tzo2(k)=zo2(j)
               tco2(k)=count2(j)
               txo1(k)=xo1(j)
               tyo1(k)=yo1(j)
               tzo1(k)=zo1(j)
               tco1(k)=count1(j)
            endif
         enddo
         i=r+1

         m=0
         mean=0
         call sort(k,tzo2,txo2,tyo2,tco2)
         do l=1,k
            if(abs(tzo2(1)-tzo2(l)).le.error1) then
```

```
      m=m+1
      mean=mean+tzo2(l)
      ptzo2(m)=tzo2(l)
      ptxo2(m)=txo2(l)
      ptyo2(m)=tyo2(l)
   endif
enddo

mean=mean/m

if(m.gt.4) then
   call straight(ptyo2,ptzo2,m,a,b)
   do l=1,k
      temp=a+b*tyo2(l)
    if(temp.le.0) then
          call system('clear')
     write (*,'(A)') '************************************'
     write (*,'(A)') '************************************'
     write (*,'(A)') '***        [[[ ERROR  ]]]        ***'
     write (*,'(A)') '***                              ***'
         write (*,'(A)') '***  Negative Slope - Bad Data  ***'
     write (*,'(A)') '************************************'
     write (*,'(A)') '************************************'
          stop
         endif
      if(temp.lt.tzo2(l)) then
         ctzo2(l)=temp
         ctxo2(l)=txo2(l)
         ctyo2(l)=tyo2(l)
         ctco2(l)=tco2(l)
      else
         ctzo2(l)=tzo2(l)
         ctxo2(l)=txo2(l)
         ctyo2(l)=tyo2(l)
         ctco2(l)=tco2(l)
      endif
   enddo
else
   do l=1,k
      if(mean.lt.tzo2(l)) then
         ctzo2(l)=mean
         ctxo2(l)=txo2(l)
         ctyo2(l)=tyo2(l)
         ctco2(l)=tco2(l)
      else
         ctzo2(l)=tzo2(l)
         ctxo2(l)=txo2(l)
         ctyo2(l)=tyo2(l)
         ctco2(l)=tco2(l)
      endif
   enddo
endif

z=z+k
k=0
do l=s,z
   k=k+1
   fmean(l)=mean
   cmean(l)=tco2(k)
   fctzo2(l)=ctzo2(k)
   fctxo2(l)=ctxo2(k)
```

```
      fctyo2(l)=ctyo2(k)
      fctco2(l)=ctco2(k)
      ftxo2(l)=txo2(k)
      ftyo2(l)=tyo2(k)
      ftzo2(l)=tzo2(k)
      ftco2(l)=tco2(k)
      ftxo1(l)=txo1(k)
      ftyo1(l)=tyo1(k)
      ftzo1(l)=tzo1(k)
      ftco1(l)=tco1(k)
   enddo
   s=i
enddo

call sort(const,fctco2,fctxo2,fctyo2,fctzo2)
call sort(const,ftco1,ftxo1,ftyo1,ftzo1)
call sort(const,ftco2,ftxo2,ftyo2,ftzo2)
call sort(const,cmean,fmean,cmean,cmean)

do l=1,const
   fmeanf(l)=fmean(l)
   fctzo2f(l)=fctzo2(l)
   ftxo2f(l)=ftxo2(l)
   ftyo2f(l)=ftyo2(l)
   ftzo2f(l)=ftzo2(l)
   ftzo1f(l)=ftzo1(l)
enddo

call sort(const,yo1,xo1,zo1,count1)
call sort(const,yo2,xo2,zo2,count2)
minyo2=yo2(1)
maxyo2=yo2(const)
min=minyo2

s=1
i=1
r=0
z=0

do while (i.lt.const)
   arr2=yo2(i)
   k=0

   do j=i,const
      if(abs(yo2(j)-arr2).le.error2) then
         k=k+1
         r=r+1
         txo2(k)=xo2(j)
         tyo2(k)=yo2(j)
         tzo2(k)=zo2(j)
         tco2(k)=count2(j)
         txo1(k)=xo1(j)
         tyo1(k)=yo1(j)
         tzo1(k)=zo1(j)
         tco1(k)=count1(j)
      endif
   enddo
   i=r+1
```

```
m=0
mean=0
call sort(k,tzo2,txo2,tyo2,tco2)
do l=1,k
   if(abs(tzo2(1)-tzo2(l)).le.error1) then
      m=m+1
      mean=mean+tzo2(l)
      ptzo2(m)=tzo2(l)
      ptxo2(m)=txo2(l)
      ptyo2(m)=tyo2(l)
   endif
enddo

mean=mean/m

if(m.gt.4) then
   call straight(ptxo2,ptzo2,m,a,b)
   do l=1,k
      temp=a+b*txo2(l)
      if(temp.lt.tzo2(l)) then
         ctzo2(l)=temp
         ctxo2(l)=txo2(l)
         ctyo2(l)=tyo2(l)
         ctco2(l)=tco2(l)
      else
         ctzo2(l)=tzo2(l)
         ctxo2(l)=txo2(l)
         ctyo2(l)=tyo2(l)
         ctco2(l)=tco2(l)
      endif
   enddo
else
   do l=1,k
      if(mean.lt.tzo2(l)) then
         ctzo2(l)=mean
         ctxo2(l)=txo2(l)
         ctyo2(l)=tyo2(l)
         ctco2(l)=tco2(l)
      else
         ctzo2(l)=tzo2(l)
         ctxo2(l)=txo2(l)
         ctyo2(l)=tyo2(l)
         ctco2(l)=tco2(l)
      endif
   enddo
endif

z=z+k
k=0
do l=s,z
   k=k+1
   fmean(l)=mean
   cmean(l)=tco2(k)
   fctzo2(l)=ctzo2(k)
   fctxo2(l)=ctxo2(k)
   fctyo2(l)=ctyo2(k)
   fctco2(l)=ctco2(k)
   ftxo2(l)=txo2(k)
   ftyo2(l)=tyo2(k)
   ftzo2(l)=tzo2(k)
   ftco2(l)=tco2(k)
```

```
      ftxo1(l)=txo1(k)
      ftyo1(l)=tyo1(k)
      ftzo1(l)=tzo1(k)
      ftco1(l)=tco1(k)
   enddo
   s=i
enddo

call sort(const,xo1,yo1,zo1,count1)
call sort(const,xo2,yo2,zo2,count2)

y=0
z=1
t=0
do while (minxo2.le.maxxo2)
   m=0
   s=0
   do j=z,const
      if(xo2(j).ge.minxo2+y.and.xo2(j).le.minxo2+area) then
         m=m+1
         axo2(m)=xo2(j)
         ayo2(m)=yo2(j)
         azo2(m)=zo2(j)
         aco2(m)=count2(j)
         axo1(m)=xo1(j)
         ayo1(m)=yo1(j)
         azo1(m)=zo1(j)
         aco1(m)=count1(j)
      endif
   enddo
   z=z+m
   y=0
   do while (minyo2.le.maxyo2)
      do k=1,m
         if(ayo2(k).ge.minyo2+y.and.ayo2(k).le.minyo2+area) then
            s=s+1
            aaxo2(s)=axo2(k)
            aayo2(s)=ayo2(k)
            aazo2(s)=azo2(k)
            aaco2(s)=aco2(k)
            aaxo1(s)=axo1(k)
            aayo1(s)=ayo1(k)
            aazo1(s)=azo1(k)
            aaco1(s)=aco1(k)
         endif
      enddo
      y=0.01
      minyo2=minyo2+area
      call sort(s,aazo2,aayo2,aaxo2,aaco2)
      do k=1,s
         t=t+1
         faaxo2(t)=aaxo2(k)
         faayo2(t)=aayo2(k)
         faazo2(t)=aazo2(1)
         faaco2(t)=aaco2(k)
         faaxo1(t)=aaxo1(k)
         faayo1(t)=aayo1(k)
         faazo1(t)=aazo1(k)
         faaco1(t)=aaco1(k)
      enddo
      s=0
```

```
         enddo
         minxo2=minxo2+area
         minyo2=min
      enddo

      call sort(t,faaco2,faayo2,faaxo2,faazo2)
      call sort(t,faaco1,faayo1,faaxo1,faazo1)

      call sort(const,fctco2,fctxo2,fctyo2,fctzo2)
      call sort(const,ftco1,ftxo1,ftyo1,ftzo1)
      call sort(const,ftco2,ftxo2,ftyo2,ftzo2)

      write(30,'(a10,a13,a20,a14,a16,a14,a15,a17,a16,a16)')
     *'"East"','"North"','"Ground Height"','"Top Height"',
     *'"North Height"','"East Height"','"Area Height"',
     *'"Difference N."','"Difference E."','"Difference A."'

      do l=1,const
         cota1=abs(fctzo2f(l)-ftzo1f(l))
         cota2=abs(fctzo2(l)-ftzo1(l))
         write(30,'(2f12.3,10f15.3)') ftxo2f(l),ftyo2f(l),ftzo2f(l),
     *        ftzo1f(l),fctzo2f(l),fctzo2(l),faazo2(l),
     *        cota1,cota2,abs(faazo1(l)-faazo2(l))
      enddo

      stop
      end

      subroutine sort(n,arr1,arr2,arr3,arr4)
      integer n, i, j, inc
      real*8 temp1, temp2, temp3, temp4
      real*8 arr1(n), arr2(n), arr3(n), arr4(n)

      inc=1
10    inc=3*inc+1
      if(inc.le.n) goto 10
20    continue
      inc=inc/3
      do i=inc+1,n
         temp1=arr1(i)
         temp2=arr2(i)
         temp3=arr3(i)
         temp4=arr4(i)
         j=i
30       if(arr1(j-inc).gt.temp1) then
            arr1(j)=arr1(j-inc)
            arr2(j)=arr2(j-inc)
            arr3(j)=arr3(j-inc)
            arr4(j)=arr4(j-inc)
            j=j-inc
            if(j.le.inc) goto 40
            goto 30
         endif
40       arr1(j)=temp1
         arr2(j)=temp2
         arr3(j)=temp3
         arr4(j)=temp4
      enddo
      if(inc.gt.1) goto 20
      return
      end
```

```
subroutine straight(x,y,ndata,a,b)
integer ndata,i
real*8 ss,st2,sx,sxoss,sy,t
real*8 a,b,x(ndata),y(ndata)

sx=0
sy=0
st2=0
b=0
do i=1,ndata
   sx=sx+x(i)
   sy=sy+y(i)
enddo
ss=float(ndata)
sxoss=sx/ss
do i=1,ndata
   t=x(i)-sxoss
   st2=st2+t*t
   b=b+t*y(i)
enddo
b=b/st2
a=(sy-sx*b)/ss
return
end
```

APPENDIX 3

European Larch **Plot EL_1**

Date of Data Acquisition: 14/03/03 N. Trees: 45

Tree No.	DBH	HEIGHT	Height FB	CrownN	CrownE
1	125	28.1	16.5	8.4	8.1
2	146.5	32.4	13.1	10.5	9.2
3	124.5	31.1	15.7	7.2	9.7
4	114.5	29	17.3	7.6	7.7
5	156	28.4	11.5	10.6	10.8
6	116	27.6	16.9	7.8	6.6
7	125	25.9	14.1	9.6	10
8	145.5	30	11.4	12.3	10.6
9	124.5	29.4	14.1	8.6	9
10	134	28.8	15.9	9	10
11	124	29.9	14.7	9.5	8.2
12	136	31.5	17.1	8.6	6.8
13	110	31.3	21.7	6.5	6.8
14	138	33.6	14	12	9.3
15	131	30.7	12.6	8	7.8
16	133	30.5	19.1	7.2	7.8
17	119.5	31.2	11.7	9.7	9.5
18	113	29.9	16.9	8.5	9.8
19	123	30.1	16.9	8.7	9
20	143	33.7	15.3	10.2	8.3
21	128	27.1	11.7	9	9.5
22	141	29.4	18.2	8.1	6.9
23	146	33.2	13.7	9.5	11.6
24	130	14.5	6.3		
25	131	30.7	14.1	10.5	9.8
26	136	30.7	12.8	10	9.9
27	108	29.4	12.3	6.9	8.4
28	155	30.2	12.9	7.8	9.4
29	155	27	9.9	7.7	8.3
30	18				
31	118	28.7	11		
32	32				
33	136	21.4	7.8	10.2	10
34	128	27.2	9.2	9.7	9.6
35	161	24.2	11.9	9.5	9.2
36	161	27.8	12.5		
37	122	29.8	17.1	4.5	5.6
38	155	31	9.9	12.5	10.8
39	157	32.9	14.6	11.5	9.8
40	118	28.7	11.9	9.9	7.1
41	142	35.4	10.8	10.6	10.8
42	147	27.8	10.6		
43	139	29.9	7.8	8.4	8.2
44	151	28.6	8.7	11	11.3
45	97	26.1	12.5	4.8	4

	European Larch	Plot EL_2			mixed
	Date of Data Acquisition: 11/03/03			N. Trees:83	
Tree No.	**DBH**	**HEIGHT**	**Height FB**	**CrownN**	**CrownE**
1	135			6	6.1
2	145	34.2	8.5	7	5.4
3	185	32.5	16.7		
4	127	31.4	12.2		
5	125				
6	80				
7	180	30.17	15.6		
8	122				
9	110				
10	119				
11	120	28	9.6		
12	170	26.4	13.2		
13	197	29.5	9.9		
14	164	29.7	15.4		
15	101			5	4.1
16	152	27.6	10.4	5.9	5.8
17	154	30.4	9.3	5	5.6
18	135	32.7	11.7	7.8	5.6
19	88			3.2	3.1
20	142	29.1	13.6	6.7	6.8
21	101			4.7	4.9
22	206	30.5	10.6		
23	163	30.5	14.1		
24	209	33.4	13.5		
25	165	32.1	15.2		
26	124				
27	173	30.7	14.2		
28	170	33.5	15.3		
29	107			4.7	5.5
30	123			5.6	5.2
31	189	29.2	11.8		
32	153	29.4	16.4		
33	225	29.7	10.9		
34	197	31.8	15.6		
35	96				
36	176	34.7	15.6		
37	95				
38	164	27.5	15.5		
39	192	34	13.5		
40	175	34.3	13.5		
41	105			6	5.2
42	97			5.4	6
43	118	30.8	10.4	6.4	6.7
44	101			5.6	5.2
45	113			5.7	6
46	96			3.8	4.2
47	222	33.4	3.8		
48	121				
49	108				
50	167	33.5	10.1		

51	190	32.8	18		
52	153	33.2	15.1		
53	175	35.1	15.2		
54	138	31.8	14.5		
55	123			6.4	7.4
56	92			5.5	5.6
57	142	32.4	12.9	6.7	7
58	124			6	6.2
59	114			4.2	4.6
60	141	31.2	12.7	7	7.2
61	113			3.9	5
62	127			5.9	6.1
63	181	30.1	9.4		
64	108			5.1	5.2
65	128				
66	121				
67	221	32.7	15		
68	168	33.1	8.3	4.2	4.5
69	104				
70	150	31.5	4.9	4.3	4.7
71	82			3.9	
72	116			5.4	6.2
73	78				
74	126				
75	180	33.2	12.7		
76	100			5.3	5
77	84			3.4	3.1
78	108			6.3	6.4
79	119			4	3.6
80	149				
81	133			5.8	6.8
82	87				
83	89			5.8	6.2

Oak Plot Ok_2 Fairy Knowe

Date of Data Acquisition: 15/03/03 **Number of trees: 174**

R31053E: 56.09.59.43397N 4.22.23.80797W 107.948

Tree No.	DBH	HEIGHT	Height FB	CrownN	CrownS
1	67	14	6		
2	60	10.1	3		
3	16				
4	43	9.6			
5	61	12.2	8.9	3.8	3.5
6	135	16.6	4.1	9.2	4.9
7	90	14.6	10.5	4.7	2
8	23.5				
9	23				
10	57	9.7			
11	92	11.7	8.6	3.8	5
12	46	9.7			
13	61	12.3	9.7	6	2
14	62	11.1	9.7		
15	13				
16	15				
17	197	24.1	5.7	15	13
18	14				
19	22				
20	20				
21	19				
22	16				
23	15				
24	13				
25	13				
26	14				
27	143	16.1	9	8.2	8.4
28	10				
29	87	17.1	9.1	6	5
30	19				
31	18				
32	125	15.7	6.1	8	7.6
33	29				
34	38	5.7			
35	110	14.7	10.8	3.6	2
36	13				
37	21				
38	14				
39	101	14.5	6	7.5	6.2
40	18				
41	82	15.3	8.6	5.5	3
42	53	9.9			
43	39	5			
44	98	17.9	9.9	5.7	5.6
45	163	22.1	3.5		
46	19				
47	121	19.5	5.6	8.8	6.6
48	17				
49	76	16.2	6.5	4.7	4.2

50	6				
51	80	22	9.3	5.8	5.1
52	17				
53	58	7.7			
54	123	14.2	8.5	10.8	6.8
55	9				
56	18				
57	11				
58	172	19.7	4.1	13	13
59	13				
60	63	13.1	7.2		
61	62	11.7			
62	26				
63	115	11.7	3.9		
64	12				
65	108	18.2	10.6	3.35	5.1
66	84	13.6	10.4	3.6	7.2
67	102	15.4	9.1	5.1	8.9
68	70	12.9	8.9	5.8	2.1
69	65	9.1			
70	21				
71	181	20	6.1	15	14
72	15				
73	90	18.2	9.5	6	4.4
74	38	6.5			
75	86	19.2	11.5	4.2	4.1
76	92	17.4	7.2	7.5	8.3
77	35	8.7		9	6
78	74	19.6	10.1	4.1	7.8
79	32	6.7			
80	23				
81	79	12.1	3.7	5.4	5
82	82	15.6	10.7	5	4.8
83	142	20.7	8.1	9.6	8.5
84	94	19.7	11.1	5.4	5
85	84	15.4	12.2	5.1	4.7
86	81	8.4	4.8	4.9	4.6
87	88	17.1	5.8	5	6.2
88	82	17.1	10.6	4.8	3.5
89	83	16.8	10.5	6	3.4
90	68	11.9	6.4		
91	14				
92	47	8.9			
93	77	12.7	10.9		
94	23				
95	17				
96	21				
97	88	17.3	8.2	5.8	8.5
98	36	6.9			
99	74	15.5	10.1	5.7	4.7
100	75	13.9	8.9	5.3	4.6
101	76	16.3	6.2	4.6	3.2
102	105	18.8	3.2	10.4	8.2
103	14				

Norway Spruce Plot NS_1 (50x50m)

Date of Data Acquisition: 15/03/03 115 trees

Tree No.	DBH	HEIGHT	Height FB	CrownN	CrownE
1	117	17.8	1.6	6	5.8
2	173	22.9	1.8	7.9	6
3	112	19.7	7	4	3.5
4	121	20.5	8.3	5	5.8
5	127	20.7	8.3	4.6	5.5
6	98				
7	128	22.1	4.1	5.3	5.2
8	155	20.6	2.1	6.9	7.2
9	82				
10	102	20.6	6	3.9	3.8
11	80				
12	120	22	6.6	5.2	4.7
13	109	19.4	6.4	4	4.6
14	111	16.4	5.8	5.6	6.2
15	74				
16	111	19.7	7.5	3.5	4.5
17	72				
18	92				
19	109	17.2	7.5	5.6	4.6
20	109	20.8	9.6	3	3.6
21	72				
22	125	20.1	7.3	5.9	5.4
23	117	19.1	6.5	5.2	4.4
24	94				
25	89				
26	74				
27	102	21.6	8.4	4.2	4.1
28	85				
29	91				
30	96				
31	117	21	7.1	5.4	5.5
32	60	9.3	4		
33	140	21	4.2	5.5	6.3
34	92				
35	107	19.6	9.1	6	5.3
36	109	20	6.5	4.2	5.6
37	129				
38	92				
39	83				
40	110	20.5	6.7	5	5.1
41	98				
42	144	20.6	8.4	5.7	5.3
43	82				
44	91				
45	117	25.4	11.9	5	4.1
46	86				
47	109	19	7.1	4.6	4.9
48	115	23.1	9.8	5.3	3.9
49	80				

50	21	7			
51	81				
52	94				
53	81				
54	89				
55	98				
56	123	19.9	6.4	5.4	6.5
57	99				
58	98				
59	95				
60	95				
61	118	12.3	2.5	8.5	7
62	105	19	3.1	6	6
63	11				
64	75				
65	108	17.8	8	5.3	5
66	98				
67	77				
68	107	22	9.5	4.8	5.2
69	90				
70	84				
71	97				
72	89				
73	113	19.5	9.4	5.1	4.8
74	69				
75	113	18.5	8.3	5.7	5.9
76	96				
77	77				
78	98				
79	109	19.1	7.4	3.8	3.6
80	88				
81	107	19.1	8.5	4.2	4
82	74				
83	136	20.7	7	5.1	4.2
84	103	19.8	6.7	5.6	4.6
85	85				
86	11				
87	75				
88	102	18.9	6	5.7	5.6
89	86				
90	86				
91	87				
92	72				
93	110	20.7	11	5.7	4.2
94	78				
95	108	19.2	9.2	4.5	5.1
96	75				
97	101	19.6	8.6	3.9	4
98	110	20.1	9.8	4	4.3
99	78				
100	135	22.7	5	6.9	5.7

Norway Spruce Plot NS_2 Drumore Wood
Date of Data Acquisition: 13/03/03 n. trees 222

Tree No.	DBH	HEIGHT	Height FB	CrownN	CrownS
1	117	23.1	5.7	4.7	5.1
2	30				
3	34				
4	64	20	7.1	4	3.8
5	103	20.8	5.3	4.8	4.6
6	63	11.4			
7	44				
8	80	17.7	4.8	3.4	2.9
9	23				
10	52	15.6			
11	66				
12	11				
13	103	20	8.1	4.2	3.8
14	112	21.8	6.3	4.1	4.9
15	19				
16	39	5.2			
17	73	12.3	5	1.8	2
18	46				
19	100				
20	12				
21	79				
22	87	14.7	4.3	2.9	2.7
23	116	19.1	5.4	5.2	4.8
24	100	18.8	5.7	4.7	4.6
25	24	3.4			
26	143	22.8	6.2	5.8	4.4
27	129	22.7	4.9	5.2	4.3
28	23				
29	41.5				
30	48				
31	138				
32	136.5	23	6.7	6.1	5.6
33	14				
34	11				
35	59				
36	109	20.1	7.2	4.5	4.3
37	68.5				
38	117	19	6.4	3.8	4
39	100	18.7	5.9	3.4	3
40	97				
41	60				
42	86	18.7	5.7	4.2	4.4
43	88	18.6	5.4	4.7	4.5
44	66				
45	65				
46	71				
47	77.5				
48	162				

49	48				
50	110	19.2		4	3.5
51	41				
52	92	21	5.4	2.8	3.1
53	70	18.5	5.1	2.5	2.8
54	28	6.7			
55	131	23.1	6.6	5.2	4.9
56	74.5				
57	52				
58	95	19		3.7	3.8
59	32	6.1		2	1.8
60	88.5	18.1		2.8	2.1
61	87	17.7		2.5	2.2
62	122	18		3.2	4
63	75	17.5		3	3.1
64	127.5	17.8		3.5	4.2
65	117	17		5.3	4.8
66	119	20.1		3.9	4.4
67	49	11			
68	135	22	7.3	4.7	4.8
69	34	6.1			
70	75				
71	87				
72	18				
73	32				
74	36.5	8			
75	91	18.3			
76	30				
77	35.5				
78	97				
79	123.5	19.3	4.6	3.6	4.5
80	141	21.4	6.5	2.8	5.4
81	154	20.8	5.7	3.8	5.6
82	72	21	4.9	2.8	3.5
83	29				
84	73				
85	92.5				
86	27.5				
87	163	18.7	6.3	3.8	5.2
88	124	18.5	5.4	4.1	4.8
89	31	5.8	6.4	2.6	2.9
90	35				
91	47				
92	90.5				
93	90				
94	63				
95	48				
96	73.5				
97	25				
98	75.5				
99	69				
100	63				